Interactions of Pure Aluminium Hydrolytic Species - Keggin Polyoxocations - and Hydroxide with Biologically Relevant Molecules

Agathe Fournier

PhD thesis submitted in partial fulfilment of the requirements of The Nottingham Trent University for the degree of Doctor of Philosophy

This research programme was carried out in collaboration with Unilever Research

School of Biomedical and Natural Sciences,

The Nottingham Trent University

May 2008

Acknowledgements

I would like to express all my gratitude to Professor Carole Perry for giving me the opportunity to do a PhD in her research group. Also I would like to thank Dr Kirill Shafran together with the past and present members of the Inorganic Chemistry Research Group for their help, support and the pleasant atmosphere of work I have experienced. I am also thankful to the friends I made over the time I spent at the Nottingham Trent University.

I gratefully acknowledge financial support and help with ^{27}Al solid-state NMR measurements from Unilever Research, Port Sunlight, Wirral, UK.

I gratefully acknowledge help from Dr. Cormac Smyth and Dr. Michael Kyle (both formerly of Ultrasonic Scientific, Dublin, Ireland) with ultrasonic measurements.

Above all, I would like to thank my family for their support and eternal encouragement.

Abstract

The general purpose of this thesis is concerned with the intricate interactions of pure aluminium species with biomolecules. Pure aluminium reference systems (aluminium monomers, Keggin aluminium polyoxocations - Al_{13} and Al_{30}, and aluminium hydroxide suspensions) were used for systematic mechanistic studies of the sol-gel transformation of aqueous solutions of aluminium-ions into aluminium (oxy) hydroxides induced by the addition of a 'soft base' - Trizma-base, which does not ionize fully in an aqueous solution. The conversion proceeds *via* forced hydrolysis-condensation of aluminium-ions into molecular clusters, structural conversion of aluminium Keggin-like polynuclear clusters into nanoparticles of aluminium (oxy) hydroxide, aggregation of primary nuclei of aluminium (oxy) hydroxide into larger clusters and finally the 'arrested growth' of the aggregates with the formation of the three-dimensional gel network.

The next part of the study concentrated on the development and the optimisation of a potentiometric method for the determination of the 'formal' hydrolysis ratio of aluminium-containing solutions. The method made it possible to establish the aluminium speciation of the selected systems.

The interactions of aluminium species with three model biomolecules - lactic acid, hen egg lysozyme and porcine mucin - were investigated. Aluminium and lactic acid underwent a strong coordination in aqueous solutions, with increasing concentrations of lactic acid appearing to force all the aluminium species initially introduced to convert into monomers and dimers as a result of an acidic hydrolysis. Subsequently, the resulting hydrolysed products formed new aluminium-lactate chelates.

The evolution of both the inorganic and biomolecular phases of the lysozyme-aluminium systems demonstrated that specific charge-stabilised bioinorganic assemblies involving aluminium species and lysozyme formed. The chemical and structural alterations of the protein on interaction with the inorganic species showed that the interactions occurred.

The interactions of aluminium with mucin appeared predominantly electrostatically driven. The formation of the aluminium-mucin entities modified the native conformation of the protein: initially organised into β-sheet structure, mucin, within the complexes, acquired a more compact organisation involving intermolecular bonding. Furthermore, in the case of the aluminium hydroxide systems, the established complexes were ordered into sheet-like structures.

Although the level of concentrations of aluminium and biomolecules exceeded those normally found in the human body and environmental media, we believe that the better understanding of aluminium species-biomolecule interactions would be of benefit to those working in the biomedical and environmental sciences.

Table of Contents

List of Figures

Page

List of Tables

Part 1

Introduction

1.1. Aluminium chemistry

The chemistry of aluminium in aqueous solution has been studied for over a century [1]; owing to its numerous applications in pharmaceutics [2, 3], clay pillaring [4-6], water treatment [7, 8, 9], ceramics [10, 11] and catalysis [12, 13] and because of the reactive properties of the colloidal products [14], the main compound of the most common mineral source of aluminium, bauxite [15-18]. The speciation of aluminium in partially neutralized solutions is of particular interest to many fields aside from chemistry, including environmental science and biology where issues such as the toxicity and transport of aluminium are important [19-23]. Basic salts containing aluminium Keggin polycations have been employed in a number of applications including clay pillaring [24], preparation of Al_2O_3 nanoparticles [25], antiperspirant actives [26], catalysts [27], and composite materials [28]. As an introduction, the hydrolysis and condensation behaviour of Al(III) in aqueous solutions will be described.

1.1.1. Water and cations in aqueous medium

The electronic structure of the water molecule is characterised by the oxygen atom being more electronegative than hydrogen ($\chi_O = 3.5$, $\chi_H = 2.1$). The electron density in the H_2O molecule is shifted toward oxygen that bears a high negative charge. According to the partial charge model detailed below, this charge can be estimated as $\delta = 0.4$. As a consequence, the water molecule exhibits a high dipolar moment ($\mu = 1.84$ Debye) and liquid water has a high dielectric constant ($\varepsilon = 78.5$ at 25^oC).
These two features of the water molecule made of the liquid a widely used dispersion liquid and a strong ligand. Its binding properties give rise to water-cation complexes that are more or less stable depending upon the size and charge of the cation, and the acidity of the medium.
The dissolution of ions allows their separation in solution. The prediction of the degree of solvation of ions with a charge higher than three is difficult because they are subject to hydrolysis reactions and, except in a highly acidic medium, the aquo complexes $[M(OH_2)_N]^{z+}$ are mostly unstable [29].

1.1.2. Acid-base properties of ions in aqueous solution

Coordinated water molecules are stronger acids than water molecules in the solvent itself. When the acidity of the medium is decreased, the water molecules tend to de-protonate according to the equation (1.1) of the general hydrolysis equilibria of cations [29]:

$$[M(OH_2)_N]^{z+} + hH_2O \overset{H_2O}{\rightleftharpoons} [M(OH)_h(OH_2)_{N-h}]^{(z-h)+} + hH_3O^+ \qquad \textbf{Equation 1.1}$$

where *h* can be defined as the hydrolysis ratio. It corresponds to the number of protons that have been removed from the solvation sphere of the aquo-cation.

During a chemical reaction, a hydroxyl group is directly bound to the metal ion in place of a water ligand. The positive charge on the metal ion creates an attraction to water, a Lewis base with a non-binding electron pair on the oxygen atom, and alters water's electron density. This in turn increases the polarity of the O-H bond, which now acts as a proton donor under the Brønsted-Lowry acid-base theory to release the hydrogen as an H^+ ion, increasing the acidity of the solution. These equilibria are specific for each element and will vary depending on the formal charge, size and nature of the element.

1.1.3. The partial charge model and its application to the aluminium cation

The acidity of the aquo-ion is dependent on proton exchange between the solvated complex and water. In a non-complexing medium, three types of ligand are likely to exist in the coordination sphere of the cation: the aquo (H_2O), hydroxo (HO^-) and oxo (O^{2-}) ligands.
The acidity of coordinated water molecules increases as the electron transfer within the M-O bond increases. In dilute solutions this leads to a whole set of solute species ranging from aquo-cations $[M(OH_2)_N]^{Z+}$ (h = 0) to neutral hydroxides $[M(OH)_Z]^0$ (h = z) or even oxo anions $[MO_{N'}]^{(2N'-z)-}$ when all protons have been removed from the coordination sphere of the metal [29]. The hydrolysis ratio increases with the pH of the solution and the oxidation state of the metal cation.

A way of controlling the hydrolyzed precursors of an element is to use a pH-charge diagram. For example, Figure (1.1) displays the pH-charge diagram [30] in which there are three domains: the lower one corresponds to aquo cations $[M(OH_2)_N]^{Z+}$, the upper one corresponds to oxo anions $[MO_{N'}]^{(2N'-z)-}$, and the intermediate one indicates the hydroxo species.

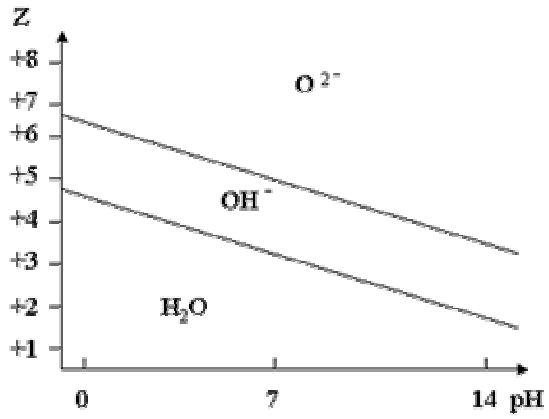

Figure 1.1. The charge-pH diagram with three domains OH_2, OH, and O^{2-}. There are only aquo ions, hydroxo ions, and oxo anions in the OH_2, OH and O^{2-} domains, respectively [30].

The extent of the hydrolysis reactions for one element, and the distribution of species associated with it can only be estimated based on the partial charge model which governs the pH-charge diagram. The speciation of a solution depends on the pH of the medium, the concentration and the nature of the element(s) present initially. The partial charge model defines the nature of the coordination sphere of a cation of charge z and coordination N as a function of the pH [31]. It follows the electronegativity equalization of the average electronegativities of the reaction products [32]. In accordance with the principle of electronegativity equalization, proton exchange between the metal complex and the medium takes place until their average electronegativities become equal. In spite of its lack of concentration and structural (as the presence of multiple bonds) considerations, the partial charge model does rationalize the chemistry of cations in solution in respect of hydrolysis and condensation processes.

Condensation between mononuclear species in aqueous solutions becomes possible only when OH groups are present in the precursor. In other words, the precursor has to be an aquo-hydroxo $[M(OH)_h(OH_2)_{N-h}]^{(z-h)+}$ or an oxo-hydroxo $[MO_{N-h}(OH)_h]^{(2N-h-z)-}$ form with both nucleophile (OH^-) and leaving (H_2O) groups present, i.e. be part of the intermediate domain, Figure (1.1). The condensation can be started by varying the pH by adding a base to a low valent metal cation such as Al^{3+}. It can also be initiated by redox reactions [16].

Elements of formal charge z = 3, such Al (III), form aquo cations in a large domain of acidity. The coordination of the metal cation decreases from octahedral to tetrahedral as the pH increases. In the M-OH_2 bond, the negatively charged oxygen atom shares electrons with both the metal M and hydrogen: $M\delta^+ \leftarrow O^{\delta-} \rightarrow H^{\delta+}$. As deprotonation goes on, electrons are more attracted by the metal. The partial charge δ_M decreases and the M-O bond becomes less polar leading to the covalent anion $[AlO_4]^{5-}$. The metal polarizes oxygen to form anionic oxo complexes. Octahedral aluminium $[Al(OH_2)_6]^{3+}$ species are observed below pH 3 whereas tetrahedral aluminates $[Al(OH)_4]^-$ are formed above pH 11. This coordination change occurs around pH ~ 6 when the partial charge of coordinated water molecules is close to zero.

1.1.4. Model of the acid-base behaviour of cations

Hydrolysis of cations converts the element to new ionic species or to precipitates by a neutralisation carried out by water molecules, Equation (1.1). Each of the species generated by the hydrolysis of a cation has a specific ratio of hydroxo-(oxo-) ligands to the number of aluminium atoms in the structural formula which can be called a 'molecular hydrolysis ratio' *h'*:

$$h' = \frac{n(OH^-) \cdot 2n(O^{2-})}{n(Al)}$$

where $n(OH^-)$ and $n(O^{2-})$ is the number of hydroxo- and oxo-ligands respectively, and n(Al) is the number of aluminium atoms per species.

The calculation of the overall hydrolysis ratio of a solution made of essentially one element, allows one to establish quantitatively the speciation distribution of that element providing that the molecular hydrolysis ratio of each species which contains this element, is known.

1.1.5. Hydrolysis, condensation and precipitation of aluminium in aqueous solution

Hydrolysis, condensation and complexation reactions of cations in aqueous solution are the phenomena involved in the formation of the solid by precipitation. Analysis of the behaviour of aluminium allows the identification of the structural relationships between the aluminium species in solution and the solid. The analysis will eventually allow an interpretation of the transformations taking place during aging of suspensions.

1.1.5.a. Hydrolysis of aluminium inorganic precursors

All ions in water are hydrated to some extent. The hydrolytic behaviour of aluminium ions in solution has only been well characterized in recent years [29, 33-36]. The Al^{3+} cation, with an ionic radius of 0.5 Å, has a primary hydration shell with six octahedrally coordinated water molecules and exists, below pH = 3, as the unhydrolyzed $[Al(H_2O)_6]^{3+}$ species, usually abbreviated as Al^{3+}.

As pH of the solution is increased, hydrolysis, with a sequential replacement of the water molecules by hydroxyl ions occurs. It can also be thought of as a progressive deprotonation of water molecules in the primary hydration shell of the metal [16, 35]. The simplest representation for Al^{3+}, omitting the hydration shell for convenience, is:

$$Al^{3+} \underset{}{\overset{+ H_2O,\ -H^+}{\rightleftharpoons}} Al(OH)_2^+ \overset{+ H_2O,\ -H^+}{\rightleftharpoons} Al(OH)_3 \overset{+ H_2O,\ -H^+}{\rightleftharpoons} Al(OH)_4^- \quad \textbf{Equation 1.2}$$

However, the hydrogen bond network in the aqueous medium ensures fast diffusion paths for the proton and the OH^- ion, so that the reaction may also proceed through a direct attack of the aquo ligand by the hydroxyl ion:

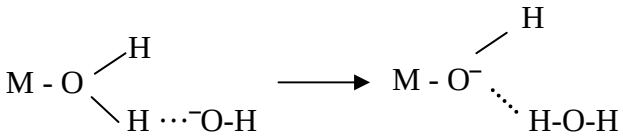

This mechanism probably occurs in the case of hydroxylation of the oxo forms. It is somewhat unlikely that the oxo ligand, which is strongly nucleophilic and has low basicity, could be substituted by the hydroxyl ion. Therefore, the reaction must proceed through direct reaction of the proton or water on the oxo ligand:

$$MO_{N'}^{q-} + H_{aq}^{+} \rightarrow MO_{N'-1}(OH)^{(q-1)-} + H_2O \qquad \textbf{Equation 1.3}$$

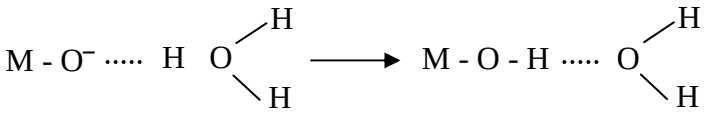

Hydroxylation of a metal cation to a hydroxo form through an oxidation or a reduction reaction constitutes the initial stage of condensation. The hydroxylated complex produced, is the precursor of condensation products.

1.1.5.b. Condensation mechanisms in aqueous solution

After the initiation of the condensation process with formation of a hydroxylated species, condensation may take place and lead to oxygen bridges between cations. Condensation reactions of aluminium species often occur at concentrations higher than 10^{-4} mol.L^{-1}, the concentration above which, monomers are unstable [29].

Condensation reactions proceed *via* the nucleophilic attack of OH^- groups onto cations [37]. Two different pathways, substitution or addition are followed depending on whether the maximum coordination of metal cation is already satisfied or not [38]. In all cases, at least one nucleophilic OH group, whose formation was initiated *via* acid-base reactions by adding a base to low-valent aquo-cations or an acid to high-valent oxy-anions, has to be present in the coordination sphere of the hydrolyzed precursor.

In the case of condensation operating *via* a nucleophilic substitution, an olation reaction, described below, takes place while a condensation *via* a two-step associative mechanism involves an oxolation

reaction. In both cases, water molecules from the coordination sphere of the metal cation are eliminated which results in the formation of polynuclear species [39, 40].

In the case of an olation reaction, there is formation of hydroxo bridges (ol bridges) [37] during a nucleophilic substitution reaction between a negatively charged OH group and a positively charged hydrated aluminium cation. As aquo-cations already exhibit their maximum coordination number, the formation of an 'ol' bridge requires the departure of one water molecule:

$$-M-OH + -M-OH_2 \rightarrow -M-OH-M- + H_2O \qquad \textbf{Equation 1.4}$$

It is kinetically controlled by the lability of the M-OH_2 bond. Olation follows a dissociative (SN_1) mechanism involving an intermediate compound of reduced coordination number.
The condensation of aquo-hydroxo cationic complexes $[M(OH)_h(OH_2)_{N-h}]^{(z-h)+}$ stops spontaneously when a finite degree of condensation is reached. The condensed species remain soluble as polycations.

Oxolation occurs *via* the creation of oxo bridges between cations that do not have aquo ligands in their coordination sphere [37]. Condensation has to proceed in this case *via* a two-step associative mechanism. It involves the condensation of two OH groups to form one water molecule which is then removed giving rise to an 'oxo' bridge. This proceeds via an associative (SN_2) mechanism as follows:

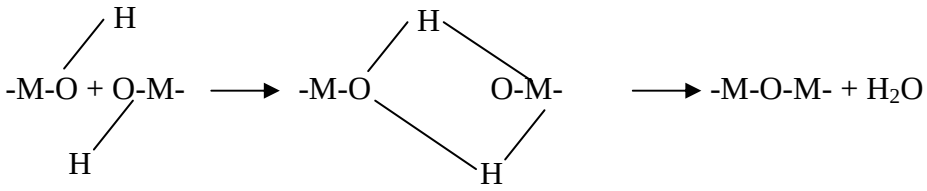

During this reaction, there is a nucleophilic addition with formation of an ol bridge, leading to an unstable transition state because of the coordination increase. Next, a proton transfer from the ol bridge to a terminal OH ligand forms a leaving water molecule. The leaving water molecule is present initially in the coordination sphere as an OH ligand and not as coordination water. As a consequence, the oxolation rate is linked to the acidity of the medium, contrary to what happens in olation.

As the degree of condensation increases, accumulation of electric charges on the condensed species decreases the nucleophilic character of the hydroxo ligands. The average electronegativity of the polycation is therefore increased which increases the charges $\delta(OH)$ and $\delta(M)$. Hence the condensation stops as soon as condensation criteria are no longer met, i.e. when OH ligands lose their nucleophilic character ($\delta(OH) > 0$) and cations lose their electrophilic character ($\delta(M) < + 0.3$).

1.1.5.c. Formation of aluminium polycations

Below pH ~ 3, the aluminium cation exists in the form of an aquo-cation $[Al(OH_2)_6]^{3+}$. An increase of the pH of the medium will initiate the formation of the doubly-charged $[Al(OH)(OH_2)_5]^{2+}$ species (h = 1), and further hydrolysis to the singly-charged $[Al(OH)_2(OH_2)_4]^{+}$ cationic monomeric species (h = 2). As well as the simple monomeric hydrolysis products, further hydrolysis leads to the uncharged metal hydroxide, $Al(OH)_3$ (h = 3) and finally the soluble tetrahedral aluminate $[Al(OH)_4^-]$ (h = 4). After formation of OH^- ligands in the first coordination sphere of the metal ion, polymeric aluminium species can be formed from a succession of condensation reactions.

The subject of aluminium polycationic species has extensively been reviewed during the past decade [41-44]. Two conflicting models describe the mechanism of aluminium hydrolysis and polymerisation in aqueous solution, namely, the "Core-links" model where hexameric cycles assemble, and the "Cage-like" Keggin-Al_{13} model where oligomeric species assemble. The two models have co-existed for more than 50 years [29, 45, 46]. Bi et al. [41] have proposed another model, a "continuous" model, consisting of the unification of both the pre-existing models. We deliberately decided to concentrate on the cage-like model, which fits better to both the experimental conditions and results (NMR proof of 4-coordinated aluminium). Nevertheless, information on the "Core-links" model is presented.

1.1.5.c.1. Formation of aluminium polycations following the "Core-links" model

In 1952, Brosset [47] interpreted his potentiometric data and put forward an early form of the "Core-links" model. Two years later, the same group [48] suggested a series of "Core-links" polymeric aluminium species whose form is $Al(Al_2(OH)_5)_n^{3+n}$. Almost at the same time, Sillen [48] put forward a theoretical "Core-links" model. Hsu and co-workers [49, 50] and Stol et al. [51] introduced and improved a "gibbsite-fragment" model or "hexameric ring scheme". The Brosset's "Core-links" model and the "gibbsite-fragment" model, developed together, form the present "Core-links" model. This model predicts the assembling of the hydroxyl aluminium changes from monomer to polymer following the hexameric ring model. It can form in its sol state, $Al_{54}(OH)_{144}^{18+}$ and then, a precipitate of $[Al(OH)_3]_n$ which maintains the sheet-structure of gibbsite or bayerite, Figure (1.2).
This model is preferred to the "Cage-like" model by the geochemists because it follows the crystallographic law of gibbsite [52].

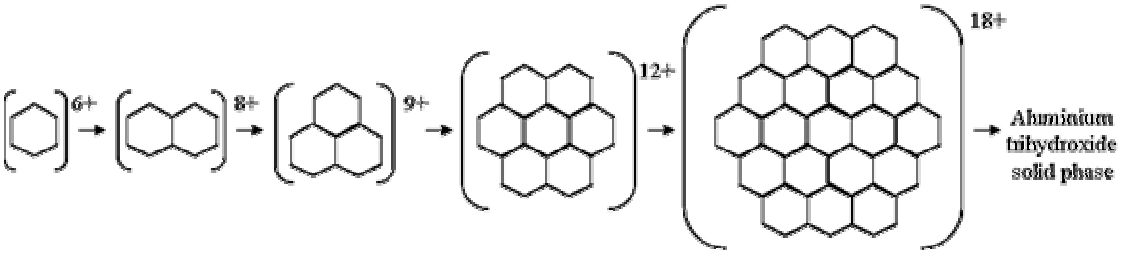

Figure 1.2. The polymerization of Al^{3+} via coalescence of the hexamer units according to the "gibbsite-fragment" model [53, 54].

1.1.5.c.2. Formation of aluminium polycations following the "Cage-like" model

Johansson [36, 55, 56] first proposed the Keggin-Al_{13} polynuclear species after he observed, from partially neutralized Al^{3+} solutions heated for 30 min at 80°C and aged for a few days, a sulfate precipitate. The structure of the Al_{13} polycation is made of a central tetrahedral AlO_4 core, surrounded by 12 aluminium octahedral AlO_6 units in the form of a cage, Figure (1.3).

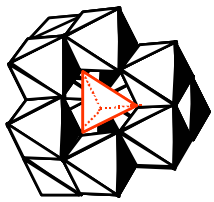

Figure 1.3. Polyhedral view of the Al_{13}-mer Keggin-type ion.

The polycation can be described as $AlO_4Al_{12}(OH)_{24}(H_2O)_{12}^{7+}$, which is usually called a "Cage-like" Keggin Al_{13} structure. This model supports the existence in solution of monomer, dimer, Keggin-Al_{13} polymer, and larger polymerized aluminium species. These species can be converted from one to another one directly [57, 58, 59a]. Since the polynuclear species of Al^{3+} in the "Cage-like" model can be identified instrumentally by using ^{27}Al magic angle spinning NMR spectroscopy [59b], this model has gained more approval and become the main viewpoint in the chemistry of flocculants [58, 60-62]. The existence of the polycation has been verified by Rausch and Bale [63] by the aid of small angle X-ray scattering.

The current status on the formation and structure of aluminium polycations explained by the "Cage-like" model of aluminium speciation will now be reviewed.

Formation of aluminium oligomers

Extensive hydrolysis of monomeric aluminium species leads eventually to the formation of small oligomeric aluminium species, such as aluminium dimers and trimers [29]. The formation of the dimeric species is initiated by the creation of a μ_2 bridge between two $[Al(OH)(H_2O)_5]^{2+}$ (h = 1) precursors. The dimerization of the h = 1 $[Al(OH)(OH_2)_5]^{2+}$ precursor leads to edge sharing dimers: , Figure (1.4).

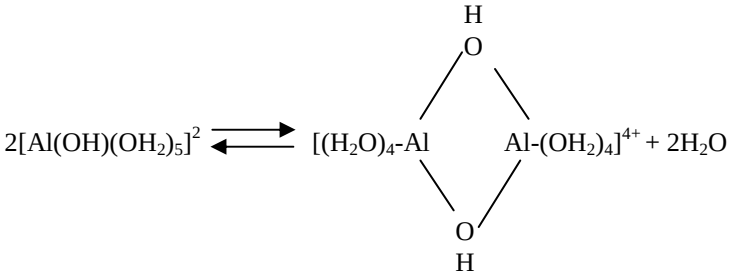

Figure 1.4. The structure of aluminium dimer.

This reaction probably follows an associative nucleophilic substitution mechanism due to the low lability of the complexing water [38].

Further hydrolysis leads to trimeric species, Figure (1.5), formed by adding one hydrolyzed monomer (h = 2) to the previous dimer:

$$[Al_2(OH)_2(OH_2)_8]^{4+} + [Al(OH)_2(OH_2)_4]^{+} \rightarrow [Al_3(OH)_4(OH_2)_9]^{5+} + H_2O \quad \textbf{Equation 1.5}$$

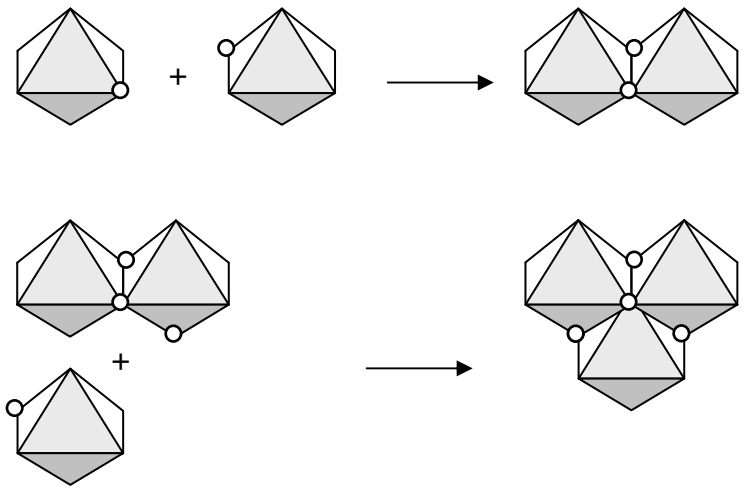

Figure 1.5. Early stages of the hydrolysis of Al^{3+} cations.
o=OH group [64].

The corresponding sulfate salts of the $[Al_2(OH)_2(OH_2)_8]^{4+}$ dimer and the more or less deprotonated cyclic trimer $[Al_3(OH)_4(OH_2)_9]^{5+}$ species have both been crystallographically characterized [36, 55]. The trimeric species preferentially exhibits a compact cyclic structure in order to minimize electrostatic repulsion between cations in edge-sharing adjacent $[AlO_6]$ octahedra. It is however possible to come across linear aluminium trimer species composed of three edge-sharing octahedra, Figure (1.6) **C**.

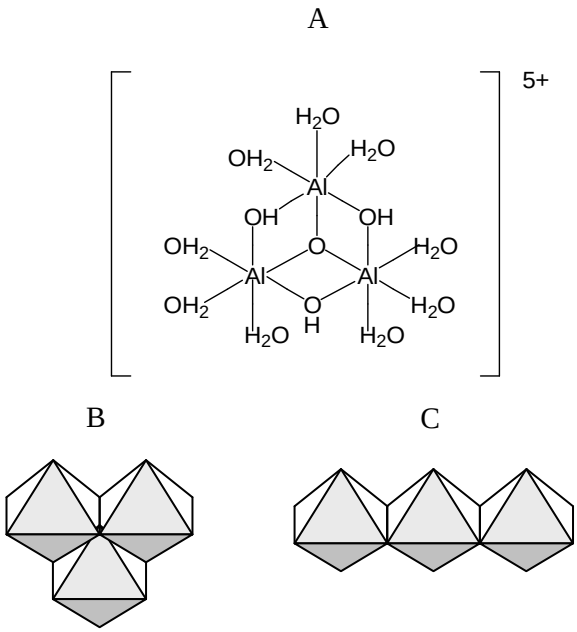

Figure 1.6. The structure of aluminium trimer (**A**), and its polyhedral representation following the cage-like (**B**) and the core-link (**C**) models.

Al^{3+} ions are bonded to a central μ_3-OH group. Electrons are strongly attracted by the small and highly polarizing Al^{3+} ions, making the μ_3-OH group highly acidic and therefore easily deprotonated.

$$[Al_3(OH)_4(OH_2)_9]^{5+} + H_2O \rightarrow [Al_3O(OH)_3(OH_2)_9]^{4+} + H_3O^+ \qquad \textbf{Equation 1.6}$$

Evidence from potentiometric titrations [65, 66] indicate that the trimer complex exists in solutions at 4 < pH < 5 but never reaches a large concentration, even in concentrated aluminium solutions, probably because of the fast formation of larger species.

Formation of aluminium polycations

As well as the simple oligomeric hydrolysis products discussed above, further addition of base in neutral solutions, leads to transformations into large aluminium polycations, the Al_{13}-mer (d ~ 1 nm) [67] and the recently characterized Al_{30}-mer (1 x 2 nm size) [68, 69], Figure (1.7).

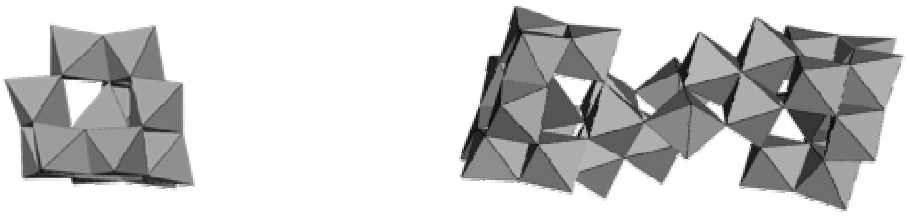

I II

Figure 1.7. Polyhedral representation of the structures of Al_{13} $[AlO_4Al_{12}(OH)_{24}(H_2O)_{12}]^{7+}$ (**I**) and Al_{30} $[Al_{30}O_8(OH)_{56}(H_2O)_{24}]^{18+}$ (**II**).

Formation of the Al_{13}-mer polyoxocation

The presence of a species with a tri-μ -OH ligand, like an aluminium trimer [70], causes further growth of condensation products by the nucleophilic character of this ligand following deprotonation. The first step of the formation of the tridecamer species is the dissociation of the tri-μ -OH bridge [16, 38]:

$$[Al_3(OH)_4(OH_2)_9]^{5+} + H_2O \rightleftharpoons [Al_3O(OH)_3(OH_2)_9]^{4+} + H_3O^+ \quad \textbf{Equation 1.7}$$

The cation formed after deprotonation has a very nucleophilic electron pair on the tri-μ -OH ligand. Formation of the $[H_3O_2]^-$ ligand can also favour deprotonation of the aquo ligands under moderate hydrolysis conditions ($h < 2.6$):

$$[Al_3O(OH)_3(OH_2)_9]^{4+} + 3OH^- \rightleftharpoons [Al_3O(OH)_3(O_2H_3)_3(OH_2)_3]^+ + 3H_2O \quad \textbf{Equation 1.8}$$

Nucleophilic attack by the resulting product on a monomeric aluminium species initiates the condensation process that generates the Al_{13} ion: because of the bulky nature of the tri-μ -OH trimer, this monomer is then forced to adopt tetrahedral coordination. The addition of the two more tri-μ -OH trimers creates the Al_{13} ion, Figure (1.8) I.

$$[Al(OH_2)_6]^{3+} + 4[Al_3O(OH)_3(O_2H_3)_3(OH_2)_3]^+$$
$$\rightleftharpoons \{Al[Al_3O(OH)_3(O_2H_3)_3(OH_2)_3^+]_4\}^{7+} + 6H_2O \quad \textbf{Equation 1.9}$$

The four trimers coordinated to the central aluminium atom may subsequently undergo intramolecular condensation by olation for molecules in the cis configuration. This last step ensures the stability of the cation.

$$\{Al[Al_3O(OH)_6(OH_2)_6]_4\}^{7+} \rightleftharpoons [Al_{13}O_4(OH)_{24}(OH_2)_{12}]^{7+} + 12H_2O \quad \textbf{Equation1.10}$$

This reaction mechanism is supported by by Akitt and Farthing [71]. Their ^{27}Al NMR investigations indicate that only small oligomers, probably trimers, condense directly without intermediates during the formation of Al_{13}-mer.

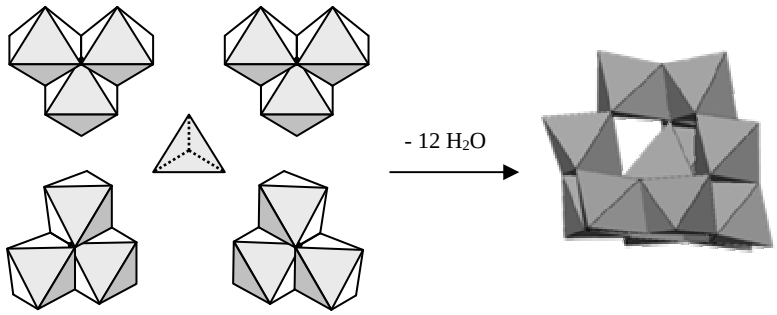

Figure 1.8. Schematic depiction of the suggested Al_{13}-mer, illustrating the structure as built from the tetrahedral AlO_4^- core and four trimers. Also shown are the structures of the tetrahedral AlO_4^- core (centre left) and the trimers (surrounding the tetrahedral AlO_4^-).

The Al_{13} polycation, Figure (1.8) has been identified by small angle X-ray methods [72, 73, 74], potentiometric titration [65] and by a narrow ^{27}Al solution NMR resonance at ~ 63.5 ppm (relative to $[Al(OH_2)_6]^{3+}$), Figure (1.10), attributed to the single tetrahedrally coordinated, by oxo bridges, aluminium (AlO_4) located at the centre of three layers of edge-sharing octahedra. The remaining aluminium atoms are hexa-coordinated with bridging hydroxides or water molecules. This type of structure is known as a Keggin structure. The tetrahedral and octahedral aluminium sites can be easily distinguished in the ^{27}Al NMR spectrum [57].

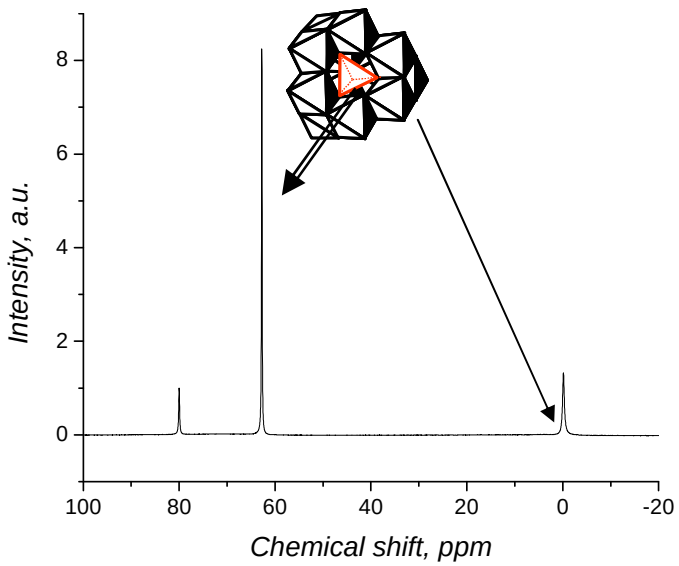

Figure 1.9. ^{27}Al solution NMR spectrum of a reference Al_{13}-mer system with the structural representation of the polycation. The arrows designate the characteristical signals of the Al_{13}-mer. The peak at 80 ppm arises from the internal reference solution of aluminate ions in D_2O.

This type of structure is known as a Keggin structure. The thermodynamic properties of these species have been reviewed by Baes and Mesmer [29] at 25 °C and more recently their evaluated data have been extrapolated up to 100 °C by Grenthe et al. [75].

Formation of the Al_{30}-mer polyoxocation

The Al_{30}-mer (1 x 2 nm size) has been recently characterized [68, 69], Figure (1.7) II and can be crystallized with a weakly interacting anion and the atom positions determined by X-ray structure analysis [61, 76]. It contains the δ-Keggin motifs as $Al_{30}O_8(OH)_{56}(H_2O)_{24}^{18+}$ (Al_{30} Kδ-T) [61] and the $Al_{13}O_4(OH)_{24}(H_2O)_{12}^{7+}$ (Al_{13} Kδ-N) species [76], Figure (1.10).

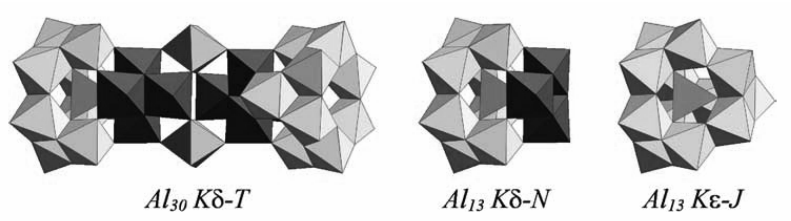

Figure 1.10. Polyhedral representation of three Keggin aluminium polycations Al_{30} Kδ-T, Al_{13} Kδ-N and Al_{13} Kε-J.

The synthesis of the Al_{30}-mer is performed either by heating solutions containing Al_{13} Kε-J and monomers at 130°C for one hour or at 20°C with aging of a solution containing Al_{13} Kε-J and monomers [77]. For Al_{30} Kδ-T, the ^{27}Al NMR in situ measurements demonstrated that the ε-Keggin $Al_{13}O_4(OH)_{24}(H_2O)_{12}^{7+}$ polycation (Al_{13} Kε-J) is the precursor species [36, 62, 78]. The existence of the Al_{30}-mer is incarnated by a ^{27}Al solution NMR signal at 70 ppm, Figure (1.11), due to the Al_{30} tetrahedral core [61, 79].

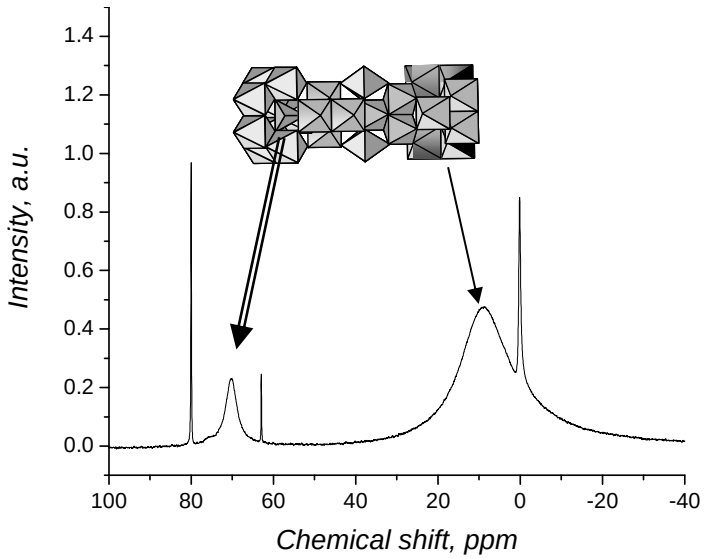

Figure 1.11. ^{27}Al solution NMR spectrum of a reference Al_{30}-mer system with the structural representation of the polycation. The arrows designate the characteristical signals of the Al_{13}-mer. The peak at 80 ppm arises from the internal reference solution of aluminate ions in D_2O.

Allouche et al. [77] determined that the presence of aluminium monomers in solution is critical to promote the synthesis of Al_{30} Kδ-T; the monomers initiate the first step of Al_{13} Kε-J conversion into Al_{30} Kδ-T. Based on those conclusions, they have developed a chemical pathway, Figure (1.12), to justify the transformation of Al_{13} Kε-J and the appearance of the Al_{30} polycation and other aluminium polycations.

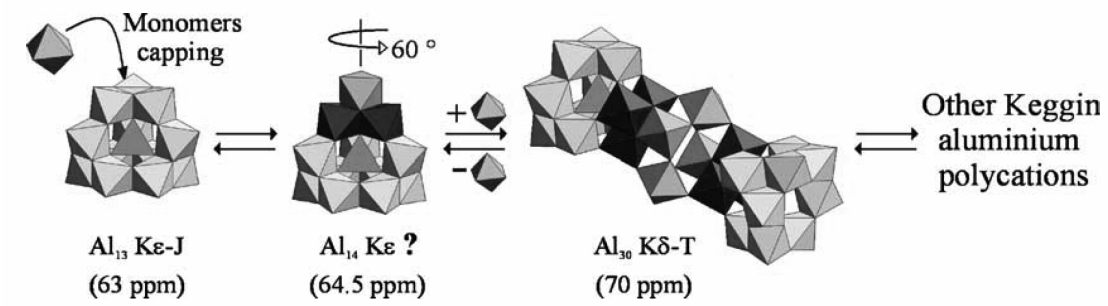

Figure 1.12. Hypothetical Al_{13} Kε-J isomerization and dimerization, initiated by aluminium monomers, to form Al_{30} Kδ-T [77].

The polycation, Figure (1.8) II, results from the combination of two δ-Al_{13} units connected by a crown of four octahedrally complexed aluminium ions. Initially, Al_{13} Kε-J is supposed to be ‘‘capped’’ by a monomer to form an intermediate species Al_{14} Kε. As Al_{13} Kε-J decreases and Al_{30} Kδ-T increases, one may safely assume that Al_{14} Kε is formed by Al_{13} Kε-J during the first stage of transformation and consumed by formation of Al_{30} Kδ-T. This will lead for a period to a constant but small amount of Al_{14} Kε. Al_{14} Kε would isomerize into Al_{14} Kδ and would further dimerize and react with two other monomers to produce Al_{30} Kδ-T.

Formation of aluminium hydroxide and oxide particles

Aluminium can form a wide range of oxides and hydroxides. Aluminium hydroxide colloids produced by aqueous and non-aqueous sol-gel routes are among the most frequent precursors to a broad range of aluminium-containing inorganic and hybrid materials [16]. The degree to which the reactions proceed and the natures of the resulting species depend on such variables as aluminium concentration, pH, temperature, and the presence of other ions.

When a certain pH (pH > 4.6) and OH/Al ratio (h > 2.5) of the partially neutralized aluminium solutions are reached, the decrease in the Al_{13} fraction and the rapid precipitation of more highly condensed, amorphous, or weakly crystalline phases made of aluminium hydroxide colloids, are

observed [29, 58, 54, 72, 80]. Using infrared, NMR spectroscopies and small-angle X-ray scattering, Bottero et al. [72] found that, when OH/Al > 2.8, the aggregation of Al_{13} led to the disappearance of tetrahedral aluminium and to the formation of polymerized octahedral layers that would finally form poorly crystalline materials. The crystalline forms of the aluminium hydroxides can be divided into the trihydroxide $Al(OH)_3$ (which exists in three forms: gibbsite, bayerite and nordstrandite) [81] and the oxide hydroxide (which exists as pseudoboehmite, boehmite or diaspore).

Bottero et al. [58] suggested that crystalline aluminium hydroxides are not formed by the condensation of the six-membered ring of octahedrally coordinated aluminium but by the structural rearrangement of Al_{13} without re-dissolution steps. However, it remains unknown whether such a mechanism can be applied to the formation of gibbsite, which is favoured in acidic situation and often requires long aging times to form [54]. As shown in Hsu and Bates [50], the transformation from polymeric aluminium species to gibbsite in partially neutralized solutions took several months and a mechanism of nucleation from the six-member polymer was proposed. The description of the mechanism is presented in the following section.

Often the insoluble aluminium hydroxides lose molecules of water to give insoluble oxides, as represented by Equation (1.11):

$$Al(OH)_z(s) \rightleftharpoons AlO_{z/2}(s) + \frac{z}{2}H_2O \qquad \textbf{Equation 1.11}$$

If the attraction of the metal ion for the pair of electrons on oxygen is strong enough, the hydroxy groups of the metal hydroxide may start to lose their remaining hydrogens as hydronium ions:

$$Al(OH)_z + zH_2O \rightleftharpoons AlO_z^{z-} + zH_3O^+ \qquad \textbf{Equation 1.12}$$

Thus the metal hydroxide may begin to act as a weak oxo acid, which finally may ionize to give an oxo anion, thus completely dismembering the water molecules that were originally attached in a hydrated ion.

1.1.5.d. Kinetics of solid formation: nucleation, growth and aging

The precipitation of a solid involves four kinetic steps [83-86]: (a) formation of a zero-charge precursor , (b) creation of nuclei, (c) growth of them and finally (d) ageing of the particles in suspension.

The presence of a zero-charge precursor $[Al(OH)_3(OH_2)_6]^0$ is required for the condensation and formation of a solid phase. The rapidity of the formation of the precursor depends on the way of its formation whether it was through the addition of a base, thermohydrolysis or the thermal decomposition of a base such as urea.

Next, the creation of nuclei through condensation (olation or oxolation) of zero-charge precursors is a function of the concentration of the precursor. Beyond a critical concentration C_{min}, the condensation

rate increases abruptly and polynuclear entities are formed throughout the solution, zone II in Figure (1.13).

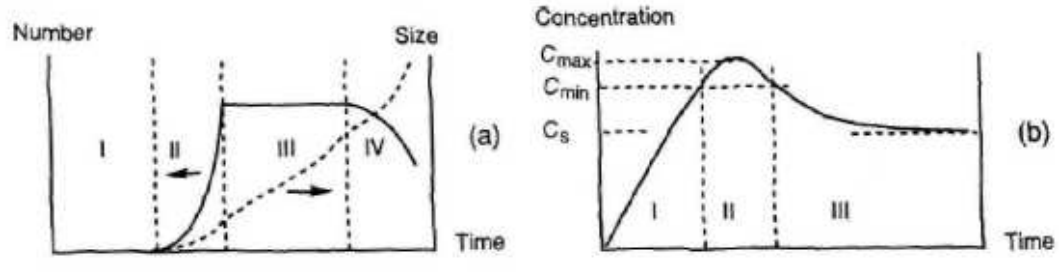

Figure 1.13. Change in (**a**) the number and sizes of particles formed in solution and (**b**) in the concentration C of the soluble precursor of the solid phase [84] during precipitation.

The unstable nature of critical-size nuclei formed during the nucleation stage leads to their growth through incorporation of the precursor molecules, which continue to be generated after nucleation. Growth of the nuclei happens through the addition of matter until the primary particle stage is reached. This step follows the same chemical mechanisms as nucleation: olation and oxolation. However, for a concentration close to C_{min}, the nucleation rate is very small and precursors condense preferentially on existing nuclei, which causes their growth until the precursor concentration reaches solution saturation, in other words the solubility limit of the solid phase, zone III in Figure (1.14).

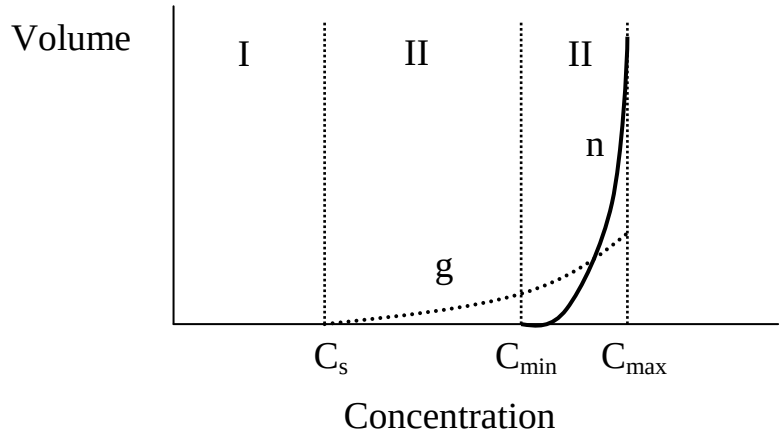

Figure 1.14. Nucleation rate *n* and growth rate *c* as a function of the precursor concentration in solution. Zones labelled I, II and III correspond to those of Figure (1.14).

Finally, ageing of the particles in suspension leads to various possible modifications of the primary particles after their growth. The increase of the average particle size and eventually their aggregation, Figure (1.13, IV), occur following the 'Ostwald ripening' phenomenon. Many small particles formed initially in a system slowly disappear except for a few that grow larger, at the expense of the small ones. The smaller particles act as "nutrients" for the bigger particles. As the larger particles grow, the

area around them is depleted of smaller particles. In addition, ageing may produce a change in morphology and crystalline structure or even cause crystallization of amorphous particles.

1.1.5.e. Precipitated aluminium hydroxides formation

Precipitated aluminium hydroxides can be formed in various ways, such as by neutralisation of the metal salt to *h*(OH/Al) ratios of approximately 3. Several studies [80, 58] have suggested that the initial stage in the formation of gels by neutralisation of aluminium solutions consists of the aggregation of tridecamer (Al_{13}-mers) units, although detailed mechanisms are still not clear. Bottero et al. [58] concluded, from NMR, infra-red and small angle X-ray studies, that the nature of the clusters formed depends very much on the OH/Al ratio. For h = 2.5 at short times, chain-like clusters of low fractal dimension and size of approximately 40 nm are formed. With increasing h the clusters become larger and more compact and there is a progressive loss of the tetrahedral aluminium. The initially precipitated form undergoes rearrangement on ageing or heating and eventually attains long-range crystalline order. The common crystalline phase is pseudoboehmite (or gelatinous boehmite). The X-ray diffraction pattern of pseudoboehmite shows broad lines that coincide with the major reflections of well-crystallized boehmite, γ-AlO(OH), but are shifted to varying degrees to higher *d*-spacings consistent with intercalation or association of water. The degree of crystalline order, particle size, and chemical composition of the gelatinous aluminas depends critically on temperature, rate of precipitation, final pH, ionic composition, concentration of starting solutions, and time of aging [29, 71]. Both amorphous and pseudo crystalline phases convert eventually to α-$Al(OH)_3$ upon aging at intermediate pH.

Thermodynamic data

Thermodynamic data available for the most established monomeric and oligomeric hydrolysed species found in aqueous solutions of aluminium-ions with non-complexing anions (chloride, nitrate, perchlorate, etc.) are summarised in Table (1.1).

Table 1.1. Thermodynamic data for the major Al^{3+} hydrolysis species (25 ºC) [19, 29].

Species	h^*	$-\log K_{x,y}$	$\pm\sigma$ $(\log K_{x,y})$**	a***	b***	$\Delta H^0_{x,y}$, kCal	$\Delta S^0_{x,y}$, kCal/K
$[Al(OH)(H_2O)_5]^{2+}$	1.00	4.97	0.02	-2.044	0.52	11.9±0.5	17.2±1.7
$[Al(OH)_2(H_2O)_4]^{+}$	2.00	9.30	0.1	-3.066	0.55	-	-
$[Al(OH)_3(H_2O)_3]$	3.00	15.00	0.2	-3.066	0.45	-	-
$[Al(OH)_4]^{-}$	4.00	23.00	0.3	-2.044	0.36	-	-
$Al_2(OH)_2(H_2O)_8]^{4+}$	1.00	7.70	0.3	-	-	18.7±2	27.5±7

Table 1.1. Continued.

Species	h^*	$-\log K_{x,y}$	$\pm \sigma$ $(\log K_{x,y})$**	a***	b***	$\Delta H^0_{x,y}$, kCal	$\Delta S^0_{x,y}$, kCal/K
$Al_3(OH)_4(H_2O)_9]^{5+}$	1.33	13.94	0.1	1.022	-	35.4±4	57±13
$[Al_{13}O_4(OH)_{24}(H_2O)_{12}]^{7+}$	2.46	98.73	0.05	-18.40	3.55	278.8±2	457±7
α-$Al(OH)_3$(gibbsite,K_{s0})	3.00	8.50	0.1	3.066	-0.45	-	-

* - hydrolysis ratio h = $[OH^-]/[Al^{3+}]$;

** - experimental error of the stability constant $K_{x,y}$; $K_{x,y}$ – the stability constant in the notation of Baes and Mesmer [29] which corresponds to hydrolysed species $Al_x(OH)_y^{(3x-y)+}$.

*** - a and b are coefficients of the extended Debye-Davies equation.

The thermodynamic data of the Al species enables one to the determination of hydrolysis constants of Al species and the stability of complexes with ligands. From the data of Table (1.1) one can see that at least eight Al species can be found at equilibrium conditions at room temperature in Al-ion aqueous solutions: Al monomers with 0<h<4, small oligomeric species such as dimers and trimers, large Al isopolycations (Al_{13}-mer) and the solid phase of Al hydroxide.

Gibbsite was included in Table (1.1) as an example of a crystalline aluminium hydroxide phase. However, depending on the hydrolysis conditions, other amorphous or crystalline aluminium hydroxide phases can be observed at equilibrium conditions (e.g. amorphous pseudoboehmite, boehmite, bayerite, diaspore, norstrandite, tohdite). Solid phases exhibit dissolution constants K_{SO} that differ from gibbsite and their presence can alter the corresponding speciation patterns significantly.

1.2. Interactions of aluminium species

1.2.1. Interaction of aluminium with biomolecules

Due to its availability and exceptional properties in both the metallic and ionic forms, aluminium is one of the most important metals for the world economy. Despite its numerous applications in fields such as catalysis [87], clay pillaring [88], water treatment [89] and cosmetics [26], many domains of aluminium chemistry and biochemistry remain unexplored, mainly due to the formation and complex inter relationships existing between aqueous ionic species or between ionic and precipitated forms of aluminium [90]. Aluminium ions undergo hydrolysis and condensation reactions in aqueous solution, leading to the formation of a range of species which can be differentiated on the basis of their nuclearity and hydrolysis ratio ($h = C(OH^-)/C(Al)_{total}$) [91]. A striking difference between aluminium and other abundant metals such as iron is the high stability of large soluble polynuclear species such as the Al_{13}-mer and Al_{30}-mer [38, 44]. Another difference is that aluminium is not essential to life, and can be classified as a detrimental element [92]. In previous studies, the interactions of aluminium

species with biopolymers have focused on monomeric forms of the aluminium ion [93] as well as on the adsorption of different ligands on aluminium hydroxide and oxide surfaces [94], differentiating between the possible complexes formed with biological ligands and demonstrating the effect of aluminium ions on the biological functions of the biopolymers.

1.2.2. Impact of aluminium on biological systems

Despite the fact that most of the aluminium entering the bloodstream (as Al(III)) is excreted within a matter of a few days or weeks, and also that the gastrointestinal tract, at least in principle, offers an effective barrier to this process, its uptake through the oral route, e.g., the administration of $Al(OH)_3$ as a high dosage antacid, gives rise to increased tissue, brain, skeletal, and urinary Al(III) levels [95, 96]. That is why an important number of speciation studies [97-102] and reviews related to the *in vivo* interacting properties of aluminium [103-107] have emerged.

The coordination chemistry of aluminium has attracted considerable attention due to its possible involvement in several toxic processes. In the last 25 years many studies demonstrated the capability of aluminium to interfere with a variety of neurological processes associated with several pathologies (Table 1.2).

Table 1.2. Involvement of aluminium in different pathological conditions.

	References
Alzheimer's disease	[108-111]
Anemia	[112, 113]
Bone disease	[114, 115]
Cancer	[114]
Cardiotoxicity	[114]
Dialysis encephalopathy	[117-119]
Gastrointestinal toxicity	[120-121]
Renal osteodistrophy	[122-123]

Aluminium overload is of interest since abnormal accumulation of aluminium has been reported in histopathological hallmarks of Alzheimer's disease such as senile plaques and neurofibrillary tangles [124-128], although whether or not the condition actually causes the disease has not been established, and aluminium overload may merely be a side-effect [129]. Because of its medicinal importance, it is of interest to compare the affinity of biomolecules for aluminium.

The Al^{3+} ion also affects vesicle fusions [130] and alters membrane permeability [131, 132]. According to Jones and Kochian [133], the plasma membrane is the most likely site of aluminium interaction and, therefore, the site of toxic effects. Aluminium has pro-oxidative properties toward biological

membranes and its implications in human pathology have described in [134]. However, there is still a lack of knowledge regarding the inorganic biochemistry of aluminium.

Among its applications, aluminium, in the form of hydroxide particles, is used in the formulation of vaccine adjuvants to stimulate the immune response [135-138]. Aluminium hydroxide adjuvants have a long history of use since they were proven effective in diphtheria, tetanus, and pertussis vaccines in the 1930s [139]. They are good adsorbents for proteins [140]. Therefore, studies devoted to the interaction of aluminium-containing adjuvants with biomolecules became of crucial importance. However, recent research [141] has demonstrated side effects (as persistent itching nodules) of the aluminium-containing vaccines after their administration. It was then suggested to avoid the uptake of aluminium adjuvants.
The selection of molecules chosen for investigation includes lactic acid, lysozyme and mucin.

1.2.2.a. Structure and properties of lactic acid from the viewpoint of an interaction study

The therapy for metal overload pathologies usually involves the administration of suitable chelating agents to selectively remove the metal from the body. Regarding aluminium, there is a need for new, safe, inexpensive and orally effective chelators [142]. The hydroxycarboxylate [143, 144] and carboxylate [145-147] type ligands are known to form soluble complexes with aluminium. In the interaction studies reported here, lactate (represented Figure (1.15) in its protonated form) was selected as a hydroxycarboxylate chelating agent.

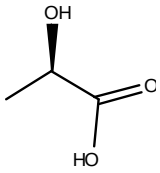

Figure 1.15. Structure of lactic acid.

Lactate is a biomolecule whose concentration in blood is usually 1-2 mmol.L^{-1} at rest, but can rise to over 20 mmol.L^{-1} during intense exercise [148]. Its detection has important applications in medicine in the diagnosis, grading and therapeutic monitoring of diseases such as cancer, stroke and heart disease [149]. The metal-binding ability of lactate has already been reported [150-152]. It is influenced by the presence of two donor groups which can be anchoring functions for metal ions [153]. Former interaction studies of aluminium with low molecular weight organic ligands [149-151] revealed the propensity of the metal to form complexes. According to the literature [152], the Al_{13} polycation did not form any complexes with lactic acid when ^{27}Al solution nuclear magnetic resonance (^{27}Al NMR) spectra of the samples were recorded shortly after the compounds were mixed together. Another study [148] has demonstrated the ability of the acid to form complexes with an initial aluminium chloride acidified solution. However, the protonation state of lactic acid was not assessed throughout the study.

Due to the lack of available data covering potentiometric, spectrophotometric, nuclear magnetic resonance spectroscopic methods and physical analysis on the interacting properties of pure aluminium hydrolytic species, aluminium monomers ($AlCl_3$), $AlO_4Al_{12}(OH)_{24}(H_2O)_{12}^{7+}$ and $Al_{30}O_8(OH)_{56}(H_2O)_{24}^{18+}$ polyoxocations (referred to as Al_{13}-mer and Al_{30}-mer for convenience) and aluminium hydroxide particles - with lactic acid, we decided to use lactic acid as an interacting ligand with the aluminium species above mentioned.

1.2.2.b. Structure and properties of lysozyme from the viewpoint of an interaction study

Lysozyme (also called Muramidase) is a basic bacteriolytic enzyme that was discovered by Fleming in 1922 [153]. It is found in mammalian urine, saliva, tears, milk, cervical mucus, leukocytes and kidneys [154].

Lysozyme, Figure (1.16), is a compact globular protein molecule with a molar mass of 14,700 Da [155]. It has a slightly ellipsoidal shape, and its dimensions are 4.50 x 3 x 3 nm [156, 157]. It is a compact protein of 129 amino acids which folds into a compact globular structure [158]. The 129 amino acid sub-units are cross-linked by four disulphide bridges [159]. There is a close cluster of basic groups (Arginine 45 and 68 in one region, Arginine 61 and 73 in a second and Arginine 5, 125 and 128 in a third) which form the highly positively charged surface regions of lysozyme, which give it a very high isoelectric point of 11.4 [160]. Beside, the majority of nonpolar (hydrophobic) groups are buried in the interior of the biomolecule [161]. The polypeptide chain forms five helical segments, a 3 stranded anti-parallel β-sheet that comprises one wall of the binding cleft. A deep cleft contains the active site which divides the molecule into two domains. These domains are linked by α-helix residues. One domain consists of residues that have β-sheet structure; the other domain has in its residues that are helical in nature [158].

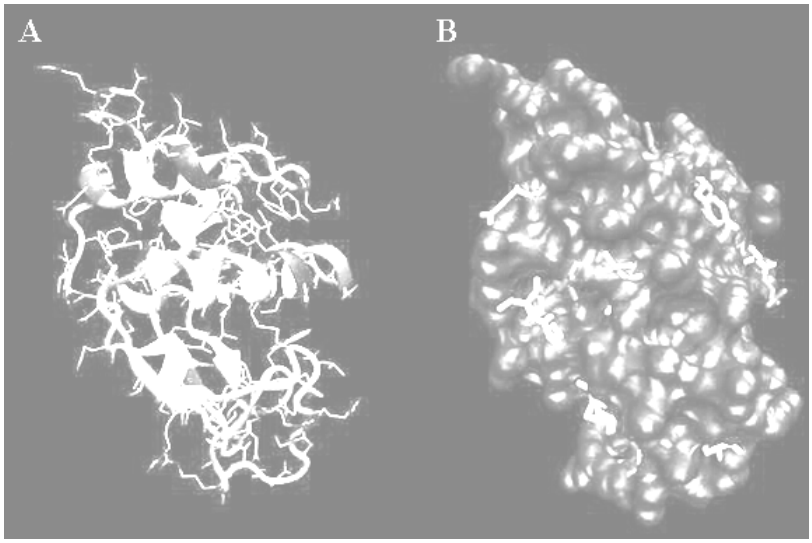

Figure 1.16. Structures of lysozyme obtained through modelling from RCSB protein data bank file 2HU1 showing the secondary structural motifs (C) and the surface residues prone to the binding of aluminium ions (D). Representation from Visual Molecular Dynamics software (VMD) [162].

Although many studies have been performed lately on the interaction between lysozyme and ligands [163-167], little is known about the secondary structure of the protein in the presence of aluminium species. The protein was selected for our studies as a widely available and cheap basic biomolecule.

1.2.2.c. Structure and properties of mucin from the viewpoint of an interaction study

Mucin is the last biomolecule selected for the interaction studies. This nitrogenous substance secreted by a mucous gland was chosen as a model ligand because of its availability, and its faculty to establish electrostatically-driven bonds with its aminoacids R-groups [168, 169]. Mucin is a block copolymer with branched and un-branched blocks [170]. Both blocks contain protein backbone chains and the branched blocks contain many highly branched oligosaccharide chains. The oligosaccharide side chains have sugar residues such as galactose, fucose, N-acetylglucosamine, N-acetylgalactosamine and sialic acid [171]. At pH > 3, both sialic acid and sulfated sugars are fully ionized and this confers a net negative charge to the molecule. Chemically, the structure of mucin has many hydrogen bond forming groups such as hydroxyl, carboxyl and amide groups. This, also, may allow the interaction between biological mucus and aluminium species. The primary alcohol of serine and threonine as well as the thiol (-SH) of cysteine allow these amino acids to act as nucleophiles during complexation reactions [172]. The protein will bear some negative charge in the present work [173], since its isoelectric point is comprised between 4.79 and 6.24.

In the presence of metal ions, mucin becomes thicker due to a change in hydration brought about by metal-induced conformational changes in the mucin macromolecule [174-181]. The association of aluminium species with mucus in the gastrointestinal tract of man has been documented [182]. Such interactions are likely to be involved in both the transport and excretion of the metal. However, the bioinorganic chemistry underlying these processes is unresolved and the interactions with aluminium polycations and aluminium hydroxides remain undefined.

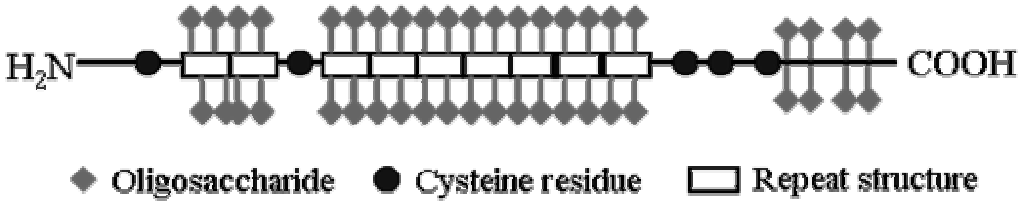

Figure 1.17. Generic structure of a mucin monomer.

The purpose of this contribution is to understand the mechanisms responsible for the formation of aluminium–mucin complexes and to observe whether the speciation of aluminium is affected by the presence of mucin.

1.2.3. Impact of aluminium on natural systems

Aluminium is an abundant element in Earth's crust: it is believed to be contained in a percentage from 7.5 to 8.1 % [183, 184]. Aluminium is very rare in its free form; dissolved monomeric aluminium occurs as aquo aluminium as well as OH^-, F^-, SO_4^{2-} and organic complexes [185, 186]. Aluminium contributes greatly to the properties of soil, where it is present mainly as insoluble aluminium hydroxide.

Aluminium's availability increases rapidly with acidity which is why the implications of the metal on the *flora* have drawn attention [187]. One of the well-known adverse effects of aluminium is on plant life under 'acid rain' conditions [188]. Dissolved Al^{3+} ions are toxic to plants; these affect roots and decrease phosphate intake. Aluminium may accumulate in plants and cause health problems for animals that consume these plants.

An increasing number of studies have been devoted to the interactions occurring between aluminium species and humic substances [189-192]. The strong aluminium complexation to humic substances [189] is of particular concern with the increasing acidification of many natural water courses as a consequence of 'acid rain'. The increased acidity levels lead directly to increased levels of 'free' Al^{3+}, readily available for interaction with dissolved humic substances. Since humic substances consist of heterogeneous mixtures of transformed biomolecules, the binding of Al^{3+} to these molecules can effectively increase the bioavailability of the metal ion to biological systems. It is therefore important to circumvent the extent and the strength of aqueous aluminium complexation.
Aluminium affects also the aquatic life as the metal is mobilized from the edaphic to the aquatic environment during acidification [193-195]. Elevated levels of aluminium are of interest because aluminium may influence the cycling of important elements such as phosphorous, organic carbon, and trace metals [196]. The presence of aluminium may also have serious ramifications for biological communities, particularly fish, inhabiting acidified aquatic systems [197]. At alkaline pH values the predominant species appears to be $Al(OH)_4^-$, whereas below pH ~ 4 the trivalent aquo ion, $A1^{3+}$, dominates; in the critical pH range from 4 to 7**,** however, there unfortunately exists little agreement as to what species are important, even in synthetic solutions containing no added ligands. Both mononuclear hydroxo complexes ($A1OH^{2+}$, $A1(OH)_2^+$, $Al(OH)_3$) and polynuclear complexes ($Al_n(OH)_m^{(3n-m)+}$) have been suggested as dissolved species in such simple systems. An understanding of the aqueous speciation of aluminium is essential for an evaluation of the processes occurring after acidic rains.

Among their applications in aqueous systems, aluminium is found to be a valuable coagulant. Pre-hydrolyzed polyaluminium coagulants are the most widely used coagulants and receive extensive research [198 (a) to (d)]. Being able to distinguish the aluminium species present in solution is a topic of high importance since the efficiency of the coagulate properties of each species is different [199, 200].

During the last few years, an increasing number of studies have demonstrated the presence of polynuclear aluminium species in the environment [200] and the toxicity of such species has been clearly demonstrated in the case of plant growth [201, 202]. It is therefore necessary to study the interactions of polycationic aluminium species with biological ligands, to identify how conformation, stability and charge (and hence their biological function) can be affected by such species; and vice versa, what is the impact of biomolecules on aluminium speciation? Our research aims to understand how charge, morphology and the structure of aluminium aqueous species influence their interaction with other molecules such as proteins. This understanding could then be used to emulate biomimetic approaches to the preparation and improvement of aluminium based materials [203]. A better control and understanding of such materials could minimise risks of release or improper use of harmful forms of the metal. Examples of the undesirable effect of existing materials and substances used include the cases of vaccine adjuvants creating aluminium sensitisation [204], or alums used for water treatment that leave traces of monomeric and polymeric aluminium ions in drinking water [205].

On the basis of the existing knowledge, the following aims were set in the present study:
First, to describe the sol-gel transformations of different aluminium reference systems. The description of the steps of the conversion of aluminium ions into aluminium (oxy) hydroxides will increase the understanding of the borderline between 'true' solutions and colloidal phases.
Since there is no available method for the determination of the 'formal' hydrolysis ratio of aluminium-containing solutions, the next part of the study will thus be concentrated on the development and the optimisation of a potentiometric method. The new approach will facilitate the study of aluminium-containing solutions.
An array of analytical techniques will be applied to the analysis of aluminium-biomolecules interactions in order to detail, if they exist, the behaviour of the new bio-materials. In this final section, the morphological analysis of aluminium-biomolecule systems will also be investigated since the structural characterisation of aluminium-biomolecules - namely lactic acid, lysozyme and mucin - assemblies has not been critically conducted yet.

1.3. References

[1] G. Tracy, W. H. Welker, J. Biol. Chem., 1915, 22, 55.

[2] R. Flarend, T. Bin, D. Elmore, S. L. Hem, Food Chem. Toxicol., 2001, 39, 163.

[3] J. J. Fitzgerald, A. H. Rosenberg, Marcel Dekker, 1999; chapter 4 Chemistry of Aluminum Chlorohydrate and Activated Aluminum Chlorohydrates, pp. 83-137.

[4] J. J. Fripiat, Catal. Today, 1988, 2, 28.

[5] M. A. Vicente, J. F. Lambert, Phys. Chem. Chem. Phys., 1999, 1, 1633.

[6] M. L. Occelli, A. Bertrand, S. Gould, J. M. Dominguez, Microporous Mesoporous Mater., 2000, 34, 195.

[7] J. Duan, J. Gregory, Adv. Colloid Interface Sci., 2003, 100-102, 475.

[8] C. T. Driscoll, in G. Sposito (Ed.), The Environmental Chemistry of Aluminium, CRC Press, 1989, p. 241.

[9] R. W. Smith, Coord. Chem. Rev., 1996, 149, 81.

[10] M. Wang, M. Muhammed, Nanostruct. Mater., 1999, 11, 8, 1219.

[11] S. L. Wang, M. K. Wang, Y. M. Tzoua, Colloids Surf., A, 2003, 231, 143.

[12] J. M. Fraile, J. A. Mayoral, A. J. Royo, Tetrahedron, 1996, 52, 9853.

[13] J. B. Hannon, S. Kodambaka, F. M. Ross, R. M. Tromp, Nature, 2006, 440, 69.

[14] S. Goldberg, J. A. Davis, J. D. Hem, in G. Sposito (Ed.), The Environmental Chemistry of Aluminum, CRC Press, 1989, Chapter 7, p. 271.

[15] K. Wefers, G. M. Bell, Oxides and Hydroxides of Aluminum, Technical Paper No. 19, Alcoa Research Laboratories, 1972.

[16] C. J. Brinker, G. W. Scherer, in: Sol–Gel Science. The Physics and Chemistry of Sol–Gel Processing, Academic Press, San Diego, 1990, p. 21.

[17] S. L. Hem, J. L. White, in: Vaccine Design - The Subunit and Adjuvant Approach, Plenum Press, New York, 1995, p. 249.

[18] P. M. Huang, M. K. Wang, N. Kampf, D. G. Schulze, in: J. B. Dixon, D. G. Schulze (Eds.), Soil Mineralogy with Environmental Applications, Soil Science Society of America, Madison, WI, 2002, p. 261.

[19] G. L. Kerven, P. L. Larsen, F. P. Blamey, C. Soil Sci. Soc. Am. J., 1995, 59, 765.

[20] D. R. Parker, P. M. Bertsch, Environ. Sci. Technol., 1992, 26, 914.

[21] D. Hunter, D. S. Ross, Science, 1991, 251, 1056.

[22] G. Furrer, B. Trusch, C. Muller, Geochim. Cosmochim. Acta, 1992, 56, 3831.

[23] R. J. P. Williams, Coord. Chem. Rev., 1996, 141, 1 and articles within the volume.

[24] J. T. Kloprogge, J. Porous Mater., 1998, 5, 5.

[25] N. Yao, G. Xiong, Y. Zhang, M. He, W. Yang, Catal. Today, 2001, 68, 97.

[26] J. J. Fitzgerald, In Antiperspirants and Deodorants; Marcel Dekker: New York; 1988, p. 119.

[27] S. M. Bradley, R. A. Kydd, J. Catal., 1993, 142, 448.

[28] J.-H. Son, H. Choi, Y.-U. Kwon, O.H. Han, J. Non-Cryst. Solids, 2003, 318, 186.

[29] C. F. Baes, R. E. Mesmer, in: The Hydrolysis of Cations, pp. 112–122, John Wiley, New York (1976).

[30] C. K. Jørgensen, Adv. Chem. Phys., 1963, 5, 33.

[31] A. Bell, E. Matijevic, J. Inorg. Nucl. Chem., 1975, 37, 907.

[32] E. Matijevic, Ann. Rev. Mater. Sci., 1985, 15, 483.

[33] R. E. Mesmer, C. F. Baes, Inorg. Chem., 1971, 10, 2290.

[34] J. J. Depuech, in NMR of Newly Accessible Nuclei, ed. P. Laszlo, vol. 2, pp. 153–195, Academic Press, New York (1983).

[35] P. M. Bertsch, M. A. Anderson, Anal. Chem., 1989, 62, 535.

[36] G. Johansson, Acta Chem. Scand., 1960, 14, 771.

[37] C. L. Rollinson, Chemistry of the Coordination Compounds, Vol. 131, Am. Chem. Soc. Master. Ser., Bailar Ed., New York, 1956, p.448.

[38] J. Jolivet, Metal Oxide Chemistry and Synthesis. From Solution to Solid State, Wiley and Sons, 2000.

[39] J. P. Jolivet, De La Solution A l'Oxyde, InterEditions-CNRS, Paris, 1994.

[40] M. Henry, J. P. Jolivet, J. Livage, Struct. Bond., 1992, 77, 153.

[41] S. Bi, C. Wang, Q. Cao, C. Zhang, Coord. Chem. Rev., 2004, 248, 441.

[42] K. Shafran, Chemical and structural studies of aluminium and zirconium aqueous chemistry Ph.D. thesis, Nottingham Trent University, 2003.

[43] W. H. Casey, B. L. Phillips, G. Furrer, Chapter Aqueous Aluminum Polynuclear Complexes and Nanoclusters: A Review, 2002, pp. 166-190.

[44] W. H. Casey, Chem. Rev. C, 2006, 106, 1.

[45] Jorgensen, L. Salem, in: The Organic Chemist's Book of Orbitals, Academic Press, 1973.

[46] J. Kragten, Atlas of Metal Ligand Equilibrium in Aqueous Solution, J. Wiley & Sons, Chichester, 1978.

[47] C. Brosset, Acta Chem. Scand., 1952, 6, 910.

[48] C. Brosset, G. Biedermann, L. Sillen, Acta Chem. Scand., 1954, 8, 1917.

[49] P. Hsu, C. Rich, Soil Science Society of America Proceedings, 1960, 24, 21.

[50] P. Hsu, T. Bates, Mineralogy Magazine, 1964, 33, 749.

[51] R. Stol, A. Van Helden, P. Bruyn, J. Colloid Interface Sci., 1976, 57, 115.

[52] R. Letterman, S. Asolekar, Water Res., 1990, 24, 931.

[53] P. M. Bertsch, in: G. Sposito (Ed.), The Environmental Chemistry of Aluminum, CRC Press, Boca Raton, 1989, pp. 117.

[54] P. H. Hsu, in: J.B. Dixon, S.B. Weeds (Eds.), Minerals in Soil Environment, Soil Science Society of America, Madison, WI, 1989, p. 331.

[55] G. Johansson, Acta Chem. Scand., 1962, 16, 403.

[56] G. Johansson, Ark. Kemi., 1963, 20, 321.

[57] J. W. Akitt, N. N. Greenwood, B. L. Khandelwal, G. D. Lester, J. Chem. Soc. Dalton Trans., 1972, 604.

[58] J. Y. Bottero, M. Axelos, D. Tchoubar, J. M. Cases, J. J. Fripiat, F. Fiessinger, J. Colloid Interface Sci., 1987, 117, 47.

[59] (a) J. Y. Bottero, J. M. Cases, F. Fiessinger, J. E. Poirier, J. Phys. Chem., 1980, 84, 2933. (b) M. Muñoz, C. I. Cabello, I. L. Botto, G. Minelli, M.Capron, C. Lamonier, E. Payen, J. Mol. Struct., 2007, 841, 96.

[60] J. W. Akitt, A. Farthing, J. Chem. Soc., Dalton Trans., 1981, 1606.

[61] L. Allouche, C. Gérardin, T. Loiseau, G. Férey, F. Taulelle, Angew. Chem. Int. Ed., 2000, 39, 511.

[62] J. A. Tosell, Geochim. Cosmochim. Acta, 2001, 65, 2549.

[63] W. V. Rausch, H. D. Bale, J. Chem. Phys., 1964, 40, 3391.

[64] H. Stünzi, L. Spiccia, F. P. Rotzinger, W. Marty, Inorg. Chem., 1989, 28, 66.

[65] L.-O. Ohman, W. Forsling, Acta Chem. Scand. A, 1981, 35, 795.

[66] T. Hedlund, S. Sjoberg, L.-O. Ohman, Acta Chem. Scand., 1987, 41, 197.

[67] J. W. Akitt, Prog. Nucl. Magn. Reson. Spectrosc., 1989, 21, 1.

[68] A. Hulanicki, R. Lewandowaki, A. Lewenstam, M. Chmurska, H. Matuszak, Mikrochim. Acta, 1985, 3, 253.

[69] N. Zhou, Y. Gu, Z. Lu, W. Chen, Talanta, 1985, 32, 1119.

[70] H. T. Evans, Inorg. Chem., 1966, 5, 967.

[71] J. W. Akitt, A. Farthing, J. Chem. Soc. Dalton, 1981, 1617.

[72] J.Y. Bottero, D. Tchoubar, J. M. Cases, F. Fiessinger, J. Phys. Chem., 1982, 86, 3667.

[73] W. V. Rausch, H. D. Bale, J. Chem. Phys., 1964, 40, 3391.

[74] D. W. Schaefer, R. A. Shellman, K. D. Keefer, J. E. Martin, Physica, 1986, 104A, 105.

[75] A. V. Plyasunov, I. Grenthe, Geochim. Cosmochim. Acta, 1994, 58, 3561.

[76] J. Rowsell, L.F. Nazar, J. Am. Chem. Soc., 2000, 122 (15), 3777.

[78] G. Johansson, G. Lundgren, L. G. Sillén, R. Söderquist, Acta Chem. Scand., 1960, 14, 769.

[77] L. Allouche, F. Taulelle, Inorg. Chem. Commun., 2003, 6, 1167.

[79] L. Allouche, C. Huguenard, F. Taulelle, J. Phys. Chem. Solids, 2001, 62, 525.

[80] S. M. Bradley, R. A. Kydd, R. F. Howe, J. Colloid Interface Sci., 1993, 159, 405.

[81] K. Wafers, C. Misra, Oxides and Hydroxides of Aluminium, Alcoa Technical Paper 19, revised 1987, Alcoa Technical Center, Alcoa, PA.

[82] P. H. Hsu, T. F. Bates, Miner. Mag., 1964, 33, 749.

[83] A. E. Nielsen, Kinetics of Precipitation, Pergamon Press, Oxford, 1964.

[84] V. K. La Mer, R. H. Dinegar, J. Am. Chem. Soc., 1950, 72, 4847.

[85] T. Sugimoto, Adv. Colloid Interface Sci., 1987, 28, 65.

[86] M. Haruta, B. Delmon, J. Chim. Phys., 1986, 83, 859.

[87] S. M. Bradley, R. A. Kydd, Catalysis Letters, 1991, 8, 185-192.

[88] E. Montarges, A. Moreau, L. J. Michot, Appl. Clay Sci., 1998, 13, 165.

[89] J. Gregory, J. Duan, Pure Appl. Chem., 2001, 73, 2017.

[90] C. C. Perry, K. L. Shafran, Journal Inorg. Biochem., 2001, 87, 115.

[91] K. L. Shafran, C. C. Perry, J. Chem. Soc., Dalton Trans., 2005, 2098.

[92] G. Berthon, Coord. Chem. Rev., 1996, 149, 241.

[93] W. R. Harris, G. Berthon, J. P. Day, C. Exley, T. Peder Flaten, W. F. Forbes, T. Kiss, C. Orvig, P. F. Zatta, J. Toxicol. Environ. Health, 1996, 48, 543.

[94] K. Rezwan, L. P. Meier, M. Rezwan, J. Voros, M. Textor, L. J. Gauckler, Langmuir, 2004, 20, 10055.

[95] A. J. Downs, in: Chemistry of Aluminium, Gallium, Indium, and Thallium, 1993, Springer.

[97] G. Van Landeghem, M. E. De Broe,P. C. D'Haese1, Clin. Biochem., 1998, 31, 385.

[98] B. Corain, G. G. Bombi, A. Tapparo, M. Perazzolo, P. Zatta, Coord. Chem. Rev., 1996, 149, 11.

[99] E. De Voto, R. A. Yokel, Environ. Health Perspect., 1994, 102, 940.

[100] M. Venturini, G. Berthon, J. Chem. Soc. Dalton Trans., 1987, 1, 145.

[101] S.-P. Bi, X.-D. Yang, F.-P. Zhang, X.-L. Wang, G.-W. Zou, Fresenius J. Anal. Chem., 2001, 370, 984.

[103] R. J. P. Williams, Coord. Chem. Rev., 2002, 228, 93.

[104] R. A. Yokel, Coord. Chem. Rev., 2002, 228, 97.

[105] X. Yang, Q. Zhang, L. Li, R. Shen, J. Inorg. Biochem., 2007, 101, 1242.

[106] A. K. Powell, S. L. Heath, Coord. Chem. Rev., 1996, 149, 59.

[107] P. Rubini, A. Lakatos, D. Champmartin, T. Kiss, Coord. Chem. Rev., 2002, 228, 137.

[107] G. D. Fasman, Coord. Chem. Rev., 1996, 149, 125.

[109] C. Exley, J. Inorg. Biochem., 1999, 76, 133.

[110] Z. M. Shen, A. Perczel, M. Hollbi,I. Nagypd1, G. D. Fasman, Biochemistry, 1994, 33, 9627.

[111] D. Drago, M. Bettella, S. Bolognin, L. Cendron, J. Scancar, R. Milaci, F. Ricchelli, A. Casini,

[112] M. Farina, F. S. Lara, R. Branda, R. Jacques, J. B. T. Rocha, Toxicol. Lett., 2002, 132, 131. L. Messori, G. Tognon, P. Zatta, Int. J. Biochem. Cell Biol., 2008, 40, 731.

[113] T. B. Drticke, Life Chem. Rep., 1994, 11, 231.

[114] T. B. Drueke, Nephrol. Dial. Transplant., 2002, 17(Suppl 2), 13.

[115] E. Bonucci, P. Ballanti, S. Berni, C. Della Rocca, Life Chem. Rep., 1994, 11, 225.

[116] P. Zatta, Trace Elem. Med., 1993, 10, 120.

[117] M. Suwalsky, B. Norris, T. Kiss, P. Zatta, Coord. Chem. Rev., 2002, 228, 285.

[118] T. Kiss, M. Kilyén, A. Lakatos, F. Evanics, T. Körtvélyesi, Gy. Dombi, Zs. Majer, M. Hollósi, Coord. Chem. Rev., 2002, 228, 227.

[119] A. Salifoglou, Coord. Chem. Rev., 2002, 228, 297.

[120] G. Lupidi, M. Angeletti, A. M. Eleuteri, E. Fioretti, S. Marini, M. Gioia, M. Coletta, Coord. Chem. Rev., 2002, 263.

[121] G. Berthon, Coord. Chem. Rev., 2002, 228, 319.

[122] M. R. Wills, J. Savory, Lancet, ii, 1983, 29.

[123] S. Daydé, M. Filella, G. Berthon, J. Inorg. Biochem., 1990, 38, 241.

[124] D. R. Crapper, S. S. Krishnan, A. J. Dalton, Science, 1973, 180, 511.

[125] D. P. Perl, A. R. Brody, Science, 1980, 208, 297.

[126] P. Zatta, Trace Elem. Med., 1993, 10, 120.

[127] G. D. Fasman, Coord. Chem. Rev., 1996, 149, 125.

[128] D. Drago, M. Bettella, S. Bolognin, L. Cendron, J. Scancar, R. Milacic, F. Ricchelli, A. Casini, L. Messori, G. Tognon, P. Zatta, Int. J. Biochem. Cell Biol., 2008, 40, 731.

[129] A. E. Martell, R. D. Hancock, R. M. Smith, R. J. Motekaitis, Coord. Chem. Rev., 1996, 149, 311.

[130] M. Deleers, J. Servais, E. Wulfert, Biochim. Biophys. Acta, 1986, 855, 271.

[131] M. Favarato, P. Zatta, M. Perazzolo, L. Fontana, M. Nicolini, Brain Res., 1995, 569, 330.

[132] P. Zambenedetti, F. Tisato, B. Corain, P. Zatta, Biometals, 1994, 7, 244.

[133] D. J. Jones, L. V. Kochian, FEBS Lett., 1997, 400, 51.

[134] P. Zatta, T. Kiss, M. Suwalsky, G. Berthon, Coord. Chem. Rev., 2002, 228, 271.

[135] Y. Shi, H. HogenEsch, F. E. Regnier, S. L. Hem, Vaccine, 2001, 19, 1747.

[136] L. S. Burrella, C. T. Johnstonb, D. Schulzeb, J. Kleinc, J. L. Whiteb, S. L. Hem, vaccine, 2001, 19, 275.

[137] S. J. Seeber, J. L. White, S. L. Hem, Vaccine, 1991, 9, 201.

[138] J. M. Heimlich, F. E. Regnier, J. L. White, S. L. Hem, Vaccine, 1999, 17, 2873.

[139] R. K. Gupta, B. Rost, E. Relyveld, G. R. Siber, in: M. Powell, M. Newman, editors. Vaccine design: The subunit and adjuvant approach. New York: Plenum, 1995. p. 229.

[140] M.-F. Chang, J. L. White, S. L. Nail, S. L. Hem, PDA J. Pharm. Sci. technol., 1997, 51, 25.

[141] E. Bergfors, B. Trollfors, A. Inerot, Vaccine, 2003, 22, 64.

[142] R. M. Garrels, F. T. Mackenzie, C. Hunt, Chemical Cycles and the Global Environment. W. Kaufmann Inc., Los Altos, CA, 1975.

[143] G. Favero, P. Jobstraibizer, Coord. Chem. Rev., 1996, 149, 367.

[144] C. J. Lind, J. D. Hem, Effects of organic solutes on chemical reactions of aluminum. U.S. Geol. Surv. Water Supply Paper, 1827-G, Washington, DC, 1975, p. 83.

[145] C. E. Roberson, J. D. Hem, Solubility of aluminum in the presence of hydroxide, fluoride, and sulfate. U. S. Geol. Surv. Water Supply Paper, 1827-C, Washington, DC, 1969, p. 37.

[146] R. W. Smith, Coord. Chem. Rev., 1996, 149, 81.

[147] B. C. Faust, W. B. Labiosa, K'O H. Dai, J. S. Macfall, B. A. Browne, A. A. Ribeiro, D. D. Richter, Geochim. Cosmochim. Acta, 1995, 59, 13, 2651.

[148] K. M. Elkins, D. J. Nelson, Coord. Chem. Rev., 2002, 228, 205.

[149] M. J. Pianna, K. O. Zahir, J. Environ. Sci. Health Part B, 2000, 35, 87.

[150] J. Luster, T. Lloyd, G. Sposito, in: N. Senesi, T. M. Miano (Eds.), Humic Substances in the Global Environment and Implications on Human Health, Elsevier Science, 1994, pp. 1019.

[151] K. M. Elkins, D. J. Nelson, J. Inorg. Biochem., 2001, 87, 81.

[152] N. M. Johnson, Science, 1979, 204, 497.

[153] W. Dickson, Verh. Internat Verein Limnol., 1978, 20, 851.

[154] C. S. Cronan, C. L. Schofield, Science, 1979, 204, 304.

[155] (a) C. T. Drisdoll, Environ. Health Perspect., 1985, 63, 93; (b) Y. Shi, H. HogenEsch, F. E. Regnier, S. L. Hem, Vaccine, 2001, 19, 1747; (c) J. Duan, J. Gregory, Adv. Colloid Interface Sci., 2003, 100, 475; (d) Z. Chen, B. Fan, X. Peng, Z. Zhang, J. Fan, Z. Luan, Chemosphere, 2006, 64, 912.

[156] J. Duan, J. Gregory, Adv. Colloid Interf. Sci., 2003, 100-102, 475.

[157] Z. Chen, B. Fan, X. Peng, Z. Zhang, J. Fan, Z. Luan, Chemosphere, 2006, 64, 912.

[158] J.-P. Boisvert, C. Jolicoeur, Colloids Surf., A Physicochemical and Engineering Aspects, 1999, 155, 161.

[159] G. Furrer, B. L. Phillips, K. Ulrich, R. Pöthig, W. H. Casey, Science, 2002, 297, 2245.

[160] D. R. Parker, T. B. Kinraide, L. W. Zelazny, Soil Science Society of America Journal, 1989, 53, 789.

[161] J. Comin, J. Barloy, G. Bourrie, F. Trolard, European Journal of Agronomy, 1999, 11, 115.

[162] O. Deschaume, K. L. Shafran, C. C. Perry, Langmuir, 2006, 22, 10078.

[163] E. Bergfors, B. Trollfors, A. Inerot, Journal of Allergy and Clinical Immunology, 2004, 113, S294.

[164] J. Berkowitz, M. A. Anderson, R. C. Graham, Water Res., 2005, 39, 3918.

[165] R. A. Yokel, P. Ackrill, E. Burgess, J. P. Day, J. L. Domingo, T. P. Flaten, J. Savory, J. Toxicol. Environ. Health, 1996, 48, 667.

[166] D. L. Jones, A. M. Prabowo, L. V. Kochian, Plant and Soil, 1996, 182, 2, 229.

[167] T. Yokoyama, H. Abe, T. Kurisaki, H. Wakita, Anal. Sciences, 1999, 15, 969.

[168] J. W. Akitt, B. E. Mann, J. Magn. Reson., 1981, 44, 584.

[169] J. W. Akitt, N. B. Milic, J. Chem. SOC.Dalton Trans., 1984, 981.

[170] S. J. Karlik, E. Tarien, G. A. Elgavish, G. L. Eichhorn, Inorg. Chem., 1983, 22, 525.

[171] P. O. Astrand, E. Hultman, A. Juhlin-Dannfelt, G. Reynolds, Journal of Applied Physiology, 1986, 61, 338.

[172] J. F .Ma, S. Hiradate, H. Matsumoto, Plant. Physiol., 1998, 117, 753.

[173] I. Sóvágó, in: Biocoordination Chemistry, ed. K. Burger, Ellis Horwood, NewYork, 1990, p. 135.

[174] R. S. Dickins, C. S. Love, H. Pushmann, Chem. Commun., 2001, 2308.

[175] E. Rakotonarivo, C. Tondre, J. Y. Bottero, J. Mallavialle, J. Water Research, 1989, 23, 137.

[176] K. Gajda-Schrantz, L. Nagy, T. Fiore, L. Pellerito, T. Gajda, J. Chem. Soc., Dalton Trans., 2002, 152.

[177] J. F .Ma, S. Hiradate, K. Nomoto, T. Iwashita, H. Matsumoto, Plant. Physiol., 1997, 113, 1033.

[178] J. F. Ma, S. J. Zheng, H. Matsumoto, S. Hiradate, Nature, 1997, 390, 569.

[179] A. Masion, F. Thomas, D. Tchoubar, J. Y. Bottero, P. Tekely, Langmuir, 1994, 10, 4353.

[180] A. Fleming, Proc. R. Soc. London (Biol), 1922, 93, 306.

[181] E. R. Berman, Biochemistry of the eye, ed. Blakemore C. New York: Plenum Press, 1991.

[182] T. Imoto, L. Johnson, A. North, D. Phillips, J. Rupley, in: Vertebrate Lysozymes. In: Boyer P. The Enzyme. New York: Academic Press, 1972; 665.

[183] W. G. Burton, K. D. Nugent, T. K. Slattery, B. R. Summers, L. R. Snyder, J. Chrom., 1988,

[184] A. A. Vertegel, R. W. Siegel, J. S. Dordick, Langmuir, 2004, 20, 6800, 443, 363.

[185] W. Humphrey, A. Dalke and K. Schulten, Journal of Molecular Graphics, 1996, 14, 33-38.

[186] E. F. Osserman, R. E. Canfield, S. Beychok, in: Lysozyme. New York: Academic Press, 1974.

[187] C. C. Blake, D. F. Koenig, G. A. Mair, A. C. North, D. C. Phillips, V. R. Sarma, Nature, 1965, 206, 757.

[188] J. V. Rinella Jr., J. L. White, S. L. Hem, J. Colloid Interface Sci., 1998, 205, 161.

[189] J. M. Teijón, M. D. Blanco, A. Rodríguez, J. A. Onrubia, I. Katime, Rev. Esp. Fisiol., 1987, 43, 81.

[190] C. Czeslik, R. Winter, Phys. Chem. Chem. Phys., 2001, 3, 235.

[191] V. Calandrini, G. Onori, A. Santucci, J. Mol. Struct., 2001, 565-566, 183.

[192] S.-Y. B. Hu, M. A. Arnold, Anal. Chem., 2000, 72, 696.

[193] T. Coradin, P. J. Lopez, C. Gautier, J. Livage, C. R. Palevol, 2004, 3, 443.

[194] S. K. Banerjee, J. A. Rupley, J. Biol. Chem., 1973, 248, 6, 2117.

[195] R. Bansil, E. Stanley, J. T. LaMont, Annu. Rev. Physiol., 1995, 57, 635.

[196] R. Bansil, B. S. Turner, Curr. Opin. Colloid Interface Sci., 2006, 11, 164.

[197] N. Thirawong, R. A. Kennedy, P. Sriamornsak, Carbohydr. Polym., 2008, 71, 170.

[198] T. A. Gerken, Critical Reviews in Oral Biology and Medicine, 1993, 4, 261.

[199] L. E. Bromberg, D. P. Barr, Biomacromolecules, 2000, 1, 325.

[200] R. L. Bertholf, M. R. Will, J. Savory, Biochem. Biophys. Res. Commun., 1984, 125, 1020.

[201] C. Exley, J. Inorg. Biochem., 1998, 70, 195.

[202] H. Y. Shrivastava, A. Dhathathreyan, B. U. Nair, Chem. Phys. Lett., 2003, 369, 534.

[203] H. Y. Shrivastava, B. U. Nair, J. Biomol. Struct. Dyn., 2003, 20, 4, 575.

[204] B. K. Varma, A. Demers, A. M. Jamieson, J. Blackwell, N. Jentoft, Biopolymers, 1990, 29, 441.

[205] J. J. Powell, C. C. Ainley, R. Evans, R. P. Thompson, Gut, 1994, 35, 1053.

Part 2

Material and Methods

2.1. Preparation of the aluminium - containing reference systems

A stock aqueous solution of aluminium chloride (~ 1.0 mol.L^{-1}) was prepared by dissolving a known amount of crystalline $AlCl_3 \cdot 6H_2O$ (Aldrich Gillingham, UK, 99 %) in distilled deionised water. Working solutions of $AlCl_3$ were prepared by dilution of the stock solution with deionised distilled water. The stock solution containing ~ 0.4 mol.L^{-1} $AlCl_3$ and acidified with ~ 0.4 mol.L^{-1} HCl, was prepared by dissolution of $AlCl_3 \cdot 6H_2O$ in distilled deionised water containing a pre-dispensed amount of 1.0 mol.L^{-1} HCl (Fisher, Loughborough, UK) in a volumetric flask of the required volume.

A model Al_{13}-mer solution was synthesised from the stock $AlCl_3$ solution by a soft hydrolysis technique - static anion exchange described elsewhere [1]. The hydrolysis ratio of an Al_{13}-mer solution was adjusted to h ~ 2.46, the molecular hydrolysis ratio of Al_{13}-mers [2]. For the preparation of a model Al_{30}-mer solution, an Al_{13}-mer solution prepared at room temperature (h ~ 2.40) was thermally aged in a water bath at 85^{o}C for 48 hours (h) as described in [1-3]. Aluminium hydroxide was prepared by adjusting the hydrolysis ratio of the stock solution of $AlCl_3$ to h ~ 2.8 using the anion exchange method [1] and by ageing the resulting solutions for 1, 6 or 8 months which led to mean particle sizes 26 ± 3 nm, 82 ± 8 nm and 100 ± 11 nm, as measured by dynamic light scattering at 90^o. The purity of solutions of Al species was verified by ^{27}Al solution NMR. The percentage of target species was found to be for Al_{13}-mer - 98.17 % of the total aluminium concentration, for Al_{30}-mer - 95.23 %; for Al hydroxide - 96.95 %. The final aluminium concentration in model solutions of the Al_{13}-mer, the Al_{30}-mer, Al hydroxide, $AlCl_3$ and $AlCl_3$ + 0.25 mol.L^{-1} HCl was close to 0.4 mol.L^{-1} as determined by means of a colorimetric method using the Ferron reagent [4]. Prior to measuring aluminium concentration the samples of 'reference' solutions were subjected to acid digestion with 1 mol.L^{-1} HCl in order to break down any polynuclear aluminium species or aluminium hydroxide present.

The formal hydrolysis ratio of commercial aluminium chlorohydrate material (ACH Microdry, Reheis, Berkeley Heights, NJ, USA) was also measured as a practical example. Approximate formula of ACH which represents basic aluminium chloride salt is $Al_2(OH)_xCl_{6-x} \times yH_2O$ (where x ~ 5 according to the

manufacturer's data and $y \sim 0.14$). An aqueous solution of this sample was prepared by dissolving 1.052 g of the fine powder in 10 mL of double distilled water to give a solution with total Al concentration of 0.8 $mol.L^{-1}$ as determined by a colorimetric method with Ferron (atomic absorption could have been used).

2.2. Preparation of biomolecules solutions

Preparation of gelation agent (GA) solution samples for gelation studies

A broad range of compounds are employed in colloidal chemistry as 'destabilising agents' (also called 'gelation agents - GAs), including inorganic salts and large organic polymers. The GAs were divided into four broad groups listed in Table (2.1), according to their mechanism of destabilization of aluminium species.

Table 2.1. The four classes of destabilising agents used throughout the experiments.

pH-independent GAs, $mol.L^{-1}$	KCl ≥ 99 %, Sigma-Aldrich
	K_2SO_4 ≥ 99 %, Sigma-Aldrich
	K_3PO_4 97 %, Aldrich
	CH_3COONa, Sigma-Aldrich
	Na_2SiO_3, Aldrich
pH-dependent GAs, $mol.L^{-1}$	$KHCO_3$ ≥ 99.5 %,, Sigma-Aldrich
	NH_3 5 M, Aldrich
	$NaAlO_2$, Riedel-de Haën (Seelze, Germany)
	$(C_2H_5)_3N$ ≥ 99 %, Sigma-Aldrich
Hybrid GA, $mol.L^{-1}$	$K_2Si(cat)_3$
Polymeric GAs, $mol.L^{-1}$	Cellulose acetate, Aldrich
	$H(OCH_2CH_2)_nOH$, Fluka (Milan, Italy)
	Poly(acrylic acid), Aldrich

The ammonia, the triethylamine and the poly(ethylene glycol) reagents were provided in the liquid form by the companies and used as supplied. The rest of the reagents used in this study were prepared by dissolution of the commercial product in double distilled water. The concentrations of the stock solution of the reagents were approximately 1 $mol.L^{-1}$ except for KCl which was prepared at 2 $mol.L^{-1}$. The $K_2Si(cat)_3$ complex was prepared according to Evans et al. [5].

Preparation of titrant solutions

Stock solutions of the five alkalis used in this study were prepared at concentrations of approx. 0.1 $mol.L^{-1}$. A stock solution of ammonia was prepared from 5 $mol.L^{-1}$ ammonia solution (Aldrich). A volumetric standard solution of 1 $mol.L^{-1}$ potassium hydroxide (Fisher) was used as the stock solution of KOH and it was sonicated prior to experiments in order to eliminate dissolved carbon dioxide. Stock solutions of the other three alkalis were prepared by dissolution of the corresponding crystalline solids (Trizma-base (Aldrich, 99.90 %), Na_2CO_3 (Aldrich, 99.995 %) and $NaHCO_3$ (Aldrich, 99.50 %)) into deionised distilled water in a volumetric flask of the required volume. Stock solutions of all five alkalis were standardised using automated potentiometric titration with a volumetric standard solution of hydrochloric acid (HCl, 1.001 ± 0.001 $mol.L^{-1}$, Fisher Scientific).

Preparation of aluminium-ion solution samples for titration

Pre-defined aliquots (0.2, 0.6 or 2 mL required to prepare solutions at a final Al concentration of respectively 0.004, 0.012 and 0.04 $mol.L^{-1}$) of the Al-containing solutions were diluted with deionised water (to make up to 20 mL of the sample solution in total) and titrated immediately with one of the five pre-standardised titrants containing 0.1 $mol.L^{-1}$ of base.

Preparation of the biomolecule solution samples for interaction studies

L-(+)-Lactic acid, ≥ 99.0 % (ex. Fluka), chicken egg white lysozyme (powder, ~ 70000 $units.mg^{-1}$ from Sigma), BSA 96 % (Sigma) and mucin (from porcine stomach Type III, bound sialic acid 0.5 - 1.5 %, partially purified powder from Sigma) were used as received. Aqueous solutions of the biomolecules (50 $mg.mL^{-1}$) were prepared immediately before use by dissolving the biomolecules in distilled deionized water.

Preparation of aluminium - biomolecule solution samples

A series of model aluminium-biomolecule solutions were prepared at room temperature by the addition of different amounts of fresh biomolecule stock solution to each of the model aluminium-containing systems. All solutions were vigorously stirred during and after mixing of aluminium-containing and biomolecule solutions (for 60 seconds (s)) using a vortex stirrer and left ageing at room temperature (25 ± 0.2 °C) for 24 h. The time of ageing was chosen on the basis of preliminary kinetic experiments which showed that most of the parameters of the aluminium-biomolecule mixtures (e.g. pH, viscosity and particle size) had stabilized after 24 h of monitoring. When the experiments were performed at constant aluminium concentration, the final aluminium concentration in the aluminium-biomolecule solutions was 0.15 $mol.L^{-1}$, and the biomolecule concentration was varied from 0 to 25 $mg.mL^{-1}$ in steps of 2.5 $mg.mL^{-1}$. For the infrared spectroscopic experiments, the measurements were performed at constant lysozyme or BSA concentration, the final protein concentration in the aluminium-protein solutions was 25 $mg.mL^{-1}$, and the aluminium concentration was varied from 0 to 0.15 $mol.L^{-1}$ in steps of 0.015 $mol.L^{-1}$.

2.3. Solution characterisation techniques

2.3.1. Potentiometry

To a large extent, the potentiometric analysis of a solution consists in determining its acidity / alkalinity. Afterwards, the pH value can be used to calculate the hydrolysis ratio of an Al-containing sample which can then be used to reveal the Al speciation of that sample [6, 7].

2.3.1.a. Principles

pH

pH is the measurement of the activity of hydrogen ions or their equivalent in solution. The pH scale is an inverse logarithmic representation of hydrogen proton (H+) concentration. As a simple definition, pH is the measurement of the hydrogen ion concentration, $[H^+]$ of a solution and is defined as the negative logarithm of the hydrogen ion concentration [8] and was introduced in 1909 by the Danish biochemist, Soren Peter Lauritz Sørensen.

$$pH = -\log[H^+] \qquad \textbf{Equation 2.1a}$$

The pH value is an expression of the ratio of $[H^+]$ to $[OH^-]$ (hydroxide ion concentration). Since the concentration of hydrogen ions and hydroxide ions are constant in a stable solution ($[H^+][OH^-] = 10^{-14}$ at temperature constant), either one can be quantified if the value of the other is known. Therefore, when determining the pH of a solution, the hydroxide ion concentration can be calculated.

While pH measurements are realised, the variation of temperature in the sample has to be considered as one of the external influences on pH measurements. Temperature affects the pH measurement in two ways. The first is a change in pH due to changes in dissociation constants of the ions in the solution being measured. This implies that as solution temperature changes, the pH value also changes. Presently available instrumentation cannot account for this change because the dissociation constants vary from solution to solution. The second reason temperature affects the pH measurement, is glass electrode resistance. Since the glass measuring electrode is an ionic conductor, it stands to reason that the resistance of the glass will change as the solution temperature changes. As temperature rises, resistance across the glass bulb decreases. This change in resistance versus temperature is constant and can be calculated depending on the specific type of glass formulation of the electrode. The pH electrode used was a combined one equipped with a temperature sensor. That characteristic of the electrode enabled one to circumvent any temperature variation during pH measurements. All the pH measurements were realised at constant temperature, 25^oC.

The combination pH electrode was used to determine the pH, it consists of a reference electrode and a measuring one joined in a single glass body assembly. The combination electrode is constructed with two types of glass. The stem of the electrode is a non-destructive glass. The tip is a specially formulated “pH sensitive” lithium ion-conductive glass consisting of the oxides of silica, lithium, calcium and other elements. The structure of the pH glass allows lithium ion electrons to be exchanged

by hydrogen ions in aqueous solutions, forming a hydrated layer. A millivolt potential is created across the interface between the pH glass and the external aqueous solution [9]. The magnitude of this potential is dependent on the pH value of the solution. Since the internal solution of the glass electrode is buffered, its pH value is kept constant, making the measured potential difference dependent only upon the pH value of the external solution being measured.

Since the hydrogen ion concentration reveals the pH of the solution studied, one can determine that concentration by firstly calculating the electric potential of the cell membrane interface between the pH combination electrode and the solution studied, with the Nernst equation (Equation (2.1)).

$$E = E_o - (RT / nF) \ln [H^+] \qquad \textbf{Equation 2.1b}$$

where E represents the Nernst potential of half-cell (V);

E_0 is the standard Nernst potential (V);

R is the universal gas constant ($J.mol^{-1}.K^{-1}$);

T is the temperature (K);

n is the number of electrons transferred in the half-reaction;

F is the Faraday constant.

pH electrodes were utilized during potentiometric titration procedures. The potentiometric titration approach was undertaken to study the speciation of aqueous aluminium solution. That analysis enabled the determination of the amount of a substance (the analyte which is the studied species) reacting with a measured volume of a solution of precisely known concentration (the titrant).

Hydrolysis ratio

Solutions of aluminium ions partially neutralised with alkali in the presence of non-complexing anions (*e.g.*, chloride) give rise to a number of identifiable soluble aluminium polynuclear hydrolytic species as well as various forms of aluminium hydroxide. Each of these species has a specific ratio of hydroxo- (oxo-) ligands to the number of aluminium atoms in the structural formula which can be called a 'molecular hydrolysis ratio' *h'*:

$$h' = \frac{n(OH^-) \cdot 2n(O^{2-})}{n(Al)} \qquad \textbf{Equation 2.2}$$

where $n(OH^-)$ and $n(O^{2-})$ is the number of hydroxo- and oxo-ligands respectively, and n(Al) is the number of Al atoms per species.

The overall hydrolysis ratio *H* is a combination of all 'molecular' hydrolysis ratios h'_n of the *n* aluminium species present in aqueous solutions at concentrations α_n:

$$H = \frac{\sum_n \alpha_n h'_n}{C(Al)_{total}} \qquad \textbf{Equation 2.}$$

where the total concentration of aluminium-ions ($C(Al)_{total}$) is defined as:

$$C(Al)_{total} = \sum \alpha_n \qquad \textbf{Equation 2.4}$$

The 'formal' hydrolysis ratio *h* can be defined as the ratio of added hydroxyl-ion concentration ($C(OH^-)_{added}$) and the total concentration of aluminium ions in the system ($C(Al)_{total}$).

$$h = \frac{C(OH^-)_{added}}{C(Al)_{total}} \qquad \textbf{Equation 2.5}$$

Under ideal experimental conditions (i.e. ideal mixing of reagents and in the absence of interfering species, etc.) the formal hydrolysis ratio *h* defined by Equation (2.5) should match the 'overall' or 'average molecular' hydrolysis ratio *H* from Equation (2.3) (*i.e.*, $h = H$). Therefore, one can use the 'formal' hydrolysis ratio *h* of hydrolysed Al-ions as an integral parameter reflecting the 'basicity' of aluminium species (*e.g.* 'degree of neutralisation' or similar parameter) or the overall 'acidity' of the system (i.e. the amount of base required to neutralise it).

Also, the condition $h = H$ discussed above provides a link between an experimentally determined formal hydrolysis ratio (*h*) and the overall hydrolysis ratio (*H*), the value of which is a function of the complete speciation of hydrolysed Al-ions in solution (Equation (2.3)). Therefore, by measuring the 'formal' hydrolysis ratio *h* one can estimate the 'average molecular' hydrolysis ratio *H* of all aluminium species present in solution, and *vice versa*.

The approach used to determine the formal hydrolysis ratio *h* of hydrolysed aluminium-ion solutions was the automatic potentiometric titration with alkali. Our approach is based on the fact that at conditions close to ideal (i.e. local pH gradients and premature aluminium hydroxide formation are minimised), the major inflexion on the pH-titration curve of aluminium-ion solution with base observed at pH around 6.9 - 7.0 corresponds to the complete precipitation of aluminium hydroxide with exact stoichiometry $n(OH) / n(Al) = 3.0$. ($K_S = 1.4.10^{-34}$). One can use this well-defined inflexion on the titration curve as a reference point and calculate the formal hydrolysis ratio *h* of an aluminium-ion solution as follows:

$$h = 3.0 - \Delta h \qquad \textbf{Equation 2.6}$$

where $\Delta h = C(OH)_{added} / C(Al)_{total}$

2.3.1.b. Apparatus for the pH analysis

The measurement of pH of aqueous solution was made using a PHM-250 pH-meter with a Red Rod glass electrode and a temperature sensor (Radiometer Analytical, Villeurbanne, France). The pH probe was calibrated using four IUPAC buffers (pH 1.689, 4.005, 7.001 and 10.008) from Radiometer. The absolute error of pH measurements was ± 0.002 pH units.

2.3.1.c. Automatic potentiometric titration setup

Potentiometric titrations were conducted using a Radiometer autotitrator TitraLab 865 (Radiometer Analytical) with TitraMaster 85 PC software. The autotitrator was equipped with a Red Rod combined glass electrode and PT100 temperature sensor. The average temperature of all measurements was 25 ± 1 °C. Four-point calibration of the pH-meter was carried out every 24 h using a set of standard pH buffer solutions (pH = 1.68 ± 0.03 *ex.* Fluka, 3.98 ± 0.02, 7.01 ± 0.02 and 10.01 ± 0.02, all *ex.* Fisher Scientific). Automated potentiometric titrations were performed in dynamic incremental mode [10] using measurement of pH as an analytical response. In order to combine good quality of titration data and minimise the time required for titration the following titration parameters were pre-optimised: maximum dose 0.06 mL, 'dynamic dose' reflecting sensitivity of the autotitrator to the change of slope of a titration curve was set to "4" (medium level). Additions of titrant were made after fluctuations of pH response reached the level of less than 0.1 $mV.s^{-1}$. The volume of the aluminium-containing sample was 20 mL and the volume of titrant added varied between 2 and 6 mL depending on the aluminium species present in the sample solution and total aluminium concentration. The described parameters of the automated titrations enabled up to 90 points on the titration curve to be achieved within a sensible titration time (in most cases less than 1 h) which led to satisfactory resolution between major titration inflexions. All titration measurements were performed in triplicate.

2.3.1.d. General pH measurements

The pH measurements were realised either on fresh samples or, for the samples containing a biomolecule, after an ageing time of 24 h at room temperature (25 ± 2 °C) in order to leave enough time for the pH to stabilize itself.

The potentiometric titrations were achieved with one of the five pre-standardised titrants listed below. Stock solutions of the five alkalis were prepared at concentrations of approx. 0.1 and 1 $mol.L^{-1}$. A stock solution of ammonia was prepared from 5 $mol.l^{-1}$ ammonia solution (Aldrich).Volumetric standard solutions of 1 $mol.L^{-1}$ potassium hydroxide (Fisher Scientific) was used as the stock solution of KOH and it was sonicated prior to experiments in order to eliminate dissolved carbon dioxide. Stock solutions of the other three alkalis were prepared by dissolution of the corresponding crystalline solids (Trizma-base (Aldrich, 99.90 %), Na_2CO_3 (Aldrich, 99.995 %) and $NaHCO_3$ (Aldrich, 99.50 %)) into deionised distilled water in a volumetric flask of the required volume. Stock solutions of all five alkalis were standardised using an automated potentiometric titration with volumetric standard solutions of hydrochloric acid (HCl, 1.001 ± 0.001 $mol.L^{-1}$, Fisher Scientific.). Pre-defined aliquots (0.2, 0.6 or 2 mL required to prepare solutions at a final Al concentration of respectively 0.004, 0.012 and 0.04 $mol.L^{-1}$) of the Al-containing solutions were diluted with deionised water (to make up to 20 mL of the sample solution in total) and titrated immediately after dilution with one of the five pre-standardised titrants.

Titrations of the four biomolecules employed through out the study were accomplished on 2.5, 20 or 25 $mg.mL^{-1}$ samples by using one of the above-mentioned titrants.

2.3.2. Conductimetry

The presence of ionised species in solution is mainly monitored by its conductivity. A good conductor such as a metal will have a high conductivity showing its ability to carry electric current.

2.3.2.a. Principle and apparatus

Placed across a conductor, the movable charges (called electrolytes) of an electrical potential difference flow and give rise to an electric current. Positively charged particles will migrate toward the negative electrode (cathode) whereas negatively charged particles will migrate toward the positive electrode (anode). The migration of particles is the electric current flow. The conductivity σ is defined as the ratio of the current density J to the electric field strength E:

$$J = \sigma E \qquad (S.m^{-1}) \qquad \textbf{Equation 2.7}$$

The conductivity measurement is directly affected by the number of dissolved ions in solution and will increase as the quantity and mobility of ions increases.
Conductivity was measured using a CDM230 conductivity meter (Radiometer Analytical). The conductivity cell consists of two parallel platinum plates at a defined distance. It is confined within a glass jacket with two pipe connectors enabling measurement in flow mode. This cell is calibrated using a conductivity standard of NaCl (1015 $\mu S.cm^{1}$ at 25 °C, Radiometer Analytical). An absolute error of the conductivity measurements was ± 0.5 % of reading.

2.3.2.b. Measurements

The conductivity of the samples was measured with the apparatus described above in automatic or manual mode. Measurements on samples containing a biomolecule were performed after sample ageing after 24 hours at room temperature (25 ± 2 °C) in order to leave enough time for the conductivity to stabilize.

2.3.3. Viscosimetry

Measuring viscosity is an effective method of determining the fluidity of a liquid. Almost all liquids are viscous fluid having viscidity. Viscous fluids are further divided broadly into two categories; Newtonian fluids (flows like water, its stress/rate of strain curve is linear and passes through the origin) that is subject to Newton's law of viscosity, and non-Newtonian fluids (the viscosity changes with the applied strain rate; then no well-defined viscosity) that is not subject to Newton's law of viscosity. The viscosity of aluminium depends on its purity, by extension, on its speciation [10]. Due to the modification of the aluminium speciation in our samples, the samples studied through out the thesis were non-Newtonian fluids.

Viscosity is the substance constant indicating the magnitude of the "fluidity" of a fluid.

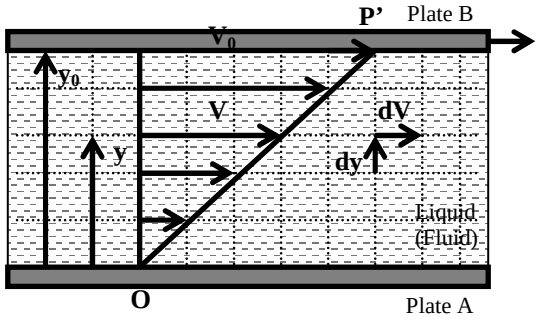

Figure 2.1. Couette flow (Newtonian fluid).

As shown on Figure (2.1), the two plates, plate A and plate B, are placed parallel to each other and filled with a liquid (fluid). The distance between plate A and plate B is y_0. Where plate A is fixed and plate B is being moved parallel to plate A at a constant speed of V_o, if the fluid between plate A and plate B is also in motion parallel to plate A and has produced a steady flow, this is called the Couette flow. Where the velocity at a given distance y between plate A and plate B is V, they are in proportion as shown in Figure x. Where the slope of the straight line connecting O and P' is D,

$$D = V / y \qquad \textbf{Equation 2.8}$$

Since it equals the increased quantity of the velocity per unit distance, i.e. the velocity gradient,

$$D = dV / dy \qquad \textbf{Equation 2.9}$$

D is called a shear rate.

In Figure (2.1), the liquid layers at distance y and at distance y + dy flow parallel to each other at speed V and at speed V + dV respectively. Because of the difference in their velocities, an internal frictional force will develop between them. The frictional force applied to the unit area of the plane parallel to the flow direction between plate A and plate B is called a tangential as shear stress.

τ stands for a tangential stress and is proportional to shear stress D. η is the proportional constant,

$$\tau = \eta D \quad \text{(Newton's law of viscosity)} \qquad \textbf{Equation 2.10}$$

Equation (2.10) represents Newton's law of viscosity where the proportional constant η is called the viscosity coefficient.

$$\eta = \tau / D \qquad \textbf{Equation 2.11}$$

The fluid subject to this law, whose viscosity η at specific temperature is constant in spite of a shear rate D or shear stress τ, is called a Newtonian fluid. If the shear rate D and shear stress τ are not proportionate, i.e. if viscosity η of the fluid is variable with the quantities of shear rate D or shear stress τ, it is called a non-Newtonian fluid. A liquid such as water, alcohol, etc. which is composed of a single substance (molecule) is a Newtonian fluid. On the other hand, a polymer solution, a colloidal solution, etc. is generally a non-Newtonian fluid.

According to Equation (2.11), viscosity is $\eta = \tau / D$. This is represented by SI system of units as follows:

- shear stress τ is force per unit area. The unit of force is Newton (N). Therefore the unit of τ is ($N.m^{-2}$) or Pascal (Pa), which is the unit of stress (pressure).
- shear rate D is defined as dV/dy by the Equation (2.9), and is represented by the unit (s^{-1}), which was given by dividing the unit [$m.s^{-1}$] of speed V by the unit (m) of distance y.

Therefore, according to (a) and (b), the unit of viscosity η is (Pa) / (s^{-1}) = (Pa.s).

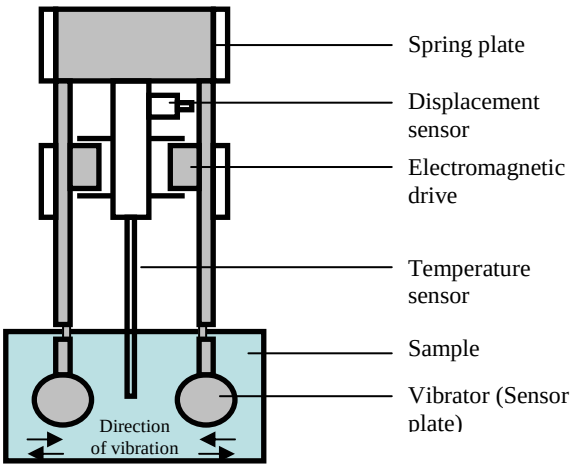

Figure 2.2. Vibro-viscometer (detection system).

2.3.3.a. Principle and apparatus

Viscosity was measured on an AND SV-10 vibro-viscometer (A&D Company Ltd., Tokyo, Japan) with gold-coated transducer and temperature sensor. The instrument has two thin sensor plates that are driven with electromagnetic force at the same frequency (30 Hz) and amplitude of less than 1 mm by vibrating at a constant sine-wave vibration in reverse phase as for a tuning-fork. The electromagnetic drive controls the vibration of the sensor plates to keep them in constant amplitude. The driving electric current, which is the exciting force, will be detected as the magnitude of viscidity produced between the sensor plates and the sample fluid. The coefficient of viscosity is obtained by correlation between the driving electric current and the magnitude of viscidity. Accuracy of the measurements is within 1 % of readings obtained. After calibration on double distilled water, the viscosity of the water was 0.894 mPa.s at 25 ^{o}C (1 atm) [11].

2.3.3.b. Measurements

Viscosity measurements were performed at 25 ± 2 °C. The readings of viscosity were acquired in 10 mL polycarbonate containers with fixed size and position.

2.3.4. Ultrasonic measurements

Ultrasonic spectroscopy was used for material characterization. A material's properties are linked to its acoustic characteristics. These can be studied by ultrasonic techniques, employing sound waves [12, 13]. The high frequency acoustic wave probes intermolecular forces in materials. Oscillating compression (and decompression) in the ultrasonic wave causes oscillation of molecular arrangements in the sample, which responds by intermolecular attraction or repulsion. The amplitudes of deformations in the ultrasonic waves employed in analytical ultrasound are extremely small, making ultrasonic analysis a non-destructive technique. An ultrasonic wave, unlike its light counterpart, is able to propagate through most materials. Another advantage is that it is relatively easy to change the wavelength of the ultrasonic wave, as ultrasonic waves are synthesized electronically unlike for optical techniques where the wave originates in a light source and therefore needs special effort to get a required spectral purity. Therefore a typical ultrasonic spectrometer can cover a broad range of wavelengths. It could be described as probing the interior of the analyzed sample with a set of fingers, which differ in their size by more than an order of magnitude!

2.3.4.a. Principle and apparatus

Ultrasonic materials analysis is based on the measurement of parameters of ultrasonic waves propagating through the sample [14-16]. This provides information on the interaction of the ultrasonic waves with the sample's interior, thus enabling analysis of its physical and chemical properties. The sample's molecules respond to the ultrasonic wave, through the intermolecular forces (intermolecular repulsion and attraction) reflecting the micro-elasticity of the sample.

The ultrasonic wave is a wave of oscillating pressure and associated longitudinal deformation. The ultrasonic spectrometer employs a principle where the path length of the ultrasonic wave in the sample exceeds the size of the sample. The general principles of high-resolution ultrasonic measurements are shown in Figure (2.3) below. Piezoelectric transducers transform the electrical signal into the oscillations of pressure, the ultrasonic wave. A second piezotransducer then transfers the received ultrasonic wave into an electronic signal, for subsequent analysis. Travelling through samples, the ultrasonic wave loses its energy (a decrease in amplitude) and changes its velocity. This decrease in amplitude and change in velocity are analysed as characteristics of the material.

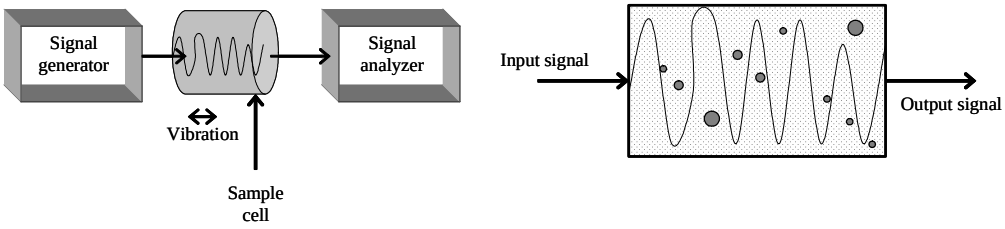

Figure 2.3. General principles of high-resolution ultrasonic measurements.

The ultrasonic properties of a sample can be characterized by two parameters: ultrasonic velocity and ultrasonic attenuation. Ultrasonic velocity (speed of sound) is determined by the elasticity and the density of the medium. Generally, the elastic response, which is extremely sensitive to molecular organization and intermolecular interactions, dominates. Travelling through a sample, ultrasonic waves lose their energy and ultrasonic attenuation is a measure of this. It characterizes the ultrasonic transparency of the sample and can be seen as a reduction of amplitude of the wave. The more homogeneous is the sample's medium, the less impeded and attenuated is the sound wave passing through it. In the case of a non-homogeneous sample, the ultrasonic wave's energy is partially absorbed by the medium, and its velocity is dispersed by some scattering effects on the particles.

2.3.4.b. Measurements

Ultrasonic titrations were performed using HR-US 102 T ultrasonic spectrometer equipped with HR-US titration accessory (both from Ultrasonic Scientific, Dublin, Ireland). The ultrasonic measurement was carried out in the ultrasonic frequency range of 5 - 15 MHz and at the temperature of 25 ± 0.1 °C maintained by an internal thermostat. Ultrasonic velocity and ultrasonic attenuation were recorded simultaneously in a differential mode using the data from two measurement cells - a cell containing the sample being titrated and the reference cell containing the same sample in unmodified form.

Titrations of Al species were performed using monotonic addition of titrant (Trizma-base solution, 1 $mol.L^{-1}$ prepared from the solid, Sigma-Aldrich, with minimum 99 % purity). Forty additions of titrant were made in total in each of the titrations with the time interval of 30 min from beginning to end as between each addition. The volume of titrant was varied in the range of 5 to 40 μL depending on the initial hydrolysis ratio h of the Al species ($h = [OH^-] / [Al]$). In general, the lower the hydrolysis ratio, the larger the volume of titration addition. The total concentration of Al species did not exceed 0.1 $mol.L^{-1}$ for all the titrations conducted.

The data was collected using a PC with dedicated software from Ultrasonic Scientific. The final titration curves were obtained by averaging the data acquired for 20 minutes (min) after each titrant addition with a 5 min delay.

2.3.5. Dynamic light scattering measurements

Particle size is of great importance in the characterization of materials [17] because it affects key colloid properties such as rheology, surface area and packing density. Moreover, its knowledge is vital information regarding the stability of a material.

2.3.5.a. Principle and apparatus

Dynamic Light Scattering (DLS - also known as PCS - Photon Correlation Spectroscopy) is a technique used to determine the diffusion coefficient of small particles in a liquid [18-20]. DLS measurements consist of the illumination of particles with a laser and the analysis of the intensity fluctuations due to the Brownian motion in the scattered light [21 a and b]. The scattered light is collected through optical fibres at different angles, and is measured by highly sensitive detector whose output is fed to a correlator.

An important feature of Brownian motion for DLS is that small particles move quickly and large particles move more slowly. For a solution of a given viscosity and at constant temperature, the relationship between the size of a particle and its speed due to Brownian motion is defined by the Stokes-Einstein Equation (2.12):

$$r = (k_B\ T)/(6\ \pi\ \eta\ D) \qquad \textbf{Equation 2.12}$$

where r is the van der Waals radius of the molecule in meters

k_B is the Boltzman constant ($1.380.10^{-23}$ $J.K^{-1}$)

T is the temperature in Kelvin

η is the viscosity of the solution in Pascal seconds

D is the self-diffusion coefficient.

Since the diffusion rate of particles is determined by their size, information about their size is contained in the rate of fluctuation of the scattered light. So by constructing the time autocorrelation function (ACF) - (Equation (2.13)) $G_2(\tau)$ of the fluctuation, one can determine the particle size distribution of the population present.

$$G_2(\tau) = \left\langle I(t)\ I(t+\tau)\ \right\rangle \qquad \textbf{Equation 2.13}$$

where I(t) is the intensity detected at time t

$I(t+\tau)$ is the intensity detected at time $t+\tau$

τ is the delay time.

The symbol $\langle\ \rangle$ refers to an average value of the product $I(t)\ I(t+\tau)$ for various times t.

A digital correlator measures the degree of similarity between two signals over a period of time. The signal intensity at (t) will be the same as itself because the signals are identical. That perfect correlation is reported as 1 and no correlation is reported as 0 (Figure (2.4)). If the comparison of the same signal at (t) with a signal at (t + τ) is realised, a decrease of the correlation between the two signal intensities will be noted. The correlation will eventually reach zero when the initial signal intensity is compared to the one of a signal at (t + ∞ τ).

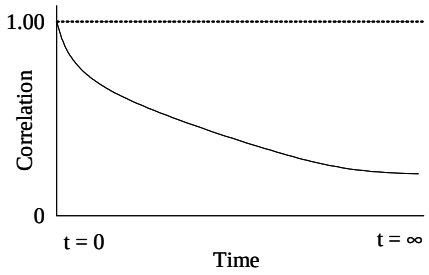

Figure 2.4. The correlation function.

Results were acquired using a Zetasizer Nano S from Malvern Instruments (Worcestershire, UK). The particle size measured in a DLS instrument is the diameter of the sphere that diffuses at the same speed as the particle being measured. Particle size distribution analysis was performed using the unimodal intensity-based model from the Coulter CONTIN program.

2.3.5.b. Measurements

The data were acquired at a measuring angle 90.0 degrees and acquisition time 120 s, temperature 25 °C, equilibration time 20 min, in triplicate. Prior to DLS measurements the samples were diluted with distilled, deionized and nano-filtered water (Whatman filter 0.1 μm) and treated for 1 min in an ultrasonic bath to break up any loose aggregates. This preparation technique was used to eliminate the effects of multiple scattering (observed in concentrated sols and leads to an under-estimation of particle size), viscosity variation and dust, leading to errors in particle size measurements.

2.3.6. Zeta-potential measurements

Almost all particulate or macroscopic materials in contact with a liquid acquire an electronic charge on their surfaces. Zeta potential is an important and useful indicator of this charge which can be used to predict and control the behaviour of colloidal suspensions. The greater the zeta potential the more likely the suspension is to be stable because the charged particles repel one another and thus overcome the natural tendency to aggregate. The measurement of zeta potential is often the key to understanding dispersion and aggregation processes.

2.3.6.a. Principle and apparatus

Zeta-potential measurements of samples were performed using a Zetasizer Nano S from Malvern Instruments using a disposable capillary cell. The development of a net charge at the particle surface affects the distribution of ions in the surrounding interfacial region, resulting in an increased concentration of counter ions close to the surface. Thus an electrical double layer exists around each particle. The liquid layer surrounding the particle exists as two parts; an inner region, called the Stern layer, where the ions are strongly bound and an outer, diffuse, region where they are less firmly attached. Within the diffuse layer there is a estimated boundary inside which the ions and particles form a stable entity. When a particle moves, ions within the boundary move with it, but any ions beyond the boundary do not travel with the particle. This boundary is called the surface of hydrodynamic shear or slipping plane. The potential that exists at this boundary is known as the zeta-potential.

Under the influence of an applied electric field, the existence of electrical charges on the surface of particles is at the origin of the movement of the particle in the liquid it is suspended in. That effect is called the electrophoresis. At the same time, viscous forces act on the particles which tend to oppose this movement. When equilibrium is reached between these two opposing forces, the particles move with constant velocity. From the velocity of a particle, which is also called electrophoretic mobility, the zeta potential of the particle can be deduced by applying the Henry equation [22]:

$$U_E = \frac{2\,\varepsilon\, z\, f(ka)}{3\,\eta} \qquad \textbf{Equation 2.14}$$

where z zeta potential

U_E electrophoretic mobility

ε dielectric constant

η viscosity

$f(ka)$ Henry's function.

Most of the time, particles are in polar media and moderate electrolyte concentration. The maximum value of $f(ka)$ is 1.5 and is referred to as the Smoluchowski approximation [23, 24].

The electrophoretic mobilities of the particles were determined using a combination of phase analysis light scattering (PALS) and Laser Doppler Velocimetry (LDV). Then, those data were converted into zeta potentials from theoretical considerations using the Smoluchowski approximation [25, 26]. The concept of zeta potential is illustrated in Figure (2.5).

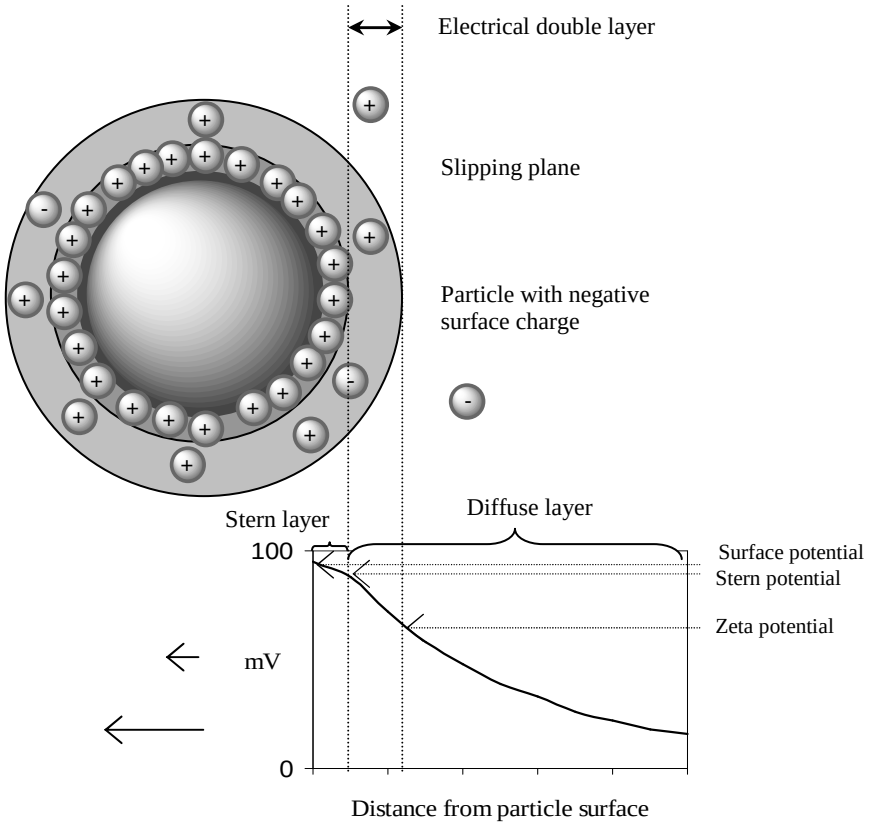

Figure 2.5. Schematic representation of zeta potential.

2.3.6.b. Measurements

1 mL aliquot of each sample was injected into the capillary cell and measurements were made at 25 °C using field strengths of approximately 10 $V.cm^{-1}$. In order to enable this conversion and to reduce the effect of viscosity the samples were diluted 100 times with deionised water immediately before measurement.

2.3.7. ^{27}Al and ^{1}H solution nuclear magnetic resonance spectroscopies

Nuclear magnetic resonance (NMR) spectroscopy is a widely used technique for speciation analysis (quantitative and qualitative) in materials science, catalysis, geochemistry, soil science, and many other fields [27-32]. In this study, ^{27}Al and ^{1}H solution NMR spectroscopies were used, particularly for the studies of aluminium biomolecule interactions in order to establish identities of the samples. However, with ^{27}Al solution NMR spectroscopy, there are several difficulties associated with the method, such as quadrupolar line broadening [33], baseline 'rolling' [32], together with the low signal-to-noise ratios [34] obtained when working at low concentrations of large aluminium species. Provided that the sample concentration is sufficiently high, those problems can be overcome through the use of computational transformations to lead to a set of spectra which are fitted in the second part of the algorithm.

2.3.7.a. Principle

Quantification

Due to the possible losses in intensity and artefacts due to NMR equipment settings and construction, the ^{27}Al NMR analysis of any system should include quantitative estimates of the intensity of the resonance related to some external standard. For this purpose, a concentric sample cell containing the sample in one compartment and a standard solution in the other was used to determine the intensity of the signal. The $[Al(H_2O)_6]^{3+}$ resonance in aqueous salt solutions and the $[Al(OH)_4]^-$ resonance in aluminate solutions are two suitable standards. $[Al(H_2O)_6]^{3+}$ solutions should be acidified ($[H^+]/[Al^{3+}] \geq 1$) to prevent self hydrolysis, and therefore give as narrow a resonance as possible, whereas an excess of alkali $[NaOH]/[Al] \geq 5$ has to be used in the case of aluminate to improve the complete detection of aluminium. The standards should in any case be calibrated against a solution of the other in a two compartment cell so as to eliminate any need for precision measurements of the cell size. The quantitative data were then extracted in the usual way by obtaining integrals. The aluminate standard is widespread as it overlaps with fewer resonances than the hexaaquo ion resonance.

2.3.7.b. Features of ^{27}Al NMR spectroscopy

The main aluminium isotope, ^{27}Al, has a natural abundance of 100 % [33]. It is characterised by a high sensitivity to detection by NMR and large chemical shift ranges, two factors that make its study relatively easy. The nucleus has a relatively small quadrupolar moment associated with a high nuclear spin ($I = 5/2$). ^{27}Al is a quadrupolar nucleus which means that its resonances are broadened relative to those of spin 1/2. This aspect of quadrupolar relaxation is counterbalanced by the additional information obtained concerning molecular symmetries from the magnitude of quadrupolar line broadenings. Furthermore, advances in high-resolution NMR spectroscopy made it possible to obtain rich information from ^{27}Al NMR spectra concerning the structure and pathways of its interactions with solvents and numerous ligands [32, 34]. Aluminium solution NMR spectra are characterised by a chemical shift range of about - 30 to + 300 ppm, normally expressed relative to the ^{27}Al resonance of $Al(H_2O)_6^{3+}$ in aqueous solution [2].

2.3.7.c. Features of ^{1}H NMR spectroscopy

Proton solution NMR (^{1}H NMR) spectra are characterised by a chemical shift in the range of - 4 to + 12 ppm, normally expressed relative to the ^{1}H resonance of tetramethylsilane as the internal standard, set as zero. To assign a molecule, the spin-spin coupling between protons is also used as an indicator. The integration curve for each proton reflects the abundance of the individual protons.

2.3.7.d. Measurements

^{27}Al solution NMR

^{27}Al solution NMR spectra were acquired using a Jeol ECX400 spectrometer (Jeol, Tokyo, Japan) operating at the following conditions: D_2O lock, single pulse method, x-pulse of 9.4 μs, 512 scans, relaxation delay 0.5 s, 10 mm sample probe, temperature 25 ^{o}C or 80 ^{o}C in the case of Al_{30} and $AlCl_3$+HCl systems. Aluminium nitrate solution (0.016 mol.L^{-1} in distilled, deionised water) was used as a primary standard for quantification. 5 mm probes with coaxial inserts (Wilmad, Buena, NJ, USA) containing 0.06 mol.L^{-1} of sodium aluminate in D_2O (99.8 %, BDH Laboratory supplies, UK) as both secondary standard and locking solution were used for acquisition. The ^{27}Al NMR FID traces were apodised using an exponential function (line broadening 10 Hz), Fourier Transformed, phased (0 and 1st order phasing) and baseline corrected using the Galactic GRAMS/32® ver. 5.1 software (Thermo Galactic, Waltham, MA, USA). The peak assigned to aluminate ions (chemical shift 80 ppm) in the secondary reference solution was used as a chemical shift reference. Quantification of the ^{27}Al NMR spectra was carried out using a local integration of the peak areas by means of the Galactic GRAMS/32® ver. 5.1 software and an algorithm developed previously [27, 35].

^{1}H solution NMR

Since it was necessary during the biochemical investigations to work with aqueous media, the water signal in the neighbourhood of $\delta \sim 4–5$ ppm interfered with the measurements. Although some signals may be hidden and integration is not possible near to the water signal, the water signal was not suppressed as the methine and the methyl signals used for quantification were not in the vicinity of the solvent signal.

2.3.8. One dimensional polyacrylamide gel electrophoresis

A molecular biological technique was undertaken to determine the molecular weight of the proteins used through that study. Polyacrylamide gel electrophoresis (PAGE) gives the molecular weight of proteins providing it they lie between 10 and 250 kDa [36-38]. Based on the manufacturer information, lysozyme and bovine serum albumin (BSA) have a molecular weight of 14.7 and 66 kDa respectively. Consequently, those two proteins are good candidates for the electrophoresis. The mucin macromolecule also used in the work, has a molecular weight in the range of $10^5 – 10^7$ Da. The high value of the molecular weight of the biomolecule made itself an inappropriate subject for the analysis. However, its results will give us a hint regarding its range of molecular weights.

2.3.8.a. Principle

A polyacrylamide gel is a separation matrix used in electrophoresis. Under the application of a directional electric field, charged protein molecules migrate in a buffer solution through the polyacrylamide gel. Polyacrylamide is a cross-linked polymer of acrylamide and a cross linking agent,

the bis-acrylamide (N,N´-methylene-bis-acrylamide). The polymerization reaction proceeds via a vinyl addition initiated by the production of free radicals. The system most commonly used for the production of free radicals involves the use of ammonium persulfate (APS) and tetramethylethylenediamine (TEMED) [39]. The cross-linked polymer network when APS, the polymerizing agent is added is shown Figure (2.6).

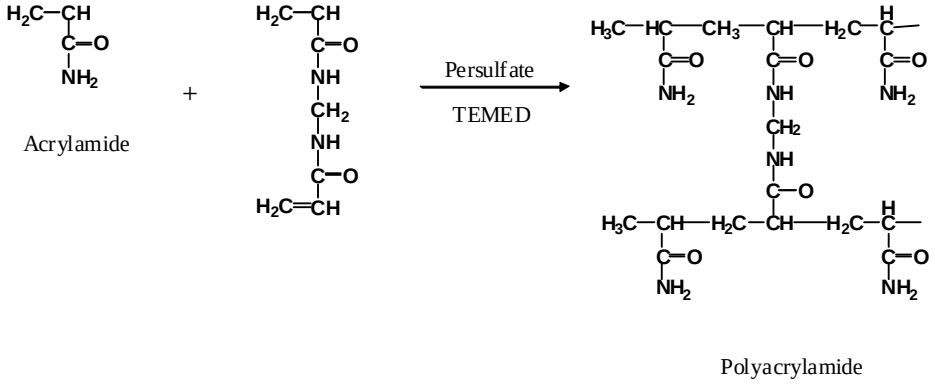

Figure 2.6. Polymerization and cross-linking of acrylamide.

The length of the polymer chains is dictated by the concentration of acrylamide used, which is typically between 3.5 and 20 % [40, 41]. The matrix separates proteins by size by forcing them through pores. The porous gels act similar to a sieve by retarding and sometimes totally obstructing the movement of large molecules while allowing smaller molecules to migrate more freely. Accordingly, the percentage of polyacrylamide chosen depends on the size of the protein that one wishes to identify or probe in the sample. Gels with a low percentage of acrylamide are typically used to resolve large proteins and high percentage gels are used to resolve small proteins.

In order to obtain a separation based only on the molecular weight of the proteins, gels are made in reducing and denaturing conditions by adding respectively β-mercaptoethanol (a reducing agent which cleaves disulfide bonds) to the samples and sodium dodecyl sulfate (SDS) in the samples' buffer and also in the loading, the gels and the electrophoresis buffers. SDS binds to the polypeptide backbone and causes unfolding of the protein. As SDS is an anionic detergent, once bound by it, the denatured proteins become negatively charged. Their rate of migration through the gel towards the anode is only proportional to their molecular weight [6]. This phenomenon is illustrated by Figure (2.7).

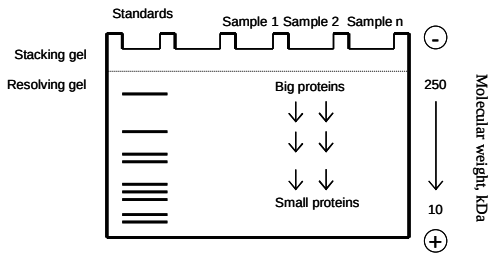

Figure 2.7. Schematic illustration of SDS-PAGE.

Protein molecular weights can be estimated by running standard proteins of known molecular weights in a separate lane of the same gel. The ratio of the distance travelled by the solute (sample's compound) to that of the solvent is known as the retardation factor (R_f) value. The R_f value is a characteristic of the solute and is used to identify its molecular weight.

2.3.8.b. Preparation of the polyacrylamide gels and measurements

For the electrophoresis of lysozyme, a 15 % resolving gel was used, and one at 7.5 % was utilized for mucin. BSA was analyzed on both gels.

A 10 % SDS solution was prepared by dissolving 10 g SDS (Sigma Aldrich) in 100 mL of distilled water. A 1.5 mol.L^{-1} Tris buffer solution for the separating gels was made by dissolving 36.4 g Tris base (Melford, Ipswich, UK) into 6 mol.L^{-1} HCl (Sigma Aldrich) until nearing pH 8.8. 8 mL of 10 % SDS was added to make a 0.4 % SDS solution. The final solution was completed with distilled water up to 200 mL. The stacking buffer requires a fair amount of HCl so ~ 70 mL of water was first added to Tris 0.5 mol.L^{-1} (6.06 g of Tris base) with 6 mol.L^{-1} HCl until nearing pH 6.8. 8 mL of 10 % SDS was added to make a 0.4 % SDS solution. The buffer solution was completed with distilled water up to 100 mL. 30 mL of acrylamide (40 % from Geneflow, Fradley, UK) was dissolved in the presence of 0.8 g of Bis-acrylamide base in 100 mL of distilled water to make a 30 % acrylamide solution. APS 10 % was prepared by dilution of 0.1 g of APS (Sigma) into 1 mL of distilled water. TEMED (Fluka).

The polyacrylamide gels were prepared in the proportions detailed in Table (2.2) being aware that the addition of the ammonium persulfate will instantly start the polymerisation of the gels.

Table 2.2. Polyacrylamide gel conditions.

7.5% resolving gel	15 % resolving gel	5 % stacking gel
1.9 mL 1.5 mol.L^{-1} Tris buffer	1.9 mL 1.5 mol.L^{-1} Tris buffer	1.25 mL 0.5 mol.L^{-1} Tris buffer
3.7 mL distilled water	1.85 mL distilled water	3.25 mL distilled water
1.9 mL acrylamide 30 %	3.75 mL acrylamide 30 %	0.5 mL acrylamide 30 %
10 µL TEMED	10 µL TEMED	10 µL TEMED
20 µL APS 10 %	20 µL APS 10 %	20 µL APS 10 %

Once electrophoresis plates are set up, the ammonium persulfate is added to the separating buffers and those latter are immediately poured. The stacking gel is poured on top of the resolving gel and a gel comb (which forms the wells and defines the lanes where proteins, sample buffer and ladders will be placed) is inserted. The preparation is left for 30 min for polymerization. During that time, the samples are mixed with a loading buffer; this latter contains 4 mL of glycerol (Fisher Scientific), 0.4 g SDS, 5

mL of the stacking buffer and distilled water up to 10 mL. Then, 4 µL of each sample (containing bromophenol blue for an easy monitoring when the gels run) and of the protein standard (Bio-Rad) were introduced in the wells previously cleaned with distilled water. The standard corresponds to ten markers (10, 15, 20, 25, 37, 50, 75, 100, 150 and 250 kDa). An electrophoresis running buffer made of 121.4 g of Tris-base, 567 g of glycine (Melford) and 40 g of SDS diluted in 4 L of distilled water, is poured in the reservoir of the electrophoresis tank. The electrode is connected to the power supply and the run of the gel started. Once the marker dyes have migrated the desired distance through the gel, the electrophoresis is stopped. For 5 min the gels are placed in a container filled with a Coomassie blue stain solution and subsequently destained with distilled water to eliminate the blue background from the gel. The Coomassie blue stain was chosen because it binds non specifically to most proteins; it is made of 200 mL of acetic acid (10 % from Fisher Scientific), 0.5 g of R250 Coomassie Blue (0.025 % from Biorad, Hemel Hempstead, UK) diluted in 1.3 L of distilled water. Gels are removed from the container and viewed with a scanner (Fujifilm).

2.3.9. Gravimetry

To expand the range of quantitative methods used for aluminium concentration determination, a gravimetric procedure was developed and tested on different model systems. Gravimetric analysis is one of the most accurate and precise methods of macro-quantitative analysis of an element in aqueous solution [42, 43]. Thermal changes in materials (e.g. phase transitions) do not involve a change of mass. The basic principle of gravimetry is to measure the mass of a sample after thermal change. In the process, the analyte is selectively converted to an insoluble form by precipitation from solution. After its isolation, the analyte is weighted.

2.3.9.a. Principle

The technique starts by the homogeneous precipitation of a sample. It is realised by increasing the pH of a boiling aqueous solution by addition of a precipitating agent, ammonia. As the ammonia is slowly liberated it raises the pH of the solution, causing metal ions that form insoluble hydroxides or hydrous oxides to precipitate. The resulting sample is washed and filtered to eliminate most of the free water and impurities (mostly the anions of the starting salt). Free from purities, the insoluble precipitate is burned to form the oxide Al_2O_3, the definite product which is subsequently weighted in a high precision balance [44]. Though the filtration step requires a long time (over 24 h), this technique is widely accepted due to its high precision/accuracy and was used to validate the other methods implemented during this study.

2.3.9.b. Measurements

The stated aluminium concentration in the initial Al_{13}-mer solution and aluminium hydroxide suspension was 0.4 $mol.L^{-1}$ and a 1 $mol.L^{-1}$ $AlCl_3$ / HCl solution was used as a model aluminium

monomer system. In a glass beaker, 5 g of a strong oxidant 0.125 mol.L^{-1} (ammonium nitrate, NH_4NO_3 ≥ 99.0 % Sigma-Aldrich) as added to 5 mL of sample. Distilled water was then added to reach a final volume of 150 mL and the solution heated to ca. 80 ^oC. A 1 mol.L^{-1} ammonia solution (concentrated aqueous ammonia 35 %, Fisher) was then added drop wise until persistence of a slight turbidity upon benzene heating, corresponding to the formation of Al hydroxide. 10 drops of methyl red $C_{15}H_{14}N_3O_2Na$ (Sigma-Aldrich) were then added as a pH indicator until a red solution was developed (Methyl red is red for pH < 4.4, yellow for pH > 6.2, and orange for 4.4 < pH < 6.2 [45]). Next, a careful drop wise addition of a dilute ammonium hydroxide 0.1 mol.L^{-1} solution (Sigma-Aldrich) was undertaken until obtaining the desired pH (< 7, to avoid the dissolution of Al hydroxide). After cooling down to room temperature, the precipitate was collected by filtration on an ashless Whatman 42 filter paper and washed with NH_4NO_3 0.125 mol.L^{-1}. Both filter and precipitate were transferred to a crucible and placed into a Muffle oven to be converted to aluminium oxide Al_2O_3 and for complete removal of the solvent by a 24 h heating at 1000 ^oC (initial temperature increase ramp: 5 ^oC per min) [46-48]. The crucible was cooled down and weighed, and the amount of alumina calculated. Aluminium concentration was deduced from the weight of alumina formed using the theoretical molecular weight and stoichiometry of the oxide.

2.3.10. Ultraviolet-visible absorption spectroscopy

Many molecules absorb ultraviolet or visible light. In this respect, Ultraviolet-visible (UV-vis) spectroscopy was used for the determination of aluminium species in solution. During the present work, the attempt was to develop a procedure based on the formation of a complex between aluminium species and a spectrophotometric reagent.

2.3.10.a. Principle and apparatus

Spectroscopy is the measurement and analysis of electromagnetic radiation absorbed, scattered, or emitted by atoms, molecules, or other chemical species [49]. The absorbance of a solution increases as attenuation of the beam increases [50, 51]. The UV-Vis spectrophotometer uses ultraviolet and visible electromagnetic radiations in the range from ca. 200 to 800 nm to energetically promote valence electrons in a molecule to an excited energy state. The absorption of light is directly proportional to the properties of the material through which the light is travelling. The Beer-Lambert law states that the absorbance is related to the path length, l, and the concentration, C, of the absorbing species:

$$A = \varepsilon \, l \, C \qquad \textbf{Equation 2.20}$$

where ε is the absorption coefficient.

Thus if ε and l are known, the concentration of the substance can be deduced from the amount of light transmitted by it.

Only chemical species having chromophore groups can be analysed using UV-Vis spectrophotometry. This implies the need to "derivatise" UV-Vis transparent substances with reagents containing chromophore groups. It is based on the formation of complexes between metal ions and organic chromophores (organic reagents) that enables quantification of metal ions using UV-Vis spectrophotometry. A large number of organic reagents have been proposed allowing determination of practically all metal ions and metalloids in the Periodic Table.

A UNICAM UV2 spectrophotometer connected to a PC with Vision32 UV-Vis software was used for all measurements. A deuterium arc lamp for UV-Range 200 - 325 nm and tungsten-halogen lamp for measurements in the 325 - 800 nm wavelengths were employed. The spectrophotometer contains a diffraction grating as a monochromator, multi-cell holder and a photomultiplier detector. The spectrophotometer allows for both spectrum scanning and fixed wavelength measurements.

2.3.10.b. Measurements

Zeroing and baseline correction of the blank sample (deionised distilled water) were performed for each sample. A 48 h aging was used to enable the full development of the complex prior to spectra acquisition from 400 to 750 nm in UV-Vis transparent plastic cuvettes 1 cm path length. For calibration, an aluminium atomic absorption standard solution (986 $\mu g.mL^{-1}$ Al in 0.7 % HCl, Aldrich) was used.

2.3.10.c. Acid Digestion coupled with ultraviolet-visible absorption spectroscopy

Introduction

Acid digestion (AD) was coupled to UV-vis spectrophotometry for the development of an aluminium concentration determination. This method was intended for the cross-verification of aluminium content in samples.

Principle and apparatus

The AD procedure consists of the total break down of aluminium species to aluminium monomers after addition of a strong acid such as hydrochloric acid HCl. The digested samples are then mixed with a complexing organic reagent solution for quantification of the Al monomer concentration by UV-visible spectrophotometry. Five organic reagents (xylenol orange ($C_{31}H_{28}N_2O_{13}SNa_4$) (Sigma-Aldrich) [52], arsenazo III ($C_{22}H_{16}As_2N_4Na_2O_{14}S_2$) (Sigma-Aldrich) [53], chrome azurol S ($C_{23}H_{13}Cl_2O_9SNa_3$) (Sigma-Aldrich) [54], Ferron ($C_9H_6INO_4S$) (Fluka) [55] and aluminon ($C_{22}H_{14}O_93NH_3$) (Sigma-Aldrich) [56]) have been tested as aluminium complexing reagents [52]. The protocol used for Ferron will be further detailed in the section Ferron assay.

Measurements

The AD was carried out using HCl 1 $mol.L^{-1}$ (Fisher). The effects of the organic reagent to aluminium concentration ratio and of the AD temperatures (25 or 50 ^{o}C) were examined for optimization of the sensitivity and reproducibility of the method. ADs were performed on three reference systems: an Al_{13}-mer solution, an aluminium hydroxide suspension with a mean particle size estimated to be 120 nm, as well as an $AlCl_3$ solution used as a blank. The digestion of the $AlCl_3$ solution was used to demonstrate the absence of treatment effect upon total aluminium concentration (the latter could be affected by eventual water evaporation, to give only one example). Depending on the initial aluminium concentration of the reference systems, three samples differing in concentration have been prepared, as listed in Table (2.3).

Table 2.3. Preparation of the AD samples (volumes (abbreviated V) are given in mL).

Initial solutions	*Reference systems: Al_{13}-mer and $Al(OH)_3$*			*Reference system: $AlCl_3$*		
[Reference systems], $mol.L^{-1}$	*0.004*	*0.012*	*0.04*	*0.004*	*0.012*	*0.04*
AD						
V (reference system) $_{added}$	0.50	1.25	5	0.2	0.5	2
V (H_2O) $_{added}$	4.50	3.75	0	1.8	1.5	0
V (HCl, 1 $mol.L^{-1}$) $_{added}$	45			18		
V (sample) $_{total}$	50			20		
AD dilution						
V (digested sample)	1	0.40	0.10	1	0.40	0.10
V (H_2O) $_{added}$	4	4.60	4.90	4	4.60	4.90
UV-Vis sampling						
V (digested diluted sample)	0.10					
V(HCl, 10^{-4} $mol.L^{-1}$ buffered at pH 3.4) $_{added}$	2.10					
V (xylenol orange, 10^{-3} $mol.L^{-1}$) $_{added}$	0.80					

The other organic reagents were respectively used to the concentration of $2.97.10^{-4}$ $mol.L^{-1}$ for chrome azurol S, 3.10^{-2} $mol.L^{-1}$ for aluminon and $7.45.10^{-5}$ $mol.L^{-1}$ for arsenazo III.

2.3.10.d. Bradford protein assay

Introduction

Several methods of determining the total protein content of a sample have been developed and widely used during this and the last century. One of the simplest and most sensitive is the Bradford total protein concentration assay, which was introduced in the mid-1970s [57]. That spectroscopic analytical technique is faster, involves fewer mixing steps, does not require heating, and gives a more stable colorimetric response than other assays (Lowry assay, the Smith copper / bicinchoninic assay for instance).

Principle and apparatus

The "Bradford" assay is a colorimetric protein assay, based on the binding specificity of the dye Coomassie Brilliant Blue-G250 to protein molecules but not to other cellular constituents [57]. This organic dye binds specifically to arginine and hydrophobic amino acid residues. The binding of the dye to protein shifts the peak absorbance of the dye. Unbound Coomassie Blue absorbs light maximally at a wavelength of 465 nm, while the absorption maximum is at 595 nm when the dye is bound to protein. The absorbance of light by the dye-protein complex at 595 nm is proportional to the amount of protein bound (over a limited range); i.e. there is a linear relationship between absorbance and the total protein concentration of the sample over a narrow range.

Measurement

The samples were subjected to a 3000 rpm centrifugation for 30 min. Then an aliquot of 0.1 mL of the sample supernatant was diluted in 9.9 mL of distilled deionized water. A volume of 1.0 mL of the resulting solution was mixed with 5.0 mL of the Bradford reagent containing 0.1 $g.L^{-1}$ Coomassie Brilliant Blue G-250 (Fluka), 5.0 % ethanol (Sigma) and 8.5 % phosphoric acid (Fisher) (filtered before use) according to the method described in [58]. The absorbance of the solutions was integrated for 15 seconds at a wavelength of 590 nm 5 min after mixing and the protein concentration was calculated from the calibration curve obtained with pure biomolecule solutions of known concentration.

2.3.10.e. Ferron spectrophotometric assay

Introduction

Beside ^{27}Al solution NMR, the concentration of aluminium can successfully be obtained by the Ferron colorimetric method. That latter offers a simple and inexpensive alternative to NMR and allows quantification at concentrations 10-100 fold lower than presently analyzable by NMR. As mentioned in a previous section (Acid Digestion coupled with ultraviolet-visible absorbance), the Ferron kinetic assay is a spectrophotometric method for determining quantitatively and qualitatively the aluminium species present in a sample. It is based on a colorimetric complexing reaction between the Ferron reagent and aluminium species. The Ferron method can conveniently differentiate between polynuclear

hydroxy- aluminium and mononuclear species based on differential reaction kinetics [55, 59-66]. However, through this work, the assay has been used only quantitatively.

Principle and apparatus

Ferron has been used in many studies of Al polymer formation. Its limit of sensitivity is 50 $g.L^{-1}$, and the response is linear up to 1500 $g.L^{-1}$ [67].

The aluminium species form colorimetric complexes with specific reaction rates with Ferron (8-hydroxy-7-iodo-5-quinolinesulfonic acid), the complexing reagent, which can be quantified by UV-vis spectroscopy by following its absorbance at 370 nm. Since Ferron is a dibasic acid (Figure (2.8)), the pH value of Ferron solution can greatly affect, and thus modify the distribution of Ferron species which will in turn affect the characteristics of the colorimetric solution.

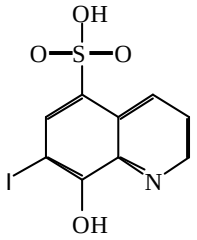

Figure 2.8. The Ferron molecule.

Around pH 5.2, Ferron reagent is partly deprotonated into mainly one form whose absorbance is the weakest at 364 nm and two other forms which yield a strong absorption background near 364 nm. According to Beer's law, as a blank solution, the choice of pH around 5.2 is favourable for the Ferron assay.

Measurement

The samples containing aluminium species and one of the four biomolecules studied through the thesis were centrifuged for 30 min at 3000 rpm using a standard laboratory centrifuge. The centrifugation speed was chosen in order to prevent free biomolecule or aluminium hydroxide colloid sedimentation. The supernatant of the solutions was then retained for residual aluminum and protein concentration measurements and the solid material used for scanning electron microscopy characterization.

The concentration of free aluminum species in supernatant solutions after centrifugation was determined using the colorimetric Ferron assay with preliminary acid digestion of the supernatant solutions to break down any polynuclear species and aluminium hydroxide that were present. For this purpose, an aliquot of 0.1 mL of the supernatant solution was mixed with 2.0 mL of 1.0 $mol.L^{-1}$ HCl and 7.9 mL of distilled, deionized water and digested for 48 h at 60 °C in a sealed tube. A 0.2 mL aliquot of the resulting solution was then mixed with 2.3 mL of deionized water and 2.5 mL of Ferron reagent (pH 5.2), containing $2 \cdot 10^{-3}$ $mol.L^{-1}$ Ferron (8-hydroxy-7-iodoquinoline-5-sulfonic acid, Fluka), 0.2 $mol.L^{-1}$ acetic acid and 0.1 $mol.L^{-1}$ hydroxylamine hydrochloride (Fisher Scientific) [55]. The absorbance of the solutions was measured at 370 nm, 1 h after mixing when the absorbance's increase

was negligible [68]. The overall concentration of aluminum-ions in the supernatant was calculated from the calibration curve obtained under the same conditions using an atomic absorption standard solution of Al- ions (0.986 $mg.L^{-1}$, Aldrich) in place of the aluminum-biomolecule samples.

2.4. Solid-state characterisation techniques

2.4.1. ^{27}Al solid state nuclear magnetic resonance spectroscopy

Solid state nuclear magnetic resonance (SSNMR) was performed to characterize solid state inorganic and bio-inorganic materials. SSNMR is clearly a very powerful technique capable of looking at a variety of materials. It does not require crystalline materials unlike diffraction techniques, and can still be used to determine local molecular environments. Its use was undertaken to corroborate the results obtained by ^{27}Al solution NMR.

^{27}Al MAS NMR spectroscopy was performed on the Al_{13}-mer and the Al_{30}-mer samples in the absence and in the presence of mucin for aluminium speciation. The aluminium concentration in the samples was kept constant at 15 $mol.L^{-1}$ and the protein's concentration equalled to 2.5, 12.5 or 25 $mg.mL^{-1}$. The experiments of SSNMR were performed by others on a Bruker DSX300 NMR spectrometer at Unilever R&D, Port Sunlight, UK. All spectra were referenced externally to solid aluminium sulphate 16 H_2O set at 0 ppm.

2.4.2. Scanning electron microscopy

Scanning electron microscopy (SEM) is a capable of delivering images of the surface of materials. SEM images have a characteristic three-dimensional appearance and are useful for judging the surface morphology, inclusions, boundary interfaces, and general characterization of a specimen surface. Furthermore, its combination with an energy dispersive X-ray analysis provides for structural and compositional studies to be performed.

2.4.2.a. Principle and apparatus [71-73]

The scanning electron microscope creates magnified images by using electrons.
Accelerated electrons in an SEM carry significant amounts of kinetic energy, and this energy is dissipated as a variety of signals produced by electron-sample interactions when the incident electrons are slowed down in the solid sample. These signals include secondary electrons (that produce SEM images), backscattered electrons, diffracted backscattered electrons (that are used to determine crystal structures and orientations of minerals), photons (characteristic X-rays that are used for elemental analysis and continuum X-rays), visible light (cathodoluminescence), and heat. Secondary electrons and backscattered electrons are commonly used for imaging samples: secondary electrons are most valuable for showing morphology and topography on samples and backscattered electrons are most

helpful for illustrating contrasts in composition in multiphase samples. X-ray generation is produced by inelastic collisions of the incident electrons with electrons in discrete orbitals of atoms in the sample. As the excited electrons return to lower energy states, they yield X-rays that are of a fixed wavelength (that is related to the difference in energy levels of electrons in different shells for a given element). Thus, characteristic X-rays are produced for each element in a material that is "excited" by the electron beam.

The SEM utilizes a focused electron beam to scan the surface of a sample and to build a three-dimensional image of the specimen. After the air is pumped out of the column, an electron gun emits a beam of high energy eletrons. The electron beam comes from a filament, made of various types of materials. The most common is the tungsten hairpin gun. This filament is a loop of tungsten which functions as the cathode. A voltage is applied to the loop, causing it to heat up. The anode plate, which is positive with respect to the filament, forms powerful attractive forces for electrons. This causes electrons to be accelerated toward the anode and to be focused to a very fine spot with the magnetic lens downward. The electron beam makes its way through electromagnetic lenses and the scanning coils force the electron beam to rapidly scan over an area of the specimen. When the electron beam hits the sample structure, it will go through it, generating physical phenomena such as secondary electrons, X rays, back scattered electrons, etc. The ejection of backscattered or secondary electrons can be viewed in the backscattered or secondary mode. The SEM at Nottingham Trent University has backscattered and secondary electron detectors. The final image is built up from the number of electrons emitted from each spot on the sample.

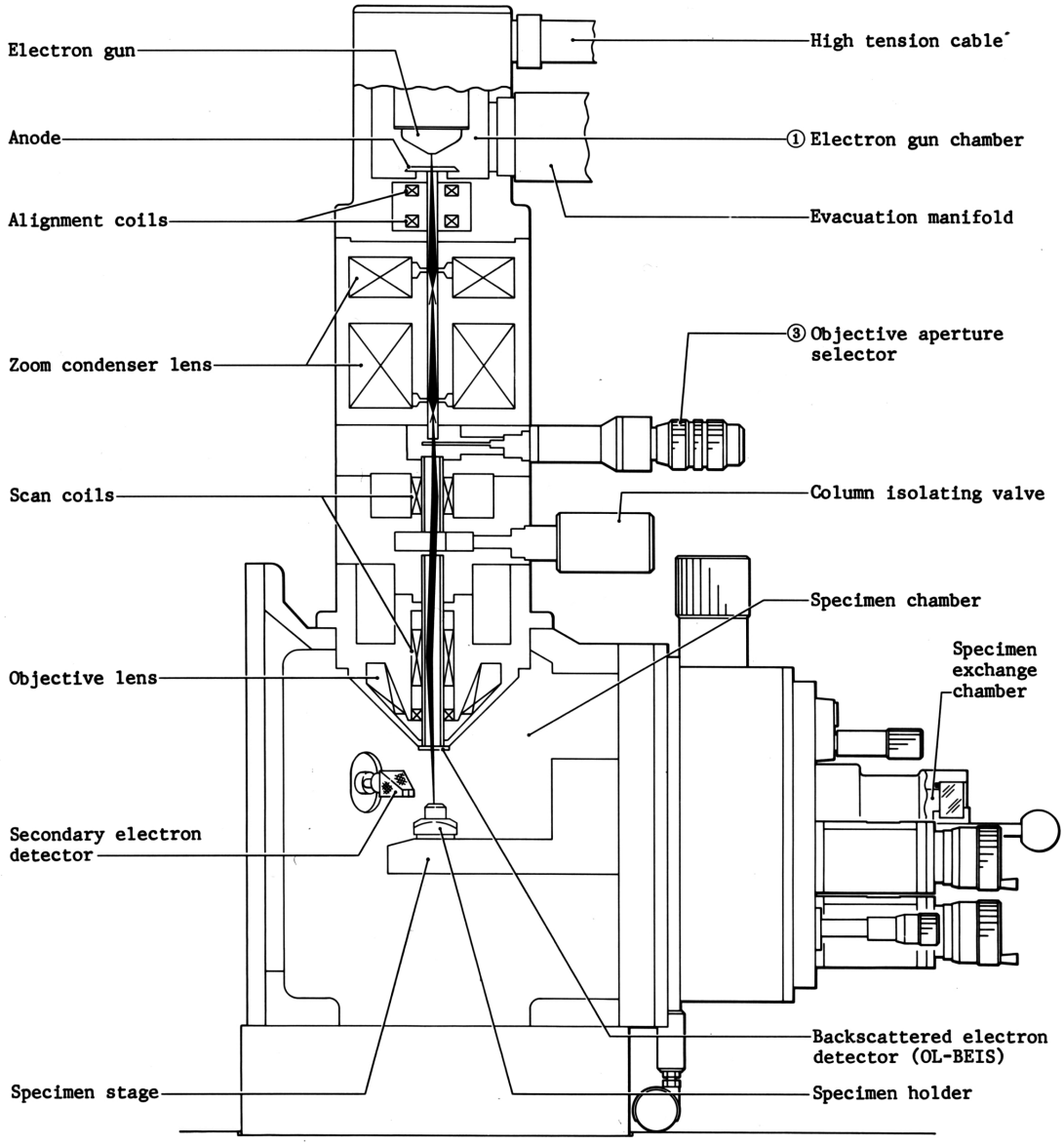

Figure 2.9. Cross-section of the JEOL JSM 840A column.

The SEM does not view a true image of the specimen, but rather produces an electronic map of the specimen. The secondary electrons are detected, converted to a voltage, and amplified. The amplified voltage is applied to the grid of the cathode ray tube (CRT) and causes the intensity of the spot of light to change. The scan rate for the electron beam can be increased so that the virtual 3-D image of the specimen can be viewed. By changing the width (w) of the electron beam, the magnification (M) can be changed where:

$$M = W / w \qquad \textbf{Equation 2.21}$$

and W is the width of the CRT. Since W is constant, the magnification can be increased by decreasing w.

The image consists of thousands of spots of varying intensity on the face of the CRT that correspond to the topography of the sample.

2.4.2.b. Microanalysis [74]

The instrument has an X-ray detector which collects the photons produced by the primary electron beam. The analyzed area is therefore the area covered by the beam. The characterization abilities of the X-ray detector are due to the fundamental principle that each element of the periodic table has a unique electronic structure and, consequently, a unique response to electromagnetic waves. The detector is able to determine the quantity of photon energy collected. A histogram of the number of photons received versus the photons energy could be plotted. The spectrums' interpretation is facilitated by a database which give the energy and intensity of the rays produced for each elements. It is also possible to select only few elements for the microanalysis. A bar chart showing the elements position and the amount of energy of their rays could be realised too.

2.4.2.c. Preparation of the samples and measurements

The samples were mounted on a metal stub (TAAB Laboratories Equipment Ltd, Reading, UK) using double sided sticky tape. Then, as the specimens are inundated by an influx of electrons a charge will tend to accumulate unless the specimen is earthed. This is typically achieved by coating objects with nanometer-thick layers of carbon or gold using a sputter coater (Edwards S150B). The coating does not make the sample itself conductive but helps to stop charging effects. For carbon coating, argon plasma is set up which coats all the surfaces it comes into contact with a very thin layer of carbon. Alternative coating with gold is possible although gold has a high atomic number and produces high topographic contrast and resolution but the information thus produced can obscure the underlying fine detail of the specimen under examination. The stub is then placed into the specimen holder, inside the microscope’s vacuum column through an air-tight door. The SEM images were acquired using a JEOL-JSM-840A SEM (JEOL), acceleration voltage 25 KeV, working distance 15 mm. The carbon coated samples were put into the SEM chamber under high vacuum. The SEM images were taken with charge-coupled device camera.

2.4.3. Infrared spectroscopy

2.4.3.a. Principle and apparatus

Introduction

Infrared spectroscopy (IR Spectroscopy) uses the infrared (wavelength range) region of the electromagnetic spectrum. As with all spectroscopic techniques, it can be used to identify a compound and to investigate the composition of inorganic compounds such as metal complexes. Among the basic spectroscopic techniques (transmission, internal reflection or attenuated total reflection (ATR), external

reflection, diffuse reflection, emission, and photoacoustic), two were used in this work – transmission and ATR – in order to assess the conformation of the biomolecule-containing materials.

General principle

Infrared spectroscopy detects the infrared intensity of vibrational characteristics of chemical functional groups in a sample versus wavelength (wavenumber) of light. When infrared light interacts with matter, chemical bonds will stretch, contract and bend. As a result, a chemical functional group tends to adsorb infrared radiation in a specific wavenumber range regardless of the structure of the rest of the molecule. The correlation of the band wavenumber position with the chemical structure is used to identify a functional group in a sample.

Table (2.4) below lists some characteristic infrared absorption band frequencies used to determine structures.

Table 2.4. Typical infrared absorption frequencies [75-76].

Functional class	Stretching vibrations			Bonding vibrations	
	Assignment	Range, cm^{-1}	Shape	Assignment	Range, cm^{-1}
Alcohol	OH free	3580-3650	sharp	O-H bending (in-plane)	1330-1430
	O-H (H-bonded)	3200-3550	broad	O-H bend (out-of-plane)	650-770
	C-O	970-1250			
Carboxylic acid and derivative	O-H	2500-3300 (acids) overlap C-H	broad	C-O-H bending	1395-1440
	C=O (H-bonded)	1705-1720 (acids)			
	C=O (H-non-bonded)	1700-1900			
	O-C	1210-1320 (acids)	sometimes 2 peaks		
	C=O	1735-1750 (esters)			
	O-C	1000-1300	2 bands		
Alkane	CH3, CH2 and CH	2800-3050	2 or 3 bands	CH2 & CH3 deformation	1350-1470
				CH3 deformation	1370-1390
				CH2 rocking	720-725

Conformational assessment of proteins by IR spectroscopy requires the investigation of the most intense absorption band in proteins, the amide I region (1590-1720 cm^{-1}) of the spectra that is sensitive

to changes in secondary structure and has been widely used for protein conformational studies [77-81]. From previous studies [77-83], the assignment of the peak maxima is known and listed in Table (2.5).

Table 2.5. Band assignments of amide I region.

Wavelength range, cm^{-1}	Secondary structure attribution
1695-1670	β-turn or β- sheet
1658-1645	α-helix
1648-1644	random chain
1635-1624	intramolecular β-sheet or extended chain
1622-1618	intermolecular β-sheet
< ~1613	side chain

Principle of Fourier Transform infrared transmission analysis

The IR radiation from the spectrometer passes through the KBr disk. After passing through the sample the measured signal is the interferogram. The detected interferogram can not be directly interpreted. It has to be "decoded" with a well-known mathematical technique, Fourier Transformation. Performing a mathematical Fourier Transform on this signal results in an infrared spectrum, which is a plot of transmittance versus wavenumber.

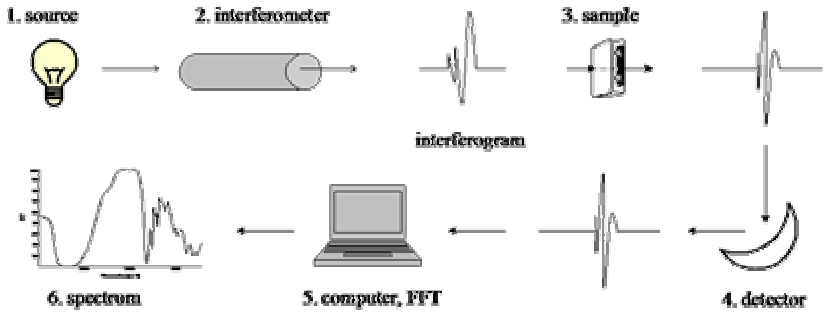

Figure 2.10. Schematic illustration of Fourier Transform infrared system.

When collecting infrared transmission data, samples are run as percentage of transmittance.

$$T(\%) = I / I_o \qquad \textbf{Equation 2.22}$$

where T is transmittance in percentage,

I is the intensity measured with a sample in the beam,

and I_0 is the intensity measured from the background spectrum.

The absorbance of the spectrum is equivalent to the transmittance and can be calculated from the transmittance spectrum using the following equation.

$$A = -\log_{10} T$$ **Equation 2.23**

where A is the absorbance.

In summary, the percentage of transmittance is similar to the absorbance. However, the use of the absorbance as a measure of the absorption is preferred to the use of the transmittance. Absorbance depends on the total quantity of the absorbing compound in the light path. A plot of absorbance against concentration shows a straight line passing through the origin (0, 0). The linear relationship between concentration and absorbance is both simple and straightforward, which is why we prefer the expression of the Beer-Lambert law using absorbance as a measure of the absorption rather than the transmittance.

Principle of Fourier Transform Attenuated Total Reflectance analysis (solid-state)

Attenuated total reflection implemented in Fourier Transform infrared (ATR-FTIR) spectroscopy is used for the analysis of the surface of materials. An attenuated total reflection accessory operates by measuring the changes that occur in a totally internally reflected infrared beam when the beam comes into contact with a sample. The infrared radiation is passed through an infrared transmitting crystal with a high refractive index, allowing the radiation to reflect within the ATR element one or more times. It then penetrates “into” the sample a finite amount with each reflection along the top surface via the so-called “evanescent” wave that decays exponentially as it moves away from the surface. In regions of the infrared spectrum where the sample absorbs energy, the evanescent wave will be attenuated or altered. The attenuated energy from each evanescent wave is passed back to the IR beam path of the spectrometer, which then exits the opposite end of the crystal and is passed to the detector in the IR spectrometer. The system then generates an infrared spectrum. From that step onwards, the data treatment is the same as for conventional transmission measurement. The type of crystal chosen depends on the spectral window required and sampling conditions. Zinc selenide (ZnSe) has a wide spectral window in the mid-IR range but can easily be damaged by strong acids or alkalis so germanium is used in such cases. The sampling surface is pressed into intimate optical contact with the top surface of the crystal.

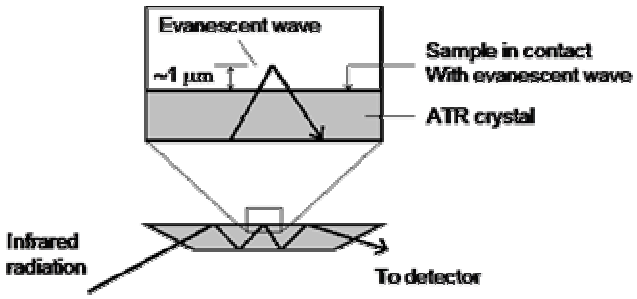

Figure 2.11. Total internal reflection at the interface of an internal reflection element. Depth of penetration of the evanescent wave is approximately 1 μm.

Compared to the infrared transmission analysis, the ATR crystal has the disadvantage of absorbing energy at much lower levels. If the sample does not have good contact with the crystal, the data will not be accurate. Most crystals have pH limitations. On the other hand, when an ATR accessory is used, most samples can be run in their natural state. The technique is easy and fast as no sample preparation is required.

Apparatus

All IR spectroscopy measurements were conduced using a Magna IR-750 infrared spectrometer (Thermo Nicolet) either by transmission IR or by ATR; experimental details for each set-up are given below.

Sample preparation - Measurements

- *Infrared transmission analysis*

A standard KBr disc technique was used. Each disc contained 2 mg of freeze dried sample mixed with ca. 198 mg of purified salt, KBr (Aldrich, FT-IR grade, ≥ 99 %) and pressed into a translucent disc using a die press operating at ca. 10 tonnes pressure per square metre. The beam of the spectrometer passed through the pellet and spectra were recorded at 4 cm^{-1} resolution, the interferometer speed set to 0.4747 $cm.s^{-1}$ with 128 scans recorded. Potassium bromide does not absorb infrared light, so spectral lines will only appear from the analyte. However, in order to prevent fluctuations in the output of the source affecting the data and to cancel out the effects of a 'parasite' compound present in a mixture, a sample of a blank potassium bromide pellet or of the pure 'parasite' compound is used as a reference. Its signal contribution to the acquired spectra is subtracted from the samples.

- *Fourier Transform attenuated total reflection analysis (solid-state)*

Samples were put down on the crystal in powdered form. The spectrometer was continuously purged with dry air/nitrogen for a minimum of 15 h prior to sample analysis. Characteristic bands around 3500 cm^{-1} and 1630 cm^{-1} are ascribed to atmospheric water vapour and the bands at 2350 cm^{-1} and 667 cm^{-1} are attributed to carbon dioxide. Prior to obtaining sample spectra, an open/beam background spectrum is collected in order to get rid of those two contributions from the clean ATR crystal. When an interferogram is measured with a sample and Fourier transformed, a sample single beam spectrum is obtained. It looks similar to the background spectrum except that the sample peaks are superimposed

upon the instrumental and atmospheric contributions to the spectrum. To eliminate these contributions, the sample single beam spectrum must be normalized against the background spectrum. Consequently, an absorbance spectrum is obtained in the same way as for transmission analysis.

In both infrared techniques used, the raw spectra were corrected for water vapour contributions. They were then truncated between 1720 and 1580 cm^{-1} (amide I bands) and curve fitted with Matlab software for the amide I band region. The number of bands was entered into the program along with their respective positions and half-heights estimated. The program iterated 1000 times the curve-fitting process by adjusting the peak high and width to achieve the best Gaussian-shaped curves that fit the original protein spectrum. Peak positions were estimated from the literature [77, 81], their variation being limited to ± 2 cm^{-1} during the fit. Protein secondary structure content was calculated from the area under the individually assigned bands and expressed as a percentage of total area in the amide I region. A representative example of the raw data and its peak fitting are shown in Figure (2.12).

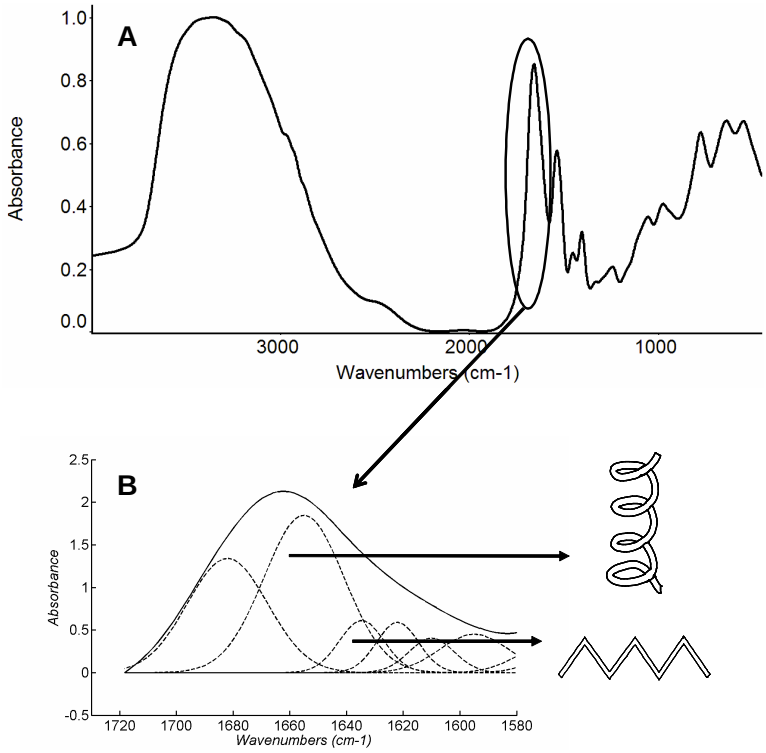

Figure 2.12. Example of infrared absorption spectrum (Al_{30}-mer - lysozyme 25 $mg.mL^{-1}$) (**A**). Enlargement of the amide I region is shown with the fitted peaks in dotted lines (**B**).

2.4.3.b. Two-dimensional correlation spectroscopy

Introduction

2D correlation spectroscopy is a popular tool in the analysis of IR spectra of proteins [84-87] where the spectral intensity is plotted as a function of two independent spectral variables, e.g., wavelength, frequency, or wavenumber. The two orthogonal axes of independent spectral variables define the 2D

spectral plane. One can enhance the spectral resolution and analyse complex or overlapped spectral features by spreading peaks along the second dimension [88]. Another other feature of two-dimensional correlation spectroscopy are the detection of the existence (or lack) of interactions among functional groups as probed through their molecular vibrations. The basic idea of 2D correlation spectroscopy is adaptable to any branch of spectroscopy, including Raman, NIR, fluorescence, X-ray, UV, etc [89]. In the present studies, the technique was applied to IR spectroscopy.

In a typical spectroscopic measurement carried out in one dimension, a selected electromagnetic probe is used by itself to study the system of interest. Characteristic interactions between the probe and constituents of the system are then analyzed in the form of a spectrum to elucidate detailed information about the system. 2D correlation spectroscopy utilizes an additional external perturbation (such as temperature [90, 91], pressure [84, 92], concentration [93, 94], stress [95] or electrical field [96]), applied during the spectroscopic measurement to stimulate the system of interest.

Principle of two-dimensional spectroscopy correlation analysis

- *Dynamic Spectrum.*

For a perturbation-induced change of the spectral intensity y (ν, t) observed during an interval of some external variable t between T_{min} and T_{max} , the external variable t is often the chronological time but can also be any other reasonable measure of physical quantity, such as temperature, pressure, concentration, voltage, etc., depending on the experiment. The spectral variable ν can be any appropriate index quantity used in spectroscopy; in the present work, infrared data. The dynamic spectrum $\tilde{y}$ (ν, t) of a system affected by the application of a perturbation is formally defined as:

$$\tilde{y}(\nu, t) = \begin{cases} y(\nu,t) - \tilde{y}(\nu) & \text{for } T_{min} \le t \le T_{max} \\ 0 & \text{otherwise} \end{cases} \qquad \textbf{Equation 2.24}$$

where $\tilde{y}$ (ν) is the reference spectrum of the system.

It is customary to set $\tilde{y}$ (ν) defined in Equation (2.25) as the reference spectrum.

$$\tilde{y}(\nu) = \frac{1}{T_{max} - T_{min}} \int_{T_{min}}^{T_{max}} y(\nu, t)\, dt \qquad \textbf{Equation 2.25}$$

- *Two-dimensional correlation function.*

The correlation spectrum can be expressed as:

$$X(\nu_1, \nu_2) = \left\langle \tilde{y}(\nu_1, t), \tilde{y}(\nu_2, t') \right\rangle \qquad \textbf{Equation 2.26}$$

The common 2D correlation intensity X (ν_1, ν_2) represents the measure of a functional comparison of spectral intensity variations *y* (ν, *t*) measured at different spectral variables, ν_1 and ν_2, during a fixed interval of the external variable *t.*

In our case, samples at different aluminium concentrations were measured, and the resulting matrix of absorbance measurements was correlated with itself (autocorrelation). The correlation properties between the vector ν_1 including a series of absorbances recorded to one wavelength and a vector ν_2 representing a series of absorbances recorded to another (or to the same) wavelength were resumed in the synchronous (real correlation) and asynchronous (imaginary number, with a phase difference). The symbol $\langle\ \rangle$ denotes any one of a class of mathematical operations, known as correlation functions, which are designed to compare the dependence of two chosen quantities on *t.* The fact that the correlation function defined by Equation (2.26) is calculated between the spectral intensity variations measured at two independent spectral variables ν_1 and ν_2 leads to the two-dimensional nature of this particular correlation analysis.

A simple convention is adopted to treat $X(\nu_1,\nu_2)$ as a complex number comprising two orthogonal (i.e., real and imaginary) components, known, respectively, as the synchronous and asynchronous two-dimensional correlation intensity.

$$X(\nu_1,\nu_2) = \Phi(\nu_1,\nu_2) + i\Psi(\nu_1,\nu_2) \qquad \textbf{Equation 2.27}$$

The synchronous two-dimensional correlation intensity $\Phi(\nu_1, \nu_2)$ represents the overall similarity between two separate spectral intensity variations measured at different spectral variables, as the value of *t* is changed. The asynchronous two-dimensional correlation intensity $X(\nu_1,\nu_2)$, on the other hand, may be regarded as a measure of dissimilarity of the spectral intensity variations.

A simplified form of the two-dimensional correlation function is known as the generalized two-dimensional correlation spectrum.

- *Generalized two-dimensional correlation.*

The generalized two-dimensional correlation formally defines the synchronous and asynchronous correlation intensity as:

$$X(\nu_1,\nu_2) = \frac{1}{\pi\,(T_{max} - T_{min})} \times \int_0^{\infty} Y_1(\omega)\, d\omega \qquad \textbf{Equation 2.28}$$

The term $\tilde{Y}_1(\omega)$ is the forward Fourier transform (FT) of the spectral intensity variations $\tilde{y}(\nu_1, t)$ observed at some spectral variable ν_1. It is given by:

$$\tilde{Y}_1(\omega) = \int_{-\infty}^{\infty} \tilde{y}(\nu_1,t)\, e^{-i\omega t}\, dt \qquad \textbf{Equation 2.29}$$

The Fourier frequency ω represents the individual frequency component of the variation of $\tilde{y}(\nu_1, t)$ measured along the external variable *t.* Likewise, the conjugate of the Fourier transform $\tilde{Y}_2^*(\omega)$ of spectral intensity variation $\tilde{y}(\nu_2, t)$ observed at spectral variable ν_2 is given by:

$$\tilde{Y}_2^*(\omega) = \int_{-\infty}^{+\infty} \tilde{y}(v_2, t)\, e^{-i\omega t}\, dt \qquad \textbf{Equation 2.30}$$

- *Numerical computation of two-dimensional spectra.*

For a set of m traces of dynamic spectra collected during the interval between T_{min} and T_{max}, along the variable t at every equally spaced increment, $\Delta t = (T_{max} - T_{min})/(m / 1)$, the synchronous 2D correlation intensity is given by a simple expression [97-98]:

$$\Phi(v_1, v_2) = \frac{1}{m-1} \sum_{j=1}^{m} \tilde{y}_j(v_1)\ \tilde{y}_j(v_2) \qquad \textbf{Equation 2.31}$$

where $\tilde{y}_j(v_i)$ is the spectral intensity at a point of physical variable t_j.

$$\tilde{y}_j(v_t) = \tilde{y}(v_t, t_j) \quad i = 1,2 \qquad \textbf{Equation 2.32}$$

The computation of asynchronous two-dimensional correlation intensity is somewhat more complicated. There are many different ways to estimate the asynchronous spectrum [97]. While these methods all give quite adequate estimation of the asynchronous two-dimensional correlation intensity, probably the simplest and most computationally efficient method currently available to estimate the asynchronous spectrum [98-99] is given by:

$$\Psi(v_1, v_2) = \frac{1}{m-1} \sum_{j=1}^{m} \tilde{y}_j(v_1) \sum_{k=1}^{m} N_{jk}\ \tilde{y}_k(v_2) \qquad \textbf{Equation 2.33}$$

The term N_{jk} corresponds to the jth row and kth column element of the discrete Hilbert - Noda transformation matrix given by:

$$N_{jk} = \begin{cases} 0 & \text{if } j = k \\ 1/\pi(k, j) & \text{otherwise} \end{cases} \qquad \textbf{Equation 2.34}$$

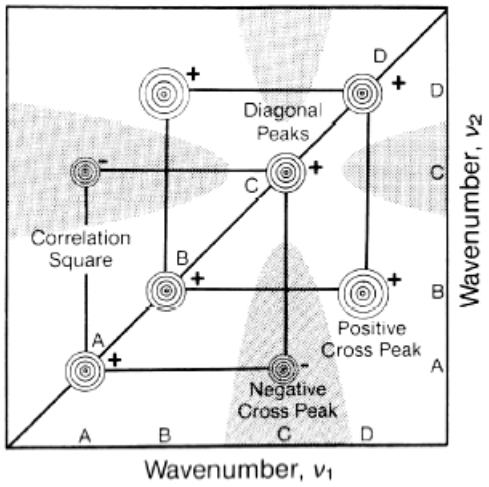

Figure 2.13. Schematic contour map of a synchronous two-dimensional correlation spectrum. Shaded areas indicate negative correlation intensity. The signs '+' and '-' refer to positive and negative peaks respectively (from [88]).

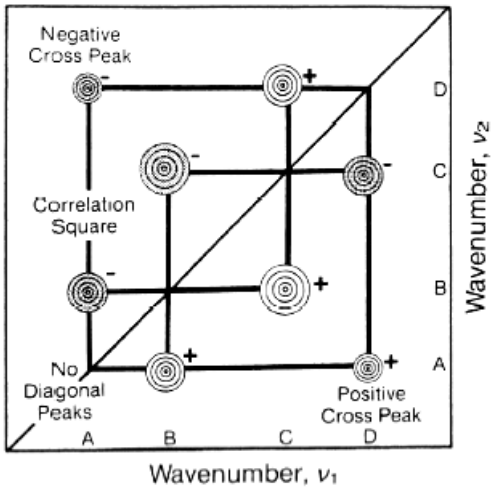

Figure 2.14. Schematic contour map of an asynchronous two-dimensional correlation spectrum. Shaded areas indicate negative correlation intensity. The signs '+' and '-' refer to positive and negative cross peaks respectively (from [88]).

Properties of two-dimensional correlation spectra

- *Synchronous spectrum*

The intensity of a synchronous two-dimensional correlation spectrum $\Phi(\nu_1, \nu_2)$ represents the simultaneous or coincidental changes of spectral intensity variations measured at ν_1 and ν_2 during the interval between T_{min} and T_{max} of the externally defined variable *t.* Figure (2.13) shows a schematic example of a synchronous two-dimensional correlation spectrum plotted as a contour map. A synchronous spectrum is a symmetric spectrum with respect to a diagonal line corresponding to coordinates $\nu_1 = \nu_2$. Correlation peaks appear at both diagonal and off-diagonal positions.

The intensity of peaks located at diagonal positions corresponds mathematically to the autocorrelation function of spectral intensity variations observed during an interval between T_{min} and T_{max}. The

diagonal peaks are therefore referred to as autopeaks. An autopeak shows the overall susceptibility of the spectral region to change in spectral intensity as an external perturbation is applied to the system.
The magnitude of an autopeak intensity, which is always positive, represents the overall extent of spectral intensity variation observed at the specific spectral variable ν during the observation interval between T_{min} and T_{max}.
Cross peaks located at the off-diagonal positions of a synchronous two-dimensional spectrum represent simultaneous or coincidental changes of spectral intensities observed at two different spectral variables, ν_1 and ν_2. It suggests the existence of a related origin of the spectral intensity variations.
The sign of cross peaks can be either positive or negative. The sign of synchronous cross peaks becomes positive if the spectral intensities at the two spectral variables corresponding to the coordinates of the cross peak are either increasing or decreasing together as functions of the external variable *t* during the observation interval. On the other hand, a negative sign of cross peaks indicates that one of the spectral intensities is increasing while the other is decreasing.

- *Asynchronous spectrum.*

The intensity of an asynchronous spectrum represents sequential, or successive, changes of spectral intensities measured at ν_1 and ν_2. Unlike a synchronous spectrum, an asynchronous spectrum is antisymmetric with respect to the diagonal line. The asynchronous spectrum has no autopeaks, consisting exclusively of cross peaks located at off-diagonal positions.
An asynchronous cross peak develops only if the intensities of two spectral features change out of phase (i.e., delayed or accelerated) with each other. This feature is especially useful in differentiating overlapped bands arising from spectral signals of different origins.
The sign of an asynchronous cross peak becomes positive if the intensity change at ν_1 occurs predominantly before ν_2 in the sequential order of *t.* It becomes negative, on the other hand, if the change occurs after ν_2. This rule, however, is reversed if $\Phi(\nu_1, \nu_2) < 0$.

2.4.1.c. Additional development in two-dimensional correlation spectroscopy: Chemometrics

In order to attain optimal measurements and to provide maximum chemical information by analyzing chemical data [100-102], chemometrics has been used by others in combination with generalised two-dimensional correlation spectroscopy. Chemometrics can use mathematical and statistical methods [100-102]. In the present work, an abstract factor analysis known as principal component analysis (PCA) was undertaken [103]. PCA acts as a filter which reconstructs less noisy data.

This technique, likewise the two-dimensional correlation spectroscopy, uses mathematical operations based on the manipulation of data using standard matrix algebra. Basically, the original spectral data matrix is decomposed into a set of a small number of underlying factors, often expressed as a product of score and loading vector matrices [100-102]. Typically, the number of factors needed to describe a dynamic spectral data set will be more than one [89]. The number of significant factors involved in the

description of a data matrix was chosen on the basis of preliminary processing experiments which showed that, with the raw matrix rank of four, the asynchronous 2D correlation spectra had significant features. The number of factors was set to four. This technique is especially well suited for the identification of the number of factors governing the data structure and also for the effective identification and rejection of noise components from a raw spectral data set prior to two-dimensional correlation analysis.

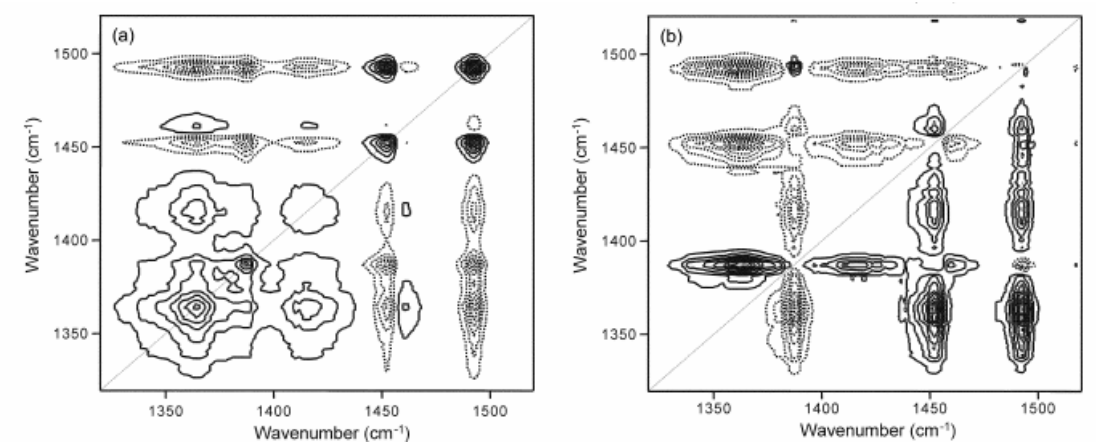

Figure 2.15. Conventional synchronous (**a**) and asynchronous (**b**) 2D correlation spectra obtained from raw spectra. Solid and dashed lines represent positive and negative cross peaks, respectively (spectra from [104]).

Figure (2.15 (a) and (b)) illustrates the synchronous and asynchronous two-dimensional correlation spectra constructed directly from the noisy dynamic spectra (raw data). While the synchronous spectrum (Figure 2.15 (a)) shows relatively little effect of noise, the corresponding asynchronous spectrum (Figure 2.15 (b)) is markedly contaminated with numerous speckles of superfluous correlation intensity spikes, caused by the unintended correlation of noise contributions.

Figure (2.15 (a) and (b)) displays synchronous and asynchronous two-dimensional correlation spectra derived from the PCA-reconstructed data. Clearly, the spectra are well conserved without curve, and peaks are present in a manner similar to those directly obtained from the original data but with much less effect of noise. Noise-induced speckles observed in Figure 2.15 (b) are virtually all removed.

2.5. References

[1] G. Tracy, W. H. Welker, J. Biol. Chem., 1915, 22, 55.

[2] R. Flarend, T. Bin, D. Elmore, S. L. Hem, Food Chem. Toxicol., 2001, 39, 163.

[3] J. J. Fitzgerald, A. H. Rosenberg, Marcel Dekker, 1999; chapter 4 Chemistry of Aluminum Chlorohydrate and Activated Aluminum Chlorohydrates, pp. 83-137.

[4] J. J. Fripiat, Catal. Today, 1988, 2, 28.

[5] M. A. Vicente, J. F. Lambert, Phys. Chem. Chem. Phys., 1999, 1, 1633.

[6] M. L. Occelli, A. Bertrand, S. Gould, J. M. Dominguez, Microporous Mesoporous Mater., 2000, 34, 195.

[7] J. Duan, J. Gregory, Adv. Colloid Interface Sci., 2003, 100-102, 475.

[8] C. T. Driscoll, in G. Sposito (Ed.), The Environmental Chemistry of Aluminium, CRC Press, 1989, p. 241.

[9] R. W. Smith, Coord. Chem. Rev., 1996, 149, 81.

[10] M. Wang, M. Muhammed, Nanostruct. Mater., 1999, 11, 8, 1219.

[11] S. L. Wang, M. K. Wang, Y. M. Tzoua, Colloids Surf., A, 2003, 231, 143.

[12] J. M. Fraile, J. A. Mayoral, A. J. Royo, Tetrahedron, 1996, 52, 9853.

[13] J. B. Hannon, S. Kodambaka, F. M. Ross, R. M. Tromp, Nature, 2006, 440, 69.

[14] S. Goldberg, J. A. Davis, J. D. Hem, in G. Sposito (Ed.), The Environmental Chemistry of Aluminum, CRC Press, 1989, Chapter 7, p. 271.

[15] K. Wefers, G. M. Bell, Oxides and Hydroxides of Aluminum, Technical Paper No. 19, Alcoa Research Laboratories, 1972.

[16] C. J. Brinker, G. W. Scherer, in: Sol–Gel Science. The Physics and Chemistry of Sol–Gel Processing, Academic Press, San Diego, 1990, p. 21.

[17] S. L. Hem, J. L. White, in: Vaccine Design - The Subunit and Adjuvant Approach, Plenum Press, New York, 1995, p. 249.

[18] P. M. Huang, M. K. Wang, N. Kampf, D. G. Schulze, in: J. B. Dixon, D. G. Schulze (Eds.), Soil Mineralogy with Environmental Applications, Soil Science Society of America, Madison, WI, 2002, p. 261.

[19] G. L. Kerven, P. L. Larsen, F. P. Blamey, C. Soil Sci. Soc. Am. J., 1995, 59, 765.

[20] D. R. Parker, P. M. Bertsch, Environ. Sci. Technol., 1992, 26, 914.

[21] D. Hunter, D. S. Ross, Science, 1991, 251, 1056.

[22] G. Furrer, B. Trusch, C. Muller, Geochim. Cosmochim. Acta, 1992, 56, 3831.

[23] R. J. P. Williams, Coord. Chem. Rev., 1996, 141, 1 and articles within the volume.

[24] J. T. Kloprogge, J. Porous Mater., 1998, 5, 5.

[25] N. Yao, G. Xiong, Y. Zhang, M. He, W. Yang, Catal. Today, 2001, 68, 97.

[26] J. J. Fitzgerald, In Antiperspirants and Deodorants; Marcel Dekker: New York; 1988, p. 119.

[27] S. M. Bradley, R. A. Kydd, J. Catal., 1993, 142, 448.

[28] J.-H. Son, H. Choi, Y.-U. Kwon, O.H. Han, J. Non-Cryst. Solids, 2003, 318, 186.

[29] C. F. Baes, R. E. Mesmer, in: The Hydrolysis of Cations, pp. 112–122, John Wiley, New York (1976).

[30] C. K. Jørgensen, Adv. Chem. Phys., 1963, 5, 33.

[31] A. Bell, E. Matijevic, J. Inorg. Nucl. Chem., 1975, 37, 907.

[32] E. Matijevic, Ann. Rev. Mater. Sci., 1985, 15, 483.

[33] R. E. Mesmer, C. F. Baes, Inorg. Chem., 1971, 10, 2290.

[34] J. J. Depuech, in NMR of Newly Accessible Nuclei, ed. P. Laszlo, vol. 2, pp. 153–195, Academic Press, New York (1983).

[35] P. M. Bertsch, M. A. Anderson, Anal. Chem., 1989, 62, 535.

[36] G. Johansson, Acta Chem. Scand., 1960, 14, 771.

[37] C. L. Rollinson, Chemistry of the Coordination Compounds, Vol. 131, Am. Chem. Soc. Master. Ser., Bailar Ed., New York, 1956, p.448.

[38] J. Jolivet, Metal Oxide Chemistry and Synthesis. From Solution to Solid State, Wiley and Sons, 2000.

[39] J. P. Jolivet, De La Solution A l'Oxyde, InterEditions-CNRS, Paris, 1994.

[40] M. Henry, J. P. Jolivet, J. Livage, Struct. Bond., 1992, 77, 153.

[41] S. Bi, C. Wang, Q. Cao, C. Zhang, Coord. Chem. Rev., 2004, 248, 441.

[42] K. Shafran, Chemical and structural studies of aluminium and zirconium aqueous chemistry Ph.D. thesis, Nottingham Trent University, 2003.

[43] W. H. Casey, B. L. Phillips, G. Furrer, Chapter Aqueous Aluminum Polynuclear Complexes and Nanoclusters: A Review, 2002, pp. 166-190.

[44] W. H. Casey, Chem. Rev. C, 2006, 106, 1.

[45] Jorgensen, L. Salem, in: The Organic Chemist's Book of Orbitals, Academic Press, 1973.

[46] J. Kragten, Atlas of Metal Ligand Equilibrium in Aqueous Solution, J. Wiley & Sons, Chichester, 1978.

[47] C. Brosset, Acta Chem. Scand., 1952, 6, 910.

[48] C. Brosset, G. Biedermann, L. Sillen, Acta Chem. Scand., 1954, 8, 1917.

[49] P. Hsu, C. Rich, Soil Science Society of America Proceedings, 1960, 24, 21.

[50] P. Hsu, T. Bates, Mineralogy Magazine, 1964, 33, 749.

[51] R. Stol, A. Van Helden, P. Bruyn, J. Colloid Interface Sci., 1976, 57, 115.

[52] R. Letterman, S. Asolekar, Water Res., 1990, 24, 931.

[53] P. M. Bertsch, in: G. Sposito (Ed.), The Environmental Chemistry of Aluminum, CRC Press, Boca Raton, 1989, pp. 117.

[54] P. H. Hsu, in: J.B. Dixon, S.B. Weeds (Eds.), Minerals in Soil Environment, Soil Science Society of America, Madison, WI, 1989, p. 331.

[55] G. Johansson, Acta Chem. Scand., 1962, 16, 403.

[56] G. Johansson, Ark. Kemi., 1963, 20, 321.

[57] J. W. Akitt, N. N. Greenwood, B. L. Khandelwal, G. D. Lester, J. Chem. Soc. Dalton Trans., 1972, 604.

[58] J. Y. Bottero, M. Axelos, D. Tchoubar, J. M. Cases, J. J. Fripiat, F. Fiessinger, J. Colloid Interface Sci., 1987, 117, 47.

[59] J. Y. Bottero, J. M. Cases, F. Fiessinger, J. E. Poirier, J. Phys. Chem., 1980, 84, 2933.

[60] J. W. Akitt, A. Farthing, J. Chem. Soc., Dalton Trans., 1981, 1606.

[61] L. Allouche, C. Gérardin, T. Loiseau, G. Férey, F. Taulelle, Angew. Chem. Int. Ed., 2000, 39, 511.

[62] J. A. Tosell, Geochim. Cosmochim. Acta, 2001, 65, 2549.

[63] W. V. Rausch, H. D. Bale, J. Chem. Phys., 1964, 40, 3391.

[64] H. Stünzi, L. Spiccia, F. P. Rotzinger, W. Marty, Inorg. Chem., 1989, 28, 66.

[65] L.-O. Ohman, W. Forsling, Acta Chem. Scand. A, 1981, 35, 795.

[66] T. Hedlund, S. Sjoberg, L.-O. Ohman, Acta Chem. Scand., 1987, 41, 197.

[67] J. W. Akitt, Prog. Nucl. Magn. Reson. Spectrosc., 1989, 21, 1.

[68] A. Hulanicki, R. Lewandowaki, A. Lewenstam, M. Chmurska, H. Matuszak, Mikrochim. Acta, 1985, 3, 253.

[69] N. Zhou, Y. Gu, Z. Lu, W. Chen, Talanta, 1985, 32, 1119.

[70] H. T. Evans, Inorg. Chem., 1966, 5, 967.

[71] J. W. Akitt, A. Farthing, J. Chem. Soc. Dalton, 1981, 1617.

[72] J.Y. Bottero, D. Tchoubar, J. M. Cases, F. Fiessinger, J. Phys. Chem., 1982, 86, 3667.

[73] W. V. Rausch, H. D. Bale, J. Chem. Phys., 1964, 40, 3391.

[74] D. W. Schaefer, R. A. Shellman, K. D. Keefer, J. E. Martin, Physica, 1986, 104A, 105.

[75] A. V. Plyasunov, I. Grenthe, Geochim. Cosmochim. Acta, 1994, 58, 3561.

[76] J. Rowsell, L.F. Nazar, J. Am. Chem. Soc., 2000, 122 (15), 3777.

[78] G. Johansson, G. Lundgren, L. G. Sillén, R. Söderquist, Acta Chem. Scand., 1960, 14, 769.

[77] L. Allouche, F. Taulelle, Inorg. Chem. Commun., 2003, 6, 1167.

[79] L. Allouche, C. Huguenard, F. Taulelle, J. Phys. Chem. Solids, 2001, 62, 525.

[80] S. M. Bradley, R. A. Kydd, R. F. Howe, J. Colloid Interface Sci., 1993, 159, 405.

[81] K. Wafers, C. Misra, Oxides and Hydroxides of Aluminium, Alcoa Technical Paper 19, revised 1987, Alcoa Technical Center, Alcoa, PA.

[82] P. H. Hsu, T. F. Bates, Miner. Mag., 1964, 33, 749.

[83] A. E. Nielsen, Kinetics of Precipitation, Pergamon Press, Oxford, 1964.

[84] V. K. La Mer, R. H. Dinegar, J. Am. Chem. Soc., 1950, 72, 4847.

[85] T. Sugimoto, Adv. Colloid Interface Sci., 1987, 28, 65.

[86] M. Haruta, B. Delmon, J. Chim. Phys., 1986, 83, 859.

[87] S. M. Bradley, R. A. Kydd, Catalysis Letters, 1991, 8, 185-192.

[88] E. Montarges, A. Moreau, L. J. Michot, Appl. Clay Sci., 1998, 13, 165.

[89] J. Gregory, J. Duan, Pure Appl. Chem., 2001, 73, 2017.

[90] C. C. Perry, K. L. Shafran, Journal Inorg. Biochem., 2001, 87, 115.

[91] K. L. Shafran, C. C. Perry, J. Chem. Soc., Dalton Trans., 2005, 2098.

[92] G. Berthon, Coord. Chem. Rev., 1996, 149, 241.

[93] W. R. Harris, G. Berthon, J. P. Day, C. Exley, T. Peder Flaten, W. F. Forbes, T. Kiss, C. Orvig, P. F. Zatta, J. Toxicol. Environ. Health, 1996, 48, 543.

[94] K. Rezwan, L. P. Meier, M. Rezwan, J. Voros, M. Textor, L. J. Gauckler, Langmuir, 2004, 20, 10055.

[95] A. J. Downs, in: Chemistry of Aluminium, Gallium, Indium, and Thallium, 1993, Springer.

[97] G. Van Landeghem, M. E. De Broe,P. C. D'Haese1, Clin. Biochem., 1998, 31, 385.

[98] B. Corain, G. G. Bombi, A. Tapparo, M. Perazzolo, P. Zatta, Coord. Chem. Rev., 1996, 149, 11.

[99] E. De Voto, R. A. Yokel, Environ. Health Perspect., 1994, 102, 940.

[100] M. Venturini, G. Berthon, J. Chem. Soc. Dalton Trans., 1987, 1, 145.

[101] S.-P. Bi, X.-D. Yang, F.-P. Zhang, X.-L. Wang, G.-W. Zou, Fresenius J. Anal. Chem., 2001, 370, 984.

[103] R. J. P. Williams, Coord. Chem. Rev., 2002, 228, 93.

[104] R. A. Yokel, Coord. Chem. Rev., 2002, 228, 97.

[105] X. Yang, Q. Zhang, L. Li, R. Shen, J. Inorg. Biochem., 2007, 101, 1242.

[106] A. K. Powell, S. L. Heath, Coord. Chem. Rev., 1996, 149, 59.

[107] P. Rubini, A. Lakatos, D. Champmartin, T. Kiss, Coord. Chem. Rev., 2002, 228, 137.

[107] G. D. Fasman, Coord. Chem. Rev., 1996, 149, 125.

[109] C. Exley, J. Inorg. Biochem., 1999, 76, 133.

[110] Z. M. Shen, A. Perczel, M. Hollbi,I. Nagypd1, G. D. Fasman, Biochemistry, 1994, 33, 9627.

[111] D. Drago, M. Bettella, S. Bolognin, L. Cendron, J. Scancar, R. Milaci, F. Ricchelli, A. Casini,

[112] M. Farina, F. S. Lara, R. Branda, R. Jacques, J. B. T. Rocha, Toxicol. Lett., 2002, 132, 131. L. Messori, G. Tognon, P. Zatta, Int. J. Biochem. Cell Biol., 2008, 40, 731.

[113] T. B. Drticke, Life Chem. Rep., 1994, 11, 231.

[114] T. B. Drueke, Nephrol. Dial. Transplant., 2002, 17(Suppl 2), 13.

[115] E. Bonucci, P. Ballanti, S. Berni, C. Della Rocca, Life Chem. Rep., 1994, 11, 225.

[116] P. Zatta, Trace Elem. Med., 1993, 10, 120.

[117] M. Suwalsky, B. Norris, T. Kiss, P. Zatta, Coord. Chem. Rev., 2002, 228, 285.

[118] T. Kiss, M. Kilyén, A. Lakatos, F. Evanics, T. Körtvélyesi, Gy. Dombi, Zs. Majer, M. Hollósi, Coord. Chem. Rev., 2002, 228, 227.

[119] A. Salifoglou, Coord. Chem. Rev., 2002, 228, 297.

[120] G. Lupidi, M. Angeletti, A. M. Eleuteri, E. Fioretti, S. Marini, M. Gioia, M. Coletta, Coord. Chem. Rev., 2002, 263.

[121] G. Berthon, Coord. Chem. Rev., 2002, 228, 319.

[122] M. R. Wills, J. Savory, Lancet, ii, 1983, 29.

[123] S. Daydé, M. Filella, G. Berthon, J. Inorg. Biochem., 1990, 38, 241.

[124] D. R. Crapper, S. S. Krishnan, A. J. Dalton, Science, 1973, 180, 511.

[125] D. P. Perl, A. R. Brody, Science, 1980, 208, 297.

[126] P. Zatta, Trace Elem. Med., 1993, 10, 120.

[127] G. D. Fasman, Coord. Chem. Rev., 1996, 149, 125.

[128] D. Drago, M. Bettella, S. Bolognin, L. Cendron, J. Scancar, R. Milacic, F. Ricchelli, A. Casini, L. Messori, G. Tognon, P. Zatta, Int. J. Biochem. Cell Biol., 2008, 40, 731.

[129] A. E. Martell, R. D. Hancock, R. M. Smith, R. J. Motekaitis, Coord. Chem. Rev., 1996, 149, 311.

[130] M. Deleers, J. Servais, E. Wulfert, Biochim. Biophys. Acta, 1986, 855, 271.

[131] M. Favarato, P. Zatta, M. Perazzolo, L. Fontana, M. Nicolini, Brain Res., 1995, 569, 330.

[132] P. Zambenedetti, F. Tisato, B. Corain, P. Zatta, Biometals, 1994, 7, 244.

[133] D. J. Jones, L. V. Kochian, FEBS Lett., 1997, 400, 51.

[134] P. Zatta, T. Kiss, M. Suwalsky, G. Berthon, Coord. Chem. Rev., 2002, 228, 271.

[135] Y. Shi, H. HogenEsch, F. E. Regnier, S. L. Hem, Vaccine, 2001, 19, 1747.

[136] L. S. Burrella, C. T. Johnstonb, D. Schulzeb, J. Kleinc, J. L. Whiteb, S. L. Hem, vaccine, 2001, 19, 275.

[137] S. J. Seeber, J. L. White, S. L. Hem, Vaccine, 1991, 9, 201.

[138] J. M. Heimlich, F. E. Regnier, J. L. White, S. L. Hem, Vaccine, 1999, 17, 2873.

[139] R. K. Gupta, B. Rost, E. Relyveld, G. R. Siber, in: M. Powell, M. Newman, editors. Vaccine design: The subunit and adjuvant approach. New York: Plenum, 1995. p. 229.

[140] M.-F. Chang, J. L. White, S. L. Nail, S. L. Hem, PDA J. Pharm. Sci. technol., 1997, 51, 25.

[141] E. Bergfors, B. Trollfors, A. Inerot, Vaccine, 2003, 22, 64.

[142] R. M. Garrels, F. T. Mackenzie, C. Hunt, Chemical Cycles and the Global Environment. W. Kaufmann Inc., Los Altos, CA, 1975.

[143] G. Favero, P. Jobstraibizer, Coord. Chem. Rev., 1996, 149, 367.

[144] C. J. Lind, J. D. Hem, Effects of organic solutes on chemical reactions of aluminum. U.S. Geol. Surv. Water Supply Paper, 1827-G, Washington, DC, 1975, p. 83.

[145] C. E. Roberson, J. D. Hem, Solubility of aluminum in the presence of hydroxide, fluoride, and sulfate. U. S. Geol. Surv. Water Supply Paper, 1827-C, Washington, DC, 1969, p. 37.

[146] R. W. Smith, Coord. Chem. Rev., 1996, 149, 81.

[147] B. C. Faust, W. B. Labiosa, K'O H. Dai, J. S. Macfall, B. A. Browne, A. A. Ribeiro, D. D. Richter, Geochim. Cosmochim. Acta, 1995, 59, 13, 2651.

[148] K. M. Elkins, D. J. Nelson, Coord. Chem. Rev., 2002, 228, 205.

[149] M. J. Pianna, K. O. Zahir, J. Environ. Sci. Health Part B, 2000, 35, 87.

[150] J. Luster, T. Lloyd, G. Sposito, in: N. Senesi, T. M. Miano (Eds.), Humic Substances in the Global Environment and Implications on Human Health, Elsevier Science, 1994, pp. 1019.

[151] K. M. Elkins, D. J. Nelson, J. Inorg. Biochem., 2001, 87, 81.

[152] N. M. Johnson, Science, 1979, 204, 497.

[153] W. Dickson, Verh. Internat Verein Limnol., 1978, 20, 851.

[154] C. S. Cronan, C. L. Schofield, Science, 1979, 204, 304.

[155] (a) C. T. Drisdoll, Environ. Health Perspect., 1985, 63, 93; (b) Y. Shi, H. HogenEsch, F. E. Regnier, S. L. Hem, Vaccine, 2001, 19, 1747; (c) J. Duan, J. Gregory, Adv. Colloid Interface Sci., 2003, 100, 475; (d) Z. Chen, B. Fan, X. Peng, Z. Zhang, J. Fan, Z. Luan, Chemosphere, 2006, 64, 912.

[156] J. Duan, J. Gregory, Adv. Colloid Interf. Sci., 2003, 100-102, 475.

[157] Z. Chen, B. Fan, X. Peng, Z. Zhang, J. Fan, Z. Luan, Chemosphere, 2006, 64, 912.

[158] J.-P. Boisvert, C. Jolicoeur, Colloids Surf., A Physicochemical and Engineering Aspects, 1999, 155, 161.

[159] G. Furrer, B. L. Phillips, K. Ulrich, R. Pöthig, W. H. Casey, Science, 2002, 297, 2245.

[160] D. R. Parker, T. B. Kinraide, L. W. Zelazny, Soil Science Society of America Journal, 1989, 53, 789.

[161] J. Comin, J. Barloy, G. Bourrie, F. Trolard, European Journal of Agronomy, 1999, 11, 115.

[162] O. Deschaume, K. L. Shafran, C. C. Perry, Langmuir, 2006, 22, 10078.

[163] E. Bergfors, B. Trollfors, A. Inerot, Journal of Allergy and Clinical Immunology, 2004, 113, S294.

[164] J. Berkowitz, M. A. Anderson, R. C. Graham, Water Res., 2005, 39, 3918.

[165] R. A. Yokel, P. Ackrill, E. Burgess, J. P. Day, J. L. Domingo, T. P. Flaten, J. Savory, J. Toxicol. Environ. Health, 1996, 48, 667.

[166] D. L. Jones, A. M. Prabowo, L. V. Kochian, Plant and Soil, 1996, 182, 2, 229.

[167] T. Yokoyama, H. Abe, T. Kurisaki, H. Wakita, Anal. Sciences, 1999, 15, 969.

[168] J. W. Akitt, B. E. Mann, J. Magn. Reson., 1981, 44, 584.

[169] J. W. Akitt, N. B. Milic, J. Chem. SOC.Dalton Trans., 1984, 981.

[170] S. J. Karlik, E. Tarien, G. A. Elgavish, G. L. Eichhorn, Inorg. Chem., 1983, 22, 525.

[171] P. O. Astrand, E. Hultman, A. Juhlin-Dannfelt, G. Reynolds, Journal of Applied Physiology, 1986, 61, 338.

[172] J. F .Ma, S. Hiradate, H. Matsumoto, Plant. Physiol., 1998, 117, 753.

[173] I. Sóvágó, in: Biocoordination Chemistry, ed. K. Burger, Ellis Horwood, NewYork, 1990, p. 135.

[174] R. S. Dickins, C. S. Love, H. Pushmann, Chem. Commun., 2001, 2308.

[175] E. Rakotonarivo, C. Tondre, J. Y. Bottero, J. Mallavialle, J. Water Research, 1989, 23, 137.

[176] K. Gajda-Schrantz, L. Nagy, T. Fiore, L. Pellerito, T. Gajda, J. Chem. Soc., Dalton Trans., 2002, 152.

[177] J. F .Ma, S. Hiradate, K. Nomoto, T. Iwashita, H. Matsumoto, Plant. Physiol., 1997, 113, 1033.

[178] J. F. Ma, S. J. Zheng, H. Matsumoto, S. Hiradate, Nature, 1997, 390, 569.

[179] A. Masion, F. Thomas, D. Tchoubar, J. Y. Bottero, P. Tekely, Langmuir, 1994, 10, 4353.

[180] A. Fleming, Proc. R. Soc. London (Biol), 1922, 93, 306.

[181] E. R. Berman, Biochemistry of the eye, ed. Blakemore C. New York: Plenum Press, 1991.

[182] T. Imoto, L. Johnson, A. North, D. Phillips, J. Rupley, in: Vertebrate Lysozymes. In: Boyer P. The Enzyme. New York: Academic Press, 1972; 665.

[183] W. G. Burton, K. D. Nugent, T. K. Slattery, B. R. Summers, L. R. Snyder, J. Chrom., 1988,

[184] A. A. Vertegel, R. W. Siegel, J. S. Dordick, Langmuir, 2004, 20, 6800, 443, 363.

[185] W. Humphrey, A. Dalke and K. Schulten, Journal of Molecular Graphics, 1996, 14, 33-38.

[186] E. F. Osserman, R. E. Canfield, S. Beychok, in: Lysozyme. New York: Academic Press, 1974.

[187] C. C. Blake, D. F. Koenig, G. A. Mair, A. C. North, D. C. Phillips, V. R. Sarma, Nature, 1965, 206, 757.

[188] J. V. Rinella Jr., J. L. White, S. L. Hem, J. Colloid Interface Sci., 1998, 205, 161.

[189] J. M. Teijón, M. D. Blanco, A. Rodríguez, J. A. Onrubia, I. Katime, Rev. Esp. Fisiol., 1987, 43, 81.

[190] C. Czeslik, R. Winter, Phys. Chem. Chem. Phys., 2001, 3, 235.

[191] V. Calandrini, G. Onori, A. Santucci, J. Mol. Struct., 2001, 565-566, 183.

[192] S.-Y. B. Hu, M. A. Arnold, Anal. Chem., 2000, 72, 696.

[193] T. Coradin, P. J. Lopez, C. Gautier, J. Livage, C. R. Palevol, 2004, 3, 443.

[194] S. K. Banerjee, J. A. Rupley, J. Biol. Chem., 1973, 248, 6, 2117.

[195] R. Bansil, E. Stanley, J. T. LaMont, Annu. Rev. Physiol., 1995, 57, 635.

[196] R. Bansil, B. S. Turner, Curr. Opin. Colloid Interface Sci., 2006, 11, 164.

[197] N. Thirawong, R. A. Kennedy, P. Sriamornsak, Carbohydr. Polym., 2008, 71, 170.

[198] T. A. Gerken, Critical Reviews in Oral Biology and Medicine, 1993, 4, 261.

[199] L. E. Bromberg, D. P. Barr, Biomacromolecules, 2000, 1, 325.

[200] R. L. Bertholf, M. R. Will, J. Savory, Biochem. Biophys. Res. Commun., 1984, 125, 1020.

[201] C. Exley, J. Inorg. Biochem., 1998, 70, 195.

[202] H. Y. Shrivastava, A. Dhathathreyan, B. U. Nair, Chem. Phys. Lett., 2003, 369, 534.

[203] H. Y. Shrivastava, B. U. Nair, J. Biomol. Struct. Dyn., 2003, 20, 4, 575.

[204] B. K. Varma, A. Demers, A. M. Jamieson, J. Blackwell, N. Jentoft, Biopolymers, 1990, 29, 441.

[205] J. J. Powell, C. C. Ainley, R. Evans, R. P. Thompson, Gut, 1994, 35, 1053.

Part 3

Pure Aluminium Species and their Gelation Behaviour

3.1. Speciation and quantification of model aluminium solutions by ^{27}Al solution NMR spectroscopy

NMR spectroscopy is a widely used technique for speciation analysis (quantitative and qualitative) in materials science, catalysis, geochemistry, soil science, and many other fields [1, 12-16]. In this study, this technique was particularly used in the studies of aluminium interactions with biomolecules in order to establish identities of the samples.

The species present in the model $AlCl_3$, Al_{13}-mer, Al_{30}-mer and aluminium hydroxide solutions were quantified using ^{27}Al solution nuclear magnetic resonance (NMR) spectroscopy. The effect of the aluminium concentration on the speciation of the Al_{13}-containing samples was explored as well for the concentration range 0.004, 0.012 and 0.040 mol.L^{-1}. The four reference systems were prepared with Al_T = 0.40 mol.L^{-1} according to the methods described in Table (3.1) and by targeting the hydrolysis ratio of each system.

Table 3.1. List of the model aluminium-ion solutions containing single hydrolytic aluminium species.

Sample	Initial Al concentration, mol.L^{-1}	hydrolysis ratio	Method of preparation
$AlCl_3$	0.40	0.0	Dissolution of $AlCl_3$ salt in water
$Al(OH)_3$		2.85	Static anion exchange and ageing at room temperature
Al_{13}		2.46	Static anionic exchange at room temperature
Al_{30}		2.40	Anionic exchange and ageing at 80 °C

In the case of an Al_{13} reference system, spectra revealed a number of other aluminium species present in the Al_{13}-containing solution (Figure (3.1)).

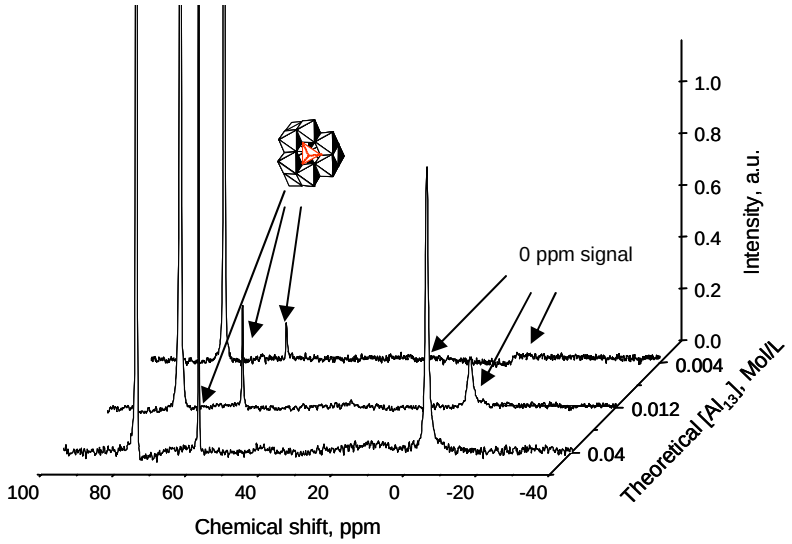

Figure 3.1. ^{27}Al NMR spectra obtained for an Al_{13} reference system prepared and measured at 25^{o}C (the 80 ppm peaks arise from the aluminate internal standard).

Assignment of the NMR signals and corresponding aluminium species is given in Table (3.2).

Table 3.2. Assignment of the ^{27}Al NMR spectra peaks.

Chemical shift (ppm)	Peak shape	Assignment	Reference
0	Relatively sharp	Al monomer	[22]
4	Broad	Al dimer	[22]
9	Very broad	Octahedral Al shell of Al_{13}-mer and Al_{30}-mer	[23]
62.5 - 63	Very sharp	Al_{13}-mer tetrahedral core	[22]
70	Broad	Al_{30}-mer tetrahedral core	[19]
80	Very sharp	Tetrahedral Al of $Al(OH)_4^-$ (reference)	[22]

On the experimental condition that the aluminate ion internal reference at 80 ppm was set as 0.06 mol.L^{-1}, the peak areas of the ^{27}Al NMR spectra were integrated. The concentration of various species with different chemical shifts could be calculated. The concentration of the Al_{13}-mer and the Al_{30}-mer were taken from the integral of the resonance peak areas at about 63 and 70 ppm multiplied by 13 and

15 respectively. The concentrations of aluminium monomer and aluminium dimer were taken from the integral intensities of the corresponding resonance peak areas at about 0 and 4 ppm respectively. The aluminium hydroxide concentration was estimated only indirectly as a difference between the total Al concentration and the sum of the concentrations of soluble Al species. The concentration of the reference systems and the correlation coefficient between the calculated and the stated values are displayed Table (3.3).

Table 3.3. Speciation of the aluminium reference systems obtained using ^{27}Al solution NMR spectroscopy.

Reference systems	Stated [Al], mol.L^{-1}	Calculated [Al], mol.L^{-1}	Correlation coefficient	^{27}Al solution NMR peaks assignment, %			
				Al_{13}-mer	Al_{30}-mer	Al monomer	Al dimer
Al_{13}	0.004	0.0036	0.9	77.08	0	17.36	5.56
Al_{13}	0.012	0.0104	0.867	86.33	0	13.67	0
Al_{13}	0.04	0.0441	1.1025	97.91	0	2.09	0
Al_{30}	0.04	0.0376	0.94	12.20	87.80	0	0
$AlCl_3$+HCl	0.012	0.012	1	0	0	97.79	2.21

When the initial concentration of the Al_{13} reference system was increased from 0.004 to 0.04 mol.L^{-1}, the concentration of the Keggin polycation increased as well, whereas the concentration of the aluminium monomer decreased. Though the monomer peak appears important in the spectra, their contribution did not exceed ~ 2.09 % of the overall concentration of soluble aluminium species detected by NMR in a 0.04 mol.L^{-1} stated Al_{13}-mer system (Table (3.3)). A too high dilution of the initial reference system had an effect on the speciation of the system. The percentage fraction of the Al_{13}-mer was measured to be 97.91 % of the total aluminium content, and the fraction of Al_{30}-mer was 87.80 % in the corresponding 0.04 mol.L^{-1} model solutions. No insoluble matter was detected in the Al_{13}-mer and Al_{30}-mer solutions as measured by quantitative ^{27}Al solution NMR and dynamic light scattering (data not shown). The fraction of aluminium hydroxide in the model hydroxide suspension exceeded 95 % of the total aluminium content.

3.2. Comparison of three methods for the quantification of aluminium concentration: acid digestion coupled with UV-visible spectrophotometry, gravimetry and ^{27}Al solution NMR spectroscopy

The characterisation of the aluminium-based systems obtained by ^{27}Al solution NMR spectroscopy was compared with two other methods, acid digestion coupled with UV-visible spectrophotometry and

gravimetry. The comparison was undertaken in order to provide a more reliable characterisation of the aluminium-based systems produced during the aluminium-biomolecule studies.

3.2.1. Quantitative methods

Acid digestion (AD) coupled with UV-visible spectrophotometry for total aluminium concentration determination.

The development of an aluminium concentration determination routine applicable during aluminium-biomolecule interaction studies was carried out by means of a spectrophotometric method relying on the development of a complex with a spectrophotometric reagent. During the present work, five organic reagents (arsenazo III, chrome azurol S, xylenol orange, ferron and aluminon- listed in Table (3.4)) were tested as aluminium complexing reagents. Each reagent was employed at a relevant concentration as ascertained from the literature [3-5, 24-28] and the relevance of the λ_{max} (complex) was concluded based on four parameters (the slope, the intercept, the correlation coefficient and a composite parameter) which will be detailed later about the xylenol orange results.

Table 3.4. Spectrophotometric reagents employed through the study.

Reagent, $mol.L^{-1}$	Ratio [reagent]/ $[Al]_{final}$	λ_{max} (complex), nm	References
Xylenol Orange, 1.10^{-3}	4.98	515	[3-5]
Chrome Azurol S, $2.97.10^{-4}$	4.44	572	[24]
Aluminon, 3.10^{-2}	22.405	524	[25-26]
Ferron, 2.10^{-3}	4.979	370	[27]
Arsenazo III, $7.45.10^{-5}$	0.082	652	[28]

A 48 h aging of the mixed solution of one reagent and one aluminium reference system was used to enable the full development of the complex prior to spectra acquisition in 1 cm quartz cuvettes using deionised distilled water as a blank. The spectrophotometric results achieved with the five reagents tested, are displayed in Figure (3.2).

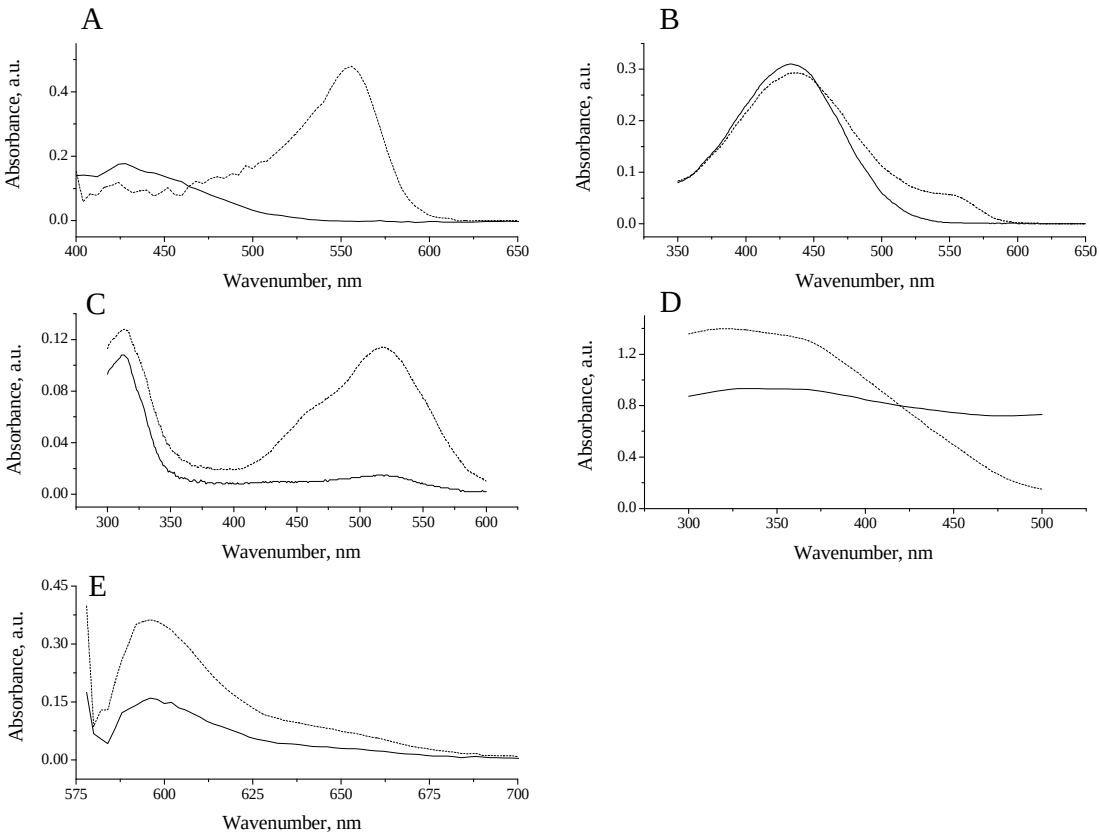

Figure 3.2. UV-vis spectral changes of xylenol orange 1.10^{-3} mol.L^{-1} (**A**), chrome azurol S $2.97.10^{-4}$ mol.L^{-1} (**B**), aluminon 3.10^{-2} mol.L^{-1} (**C**), Ferron 2.10^{-2} mol.L^{-1} (**D**) and arsenazo III $7.45.10^{-5}$ mol.L^{-1} (**E**) after addition of Al_{13}-mer in solution. The concentration of the Al_{13}-mer was in (A) $1.60.10^{-4}$ mol.L^{-1}, in (**B**) 2.92.10-^{6} mol.L^{-1}, in (**C**) $3.21.10^{-5}$ mol.L^{-1}, in (**D**) $6.43.10^{-5}$ mol.L^{-1} and in (**E**) $7.30.10^{-5}$ mol.L^{-1}. Solid lines are for pure reagent solutions and dashed lines for the aluminium-reagent complexes.

The largest and non dubious separation between the maximum absorption wavelengths of the complex and free organic reagent molecules was observed in the case of xylenol orange (Figure (3.2 (**A**)). Moreover, calibration with an aluminium standard solution (aluminium atomic absorption standard solution (986 μg / mL Al in 0.7 % HCl, Aldrich)) resulted in more reliable values for this reagent than for the four other ones on the basis of the calibration regression coefficient, R^2 (values are represented in Table (3.5)).

Table 3.5. Calibration regression coefficient, R^2 of the calibration lines obtained with UV-vis spectrophotometric reagents.

Reagent, mol.L-1	Ratio [reagent]/ [Al]final	R^2
Xylenol Orange, 1.10-3	4.98	0.9991
Chrome Azurol S, 2.97.10-4	4.44	0.9322

Table 3.5. Continued.

Reagent, mol.L^{-1}	Ratio [reagent]/ $[Al]_{final}$	R^2
Aluminon, 3.10^{-2}	22.405	0.9272
Ferron, 2.10^{-3}	4.979	0.9859
Arsenazo III, $7.45.10^{-5}$	0.082	0.9466

Xylenol orange (3,3'-bis[N,N-di(carboxymethyl)aminomethyl]-o-cresolsulfonephthalein) (Figure (3.3)), is a water-soluble dye containing a triphenylmethane group.

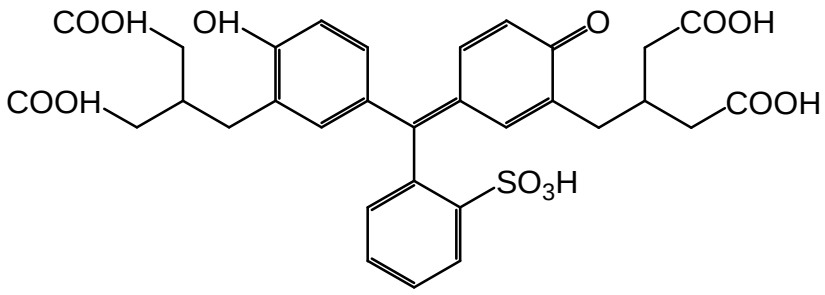

Figure 3.3. Xylenol orange ($C_{31}H_{32}N_2O_{13}$) molecular structure. The sulphonic group is deprotonated in the 'H_5XO^-' form.

From the literature [3-5], it bears 10 different acid sites. However, the form of the organic reagent used for analytical purposes is the mono-deprotonated 'H5XO⁻' species ($0 \leq pH \leq 3$), a purple coordination compound with a maximum absorption at 555 nm being formed with aluminium (spectra are shown in Figure (3.3)).

Acid digestion was performed using a strong acid (HCl, 1 mol.L^{-1}) in order to break down all aluminium species to Al monomer. The digested samples were mixed with a complexing organic reagent solution for quantification of the monomer concentration by UV-vis spectrophotometry. The effects of organic reagent to aluminium concentrations ratio and of the acid digestion temperatures (25 or 50 °C) were examined for optimization of the sensitivity and reproducibility of the method. Acid digestions were performed on three reference systems: an Al_{13} solution, an aluminium hydroxide suspension with a mean particle size estimated to 120 nm, as well as an $AlCl_3$ solution used as a blank. The digestion of the $AlCl_3$ solution was used to demonstrate the absence of treatment effect upon total aluminium concentration (the latter could be affected by eventual water evaporation, to give only one example). Depending on the initial aluminium concentration of the reference systems, three samples differing in concentration were prepared, as listed in Table (3.6). The measurements were performed on the samples freshly prepared to the according dilutions.

Table 3.6. Preparation of the AD samples (volumes (abbreviated V) are given in mL).

Initial solutions	Reference systems: Al_{13}-mer and $Al(OH)_3$			Reference system: $AlCl_3$		
[Reference systems], $mol.L^{-1}$	0.004	0.012	0.04	0.004	0.012	0.04
AD						
V (reference system) $_{added}$	0.50	1.25	5	0.2	0.5	2
V (H_2O) $_{added}$	4.50	3.75	0	1.8	1.5	0
V (HCl, 1 $mol.L^{-1}$) $_{added}$	45			18		
V (sample) $_{total}$	50			20		
AD dilution						
V (digested sample)	1	0.40	0.10	1	0.40	0.10
V (H_2O) $_{added}$	4	4.60	4.90	4	4.60	4.90
UV-Vis sampling						
V (digested diluted sample)	0.10					
V(HCl, 10^{-4} $mol.L^{-1}$ buffered at pH 3.4) $_{added}$	2.10					
V (xylenol orange, 10^{-3} $mol.L^{-1}$) $_{added}$	0.80					

An initial calibration experiment was performed with the measurement of aluminium concentration in 9 buffered (10^{-4} $mol.L^{-1}$ HCl, pH = 3.4) Al^{3+} solutions prepared from the atomic absorption standard solution. The measurement wavelength was optimised on the basis of four parameters: the slope *a*, the intercept *b* and correlation coefficient R^2 of the linear calibration, together with a composite parameter, $K = a \cdot (1 - R^2)$, given by an optimisation function taking into account all three first parameters (Figure (3.4)).

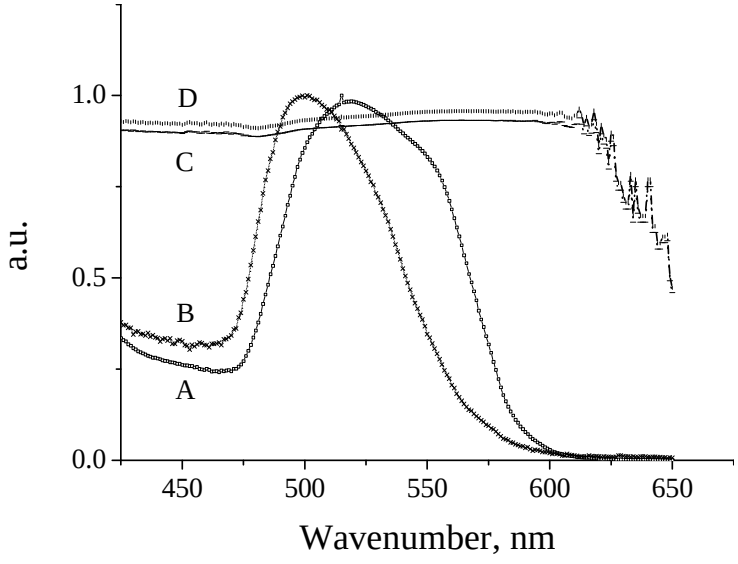

Figure 3.4. Optimisation parameters of the 'xylenol orange-aluminium' analytical reaction. Curves (**A**) to (**D**) represent respectively the slope (**A**), the intercept (**B**), the correlation coefficient R^2 (**C**) and the composite parameter K (**D**).

The maximum slope (optimum sensitivity) of the calibration line was observed for a wavenumber λ = 520 nm, whereas the minimum intercept (lowest background signal) was obtained for λ > 575 nm, and the calibration plot reached its highest linearity (R^2 close to 1) for 475 < λ < 605 nm. Finally, the global parameter K gave a clear range of applicability of the technique from 475 to 605 nm. On the basis of the K parameter, the optimum calibration and measurement wavelength was 515 nm. Figure 3.4 shows the calibration plot obtained for this wavelength.

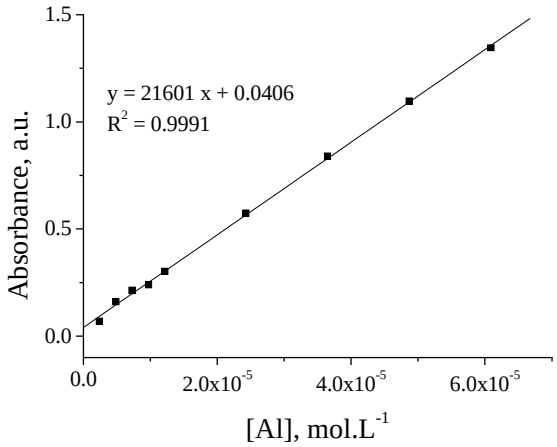

Figure 3.5. Calibration of Al standard solution ($3.65.10^{-2}$ mol.L^{-1}) diluted to various concentrations with xylenol orange 10^{-3} mol.L^{-1} at λ_{max} 515 nm.

Whichever aluminium reference system was used, the use of a 50 ^{o}C heating throughout digestion allowed a full breakdown of the species 3 times faster than when the same treatment was carried out at room temperature. Figure (3.6) illustrates the digestion temperature-dependence in the case of the Al_{13} reference system at 0.04 mol.L^{-1}. Acid digestions were therefore performed at 50 ^{o}C for 48 h under efficient stirring using an open top water bath fitted with a multi-position magnetic stirrer and high-precision circulator (± 0.1 ^{o}C).

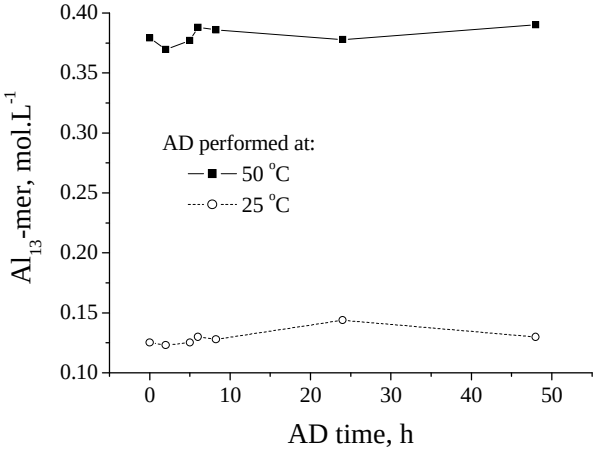

Figure 3.6. Evolution of the concentration of an initial Al_{13}-mer reference system 0.04 mol.L^{-1} as a function of time with acid digestion performed at 25 and 50 ^{o}C.

As expected, the concentration of the $AlCl_3$ reference system was 1 mol.L^{-1} from the beginning of the acid digestion process (Figure (3.7)) with a slight underestimation in the cases where the initial aluminium concentrations were 0.012 and 0.04 mol.L^{-1}. Therefore, one can conclude that the acid digestion coupled with UV-vis monitoring procedure did not affect aluminium concentration determination and can be used as a quantitative analytical technique. In the case of the Al_{13}-mer and the aluminium hydroxide reference systems, the initial aluminium concentration had no effect on the digestion process since the determined concentrations of those systems were equal to the concentration initially introduced (Figure (3.7) curves 4 to 9). For Al_{13}-mer solutions, the concentration detected reached the expected 0.4 mol.L^{-1} concentration from the first measurements carried out straight after the beginning of the acid digestion treatment, whereas the complete dissolution of aluminium hydroxide required an 8 h digestion treatment. For any aluminium speciation (different proportions of Al_{13}-mer and aluminium hydroxide), a 10 h acid digestion will therefore be desirable for the determination of total aluminium concentration.

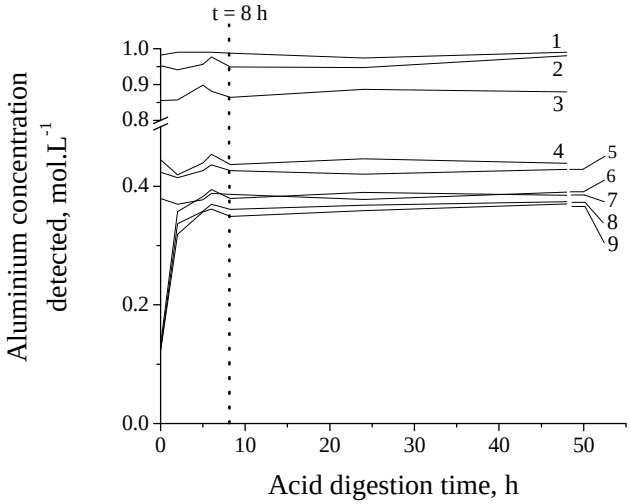

Figure 3.7. Evolution of aluminium concentration detected as a function of digestion time (digestion performed at 50 ^{o}C). Lines 1 to 3 represent the $AlCl_3$ reference systems at 4, 12 and 40 mmol.L^{-1}, lines 4 to 6 Al_{13}-mer reference systems at 4, 12 and 40 mmol.L^{-1} and lines 7 to 9 the aluminium hydroxide reference systems at 4, 12 and 40 mmol.L^{-1}.

Gravimetry

The aluminium reference system concentrations obtained by gravimetry were in good agreement with the stated ones as stipulated by the results displayed in Table (3.7). Furthermore, the gravimetric procedure (performed in triplicate for all the systems) gave good reproducibility as emphasised by the root mean squared deviation (RMSD) value below 1.50 % (Table (3.7)) for all reference systems used.

Table 3.7. Al concentration in reference systems as determined from gravimetric analysis.

Reference system	Al_{13}-mer	$AlCl_3$+HCl	Al hydroxide
$[Al]_{stated}$, $mol.L^{-1}$	0.4	1	0.4
$[Al]_{calculated}$, $mol.L^{-1}$	$0.394 \pm 1.39.10^{-3}$	$1.016 \pm 1.50.10^{-2}$	$0.407 \pm 5.90.10^{-3}$
RMSD, %	0.35	1.47	1.45

In addition to the quantitative analysis, a pure aluminium powder free from any contaminant can be recovered with high efficiency. Indeed, having a low solubility, the precipitate can easily be recovered by filtration.

3.2.2. Discussion and conclusions

Acid digestion coupled with UV-vis spectroscopy

An aluminium quantification procedure based on the formation of a complex between a metal ion and a UV-vis reagent, xylenol orange, was successfully developed and optimised. Calibration experiments were carried out to optimise the measurement wavelength to be used for the assay. For the measurement of any given sample, the proposed procedure implements an acid digestion treatment at 50 ^{o}C prior to mixing with the organic reagent. The breakdown of aluminium species in acidic media was demonstrated to be remarkably accelerated when using the highest temperature digestion conditions tested (50 ^{o}C). After optimisation, acid digestion coupled with the UV-vis procedure was demonstrated to be a method too time-consuming. The implementation of the acid digestion in itself requires at least 48 h. Although this simple method is sensitive, precise and accurate for the determination of aluminium in solution, it was not selected for our further studies.

Gravimetry

Results demonstrated that gravimetry can be applied to quantify aluminium-containing solutions. Moreover, whatever the reference systems used, the statistical parameters are lower than 2 %, which makes gravimetry an accurate and reliable tool to estimate the concentration of a solution containing aluminium species. However, a comparison of this method with a qualitative analysis such as ^{27}Al solution NMR is still required to establish the identity of a sample since gravimetry does not provide the aluminium speciation of the sample. The relevance of the spectrophotometric and gravimetric data can be checked by comparison with the ^{27}Al NMR peak areas, for example in the case of samples from the Al_{13} 0.4 $mol.L^{-1}$ solution.

^{27}Al solution NMR

^{27}Al solution NMR analysis is a convenient method for the selective determination of relevant Al species in solutions. Provided that the sample volume is sufficiently high, a given solution can be studied almost without any sample preparation. The species concentration is found to vary from the theoretical concentration values at ~ 5 % with ^{27}Al NMR. This divergence is probably due to the computing transformations required to convert the spectra.

Comparison between the three implemented techniques

Data obtained by the different quantitative methods demonstrate that, as illustrated by the correlation coefficients in Table (3.8), quantification of aluminium concentrations can be assessed reproducibly by all three methods.

Table 3.8. Summary of the quantitative data obtained by three analytical techniques.

Methods	Reference systems	$[Al]_{stated}$, $mol.L^{-1}$	$[Al]_{calculated}$, $mol.L^{-1}$	Correlation coefficient
AD / UV-Vis	Al_{13}-mer	0.4	0.448	1.12
	$AlCl_3$	1	1.013	1.013
	$Al(OH)_3$	0.4	0.408	1.02
Gravimetry	Al_{13}-mer	0.4	0.394	0.985
	$AlCl_3$+HCl	1	1.016	1.016
	$Al(OH)_3$	0.4	0.407	1.0175
^{27}Al solution NMR	Al_{13}-mer	0.004	0.0036	0.9
		0.012	0.0104	0.867
		0.04	0.0441	1.1025
	Al_{30}-mer	0.04	0.0376	0.94
	$AlCl_3$+HCl	0.012	0.012	1

The detection limits of the aluminium concentration of the acid digestion coupled with UV-vis spectrophotometric technique developed in the work are between $2.9.10^{-5}$ and $1.6.10^{-4}$ $mol.L^{-1}$. The lower limit of detection of gravimetric analysis is determined primarily by the sensitivity of the balance, and the weight stability of the substrate used to collect and weigh the sample. These factors should be chosen to ensure whenever possible that the lower limit of detection is an order of magnitude lower than the appropriate exposure limit. In the present work, this method was applied to aluminium contents between 0.05 % (mass fraction) and 0.138 % (mass fraction). It is the equilibrium solubility of a sample which controls the highest limit of detection. Though the comparison of the calculated aluminium concentration resulted in good consistency between gravimetric, spectrophotometric and ^{27}Al solution NMR techniques, it was decided not to use the acid digestion coupled with UV-vis and the gravimetric methods further for the sake of the rapidity of the experiments. Finally, the technique selected for the next experiments was ^{27}Al solution NMR where the aluminium concentration has to be higher than 1.10^{-4} $mol.L^{-1}$ in aluminium sulphate for detection using a 400 MHz spectrometer operating at 104.2 MHz.

3.3. Fundamental studies of aggregation / gelation phenomena in hydrolyzed aluminium ions solutions

The idea behind performing “controlled destabilization” experiments was to identify a range of reagents that can destabilize different aluminium species to produce gels. This experiment had the

potential to unveil which of the many functionalities present in biomolecules might have the most important impact on the gelation phenomenon, by analogy with effects observed with simple gelling agents (GAs). A broad range of compounds employed in colloidal chemistry as 'destabilising agents', including inorganic salts and large organic polymers with a range of functionalities have been tested on three reference systems: Al_{13}-mers; Al_{30}-mers and monodisperse aluminium hydroxide particles. The GAs can be divided into four broad groups listed in Table (3.9), according to their mechanism of destabilization of aluminium species.

Table 3.9. The four classes of destabilising agents used throughout the experiments

Category of GAs	GAs	References
pH-independent GAs, mol.L^{-1}	KCl	[29-30]
	K_2SO_4	[31]
	K_3PO_4	[32]
	CH_3COONa	[33]
	Na_2SiO_3	[34]
pH-dependent GAs, mol.L^{-1}	$KHCO_3$	[35]
	NH_4OH	[36]
	$NaAlO_2$	[37-38]
	$(C_2H_5)_3N$	[39]
Hybrid GA, mol.L^{-1}	$K_2Si(cat)_3$	[40]
Polymeric GAs, mol.L^{-1}	Cellulose acetate	[41-43]
	$H(OCH_2CH_2)_nOH$	[44-45]
	Poly(acrylic acid)	[46]

pH-independent GAs refer to reagents whose stability is not affected upon variation of their medium's pH. Some of them are even being referred to as buffers. KCl was chosen for its well-reproducible and well-repeatable and measurable properties [29]. K_2SO_4 [31] and K_3PO_4 [32] were selected because they are widely used chemicals as a fertilizer. So it is more likely to find those chemicals in soils where aluminium is also present [30]. Although CH_3COONa is sensitive to pH variations because it has a carboxylate function, in the context of our work, this reagent is in its protonated form. Then it is considered presently as a pH-independent GA. Its use is justified by for a wide range of applications such as in the textile industry and in the food industry [33]. Na_2SiO_3 was used because of the property

of the silicate ion, in acidic solutions, to react with hydrogen ions to form silicic acid. Then, when heated the silicic acid forms silica gel [34]. The gelation ability of the silicate ion was the reason for the inclusion of this reagent.

pH-dependent GAs denote reagents whose protonation state may vary in the pH range used for the samples. $KHCO_3$ was one of the pH-dependent GAs employed since dissolved inorganic carbonate species are known to interact with aluminium hydroxide [35]. NH_4OH appeared to be a good titrant for the potentiometric determination of the 'formal' hydrolysis ratio of aluminium species in aqueous solutions. The reagent was able to precipitate aluminium hydroxide colloids in solutions whose pH was higher than 6. The behaviour of the aluminium species in the presence of NH_4OH, a weak base was studied as well. The soluble ammonium hydroxide produces ammonium ions and hydroxide ions in solution in equilibrium with NH_3 and water. The NH_3 molecules will hydrolyze the aluminium species [36] and will possibly produce a complex. $NaAlO_2$ was chosen for our gelation studies since it is a derivative product of aluminium hydroxide. Once heated in the presence of a caustic soda solution, aluminium hydroxide, the aluminium species the likeliest to undertake a sol-gel transition [37], produces sodium aluminate [38]. Finally, $(C_2H_5)_3N$ was picked for reagent because of its ability to complex borane [39]. Since the elements aluminium and boron are both in the boron group of chemical elements, it would be possible to observe the development of a complex between aluminium and $(C_2H_5)_3N$.

By using the term **'**hybrid' GA, we mean that the reagent came from the complexation of the orthosilicic acid with the catechol species 1,2-dihydroxybenzene. The $K_2Si(cat)_3$ complex was partially decomposed into orthosilicic acid and 1,2-dihydroxybenzene (catechol) in the samples as the pH in the samples was initially below 7. The catechol released by the complex is known to bind aluminium strongly [40] (stability constant for Al^{3+} and catechol $10^{8.1}$). That is why it was utilized herein.

The last reagent category encompasses the polymeric GAs. They basically consist of large molecular mass molecules composed of repeating structural units, or monomers, connected by covalent chemical bonds. Cellulose acetate and poly(acrylic acid) display ionisable functional groups susceptible to interact with aluminium species. Cellulose acetate membrane is commonly used in ultrafiltration (UF) and reverse osmosis membrane processes [41]. Cellulose acetate / sulfonated poly(ether ether ketone) blend UF membranes have been used for separating chromium (III) ions [42]. Recently, cellulose acetate/poly(ether imide) blend UF membranes have been prepared and applied for the rejection of proteins and metal ions [43]. In the present investigation, interactions between ionisable functional groups of acetate cellulose and the aluminium species are expected. Similarly, complexation between the carboxylate groups of poly(acrylic acid) and the positively charged aluminium species are most likely to happen since poly(acrylic acid) had already proven its ability to complex copper (II) [46]. Polyethylene glycol is likely to establish hydrogen bonded aluminium complexes in the same way as it does in the presence of a poly(methacrylic acid) network [44-45].

3.3.1. Preparation and characterisation

The GAs listed in Table (3.9) were added, at the concentration mentioned in Table (3.10), to a chosen aluminium reference system and the volume made up to 10 mL with distilled water in a 15 mL plastic tube. The final reference system concentration was 0.1 $mol.L^{-1}$, and depending on the nature of the GAs, these latter have been introduced in ratios [Al] / [GA] between 0.1 and 1.5 except when a polymer GA was employed where ratios were between 100 and 10000 (ratios are represented in Table (3.10)). The high excess of GAs in the mixtures was deliberately executed to favour the interaction of the agents with the polymeric aluminium species. And in the case of the polymeric GA-containing solutions, a large excess of aluminium species was added in the solutions in order to facilitate their penetration in the polymer network.

Table 3.10. GAs concentration and aluminium to GA ratios used throughout the study.

GAs	$[GA]_{sample}$, $mol.L^{-1}$	Ratios [Al] / [GA]
KCl	2	0.05
K_2SO_4	0.5	0.2
K_3PO_4	0.2	0.5
CH_3COONa	0.5	0.2
Na_2SiO_3	0.2	0.5
$KHCO_3$	0.5	0.2
NH_4OH	0.5	0.2
$NaAlO_2$	0.075	1.333
$(C_2H_5)_3N$	0.2	0.5
$K_2Si(cat)_3$	0.2	0.5
Cellulose acetate	1.10^{-4}	1.10^{3}
$H(OCH_2CH_2)_nOH$	1.10^{-3}	1.10^{2}
Poly(acrylic acid)	1.10^{-5}	1.10^{4}

The solutions were kept at ambient temperature and visual observation made for 0, 1 and 24 h aging. pH measurements were carried out at t = 24 h.

3.3.2. Results and discussion

On the basis of pH measurements performed 24 h after addition of the GAs, and qualitative visual observations there was a clear difference in the action of different types of GAs (Table (3.11)).

Table 3.11. Assessment of the rate of gelation with screening experiments. pH measurements were performed 24 h after addition of the GAs.

Al-containing systems 0.1 mol.L^{-1}		Al_{13}-mer				Al_{30}-mer				Aluminium hydroxide			
Time after addition of the GAs, hours		0	1	24	pH	0	1	24	pH	0	1	24	pH
Blank		-	-	-	4.238	-	-	-	4.357	-	-	-	4.490
pH-independent GAs	KCl	-	-	-	4.170	-	-	-	4.152	-	-	-	5.710
	K_2SO_4	s	s	+	5.030	p	p	+	4.696	+	+	+	6.918
	K_3PO_4	s	s	s	11.561	s	s	p	11.074	+	+	+	11.601
	CH_3COONa	-	-	-	5.253	-	-	-	4.956	-	-	-	6.194
	Na_2SiO_3	s	s	s	8.091	s	+	+	6.405	+	+	+	11.020
pH-dependent GAs	$KHCO_3$	p	p	p	5.965	s	s	p	5.903	+	+	+	7.310
	NH_4OH	s	+	+	5.912	s	s	+	5.976	+	p	p	9.326
	$NaAlO_2$	s	p	p	7.113	s	p	p	6.989	s	p	p	11.710
	$(C_2H_5)_3N$	p	-	-	6.800	s	-	-	6.610	s	-	-	8.530
Hybrid GA	$K_2Si(cat)_3$	p	p	p	6.630	-	+	p	6.344	-	s	s	5.340
Polymeric GAs	Cellulose acetate	-	+	+	4.060	-	+	+	2.484	+	+	+	2.870
	$H(OCH_2CH_2)_nOH$	-	-	-	4.210	-	-	-	4.062	-	-	-	5.107
	Poly(acrylic acid)	-	s	s	4.230	+	+	+	4.380	+	+	+	5.342

"+" and "-" mean respectively gel and no gel formation; "p" and "s" correspond respectively to the formation of a precipitate or a suspension in solution.

There were several hints provided by the screening tests of various GAs. Among the pH-independent GAs tested, KCl did not show any effect on the aluminium species. Similarly, CH_3COONa did not cause the gelation of the aluminium species. The absence of deprotonated sites in the pH conditions studied for both agents explained those observations. In contrast, K_2SO_4, K_3PO_4 and Na_2SiO_3 have reacted positively to the suspension - gelation test although the K_3PO_4-containing samples and some of

the Na_2SiO_3-containing samples were highly basic solutions. The occurrence of hydrogen bonding within the samples, beside electrostatic interactions, could be at the origin of the formation of a gel in those mixtures.

Except in the presence of $(C_2H_5)_3N$, what strikes the eye of the observer is that the pH-dependent GAs caused significant effects on the aluminium species. $KHCO_3$, NH_4OH and $NaAlO_2$ have affected the aluminium species present. Broadly speaking, both the Al_{13}-mer and the Al_{30}-mer have responded, in a similar way, to the three agents listed above. The two polycations are highly positively charged which has assisted in the establishment of electrostatic interactions with the agents, which, under the pH conditions measured (disclosed in Table (3.11)), bore negative charges. However, bicarbonate solutions have a stronger effect than other bases tested, probably due to the additional effect of charge-neutralization by means of complexation of aluminium species with dissolved carbonate-ions. This fact will limit the use of bicarbonate and carbonate solutions for quantitative titration experiments, as it is most likely that the major inflexion point of the formation of aluminium hydroxide would be 'obscured' by complexation with carbonate. During the visual evaluation of the gelation of the mixtures, the effectiveness of NH_4OH will be of great interest for titration purposes. That base can be used for the titrimetric determination of the hydrolysis ratio of aluminium-containing solutions. $(C_2H_5)_3N$ only slightly destabilized charged aluminium species when the agent was added to the samples. Its effect was not visible one hour after its addition. The very limited effect of the reagent can be explained by its high pK_a value (pK_a = 10.78).

Aluminium chloride solutions were known to precipitate silica and to form aluminium-rich silica materials [40]. Likewise, the aluminium polycations and the aluminium hydroxide colloids employed in the present work were affected by the potassium tris (catecholato) silicate (IV) agent. Either a precipitate (in the case of the aluminium-mers samples) or a suspension was formed in the presence of $K_2Si(cat)_3$ in the samples.

Finally, polymeric GAs which are acidic polyelectrolytes caused serious destabilization of the aluminium-containing reference systems even at extremely low concentrations (milligrams per litre or lower) depending on the number and acidity of the groups. A side effect can be identified by pH measurements which indicated that the final pH of the co-gel formed from the most acidic gellants with aluminium-containing systems was significantly lower and dropped below pH = 3.0 at the latter stage of pH monitoring in the case of Al_{30}-mers and aluminium hydroxide colloids.

In terms of comparative 'activity' and susceptibility to various forms of colloidal 'destabilization', aluminium hydroxide suspension was the best aluminium-containing reference system, since it was the only system susceptible to all types of GAs tested and showed the most frequent formation of a gel (formation of a gel with six of the reagents tested after 24 h), compared to Al_{13}-mer and Al_{30}-mer. Al_{13}-mer solutions were able to form gels with three GAs, while the Al_{30}-mer solution gelled in the presence

of five of the GAs. The Al_{30}-mer was therefore positioned between the Al_{13}–mer and aluminium hydroxide in terms of relative stability towards aggregative destabilization.
In general, the Al_{30}-mer samples disclosed a higher acidity than the Al_{13}-mer samples. Although in some cases the pH difference was not substantial, the higher acidity made the Al_{30}-mer solutions more sensitive to GAs addition.

3.3.3. Conclusion

The screening test described in this section has shown a high efficiency at testing a large number of compounds for their destabilizing effect on aluminium species. The number of organic polymers could be extended in order to test more functionality for potential co-gellant applications. Water-soluble acidic derivatives of cellulose were of special interest due to their relative harmlessness and potential co-gellant action. In order to test 'hybrid' GAs in-depth, buffered solutions of these agents should be introduced at pH ca. 4.2 (similar to the pH of the Al_{13}-mer, Al_{30}-mer and not far from the pH of aluminium hydroxide nanosuspensions).

3.4. A multi-technique study of the effect of aqueous aluminium speciation on hydrolytic gelation of aluminium (oxy) hydroxide

Conversion of aluminium (Al) ions into aluminium (oxy) hydroxides and oxides is technologically and environmentally important process upon which a diverse range of applications is based including preparation of alumina-based catalysts, cosmetic products, vaccine adjuvants, ceramics, pillared clays, sweep-flocculation for fresh water treatment, etc. [47-51]. This conversion can be conducted in aqueous or non-aqueous conditions, in acidic or alkaline medium [51-53] and different structures of aluminium (oxy) hydroxide can be obtained including amorphous 'pseudoboehmite', crystalline boehmite, gibbsite, bayerite and diaspore [54, 55]. The structure of the resulting (oxy) hydroxide material in aqueous solutions depends on the conditions of neutralisation such as pH, temperature, pressure, aluminium concentration, type and strength of neutralising agent, the presence of anions, ligands and macromolecules, etc. [47, 51-53]. Most of these conditions define molecular speciation of aluminium ions in the process of conversion which in turn may influence the outcome of the transformation into insoluble (oxy) hydroxide. Although the crucial role of molecular speciation of aluminium ions in the formation of Al (oxy) hydroxide is beyond any doubt [51, 52], the actual mechanism of such transformation is still a matter of debate [51, 52, 55]. The reason for this is the complexity of the system in question owing to the diversity of molecular aluminium precursors and, especially, a sheer number of factors involved in the conversion process.
Indeed, in aqueous solutions, in the presence of non-complexing anions (halides, nitrate, perchlorate, etc.), a number of molecular aluminium species can be found in a dynamic equilibrium. These include monomeric forms of Al ions ($[Al(H_2O)_6]^{3+}$, $[Al(OH)(H_2O)_5]^{2+}$, $[Al(OH)_2(H_2O)_4]^{+}$, etc.), several polynuclear Al clusters such as small oligomeric species Al_n (where $n < 13$), *e.g.* Al dimers ($[Al_2(OH)_2(H_2O)_8]^{4+}$) and trimers ($[Al_3(OH)_4(H_2O)_9]^{5+}$) as well as larger Al tridecamers

($[Al_{13}O_4(OH)_{24}(H_2O)_{12}]^{7+}$ or 'Al_{13}-mer') of ε-Baker-Figgis structure [48, 53, 56, 57]. At prolonged ageing of weakly acidic Al-ion solutions at elevated temperature other polynuclear species can be identified including the recently discovered $[Al_{30}O_8(OH)_{56}(H_2O)_{26}]^{18+}$ species or the 'Al_{30}-mer' [58-60]. These giant Al polycations containing 30 Al atoms actually consist of two δ-Baker-Figgis Al_{13} moieties bridged by four additional Al atoms. Other hydrolytic Al clusters such as Al tetramers, hexamers, etc. have also been postulated, although direct evidence of their existence is still lacking [48, 57].

At the colloidal level of transformation of molecular Al hydrolytic clusters into Al (oxy) hydroxide, one can expect either formation of gel, flocculation, or precipitation depending on the conditions and the kinetics of the nucleation, particle growth and aggregation [51, 52, 55, 57]. For instance, amorphous 'pseudoboehmite' type material is formed by forced hydrolysis of aqueous Al-ions in circumneutral conditions [61]. This material is highly disordered and tends to form gels or coagulates [52, 61]. Ordered, crystalline forms of Al hydroxide (e.g. gibbsite or bayerite) form slowly in the conditions of non-neutral pH (pH > 8.0 or pH < 5.5) and they will tend to separate early from the aqueous phase as well-defined precipitates [51, 54, 55, 61]. Therefore, finding ways to control the stoichiometric conditions (and the pH as a function of stoichiometry of aluminium and neutralising agent) and the kinetics of aluminium (oxy) hydroxide formation are important for the preparation of advanced materials with tailor-made morphological, structural and surface characteristics [51, 52].

The type and strength of neutralising agent (e.g. alkali for acidic Al-ion solutions) have been found to strongly affect the kinetics of nucleation and colloidal particle growth and, therefore, predefine the pathway of colloidal sol-gel transformation, particle coagulation or precipitation. Alkalis with lower pK_a (pK_a < 7.0) tend to create gels of Al (oxy) hydroxide, while stronger bases with pK_a > 10.0 form predominantly precipitates. Concentration of aluminium ions is also an important factor of the colloidal transformation of Al-ions into (oxy) hydroxide. Generally, the higher the concentration of aluminium the harder it is to control the homogeneity of the system and, therefore, to prevent premature aggregation and precipitation [62, 63]. However, the ability of the aluminium-ion solutions to form gels also increases dramatically with the increase of aluminium concentration [64].

Sol-gel transformations of Al-ions into Al hydroxide produced by a weak base (Trizma-base, pK_a = 8.3) were investigated in aqueous solutions. Along with native aqueous solution of aluminium chloride, the following aluminium species were prepared using the 'soft hydrolysis' method: Al_{13}-mers, Al_{30}-mers and monodisperse suspension of Al hydroxide nanoparticles. The 'soft hydrolysis' method is based on the static anion exchange technology which allows for obtaining solutions of single pure hydrolytic species of aluminium with minimised impurities of other species of the same metal.

In addition to potentiometric titration, four techniques: pH-metry, conductivity, dynamic viscosity measurements and ultrasonic spectrometry were used to monitor the sol-gel transformations. The latter technique is an emerging tool for characterisation of colloidal processes [65-67] which has been applied previously by our group for the studies of aqueous acid-base titrations including Al hydroxide formation [68, 69].

3.4.1. Materials and Methods

Sample preparation

A stock solution of aluminium chloride (1.0 mol.L^{-1}) was prepared by dissolving an appropriate amount of crystalline $AlCl_3 \cdot 6H_2O$ 99 % (Aldrich, Gillingham, UK) in distilled, deionised water. Working $AlCl_3$ solutions were prepared by dilution of the stock solution.

Model solutions of Al_{13}-mer and Al_{30}-mer as well as Al hydroxide suspension were prepared from the stock $AlCl_3$ solution by the static anion exchange developed by our group [24]. For the preparation of the Al_{13}-mers the formal hydrolysis ratio of the solution (the formal hydrolysis ratio is the ratio of the concentration of added alkali and total aluminium concentration $h = C((OH^-)_{added}/C(Al)_{total})$ was adjusted to $h \sim 2.46$, close to the theoretical hydrolysis ratio $h = 2.462$ of these species [62]. For the preparation of a model Al_{30}-mer solution, the Al_{13}-mer solution prepared at room temperature at $h \sim 2.40$ was thermally aged at 85 °C for 48 h as described in the previous work [70]. The sol of aluminium hydroxide was prepared at room temperature by adjusting the hydrolysis ratio of the stock solution of $AlCl_3$ to $h \sim 2.85$ also using the static anion exchange method [70] followed by ageing the resulting sol for 2 months which led to mean particle size of 55 ± 6 nm, as measured by dynamic light scattering (DLS). Summary of the data on model solutions containing four Al species is given in Table (3.12).

Table 3.12. The list of the model aluminium-ion solutions containing single hydrolytic aluminium species.

Sample	Initial Al concentration	% fraction of target Al species	hydrolysis ratio	Titrant concentration (Trizma-base)	Method of preparation
$AlCl_3$	0.400 mol.L^{-1}	99.00	0.0	0.783 mol.L^{-1}	Dissolution of $AlCl_3$ salt in water
$Al(OH)_3$		95.00	2.85		Static anion exchange and ageing at room temperature
Al_{13}		97.92	2.46		Static anionic exchange at room temperature
Al_{30}		93.80	2.40		Anionic exchange and ageing at 85 °C

As follows from the data of Table (3.12), high percentages of the target species have been detected using quantitative ^{27}Al NMR spectroscopy as described below. No insoluble matter was detected in the Al_{13}-mer and Al_{30}-mer solutions as measured by quantitative ^{27}Al solution NMR and DLS.

The total amount of aluminium in the model solutions of aluminium species was measured by means of a spectrophotometric method using Xylenol Orange (*ex.* Sigma-Aldrich, Gillingham, UK) as analytical reagent [1]. The total concentration of aluminium in the model solutions of aluminium species was found to be 0.400 ± 0.002 Mol.L^{-1}. This measurement was validated using a gravimetric procedure based on the precipitation of aluminium hydroxide with ammonia and consequent calcination of the precipitate at 1000 °C as described in [1].

Quantitative measurement of aluminium speciation using ^{27}Al solution NMR spectroscopy

The speciation in the model $AlCl_3$, Al_{13}, Al_{30} and aluminium hydroxide solutions was quantified using ^{27}Al solution nuclear magnetic resonance (NMR) spectroscopy. For this purpose the NMR spectra of samples from Al_{13} and aluminium hydroxide systems were acquired at 25 ^{o}C and those of the Al_{30} system at 85 ^{o}C using a JEOL ECX400 spectrometer (Jeol, Tokyo, Japan). The procedure employed has been detailed in the Material and Methods (2.3.7.d.) section of the thesis.

The amount of Al hydroxide was estimated from ^{27}Al NMR measurements indirectly as a difference of the total aluminium concentration and the sum of all soluble aluminium species detected by NMR [2, 73].

Multi-probe titration setup

The experimental setup for carrying out the titrations of aluminium species with Trizma-base is schematically depicted in Fig. (3.8). It consists of a combined Red Rod glass electrode (Radiometer Analytical, Villeurbanne, France) linked to a PHM-250 pH-meter (Radiometer Analytical, Villeurbanne, France), a pH probe (1), a two-plate conductivity probe (Radiometer Analytical, Villeurbanne, France) (2) connected to CDM-230 conductivity meter (Radiometer Analytical, Villeurbanne, France). Viscosity probe (3) in the experimental setup, Figure (3.8), represents a parallel plate gold-coated transducer with a temperature sensor (dark rod in the middle) connected to an AND SV-10 vibro-viscometer (AND A&D Ltd., Japan). These three probes are immersed simultaneously in a 75 ml solution of Al species in the 150 ml crystallising dish. The vessel containing sample solution (4) is set on top of the magnetic stirrer (5) and is stirred using a magnetic stirrer bar. The titrant solution is dispensed from an EDOS 5222 liquid handling device (Eppendorf, Cambridge, UK) (6) using a Combitip Plus syringe (Eppendorf, Cambridge, UK) (7). Viscosimeter, pH-meter and conductivity meter were connected to a PC (8) and readings of viscosity, pH and conductivity were taken in parallel every 10 seconds.

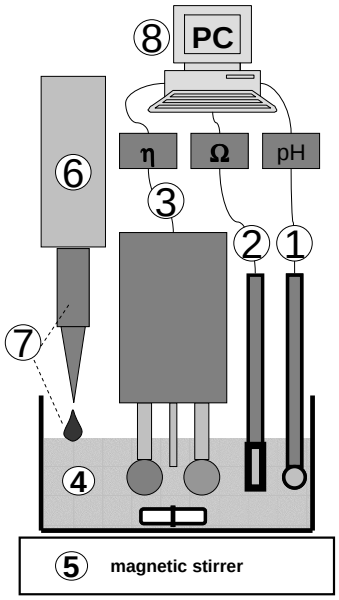

Figure 3.8. Schematics of the multi-probe titration setup.

The conductivity probe was calibrated using a standard solution of NaCl (1015 μS.cm^{-1}, Radiometer, Villeurbanne, France) and the pH probe calibrated using four IUPAC buffer solutions (pH = 1.68 ± 0.03 (ex. Fluka, Milan, Italy); 3.98 ± 0.02; 7.01 ± 0.02 and 10.01 ± 0.02, all ex. Fisher Scientific, Loughborough, UK, unless otherwise mentioned).

Titration procedure

A stock solution of the titrant, Trizma™ (2-Amino-2-(hydroxymethyl) propane-1,3-diol) was prepared by dissolving 94.95 g of a commercial-grade Trizma-base 99.9 % (crystalline powder *ex.* Aldrich, Gillingham, UK) in 1 litre of distilled deionised water to achieve a concentration of 0.783 mol.L^{-1}, as measured by the potentiometric titration with a volumetric standard solution of hydrochloric acid (1 mol.L^{-1}, *ex.* Fisher Scientific, Loughborough, UK).

Titrations were conducted in the following manner. A fixed volume of 80 ml of undiluted sample containing one of four aluminium species under investigation at the total Al concentration of 0.400 ± 0.002 mol.L^{-1} was placed in a 150 ml Pyrex ® crystallising dish. This vessel was chosen due to convenient shape allowing for accommodation of all three probes in one sample or a reasonable volume. Titrations were performed at room temperature (25 ± 1 ^{o}C) in a monotonic mode (equal additions of titrant) using undiluted Trizma-base solution (0.783 mol.L^{-1}) as a titrant. For this purpose, 80 successive additions of 0.2 ml of the titrant were made at 3 min time intervals between the additions using a pre-programmed EDOS 5222 automated liquid handling unit (Eppendorf, Cambridge, UK) under continuous stirring at 300 rpm. The data readings from the inserted probes were acquired every 10 s for 240 min of each experiment. All titrations were made in duplicates.

The probe of the vibro-viscometer SV-10 is generally sensitive to the level of immersion of the sensor plates in solution. During the titrations the volume of sample constantly increases due to additions of titrant. In order to compensate for this effect, 'blank titrations' were run in duplicate in which monotonic additions of titrant (Trizma) were made in the same conditions as in the titrations of Al species solutions. The difference in values of dynamic viscosity measured in 'blank titrations' from the original value (normally, close to ~ 1 mPa·s) was subtracted then from the titrations of Al species solutions.

Ultrasonic measurements

The use of ultrasonic measurements for monitoring of the acid-base reactions involving aqueous solutions of aluminium ions has been reported by our group [68, 69]. Previously we have concentrated our effort on the use of external ultrasonic transducer working in back-reflection mode described in detail elsewhere [74]. An obvious advantage of such external transducer is the possibility to adapt ultrasonic measurements to a broad range of experimental settings including field conditions. Ultrasonic spectroscopy using the external ultrasonic transducer has been shown to provide some valuable analytical information at a very high measurement speed [68, 69]. The speed of measurement was found to be advantageous comparing to the conventional pH measurements when studying non-equilibrium changes in acid-base reactions including neutralisation of aluminium-ions with base. Good temperature control was found to be the key issue when measuring ultrasonic velocity. The use of the

proposed external ultrasonic transducer and of the mathematical algorithm to compensate for temperature deviations, was proposed to tackle the conditions of uncontrolled temperature operation [75]. Ultrasonic velocity has been found to be the most appropriate measurement parameter when using external ultrasonic transducer while the measurement of ultrasonic attenuation was less successful [68].
In the present study ultrasonic titrations were performed using a dedicated analytical instrument - HR-US 102 P high-resolution ultrasonic spectrometer (Ultrasonic Scientific, Dublin, Ireland) containing parallel ultrasonic transmission-based cells with fixed geometry and an external titration accessory (Ultrasonic Scientific, Dublin, Ireland). The ultrasonic measurements were carried out in the ultrasonic frequency range of 5-15 MHz (specifically, 8 and 15 MHz) at the temperature of 25 ± 0.01 °C maintained by the incorporated thermostat. Ultrasonic velocity and ultrasonic attenuation were recorded simultaneously in a differential mode using the data from two measurement cells - a cell containing the sample being titrated and the reference cell containing distilled water as a reference.
Ultrasonic titrations of aluminium species were performed using monotonic addition of titrant (Trizma-base solution, 0.8 mol.L^{-1}). 80 additions 200 µl of titrant were made to a sample solution containing 80 ml of undiluted Al-ion solution at time intervals of 3 or 30 min (the latter titrations took one full day to run). Double stirring system operating at 300 rpm stirring speed was used for sample homogenisation. The data of the ultrasonic titrations was collected using a PC with the dedicated software from Ultrasonic Scientific (Dublin, Ireland). 'Blank titrations' of distilled water with Trizma-base titrant were also recorded in the same conditions as the titrations of Al species and the measured values of differential ultrasonic viscosity and attenuation were used for the correction for the effect of increasing volume and dilution of the Al species samples.

3.4.2. Results and discussion

The results of titrimetric measurements of sol-gel transformation of four distinct aluminium species into Al (oxy) hydroxide as monitored by four different techniques are presented in Fig. (3.9) (method-wise).

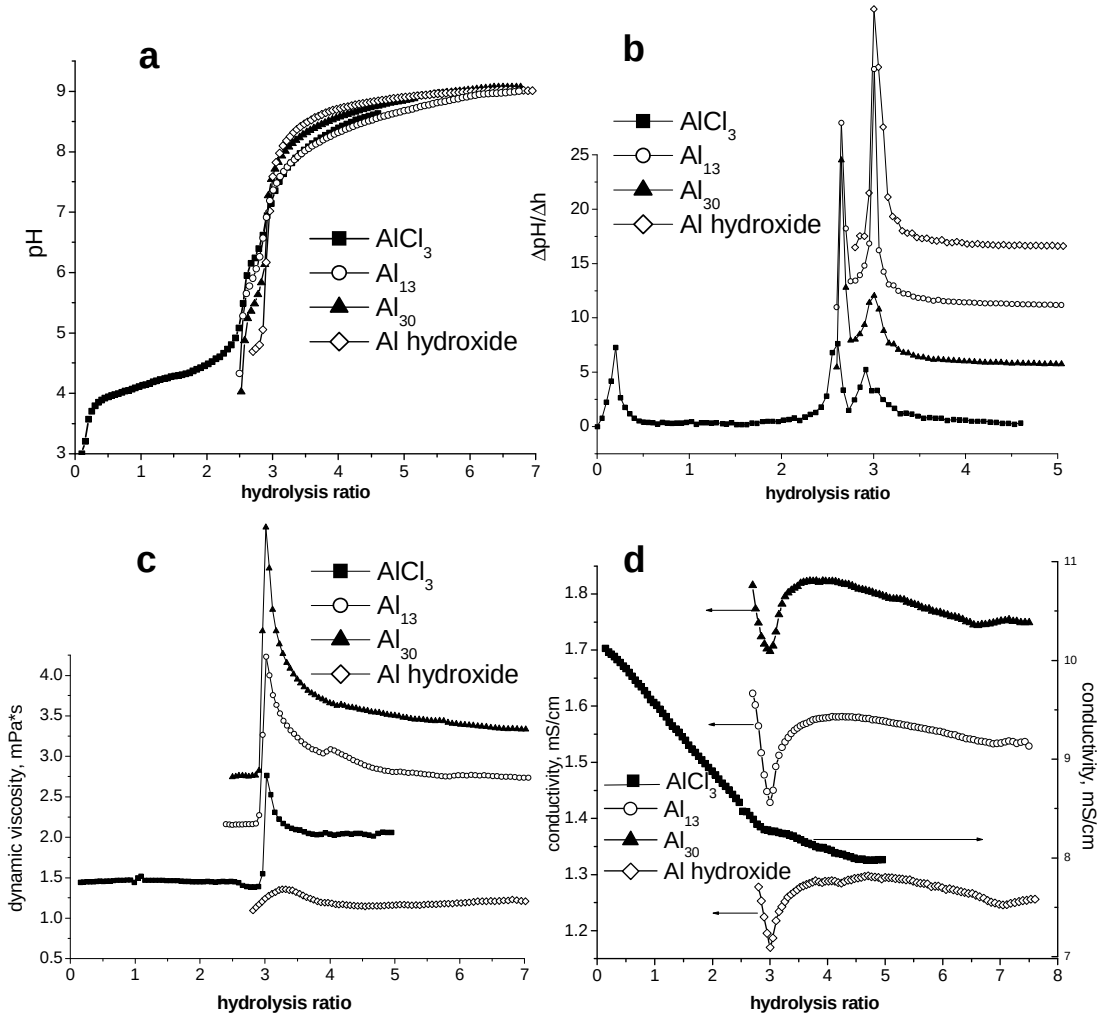

Figure 3.9. Multi-technique titrations of model aluminium-ion solutions (0.4 Mol.L^{-1}) containing single aluminium species using Trizma-base as a titrant. (**a**) pH curves; (**b**) first derivative pH curves (ΔpH/Δh, x-offset 70 %); (**c**) dynamic viscosity curves (x-offset 80 %); (**d**) Conductivity measurements.

As follows from Fig. (3.9) **a**, the overall shape of the pH-metric titration curves remains quite similar for all four species under investigation. Indeed, the starting point of the pH-metric curves depends on the initial formal hydrolysis ratio and initial pH of the respective Al species which are $h \sim 0.0$ and pH = 2.8 for $AlCl_3$, $h \sim 2.46$ and pH = 4.2 for Al_{13}-mers, $h \sim 2.40$ and pH = 3.9 for Al_{30}-mers; $h \sim 2.85$ and pH = 4.7 for Al hydroxide suspension. All four pH-metric titration curves tend to converge around the major inflexion at $h \sim 3.0$ that corresponds to the completion of formation and charge neutralisation of aluminium hydroxide.

First derivatives of the pH-metric titration data presented in Fig. (3.9) **b** offer a better insight into the main features of the pH-metric titration curves. The data of Fig. (3.9) **b** indicates that the pH-metric curve of $AlCl_3$ titration with Trizma (Fig. (3.9) **a**) contains an additional inflexion at the beginning of the titration with the maximum at $h \sim 0.2$. This inflexion corresponds to the process of neutralisation of protons released by (auto) hydrolysis of monomeric Al ions [76, 77]. The plateau on the first derivative pH-metric titration curve of $AlCl_3$ corresponds to the region of pH ($3.8 < pH < 4.8$) and hydrolysis

ratios ($0.2 < h < 2.5$) where hydrolysis becomes less significant and the neutralisation reaction of Al-ions with base is dominated by the consumption of hydroxyl-ions by the ongoing condensation into Al polynuclear hydrolytic species. The contribution of the Keggin-like Al_{13}-mer becomes important in this range of hydrolysis ratios and reaches maximum at $h \sim 2.46$ (the theoretical hydrolysis ratio of the Al_{13}-mer species). The next inflexion which can be observed on the curves of $AlCl_3$, Al_{13}-mers and Al_{30}-mers is at $h \sim 2.59 \pm 0.03$ (Fig (3.9) **b**). We assume that the small jump on pH-metric curves at $h \sim 2.59$ (or the peak on the first derivative pH-curves in Fig. (3.9) **b**) highlights the point where further formation of Al Keggin ions is impossible (the maximum hydrolysis ratio for these ions - $h = 2.462$ for Al_{13} and $h = 2.40$ for Al_{30} - has already been reached) and further additions of base result in rapid increase of pH. The following mini-plateau at $2.6 < h < 2.9$ ($5.3 < pH < 6.3$) in Fig. (3.9) **a**, which coincides with the 'gap' or a local minimum between the inflexions at $h \sim 2.6$ and $h \sim 3.0$ in Fig. (3.9) **b** is the region where simultaneous structural conversion from Keggin-like structure into disordered structure of Al (oxy) hydroxide (most probably, pseudoboehmite) takes place [76-78]. In this process the pH is steadied due to consumption of hydroxyl-ions by the structural conversion mentioned above. Finally in the vicinity of the major inflexion point at $h \sim 3.0$ which is common for all four Al species in question (Fig. (3.9) **b**) the process of structural conversion is practically completed. This process coincides with charge neutralisation and exhaustion of all 'acidic' sites in Al with the hydroxide particles.

As follows from the data of Fig. (3.9) **b**, the major inflexions at $h \sim 2.6$ and $h \sim 3.0$ are very well reproduced in all four Al systems under investigation (except the first inflexion at $h \sim 2.6$ for Al hydroxide) as indicated by the positions of the maxima of the corresponding inflexion peaks of the first derivative pH-metric curves. Slight differences in the shape of the inflexion peaks in Fig. (3.9) **b** are probably an indirect consequence of different nature of starting molecular precursors. There is also a small but systematic difference in the position of the second inflexion at $h \sim 2.6$ between $AlCl_3/Al_{13}$ ($h \sim 2.61 \pm 0.02$) and Al_{30} ($h \sim 2.57$). Similarity of $AlCl_3$ and Al_{13}-mers is explained by the fact that in the course of $AlCl_3$ neutralisation at room temperature the Al_{13} species are predominantly formed [51-53, 76-78]. The mentioned systematic difference of inflexions at $h \sim 2.6$ for Al_{13} and Al_{30} species arises from their differing 'intrinsic acidity' manifested as a 'theoretical hydrolysis ratio' or the ratio of oxo-/hydroxyl-ligands and Al atoms in the structural formula ($h = 2.462$ for Al_{13} and $h = 2.40$ for Al_{30}).

Viscosity changes in the course of acid-base titration of Al species with Trizma-base were monitored using a novel approach in dynamic viscosity measurements known as 'vibro-viscometry' [79]. This approach is based on the measurement of the force required to oscillate (or vibrate) in-plane the two thin metal sensor plates [79]. The method is sensitive and is able to measure dynamic viscosity η in a wide range (0.3-3000 mPa·s) suitable for aqueous solutions (η=0.98 mPa·s for pure water) with good time resolution (down to 0.5 s). The sensor probe of vibro-viscometer is quite compact in size and allows for accommodation of other probes. The results of dynamic viscosity measurements are shown in Fig. (3.9) **c**.

As indicated by the data of Fig. (3.9) **c**, at hydrolysis ratios below $h \sim 3.0$ the value of dynamic viscosity of Al species solutions is very close to 1 mPa·s. At $h \sim 3.0$ there is a single jump in dynamic viscosity in the course of acid-base titration of all four Al species in question. This jump corresponds to

the point of abrupt sol-gel transition of all four aluminium precursors into amorphous aluminium oxyhydroxide. The position of this jump ($h \sim 2.96 \pm 0.6$) is quite reproducible (experiments performed in triplicate) and is very close to the main inflexion observed on the potentiometric titration curves at $h \sim 3.0$ (Fig. (3.9) **a** and **b**; in the case of Al hydroxide precursor - slightly higher at $h \sim 3.2$). At higher hydrolysis ratios, the viscometric titration curves for all four Al species display a slow decay in viscosity values. Interestingly, the value of dynamic viscosity at $h > 3.0$ never reaches the original level of $\eta \sim 1.0$ mPa·s. This can be explained by the softness of the Trizma-base used as a titrant ($pK_a = 8.3$). The pH of solutions at $h > 3.0$ never exceeds pH ~ 9.1 (Fig. (3.9) **a**) which is probably insufficient to cause complete breakdown of Al hydroxide gel into $Al(OH)_4^-$ monomers as expected from the data with stronger alkalis [73, 76].

The magnitude of the major viscosity jump at $h \sim 2.9$ in Fig. (3.9) **c** appears to correlate well with the nature of aluminium precursors of sol-gel transformation. During hydrolysis-condensation of $AlCl_3$ solutions at $h < 3.0$ forced by the additions of Trizma-base the formation of Al monomeric clusters proceeds in an uncontrollable manner and, hence, is prone to the effect of so called 'local pH gradients' [62]. This phenomenon is common for solutions of Al-ions supersaturated with respect of Al hydroxide ($C(Al) > 5 \cdot 10^{-6}$ mol.L^{-1}). When reasonably strong alkali ($pK_a > 10.0$) is added to such supersaturated solutions, the mixing of alkali with Al-ion solution is insufficient to prevent the reaction of aluminium hydroxide formation to proceed locally [52, 62]. The premature formation of aluminium hydroxide proceeds far below the actual conditions for such process ($h << 2.5$). Al hydroxide is very difficult to dissolve back into molecular Al species in the weakly acidic conditions of the reaction. As a result of 'local pH gradients' and premature formation of Al hydroxide the concentration of Al_{13}-mers is much lower than 100 % of total Al content as one would expect in the vicinity of $h = 2.462$**.** This is the reason for the need of special methods such as static anion exchange to be developed for the production of relatively pure Al_{13}-mer solutions [70]. Heterogeneity in the $AlCl_3$ solution freshly neutralised with Trizma-base probably leads to a relatively low jump in dynamic viscosity ($\Delta\eta \sim 1.25$ mPa·S) observed on the corresponding curve in Fig. (3.9) **c** around $h \sim 2.96$.

The magnitude of the jump of dynamic viscosity at the point of sol-gel transition observed at $h \sim 2.96$ in the titration curves depicted in Fig. (3.9) **c** is reproducibly higher for the Al_{30}-mer solutions ($\Delta\eta \sim 3.25$) than for the Al_{13}-mer solutions ($\Delta\eta \sim 2.05$). Possible reason behind this trend could be in (*a*) higher molecular weight and somewhat larger size of the Al_{30}-mers; (*b*) higher 'intrinsic' acidity of the Al_{30}-mers comparing to that of the Al_{13}-mer as manifested in its lower theoretical hydrolysis ratio. This hypothesis agrees well with the literature data showing that Al_{30}-mers can be coagulated easier and better than Al_{13}-mer solutions [80]. However, further studies are necessary in order to understand this trend in sol-gel transition of Al hydrolytic clusters.

In the case of Al hydroxide suspension the magnitude of the viscosity jump ($\Delta\eta \sim 0.42$) is the lowest among the four Al-based systems studied (Fig. (3.9) **c**). One could assume that in the case of Al hydroxide system the hydrolysis ratio is quite high ($h \sim 2.85$) and it exceeds certain 'critical level' required for the formation of a robust gel phase. This also may indicate that the mean particle size of the suspension should be smaller than 55 nm observed for the given Al hydroxide suspension in order to exhibit sol-gel transition as indicated by a discernible viscosity jump.

Although the 'viscosity jump' observed in viscosimetric titrations in Fig. (3.9) **c** provides only a semi-qualitative measure one could assume that this jump at $h \sim 2.96$ is related to the 'quality' or robustness of the aluminium hydroxide gels (Fig. (3.9) **c**). The magnitude of 'viscosity jump' $\Delta\eta$ increases in the following order $\Delta\eta$(Al hydroxide) < $\Delta\eta(AlCl_3)$ < $\Delta\eta(Al_{13})$ < $\Delta\eta(Al_{30})$ and, thus, the gel robustness should follow a similar trend according to this hypothesis.

Our previous observations of the transformations of Al-ions into Al hydroxide in aqueous solutions and the literature data [62, 76-78, 81] suggest that this process depends strongly on the strength of base used as a titrant. In the case of very weak bases such as sodium or potassium bicarbonate ($pK_a = 6.35$) gelation occurs quite early in the course of titration - around $2.6 < h < 2.8$ depending on the concentration of aluminium. The second inflexion at $h \sim 2.9$-3.0 is much less profound in the titrations with weak bases. In the case of stronger bases ($8 < pK_a < 10$) such as ammonia [76] gelation in hydrolysed Al-ion solutions normally does not happen below hydrolysis ratio $h \sim 3.0$. Instead, formation of a gelatinous Al (oxy) hydroxide precipitate is observed in the case of ammonia [62, 76]. Finally, when using strong bases such as sodium carbonate ($pK_a \sim 10.6$) and, especially, sodium or potassium hydroxides ($pK_a > 15$) [62, 76], gelatinous, readily re-dispersible precipitates are usually formed at $2.6 < h < 2.8$ (mainly due to 'local pH gradients' which are described above and in more detail, previously [62]) with subsequent conversion into sparingly soluble precipitate of Al (oxy) hydroxide at $h \sim 3.0$. Trizma base with $pK_a = 8.3$ is at the borderline of weak and medium-strong bases. Therefore, as expected, its behaviour in neutralisation of Al-ions is close to that of ammonia in terms of the formation of Al (oxy) hydroxide near $h \sim 3.0$. However, unlike for ammonia, a gel is formed instead of a precipitate when titrating with Trizma.

The changes in conductivity of the samples containing four different aluminium species titrated with Trizma-base can be followed from the data of Fig. (3.9) **d**. The general levels of solution conductivity are in a good agreement with the chemical nature of aluminium species. Solution of $AlCl_3$ displays the highest conductivities throughout the titration (right-hand conductivity scale in Fig. (3.9) **d**). Conductivity levels Ω (mS/cm) of the Al_{13}-mer, Al_{30}-mer and Al hydroxide solutions are decreasing the following order: $\Omega(Al_{30}\text{-mer}) > \Omega(Al_{13}\text{-mer}) > \Omega$(Al hydroxide) according to the formal charge of these species which changes in the order $z = 18$ (Al_{30}-mer) > $z = 7$ (Al_{13}-mer) > $z << 7$ (Al hydroxide). In the case of Al hydroxide the exact charge of individual particles is not known, nonetheless, judging by the highly positive zeta-potential $\zeta \sim 40$-50 mV of this type of colloidal systems measured previously [81] there is still certain positive charge associated with these particles at weakly acidic pH (I.E.P. of Al hydroxide is normally around pH ~ 7). This charge, however, is much lower than the charge of any molecular cluster of aluminium, *e.g.* Al_{13}-mers. It can be shown that the formal charge z of aluminium species is directly related to the 'intrinsic acidity' of these species expressed by their theoretical hydrolysis ratio h':

$$z = (3 - h') \cdot n(Al) \qquad (1)$$

where n(Al) is the number of aluminium atoms in aluminium species.

The conductivity curves obtained from the titrations of Al_{13}, Al_{30} and aluminium hydroxide are quite similar in shape and contain a reasonably sharp negative peak with the minimum exactly at hydrolysis ratio h = 3.0 (Fig. (3.9) **d**). The drop in conductivity before the major inflexion corresponding to the formation of Al hydroxide on all four conductivity curves in Fig. (3.9) **d** can be explained by steady conversion of aluminium molecular clusters into Al hydroxide which continues up to the hydrolysis ratio h ~ 3.0. In the case of Al_{13}-mers, Al_{30}-mers and Al (oxy)hydroxide nanoparticles, when the critical point of charge neutralisation is reached at h = 3.0 the conductivity starts to build up at h > 3.0 due to the excess of hydroxyl-ions supplied by the additions of Trizma-base. After reaching a plateau in the range of 3.5 < h < 4.5 all three conductivity curves show a trend of decreasing the conductivity values at higher hydrolysis ratios. This behaviour is due to the fact that above pH = pK_a (Trizma) = 8.3 the dissociation of the organic base used as a titrant rapidly decreases and at some point stops completely.

In the case of the titration of $AlCl_3$ solution, the conductivity curve shows different trend as it continues to decrease after reaching h = 3.0 on the titration curve (Fig. (3.9) **d**). One could explain this observation by a very the formation of a very weak gel as indirectly demonstrated by viscosity measurements discussed above (Fig. (3.9) **c**). This weak gel starts to dissolve immediately after reaching h = 3.0 even at very small excess of free base.

Ultrasonic titrations of Al aqueous species with Trizma base were conducted separately due to small volume of the cells of the ultrasonic spectrometer used in this study. Nonetheless, the conditions of the bulk titrations monitored with the other three probes described above were reproduced in the ultrasonic titrations, albeit on a smaller scale. The results of ultrasonic titrations are shown in Fig. (3.10).

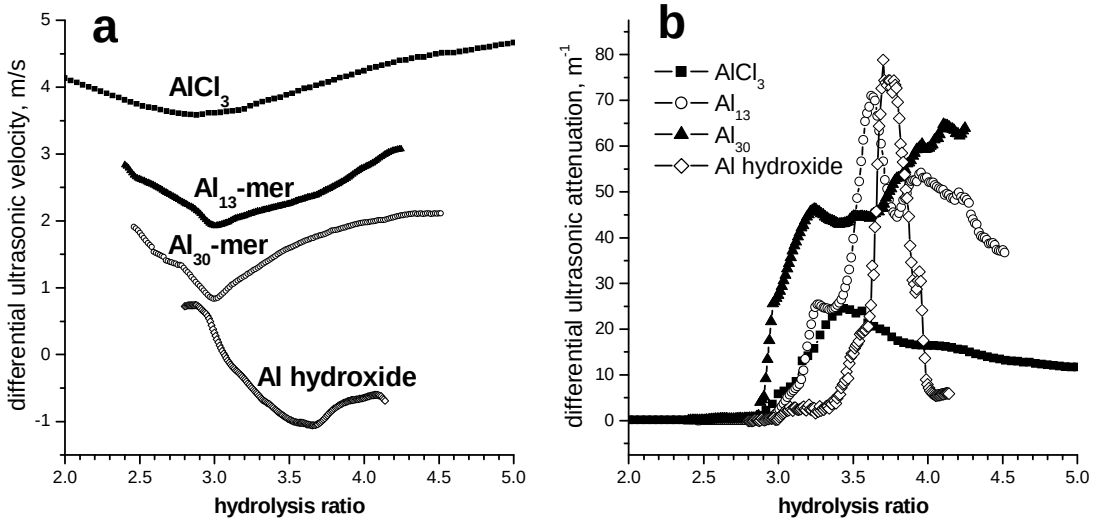

Figure 3.10. Results of ultrasonic titrations of four aluminium species (0.4 $Mol.L^{-1}$ total aluminium content) with Trizma-base. (**a**) Differential ultrasonic velocity *vs.* hydrolysis ratio; (**b**) differential ultrasonic attenuation *vs.* hydrolysis ratio (x-axis is truncated below h = 2.0 for the purpose of clearer data presentation).

As follows from Fig. (3.10) **a**, the values of differential ultrasonic velocity strongly depend on the hydrolysis ratio in the course of titrations of Al species with Trizma-base. In the acidic conditions (h < 3.0) velocity of ultrasound decreases to its absolute minimum on the curve at h ~ 3.0 (h ~ 3.7 for Al

hydroxide). It is known that ultrasonic velocity in liquids depends on the characteristics of bulk medium such as solution density and viscosity. Viscosities of Al species solutions do not change much in weakly acidic conditions (h < 3.0) as has been demonstrated above (Fig. (3.9) **c**). Therefore, the decrease of ultrasonic velocity is due to the variations in solution density. In the course of titration, the charge of aluminium species decreases due to forced hydrolysis-condensation and so, most probably, does the density of the sample solutions and, as a consequence, velocity of propagating ultrasound. At hydrolysis ratios above the major inflexion in the titration curves (h = 3.0) viscosity builds up significantly as well as the concentration of free hydroxyl-ions introduced by the excess of Trizma-base as has been shown by viscosity and conductivity measurements (Fig. (3.9) **c** and **d**). As a result, weak gels of Al (oxy) hydroxide start to dissolve and form smaller, negatively charged particles as well as monomeric $Al(OH)_4^-$ as a final product of dissolution in basic conditions [51, 76, 77]. This helps to explain both the increase in conductivity (Fig. (3.9) **d**) and in ultrasonic velocity (Fig. 10 **a**) above h = 3.0. Comparing Fig. (3.9) **d** and Fig. (3.10) **a** one can see that there is a certain degree of correlation of ultrasonic velocity curves with conductivity curves (note the difference in x-axis scales in Fig. (3.9) **d** and Fig. (3.10) **a**) as well as with the formal charge of the Al species under investigation. The overall levels of speed of ultrasound V decrease in the following order V(Al hydroxide) < $V(Al_{13})$ < $V(Al_{30})$ < $V(AlCl_3)$ in a good agreement with the conductivity data discussed above, Fig. (3.9) **d**, and with the formal charge of these species.

Behaviour of differential ultrasonic attenuation as a function of hydrolysis ratio in the course of ultrasonic titrations of Al species with Trizma-base can be traced in Fig. (3.10) **b**. Similarly to the dynamic viscosity data (Fig. (3.9) **c**), the ultrasonic attenuation starts to increase rapidly above the hydrolysis ratio of $h \sim 2.8$. For the molecular Al species ($AlCl_3$, Al_{13}-mers, Al_{30}-mers) this parameter rapidly reaches local maximum in the range of $3.2 \leq h \leq 3.6$. In the case of $AlCl_3$ titrations, after reaching a clear maximum at $h \sim 3.4$ the ultrasonic attenuation curve starts to decrease steadily. For the Al_{13}-mer solutions, the behaviour of ultrasonic attenuation is more complicated as it has at least three clear maxima on the ultrasonic titration curve (Fig. (3.10) **b**) at $h \sim 3.3$, $h \sim 3.6$ and $h \sim 4.0$. The curve of ultrasonic attenuation vs. hydrolysis ratio for Al_{30}-mer has one clear maximum at $h \sim 3.3$ which coincides with the Al_{13}-mer. Above this hydrolysis ratio the ultrasonic attenuation signal of the Al_{30}-mer solution tends to increase constantly unlike any other Al species. Finally, in the case of Al hydroxide there is a relatively sharp peak on ultrasonic attenuation curve with the maximum at $h \sim 3.7$-3.8, above which this parameter quickly decays.

When the pH and hydrolysis ratio are high enough for initiating 'alkaline' breakdown of Al hydroxide, the particle size of Al hydroxide starts to decrease as reflected by the decreasing ultrasonic attenuation above certain 'critical' hydrolysis ratio. The values of 'critical hydrolysis ratio' h' form the following approximate trend: $h'(AlCl_3) = 3.4 < h'(Al_{13}) = 3.6 < h'$(Al hydroxide) $= 3.75 < h'(Al_{30}) = 4.2$. One can hypothesise that the robustness of aluminium hydroxide gels towards breakdown induced by further dilution and/or excess of base follows the same trend.

In order to explain peculiarities of ultrasonic attenuation curves described above one needs to mention that the value of ultrasonic attenuation depends on absorption and scattering from the solid particles present in solution [65, 66 a]. The size and/or the concentration of the particles must be quite large to

cause absorption or scattering of ultrasonic waves with the frequency range of 5-15 MHz [66 b]. This fact explains why ultrasonic attenuation is relatively insensitive to the formation of primary ultra-fine particles of Al hydroxide dominating speciation patterns of Al-ions at $h < 2.8$ (this transformation can be detected at least qualitatively using DLS [2, 73, 76]). Ultrasonic attenuation appears to be reasonably sensitive to the appearance of larger particulates of sub-micrometer size near the point of electroneutrality (IEP) of Al hydroxide at $h = 3.0$. In this range DLS technique has detected a broad range of particulates with the sizes $100 < d < 2000$ nm [73, 76]. Also, increasing interactions between Al (oxy) hydroxide particles induces the increase of viscosity of the medium and, as a consequence, leads to increased absorption of ultrasonic waves. Therefore, the fluctuations of ultrasonic attenuation observed in Fig. (3.10) **b** at $h \geq 2.8$ are owing to the variations in both scattering and absorption of ultrasonic waves. This could explain the complexity of the observed ultrasonic attenuation curves as well as why the maxima in ultrasonic attenuation do not exactly coincide with the features of the titration curves measured with other techniques in this work.

The steepness of the increase in ultrasonic attenuation at the onset of gelation ($2.8 < h < 3.0$) appears to be correlated with the differing 'intrinsic acidity' of aluminium species used as precursors in sol-gel transformation. The steepness of the incline of ultrasonic attenuation in the discussed region of ultrasonic titrations is the highest for the Al_{30}-mer (Fig. (3.10) **b**) followed by Al_{13}-mers and Al hydroxide. In the case of $AlCl_3$ the steepness of the initial incline of the ultrasonic attenuation curve is close to that of the Al_{30}-mer. However, due to the 'local pH gradient' effects discussed above the overall increase of ultrasonic attenuation in the case of $AlCl_3$ is much lower than for other aluminium precursors and the initial incline does not match the highest 'acidity' of aluminium monomers.

3.4.3. Conclusions

Sol-gel transformation of aqueous solutions of aluminium-ions into aluminium (oxy) hydroxides induced by the addition of a 'soft base' - Trizma-base has been investigated using monotonic single-batch titrations and a bundle of four complimentary techniques for monitoring pH, conductivity, viscosity and parameters of ultrasound (ultrasonic velocity and attenuation). Pure aluminium species such as aluminium monomers, tridecamers ($[Al_{13}O_4(OH)_{24}(H_2O)_{12}]^{7+}$ or 'Al_{13}-mers', 'Al_{30}-mers' ($[Al_{30}O_8(OH)_{56}(H_2O)_{26}]^{18+}$) and monodisperse aluminium hydroxide particles synthesised using a patented technology of static anion exchange were used as precursors to aluminium (oxy) hydroxide gels. The multi-probe monitoring of the formation of aluminium oxy (hydroxide) has revealed that in the presence of non-complexing chloride-ions regardless of molecular nature of aluminium species sol-gel transformation proceeds via a similar pathway:

(1) Forced hydrolysis-condensation of Al-ions into molecular clusters of precisely defined structure - Al_{13}-mers at room temperature and Al_{30}-mers at elevated temperature (or prolonged reaction times). The end of this process is marked by the inflexion in the pH-metric titration curves at $h \sim 2.59 \pm 0.03$. Both conductivity and ultrasonic velocity measurements indicate the decrease of charge of Al species as a result of hydrolysis-condensation into larger structures. This process is fully complete at $h \sim 3.0$.

(2) Structural conversion of aluminium Keggin-like polynuclear clusters into nanoparticles of

aluminium (oxy) hydroxide above the first pH-metric inflexion $h \sim 2.59$. The course of this transformation depends on the molecular nature of the precursor.

(3) Aggregation of primary nuclei of aluminium (oxy) hydroxide into larger clusters which has been detected by the increasing scattering of ultrasonic waves resulting in elevated levels of ultrasonic attenuation (amplitude) in the vicinity of $h \sim 3.0$.

(4) 'Arrested growth' of the aggregates with the formation of the three-dimensional gel network which happens around the major inflexion in the potentiometric titration curves at $h = 3.0$. This event was detected by the dynamic viscosity probe (a jump on the corresponding titration curves). It is hypothesised that the amplitude of the viscosity jump can be related to the chemical stability and, possibly, mechanical properties of the gels. The amplitude of the viscosity jump agrees well with the molecular nature of aluminium species in question (their size, formal charge and 'intrinsic acidity' as manifested by the formal hydrolysis ratio).

(5) Breakdown of gel structures in the excess of free base (Trizma) is a complex phenomenon and it is best monitored by a combination of conductivity, ultrasonic velocity and attenuation measurements. Depending on the molecular nature of the precursors, the breakdown of gels follows very different patterns. In the case of the Al_{30}-mer the breakdown pattern is the most complex as it is not complete on the hydrolysis ratio scale of the experiment ($h \leq 4.4$) according to the ultrasonic attenuation data.

The effect of the strength of alkali (Trizma-base) used as a titrant on the type and pathway of sol-gel transformation has been outlined. It has been shown that the sol-gel transition pathway observed in the present study is due to weak-medium strength of Trizma-base ($pK_a = 8.3$).

Summarising the above, the combination of four complimentary monitoring techniques was able to trace down all major steps of sol-gel transformation as well as further fate of the gel network in the conditions of increasing base concentration. The use of ultrasonic spectrometry is shown to be especially beneficial for the monitoring of the later stages of aluminium (oxy) hydroxide formation and its eventual breakdown by the excess of base.

3.5. References

[1] K. L. Shafran, O. Deschaume, C. C. Perry, Adv. Eng. Mater., 2004, 6, 836.

[2] K. L. Shafran, C. C. Perry, Dalton Trans., 2005, 2098.

[3] A. R. Coscione, J. C. de Andrade, R. J. Poppi, C. Mello, B. van Raij, M. F. de Abreu, Anal. Chim. Acta, 2000, 423, 1, 31.

[4] A. Majeed, N. Javed, M. S. Khan, Pak. Science International (Lahore), 1996, 8, 1, 25.

[5] S. Lu, Fenxi Huaxue, 1985, 13, 8, 638.

[6] L. P. Holmes, D. L. Cole, E.M. Eyring, J. Phys. Chem., 1968, 72, 301.

[7] W. Blum, J. Amer. Chem. Soc., 1916, 38, 1282.

[8] A. K. De, in A Text Book of Inorganic Chemistry, 9th ed., New Age International (P) Limited, Publishers, 2003.

[9] J. Rosell, L. F. Nazar, J. Am. Chem. Soc., 2000, 122, 3777.

[10] L. Allouche, F. Taulelle, Inorg. Chem. Commun., 2003, 1167.

[11] J. R. Rustad, J. S. Loring, W. H. Casey, Geochim. Cosmochim. Acta, 2004, 68, 301.

[12] K. A. Evans, in Chemistry of Aluminium, Gallium, Indium and Thallium, ed. A.J Downs, 1993.

[13] J. J. Fitzgerald, A. H. Rosenberg, in Antiperspirants and Deodorants, Chapter 5 Chemistry of aluminium hydrolysis complexes, ed. Marcel Dekker, 1999.

[14] D. F. Baes Jr., R. E. Mesmer, in The hydrolysis of cations, Wiley-Interscience, 1976.

[15] P. M. Bertsch, D. R. Parker, in The Environmental Chemistry of Aluminium, Chapter Aqueous polynuclear aluminium species, ed. G. Sposito, Lewis publishers, CRC Press, 2nd edn., 1996, pp. 117-168.

[16] W. H. Casey, B. L. Philips, G. Furrer, Rev. Mineral. Geochem., 2001, 44, 167.

[17] J. W. Akitt, A. Farthing, New J. Magn. Reson. 1978, 32, 345.

[18] C. C. Perry, K. L. Shafran, J. Inorg. Biochem., 2001, 87, 115.

[19] L. Allouche, C. Gerardin, T. Loiseau, G. Ferey, F. Taulelle, Angew. Chem., Int., 2000, 39, 511.

[20] P. M. Bertsch, W. J. Layton, R. I. Barnhisel, Soil Sci. Soc. Am. J,. 1986, 50, 1449.

[21] P. M. Bertsch, G. W. Thomas, R. I. Barnhisel, Soil Sci. Soc. Am. J., 1986, 50, 825.

[22] J. W. Akitt, Prog. Nucl. Magn. Reson. Spectrosc., 1989, 21, 1-2, 1.

[23] E. Morgado, Y. L. Lam, L. F. Nazar, Colloid Interface Sci., 1997, 188, 257.

[24] Y.-P. Qin, E.-X. Wang, Dianchi, 2004, 34, 4, 307.

[25] M. A. Zayed, B. N. Barsoum, A. E. Hassan, Egyptian Journal of Chemistry, 1998, 41, 1-6, 187.

[26] J. Aleksandrowicz, M. Fiejka, T. Wysokinska, Medycyna Doswiadczalna i Mikrobiologia, 1991, 43, 3-4, 175.

[27] J. W. Akitt, A. Farthing, J. Chem. Soc. Dalton Trans., 1981, 2-5, 1606.

[28] S. Pokharna, K. D. Gupta, R. Mahla, C. Kirpalani, Asian J. Chem., 2004, 16, 3-4, 1765.

[29] J. Burgess, in Ions in Solution: Basic Principles of Chemical Interactions. Ellis Horwood, by Chichester / Halsted Press,. New York 1988.

[30] B. Mitrović, R. Milačić, B. Pihlar, Analyst, 1996, 121, 627.

[31] N. Senesi, M. Polemio, Nutrient Cycling in Agroecosystems, 1981, 1, 289.

[32] D. J. Greenwood, T. V. Karpinets, Soil Use and Management, 1997, 13, 178.

[33] S.-H. Lee, S.-M. Park, Y. Kim, Carbohydr. Polym., 2007, 70, 1, 53.

[34] D. K. Rai, S. Chandra, J. Phys. D: Appl. Phys., 1997, 30, 2078.

[35] E. C. Scholtz, J. R. Feldkamp, J. L. White, S. L. Hem, J. Pharm. Sci., 1984, 73, 967.

[36] T. J. Kloprogge, D. Seykens, J. B. H. Jansen, J. W. Geus, J. Non-Cryst. Solids, 1993, 152, 207.

[37] C.J. Brinker, G.W. Scherer, in Sol-gel science: the physics and chemistry of sol-gel processing (1990) Academic Press. 908 p.

[38] D. Helmut, H. Wolfgang, H. Dietmar, "Process and apparatus for the manufacture of sodium aluminate", European patent, No. 387492 (19 September 1990).

[39] R.O. Hutchins, K. Learn, B. Nazer, D. Pytlewski, Org. Prep. Proced. Int., 1984, 16, 335.

[40] C. C. Perry, T. Keeling-Tucker, J. Inorg. Chem., 2000, 78, 331.

[41] A. Nagendran, D. L. Arockiasamy, D. Mohan, Int. J. Polymer. Mater., 2008, 57, 2, 138.

[42] G. Arthanareeswaran, P. Thanikaivelan, N. Jaya, D. Mohan, M. Raajenthiren, J. Hazard. Mater. B, 2007, 139, 44.

[43] A. Nagendran, D. Mohan, Adv. Technol., 2007, 19, 1, 24.

[44] O. E. Philippova, N. S. Karybiants, S. G. Starodubtzev, Macromolecules, 1994, 27, 2398.

[45] V. D. Skirda, I. Y. Aslanyan, O. E. Philippova, N. S. Karybiants, A. R. Khokhov, Macromol. Chem. Phys., 1999, 200, 2152.

[46] F. Yamashita, T. Komatsu, T. Nakahawa, Bull. Chem. Soc. Jpn., 1976, 79, 2072.

[47] Chemistry of Aluminium, Gallium, Indium and Thallium, by A.J. Downs (Ed.), Chapman and Hall, London, 1993.

[48] The Environmental Chemistry of Aluminium, by G. Sposito (Ed.), Boca Raton, Lewis, 1996.

[49] D.J. Chadwick, J. Whelan (Eds.), Aluminium in Biology and Medicine, Wiley-Interscience, Chichester, 1992.

[50] J.T. Kloprogge, J. Porous Mater., 5 (1998) 5.

[51] C.J. Brinker, G.W. Scherer, Sol-Gel Science: The Physics and Chemistry of Sol-Gel Processing, New York, Academic Press, 1990.

[52] J.-P. Jolivet, Metal Oxide Chemistry and Synthesis. From Solution to Solid State, Chichester, Wiley and Sons, 2000.

[53] D.T. Richens, The Chemistry of Aqua Ions. Synthesis, Structure and Reactivity, John Wiley & Sons, Chichester, 1997.

[54] (a) K. Wefers, C. Misra, Oxides and Hydroxides of Aluminum. Alcoa Technical Paper No. 19, Revised, Alcoa, 1987, p. 92; (b) J.D. Hem, C.E. Roberson, ACS Symp. Ser., 416 (1990) 429.

[55] P.M. Huang, M.K. Wang, N. Kämpf, D.G. Schulze, in: J.B. Dixon, D.G. Schulze (Eds.), Soil Mineralogy With Environmental Applications, Soil Science Society of America, Inc. Book Series Number 7, Soil Science Society of America, Madison, WI, 2000, p. 261–290.

[56] D.F. Baes Jr., R.E. Mesmer, Boron, Aluminium and Scandium, in: The Hydrolysis of Cations, New York, Wiley-Interscience, 1976, p.112-123.

[57] (a) J.J. Fitzgerald, Chemistry of Aluminium Hydrolysis Complexes, in: Antiperspirants and Deodorants, New York, Marcel Dekker, 1988, p.119-296; (b) J.J. Fitzgerald, A.H. Rosenberg, Chemistry of Aluminum Chlorohydrate and Activated Aluminum Chlorohydrates, in K. Laden (Ed.), Antiperspirants and Deodorants, New York, Marcel Dekker, 1999, p.83-136.

[58] L. Allouche, C. Gerardin, T. Loiseau, G. Ferey, F. Taulelle, Agew. Chem. Int. Edit., 2000, 511, 39.

[59] J. Rowsell, L.F. Nazar, J. Am. Chem. Soc., 2000, 122, 3777.

[60] W.H. Casey, Chem. Rev., 2006, 106, 1.

[61] M. Henry, J.P. Jolivet, J. Livage, Struct. Bond., 1992, 77, 153.

[62] A. Fournier, K.L. Shafran, C.C. Perry, Anal. Chim. Acta, 2008, 607, 61.

[63] A.C. Vermeulen, J.W. Geus, R.J. Stol, P.L. DeBruyn, J. Colloid Interf. Sci., 1975, 51, 449.

[64] A.S. Dukhin, P.J. Goetz, T.H. Wines, P. Somasundaran, Colloids Surf., A - Physicochemical and Engineering Aspects, 2000, 170, 127.

[65] R.E. Challis, M.J.W. Povey, M.L. Mather, A.K. Holmes. Reports on Progress in Physics, 2005, V. 68, 7, pp. 1541-1637.

[66] (a) A.K. Holmes, R.E. Challis, J. Colloid Interface Sci., 216 (1999) 50; (b) F. Priego-Capote, M. D. Luque de Castro, Trends Anal. Chem., 2004, 23, 829.

[67] A.N. Kalashnikov, K.L. Shafran, R.E. Challis, C.C. Perry, M.E. Unwin, A.K. Holmes, V. Ivchenko, IEEE Ultrasonics Symposium, 2004, 1, 549.

[68] A.N. Kalashnikov, K.L. Shafran, V.I. Ivchenko, R.E. Challis, C.C. Perry, IEEE Transactions on Instrumentation and Measurements, 2007, 56, 1329.

[69] (a) K.L. Shafran, O. Deschaume, C.C. Perry, J. Mat. Chem., 2005, 15, 3415; (b) O. Deschaume, K.L. Shafran, C.C. Perry, Process of preparing aluminium species, International Patent WO2006/103092 A1; Filed on 05/10/2006.

[70] Z. Marczenko, M. Balcerzak, E. Kloczko, in: Separation, Preconcentration and Spectrophotometry in Inorganic Analysis, Amsterdam, Elsevier, 2000.

[73] (a) Ultrasonic Pulser Receiver. (2006, Jun.), Available online at: www.ndtsolutions.com; (b) R. C. Asher, Ultrasonic Sensors, Bristol, PA: IOP, 1997.

[74] A. N. Kalashnikov, V. Ivchenko, R. E. Challis, A. K. Holmes, "Compensation for temperature variation in ultrasonic chemical process monitoring," in Proc. IEEE Ultrason. Symp., Rotterdam, The Netherlands, 2005, p. 1151-1154.

[75] C.C. Perry, K.L. Shafran, J. Inorg. Biochem., 2001, 87, 115.

[76] S.P. Bi, X.D. Yang, F.P. Zhang, X.L. Wang, G.W. Zou, Fresenius J. Anal. Chem., 2001, 370, 984.

[77] (a) S.M. Bradley, R.A. Kydd, R. Yamdagni, Dalton Trans., 9 (1990) 2653-2656; (b) G. Fu, L.F. Nazar, A.D. Bain. Chem. Mater., 1991, 3, 602.

[78] Viscometer for particle sizing, Mater. Today, 2005, 8, 66.

[79] Z. Chen, B. Fan, X. Peng, Z. Zhang, J. Fan, Z. Luan, Chemosphere, 2006, 64, 912.

[80] J. Aveston, J. Chem. Soc.-London, 1965, 111, 4438.

[81] O. Deschaume, K.L. Shafran, C.C. Perry, Langmuir, 2006, 22, 10078.

Part 4

Speciation of Pure Aluminium Species

The 'formal' hydrolysis ratio (h = $[OH^-]/[Al^{3+}]$) of hydrolysed aluminium-ions is an important parameter required for the exhaustive and quantitative speciation-fractionation of aluminium in aqueous solutions. This work describes a potentiometric method for determination of the formal hydrolysis ratio based on an automated alkaline titration procedure. The method uses the point of complete precipitation of aluminium hydroxide as a reference (h = 3.0) in order to calculate the initial formal hydrolysis ratio of aluminium hydrolytic species. Several solutions of pure hydrolytic species including aluminium monomers ($AlCl_3$), Al_{13}-mers, Al_{30}-mers and aluminium hydroxide have been used as 'reference standards' to validate the proposed potentiometric method. Other important variables in the potentiometric determination of the hydrolysis ratio have also been optimised including the concentration of aluminium and the type and strength of alkali (Trizma-base, NH_4OH, $NaHCO_3$, Na_2CO_3 and KOH). The results of the potentiometric analysis have been cross-verified by quantitative ^{27}Al solution NMR measurements. The 'formal' hydrolysis ratio of a commercial basic aluminium chloride has been measured as an example of a practical application of the developed technique.

4.1. Automated pH-metric titrations of aluminium-ions. The effect of aluminium speciation

Typical examples of automated pH-metric titration curves obtained from titration of the Al-containing systems (0.004 $mol.L^{-1}$ solutions) with Trizma (free base, 0.1 $mol.L^{-1}$) are presented in Fig. (4.1). Initial titration curves ('integral mode' - pH *vs.* h) were re-calculated from the initial data (pH *vs.* volume of titrant) using the hydrolysis ratio as the x-axis, lines in Fig. (4.1). The first derivative curves ($\Delta pH/\Delta h$ vs. h) were obtained from the initial titration curves and these are presented in Fig. (4.1) as triangle symbol and line curves.

Potentiometric titration curves presented in Fig. (4.1) exhibit different numbers of inflexion points depending on the initial Al species present in the samples. For $AlCl_3$ solutions (with and without added HCl) there are three inflexions on the titration curves which correspond to early hydrolysis-

condensation of Al-ions (broad inflexion peak at $h \sim 0.25$, Fig. (4.1) **a** and **b** [1], followed by a long plateau due to the predominant formation of Al_{13}-mers. The second inflexion point at $h \sim 2.75 \pm 0.01$, Fig. (4.1) **a** and **b** arises from the breakdown of the structure of the dominant Al_{13}-mer clusters with their simultaneous conversion into colloidal Al hydroxide [1, 2]. The third inflexion observed during titrations of $AlCl_3$ with Trizma is due to the formation of Al hydroxide at $h = 3.0$, Fig. 1 **a** and **b**.

In the case of the samples containing pure Al hydrolytic clusters such as Keggin Al_{13}-mers and Al_{30}-mers there are only two inflexions observed on the titration curves, Fig. (4.1) **c** and **d**. These inflexions are of the same origin as the last two inflexion points in the titration of $AlCl_3$ discussed above. The inflexion of the Al_{30}-mer structural collapse is located at systematically lower hydrolysis ratio ($h = 2.53 \pm 0.02$) than the same peak for the Al_{13}-mer ($h = 2.58 \pm 0.02$). The peak of the major inflexion in Fig. (4.1) **c** and **d** is again very close to 3.0 ($h = 2.98 \pm 0.02$). The same is true for the potentiometric titration of Al hydroxide with Trizma which shows only one major inflexion at $h = 3.0$. Therefore, the data of Fig. (4.1) gives support for our main assumption that, providing all other conditions are met, one can use the position of the inflexion point at ca. $h = 3.0$ as a reference value in order to calculate the 'formal' hydrolysis ratio of samples of unknown Al speciation.

Additional data processing of the first-derivative titration curves was performed using peak-fitting module of Microcal Origin 6.1 software (Microcal Software Inc., MA, USA). Peak-fitting was used to refine the position of the inflexion points and resolve overlapping inflexions better. Two examples of the peak-fitting results are given in Fig. (4.2). The peaks on the first derivative pH-metric titration curves were fitted with a symmetrical Gaussian function with high goodness of fit (the correlation coefficient R^2 of the fitted curves was 0.9806 and 0.9976 for the titrations presented in Fig. (4.2). The maxima of the fitted peaks located precisely at the inflexion points made it easier to assign the reference of value of $h = 3.00$ to the major inflexion peak of Al hydroxide precipitation. This, in turn, enabled more precise and reproducible results of the formal hydrolysis ratio determination to be achieved using the proposed titrimetric procedure.

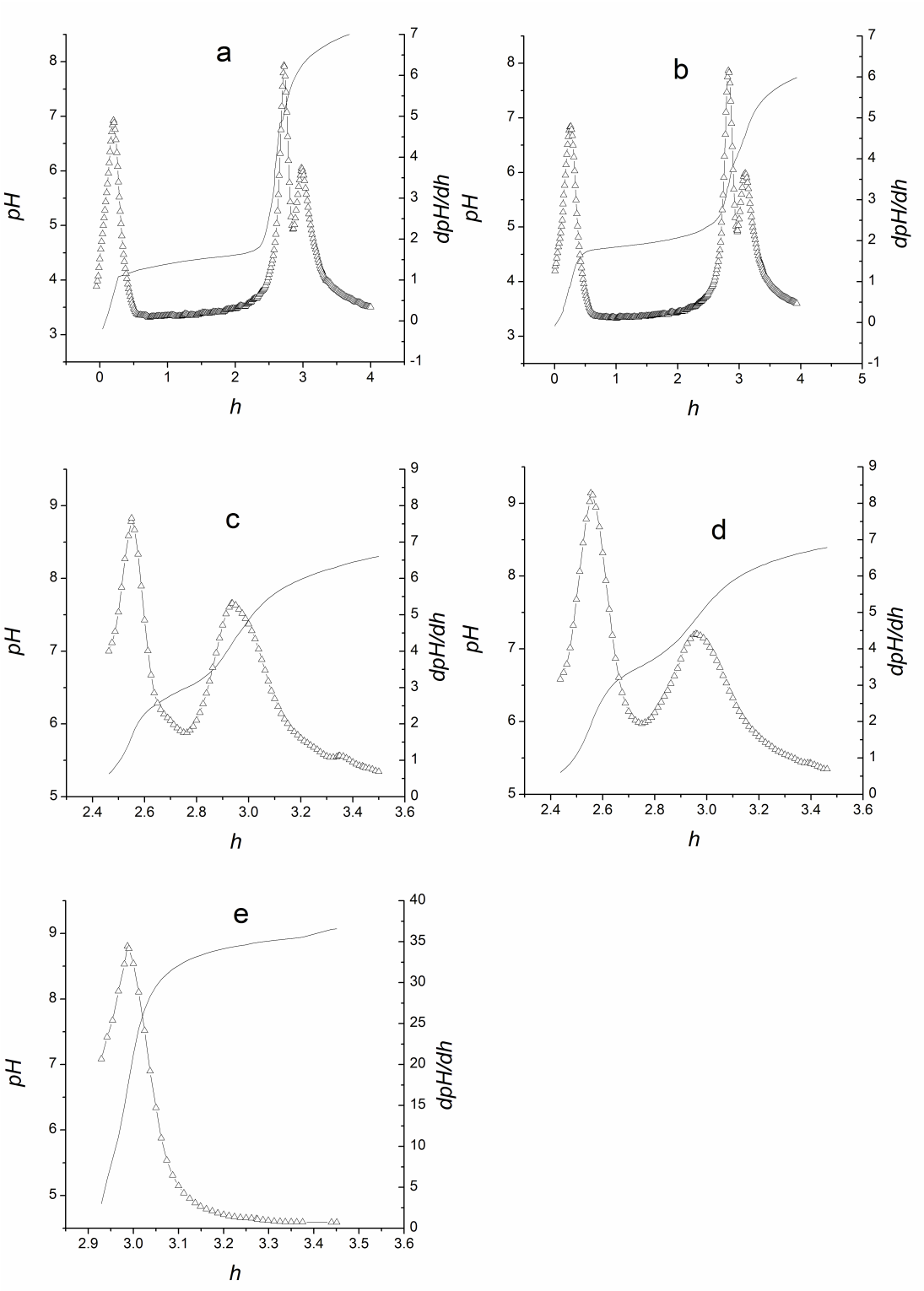

Figure 4.1. Integral (solid lines) and first-order derivative (solid lines with triangular symbols) curves of potentiometric titration of aqueous solutions of $AlCl_3$+HCl (***a***), $AlCl_3$ (***b***), Al_{13} (***c***), Al_{30} (***d***) and Al hydroxide (***e***) (all -with 0.004 mol.L^{-1} Al concentration) with Trizma base (0.1 mol.L^{-1}).

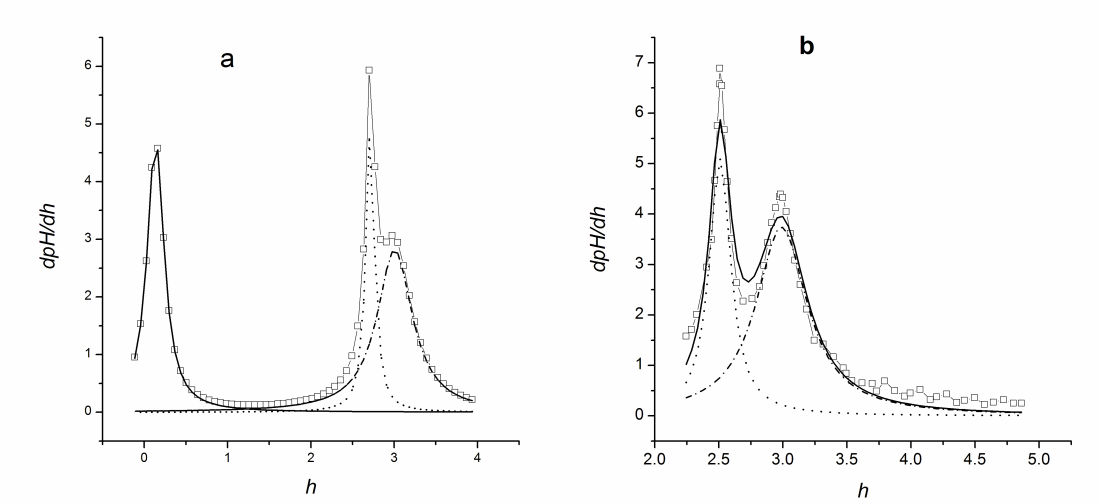

Figure 4.2. Examples of peak-fitting of the first derivative titration curves of $AlCl_3$ (***a***) and Al_{13}-mer (***a***) 0.004 mol.L^{-1} solutions obtained from titration with Trizma base (0.1 mol.L^{-1}). Lines with square symbols represent original first derivative curve data. Solid lines represent theoretical curves which are the sums of all fitted peaks. Fitted peaks are shown by dotted, dash-dotted and dashed lines.

4.2. Optimisation and validation of potentiometric measurements of hydrolysis ratio of aluminium-ion solutions

4.2.1. The effect of total aluminium concentration on pH-metric titrations of aluminium-ions

Total concentration of aluminium is an important parameter affecting the results of the potentiometric determination of the 'formal' hydrolysis ratio. In the present study this parameter was varied from 0.001 to 0.06 mol.L^{-1}. The set of titrations of Al_{13}-mer solutions with Trizma-base is shown in Fig. (4.3) **a** as an illustrative example of the effect of total Al concentration. Comparison of the determined values of formal hydrolysis ratio is given in Fig. (4.3) **b**.

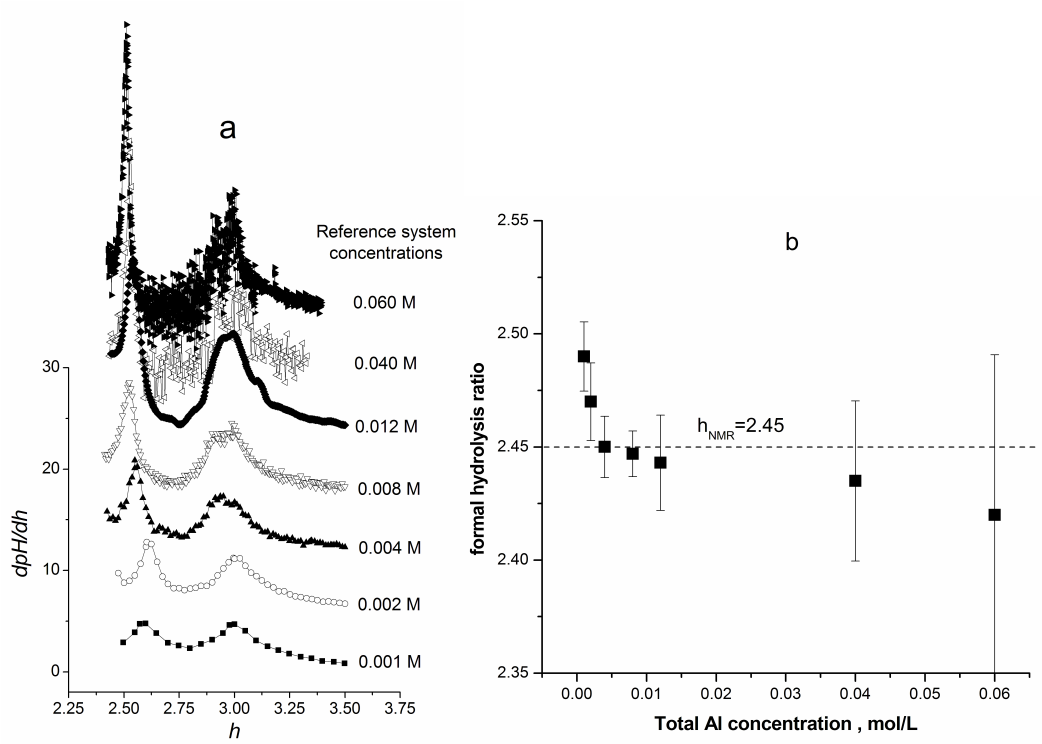

Figure 4.3. First-order derivative titration curves obtained from titrations of the Al_{13} reference system at various aluminium concentrations with 0.1 mol.L^{-1} Trizma-base (***a***). Formal hydrolysis ratios of Al_{13} solution determined from the titrations in Fig. (4.3) **a**.

From the data of Fig. (4.3) **a** one can find that for more concentrated Al_{13}-mer solutions ([Al] ≥ 0.04 mol.L^{-1}) there is a problem of assigning the major inflexion point (h = 3.0) which arises from higher local pH gradients and higher solid loading in the corresponding samples in the vicinity of Al hydroxide precipitation as a result. This effect is reflected by the increased noise of the titration data at higher Al concentrations, and sometimes, by strongly skewed or bifurcate major inflexion peak in the first-order derivative curves, Fig. (4.3) **a**. Similar trend was found for the other four reference systems of hydrolysed Al-ion species studied (results are not reported for the sake of brevity).

As follows from Fig (4.3) **b**, titrations at total aluminium concentration in the samples higher than 0.012 mol.L^{-1} led to a small but systematic underestimation of the formal hydrolysis ratio comparing to the reference value of h = 2.45 as measured by quantitative ^{27}Al NMR (represented as a horizontal dashed line in Fig. (4.3) **b**). The latter value is very close to the theoretical hydrolysis ratio of the Al_{13}-mer (h' = 2.462, absolute difference between measured values ~ 0.5 %). The so called 'local pH gradients' can strongly affect the results of experiments based on the neutralisation of aluminium ions with alkali. The origin of this phenomenon lies in the supersaturated nature of Al-ion solutions and, as a result, their instability towards the premature formation of Al hydroxide. When a strong alkali is added drop-wise, there is always an initial pH gradient between the localised alkali droplet and the bulk of the Al-ion solution before complete mixing takes place. The combined action of the supersaturation of the Al-ion solution and the local pH gradient (also called 'alkaline shock') results in premature formation of Al hydroxide which hinders a variety of experimental studies including potentiometric

measurements [1, 3]. This adverse effect cannot be eliminated completely by improving conditions of physical mixing (*e.g.* higher stirring rate, slower reagent addition, higher temperature, etc.). Another complication arising from the supersaturated nature of Al-ion solutions at higher Al concentrations ($C(Al) \geq 10^{-2}$ mol.L^{-1}) is the possibility of gel phase formation in the vicinity of the major inflexion point in the titration at $2.5 \leq h \leq 3.0$. The formation of a gel due to the high solid loading of hydrolysed Al-ion solutions with ultra-fine Al hydroxide particles can lead to incorrect pH measurements due to (*a*) increased viscosity, (*b*) blockage of the active surface of the glass pH electrode by Al hydroxide gel.

Another extreme one should try to avoid in the titrimetric determination of the formal hydrolysis ratio is high dilution of Al-containing samples. Increasingly dilute Al-ion solutions can cause changes in the Al speciation and alter the resulting hydrolysis ratio of the system, therefore biasing the results of the proposed method. This is reflected indirectly in the results of pH-metric titrations of Al_{13}-mers given in Fig. 3b which indicate that at [Al] < 0.004 mol.L^{-1} the determined value of the formal hydrolysis ratio was overestimated compared to NMR value of $h = 2.45$ with high statistical significance.

The optimum range of aluminium concentrations for the titrimetric determination of the formal hydrolysis ratio was found to be between 0.004 and 0.012 mol.L^{-1}. The values of h were the closest to the theoretical hydrolysis ratios of the corresponding Al species (as well as hydrolysis ratios estimated with ^{27}Al NMR, were applicable) and the analytical error was at minimum (relative standard deviation < 2 %). Therefore, this range of Al concentrations can be recommended for accurate and reproducible determination of the 'formal' hydrolysis ratio of Al-ion based systems.

4.2.2. The effect of alkali strength on pH-metric titrations of aluminium-ions

Another very important parameter of the pH-metric determination of the 'formal' hydrolysis ratio is the type and strength of alkali employed as a titrant. We have compared five alkalis of different strengths varying from a very weak base ($NaHCO_3$) to a very strong base (KOH). The results of the automated pH-metric titrations of the Al_{30}-mer reference system (h' = 2.40) are shown in Fig. (4.4) as an illustrative example.

As follows from Fig. (4.4), for KOH, the separation between inflexions corresponding to the structural transformation of Al_{30}-mers into Al hydroxide ($h \sim 2.46$) and precipitation of Al hydroxide ($h \sim 3.0$) is the largest among the alkalis compared. The peak of the major inflexion at $h = 3.0$ on the 'ΔpH/Δh vs. h' curve is also the sharpest for KOH (Fig. (4.4) **b**) and is more distinct than the broad and diminished peak of the first inflexion ($h \sim 2.46$). For weaker alkalis ($NaHCO_3$ and Trizma, Fig. (4.4) **a** and **d**), one can observe the broadening of the second inflexion at $h = 3.0$ as well as a constant drift of the first inflexion towards higher hydrolysis ratios (bearing in mind that the position of the second peak is set manually to $h = 3.0$ as a reference point).

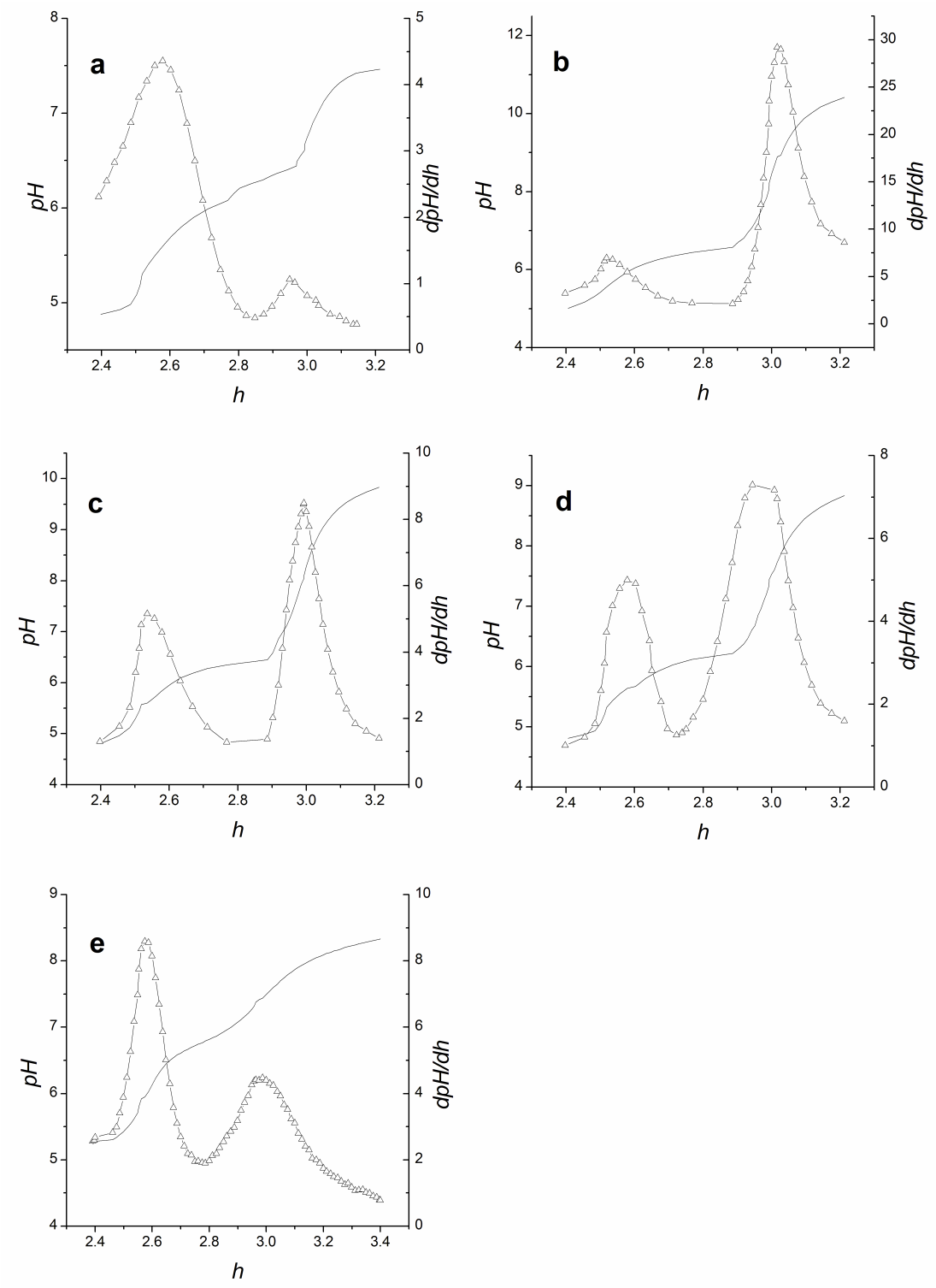

Figure 4.4. Automated potentiometric titrations (integral and first-order derivative curves) of the Al_{30}-mer solution (0.004 mol.L^{-1}) with different bases: $NaHCO_3$ (***a***), KOH (**b**), Na_2CO_3 (***c***), NH_3 (***d***) and Trizma-base (***e***) (concentration of all bases - 0.1 mol.L^{-1}).

The gap between the first and second inflexion points reaches a minimum for $NaHCO_3$ ($\Delta h \sim 0.35$). In this case the second inflexion was found to be consistently below the postulated reference point $h = 3.0$ (the value of the formal hydrolysis ratio was estimated to be $h \sim 2.96$ as calculated using Eq. (2.6) from

Material and Methods section, and known values of Δh and h). This feature of the titration of Al ions with $NaHCO_3$ has been observed previously [1] and most probably arises from the buffering effect of sodium bicarbonate which reaches a maximum in the vicinity of pH = $pK_{a1}(NaHCO_3)$ = 6.35. Comparison of the results of determination of the 'formal' hydrolysis ratio for two 'reference' systems of Al_{13}-mer and Al_{30}-mer solutions using five alkalis of different strength is presented in Fig. (4.5).

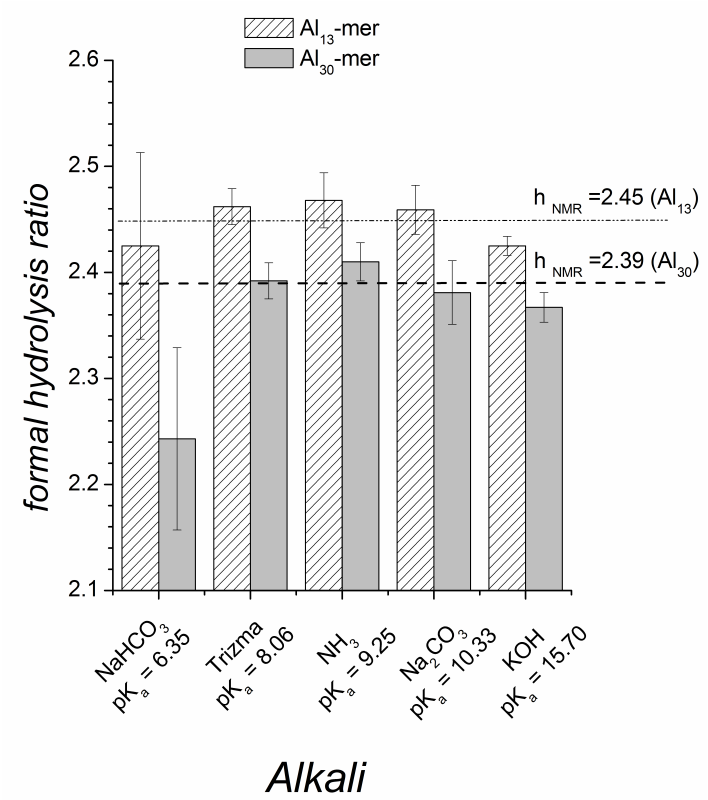

Figure 4.5. The effect of alkali strength (as indicated by its pK_a) on the value of the formal hydrolysis ratio of the Al_{13}-mer and Al_{30}-mer reference solutions (total aluminium concentration - 0.004 mol.L^{-1}) measured potentiometrically. Horizontal lines indicate the values of the hydrolysis ratio of the Al_{13}-mer solution determined independently by ^{27}Al solution NMR spectroscopy. Concentration of all alkalis used to collect the data presented in this graph was 0.1 mol.L^{-1}.

The data of Fig. (4.5) indicates that the results of the determination of 'h' with Na_2CO_3, NH_3 and Trizma-base are closest to the theoretical values for the Al_{13}-mer (h' = 2.46) and the Al_{30}-mer (h' = 2.40) as well as reference values obtained from the ^{27}Al solution measurements (h = 2.45 ± 0.01 for the Al_{13}-mer and h = 2.39 ± 0.02 for the Al_{30}-mer). The data from the titrations with sodium bicarbonate are subject to larger error compared to other alkalis. This fact can be explained by the fact that the inflexion corresponding to Al hydroxide is skewed by the buffering effect of CO_2(aq.) - HCO_3^- system and possible gel formation as pointed out above. Use of potassium hydroxide as a titrant leads to statistically significant underestimation of the formal hydrolysis ratio of both Al hydrolytic clusters (Fig. (4.5)) most probably due to the strongest 'alkali shock' or local pH gradient upon the addition of this strong base.

On the basis of the above comparison of five different alkalis the optimum window of alkali strength for the determination of the 'formal' hydrolysis ratio of Al species in solution is in the range of 8.0 ≤

$pK_a \leq 10.4$ (*e.g.* Trizma, NH_4OH or Na_2CO_3). Sodium bicarbonate ($pK_a << 8.0$) and strong alkalis such as KOH or NaOH ($pK_a >> 10.4$) are not recommended for this purpose.

4.2.3. Comparison of pH-metric titrations and quantitative ^{27}Al solution NMR for the determination of the 'formal' hydrolysis ratio

Accuracy of the 'formal' hydrolysis ratio *h* of the reference systems containing various Al species determined by means of the proposed potentiometric method was cross-verified using quantitative ^{27}Al solution NMR analysis of Al speciation. ^{27}Al NMR spectra of the five 'reference' systems used in this study are presented in Fig. (4.6).

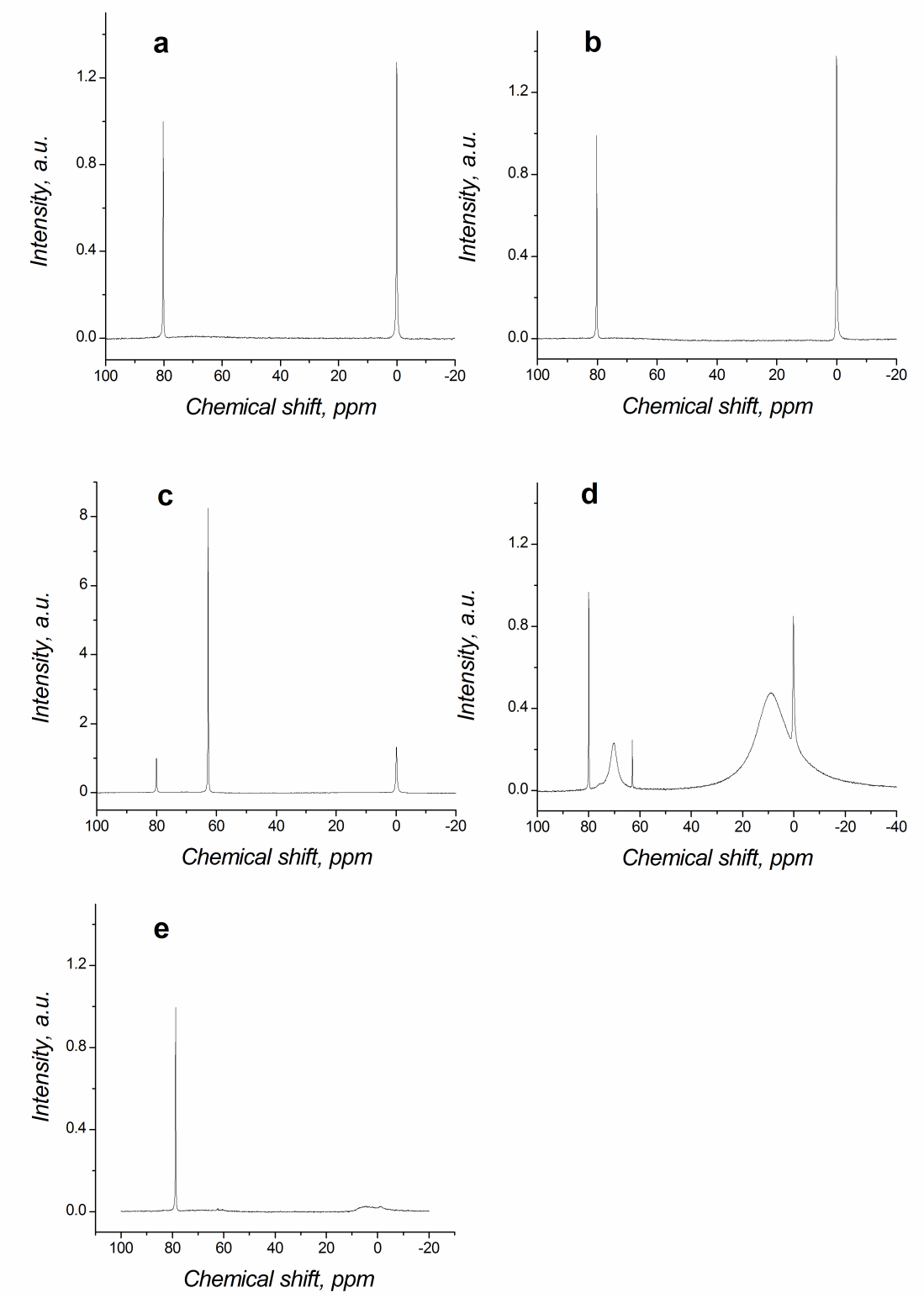

Figure 4.6. ^{27}Al solution NMR spectra of the initial Al reference systems: $AlCl_3$+HCl (***a***), $AlCl_3$ (***b***), Al_{13} (***c***), Al_{30} (***d***) and Al hydroxide (***e***) (0.04 mol.L^{-1}) solutions. The peak at 80 ppm in all spectra arises from the internal standard ($NaAlO_2$ in D_2O). All spectra apart from (***d***) were recorded at 25 °C, the spectrum (***d***) - at 70 °C.

The peak at 80 ppm in all of the NMR spectra in Fig. (4.6) corresponds to the signal of the external

standard - $NaAlO_2$ solution in D_2O. For $AlCl_3$ solutions (with or without added HCl), the only signal present in the ^{27}Al NMR spectra is the peak at ~ 0 ppm, Fig. (4.6) **a** and **b**, arising from Al monomeric species [4]. The spectrum of the Al_{13}-mer reference solution contains two signals; strong and sharp peak at 63 ppm arising from the tetrahedral 'core' Al atom of the Al_{13}-mer [4] and a relatively small signal of Al monomers at 0 ppm, Fig. (4.6) **c**. Since the ^{27}Al NMR spectrum was performed at 25^oC, the signal of the octahedrally coordinated aluminium does not appear. The spectrum of the Al_{30}-mer solution, Fig. (4.6) **d**, along with the peaks described above contains broad peaks at 70 and 10 ppm arising from the tetrahedral and octahedral Al atoms of the Al_{30}-mer structure respectively [5]. In the spectrum of Al hydroxide suspension (Fig. (4.6) **e**) only very tiny peaks at 63 and 0 ppm (not visible in the figure) arising from respectively the Al_{13}-mer and Al monomers can be observed. This fact indicates that the majority of Al-ions have been converted into Al hydroxide phase undetectable by solution NMR. The acquired ^{27}Al solution NMR spectra were subjected to a data treatment described previously [6] in order to obtain quantitative information on Al speciation, Table (4.1).

Table 4.1. Quantitative speciation of five Al-containing reference systems ($C(Al)_{total}$ = 0.004 $mol.L^{-1}$) by ^{27}Al solution NMR.

Species	**Al reference systems**			
distribution / %	**$AlCl_3$+ HCl**	**$AlCl_3$**	**Al_{13}**	**Al_{30}**
Al hydroxide				
Al monomers	100.0	99.06	0.73	0.21
0.90				
Al oligomers (Al_2, Al_3)	0.0	0.94	0.0	0.0
0.75				
Al_{13}-mers	0.0	0.0	98.17	4.56
1.40				
Al_{30}-mers	0.0	0.0	1.10	95.23
0.0				
Al hydroxide	0.0	0.0	0.0	0.0
96.95				

As follows from Table (4.1) reference systems of hydrolysed Al species (Al_{13}-mers, Al_{30}-mers and Al hydroxide) demonstrate high purity which has been achieved due to the use of the static anion exchange technique used for the synthesis of these samples [7].

The results of comparison of the formal hydrolysis ratio determined by means of the potentiometric method proposed in the present study and by quantitative ^{27}Al NMR spectroscopy described in [3] are summarised in Table (4.2).

The data of Table (4.2) shows the results of the potentiometric titration method follow very closely the data obtained from quantitative ^{27}Al NMR measurements. The largest difference between NMR and potentiometric results was in the case of Al hydroxide. However, the formal hydrolysis ratio of Al hydroxide was determined by NMR indirectly, and in the calculation the hydrolysis ratio of colloidal

Al hydroxide was arbitrarily set to $h'(Al(OH)_3)$ = 3.0 which is generally not the case below the precipitation point (h = 3.0, pH ~ 6.9 - 7.0). Therefore, potentiometric titration in this case provides a less ambiguous value of h than NMR spectroscopy.

Table 4.2. Results of determination of the 'formal' hydrolysis ratio h of five Al reference systems (Al concentration in all of the samples - 0.004 mol.L^{-1}) by automated potentiometric titrations using 0.1 mol.L^{-1} Trizma base as a titrant and by quantitative ^{27}Al solution NMR technique.

Reference systems	**$C(Al)_{total}$ mol/L**	**Titrimetry**			**NMR**	**Difference**
		***h*(Al hydroxide)**	**Δh**	***h*(pH)=3 - Δh**	***h*(NMR)**	***h*(pH)–*h*(NMR)**
$AlCl_3$+ HCl						
0.418	3.000	3.380	- 0.380	- 0.375*	- 0.005	
$AlCl_3$						
0.400	3.000	3.006	- 0.006	0.006	- 0.012	
Al_{13}						
0.353	3.000	0.547	2.453	2.450	0.003	
Al_{30}						
0.419	3.000	0.608	2.392	2.390	0.002	
Al hydroxide						
0.300	3.000	0.041	2.959	2.929	0.030	

$C(Al)_{total}$ is the total Al concentration of the initial Al reference system, h (Al hydroxide) is the hydrolysis ratio assigned to the inflexion of Al hydroxide precipitation, $\Delta h = C(OH)_{added}/ C(Al)_{total}$ is the measured value of change in hydrolysis ratio during titration; h (pH) is the 'formal' hydrolysis ratio of Al-ion solution determined using pH-metric titrations and h (NMR) is the same parameter determined by ^{27}Al NMR method.

* - in the case of the system '$AlCl_3$ + HCl' the formal hydrolysis ratio was calculated using Eq. 2 from fixed initial concentrations of both constituents, $AlCl_3$ (h' = 0.0) and HCl (h' = -1), rather than from ^{27}Al NMR data alone.

4.3. Determination of the formal hydrolysis ratio in a commercial sample of aluminium basic chloride

The optimised and validated potentiometric method described in this study was tested on a commercial solution of basic aluminium chloride salt - ACH Microdry (Reheis, Berkeley Heights, NJ, USA) of unknown composition and the results were compared with the data of ^{27}Al NMR. An example of the titration of the ACH solution with Trizma is shown in Fig. (4.7).

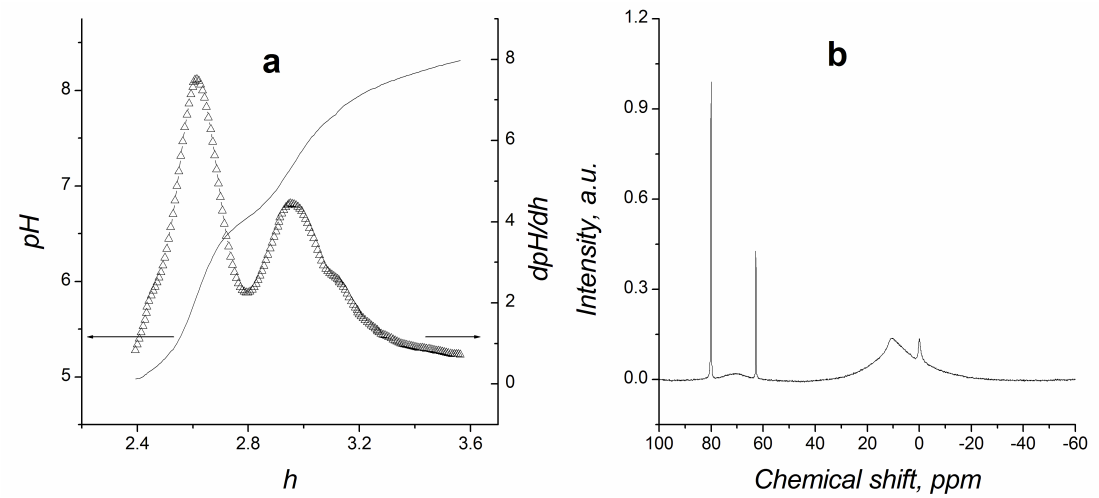

Figure 4.7. Automated potentiometric titration of an 0.4 mol.L^{-1} aluminium chlorohydrate solution (ACH Microdry, Reheis, Berkeley Heights, NJ, USA) with Trizma-base 0.1 mol.L^{-1} (pH-metric curve (line) with its derivative curve (line with symbol)) (***a***) and its ^{27}Al solution NMR spectra recorded at 25 °C (***b***). The peak at 80 ppm arises from the internal standard ($NaAlO_2$ in D_2O).

From the data of Fig. (4.7) one can find that Keggin-like ions (Al_{13} and Al_{30}) constitute a major part of the commercial ACH sample as follows from the profound first inflexion peak at $h \sim 2.60$. This result was confirmed by ^{27}Al NMR data according to which the fraction of Al_{13}-mers is *ca.* 9 % of the total Al content and the fraction of Al_{30}-mers is 83 % making a total of 92 % (other Al species such as Al monomer, oligomers and hydroxide are of minor importance as none of them exceeds 5 % of total Al content). The value of the 'formal' hydrolysis ratio determined by pH-metric titration is $h \sim 2.392 \pm 0.023$ which is close to the value determined by ^{27}Al solution NMR ($h = 2.407 \pm 0.021$). The difference between the methods is less than 0.7 % and the relative standard deviation (RSD %) of potentiometric determination did not exceed 1.0 %.

4.4. Conclusions

Summarising the results of the present investigation one can conclude that the value of 'formal' hydrolysis ratio is an important analytical parameter defining the overall 'basicity' or 'acidity' of hydrolysed Al-ion solutions and it has direct connection with the overall molecular hydrolysis ratio defined by complete Al speciation-fractionation.

The proposed potentiometric method of determination of the formal hydrolysis ratio can find practical applications in the areas where the knowledge of total aluminium speciation would be beneficial, for instance, in the synthesis of structural and ceramic materials, for the use of Al species as water treatment agents and antiperspirant actives, for clay pillaring agents in catalytic applications, etc. The advantage of the proposed method compared with other techniques of determining the 'basicity' of Al-ion solutions and basic aluminium salts including potentiometric methods [8, 9] is that the present method uses a well-defined reference point which corresponds to the precipitation of Al hydroxide which in the presence of non-complexing anions and in the absence of local pH perturbations must be

at h = 3.0. Also, the proposed method has been carefully optimised using a number of important parameters and cross-verified by means of quantitative ^{27}Al NMR technique.

An optimum range of aluminium concentrations was identified in this study to be within the range of 0.004 - 0.012 mol.L^{-1} in which both excessive dilution and local pH gradients due to alkali addition are minimised. The best alkalis to use for the potentiometric titration are Trizma-base, NH_3 and Na_2CO_3. The present study has shown that the strength of alkali must be within an optimum range of pK_a ($8.0 \leq pK_a \leq 10.33$). Below this range the self-buffering effect of weak base does not allow for the reference point of Al hydroxide precipitation to be established correctly. Stronger alkalis (*e.g.*, KOH) lead to underestimated results due to enhanced local pH gradients.

Precision and accuracy of the proposed potentiometric method was tested using a set of five 'reference' systems with known amounts of aluminium and pre-defined Al speciation patterns. The titrimetric technique of the 'formal' hydrolysis ratio determination is precise (relative standard deviation did not exceed 2 % for all titrations conducted). The accuracy of the technique was cross-verified using an independent analytical method - quantitative ^{27}Al NMR spectroscopy. It was found that the results from pH-metric titrations of all five 'reference' systems containing Al monomers ($AlCl_3$ solutions with and without HCl), Keggin Al_{13}-mers and Al_{30}-mers and Al hydroxide particles do not differ from the NMR results by more than 3 % (absolute difference). The proposed method of potentiometric determination of the 'formal' hydrolysis ratio was tested on a commercial sample representing basic aluminium chloride ('aluminium chlorohydrate' or ACH). It was found that the hydrolysis ratio of the commercial basic aluminium chloride is determined primarily by Keggin-like polyoxocations and Al hydroxide present in the sample and is within 0.7 % absolute difference of measured values from ^{27}Al NMR determination.

4.5. References

[1] C.C. Perry, K.L. Shafran, Journal of Inorganic Biochemistry, 2001, 87, 115.

[2] S. Bi, C. Wang, Q. Cao, C. Zhang, Coordination Chemistry Reviews, 2004, 248, 441.

[3] K.L. Shafran, C.C. Perry, Dalton Trans., 2005, 12, 2098.

[4] J.W. Akitt, Prog. Nucl. Magn. Reson. Spectrosc., 1989, 21, 1.

[5] L. Allouche, C. Gerardin, T. Loiseau, G. Ferey, F. Taulelle, Angew. Chem. Int. Ed., 2000, 39 511.

[6] K.Shafran, O.Deschaume, C.C.Perry, Adv. Eng. Mater., 2004, 6, 836.

[7] K.L.Shafran, O. Deschaume, C.C. Perry, J. Mat. Chem., 2005, 15, 3415.

[8] K.E. Hancock, G.E. Peck, D.L. Perry, J.L. White, S.L. Hem, J. Colloid Interface Sci., 1996, 183, 431.

[9] J. Klein, M. Ushio, L.S. Burrell, B. Wenslow, S.L. Hem, J. Pharm. Sci., 2000, 89, 311.

Part 5

Complexation Properties of Lactic Acid, a Strongly Binding Ligand towards Aluminium Polyoxocations and Aluminium Hydroxide Colloids

The formation of complexes between aluminium species and lactic acid was investigated by ^{27}Al and ^{1}H solution NMR and Fourier transform infrared spectroscopic methods and spectrophotometric technique in aqueous solutions at room temperature. The aim of this study was to observe the effect of lactic acid, a strongly binding ligand, on four different hydrolysed aluminium-ion solutions, namely $AlCl_3$, Al_{13}-mer, Al_{30}-mer and an aluminium hydroxide suspension with particles size of 100 ± 11 nm.

5.1. Preparation of the aluminium-lactic acid reaction systems

A series of model aluminium-biomolecule solutions were prepared at room temperature by the addition of different amounts of fresh biomolecule stock solution to each of the four model aluminium-containing systems as described in [1]. The final aluminium concentration in the aluminium-biomolecule solutions was 0.15 $mol.L^{-1}$, and the lactic acid concentration was varied from 2.5 to 25 $mg.mL^{-1}$ in steps of 2.5 $mg.mL^{-1}$. Although the concentration of blood lactic acid is usually berween 1.10^{-3} $mol.L^{-1}$ and 2.10^{-2} $mol.L^{-1}$ [2(a)] (0.0901 and 0.8016 $mg.mL^{-1}$ respectively), the experiments were prepared with lactic acid at concentrations above the biological concentrations in order to make comparisons between the different biological compounds used throughout the study. Table (5.1) displays the aluminium:lactic acid molecular ratios. Aluminium hydroxide particles were modelled as cylinders with 2 nm height and 50 nm radius. Moreover the density chosen was 2.42 $g.cm^{-3}$ [2(b)].

Table 5.1. Interval of molecular aluminium species: lactic acid ratios used.

Al hydroxide : lactic acid	Al_{30}-mer : lactic acid	Al_{13}-mer : lactic acid	$AlCl_3$: lactic acid	[lactic acid], $mol \cdot L^{-1}$
$6.97 \cdot 10^{-5}$: 1	0.180 : 1	0.416 : 1	5.405 : 1	$2.78 \cdot 10^{-2}$
$7.00 \cdot 10^{-6}$: 1	0.018 : 1	0.042 : 1	0.541 : 1	$2.78 \cdot 10^{-1}$

5.2. Chemical and physical properties of the aluminium: lactic acid solutions.

Lactic acid is a weak hydroxycarboxylic acid with a pK_a of 3.85. In order to illustrate the species distribution of a lactic acid solution *vs.* pH, the version 3.1 of SPARC on-line calculator 14 (http://ibmlc2.chem.uga.edu/sparc/) was used. The deprotonation of the carboxylic group was ~ 100 % at pH above 6, Figure (5.1). For a pH value between 3.85 and 6, lactic acid solutions also contained some of the deprotonated form, lactate. Therefore, aluminium-lactate assemblies could be formed from pH 3 upwards.

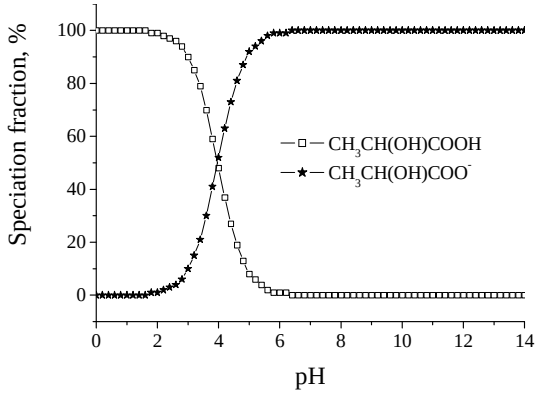

Figure 5.1. Speciation plot of a pure lactic acid solution.

Interactions of aluminium species and lactate were first investigated by pH, conductivity and viscosity measurements. The measurements were carried out simultaneously, after ageing the samples for 24 h and data are presented in Figure (5.2). No precipitate was detected in the samples.

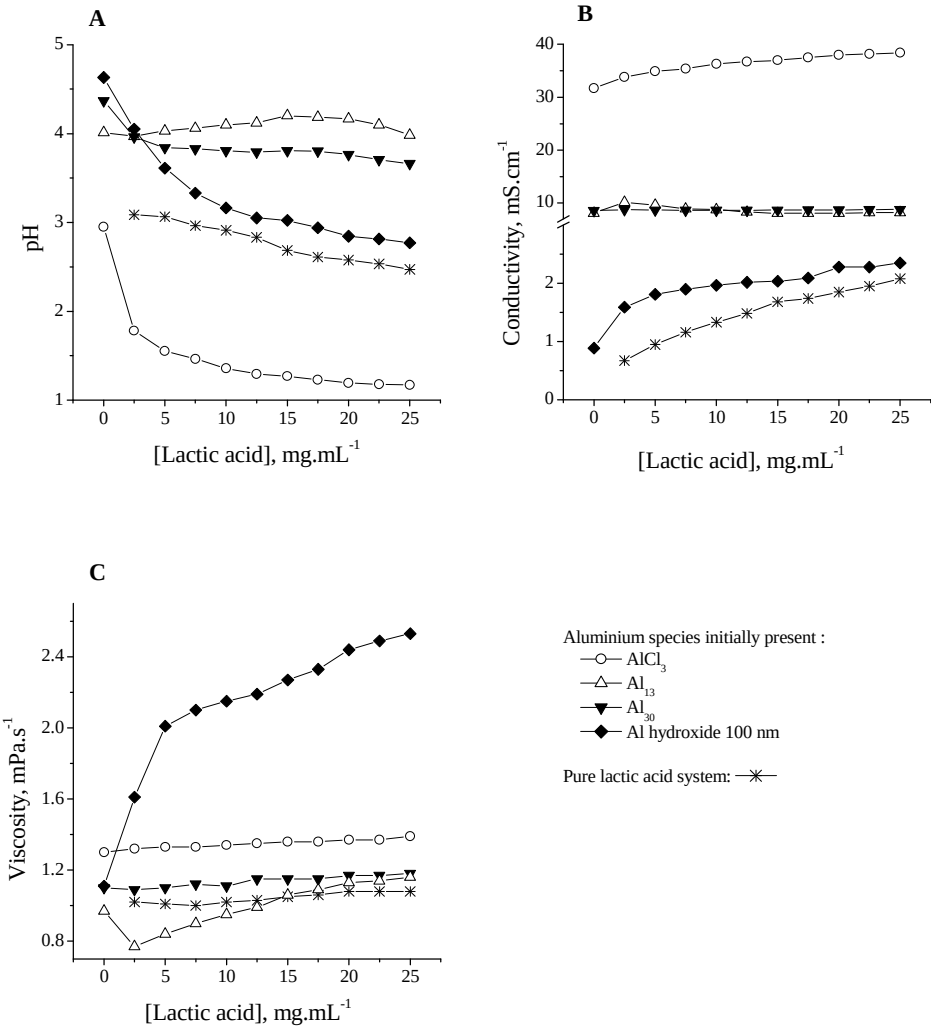

Figure 5.2. (**A**) pH, (**B**) conductivity and (**C**) viscosity of pure lactic acid solutions and aluminium species-lactic acid solutions prepared at various lactic acid concentrations.

Pure lactic acid 2.5 mg.mL^{-1} in aqueous solution had a pH around 3.1 as indicated by Figure (5.2 - **A**). At this pH, the protonated form of lactic acid is predominant according to Fig. 5.1. An increase in lactic acid concentration caused a decrease in pH attributable to a concentration-effect of the acid. Similarly, the pH of the aluminium monomer-lactate systems decreased with an increase in lactic acid concentration, due to additions of this acid to the Al-ion solutions. Addition of lactic acid to the mixtures containing the Al_{13}-mers caused the breakdown of the aluminium polycations due to the decrease of the pH of the medium, and the formation of aluminium-lactate complexes as evidenced by ^{27}Al and ^{1}H NMR spectroscopies (see below). Buffering effect of the medium containing Al_{13} species with the increasing concentration of lactic acid is also an indirect evidence of the breakdown of aluminium polycations. For the Al_{30}-lactate samples, the trend was similar to that observed with the Al_{13}-lactate mixtures. The added lactic acid promoted the acidic breakdown of the Al_{30}-mer and at the same time, lactate was complexed by the breakdown products of the Al_{30}-mers polycations. As a result of this process the pH of solution was maintained at the same level in spite of increasing lactic acid concentration. The initial pH of the

aluminium hydroxide-lactate systems was systematically higher than that of the aluminium polycations-lactate samples and decreased most dramatically among aluminium species studied with the increasing lactic acid concentration. The drop of pH was probably a consequence of slower breakdown kinetics of Al hydroxide and, therefore, slower buffering effect on the time scale of the experiment.

The systems containing aluminium species had a higher conductivity than those made of pure lactic acid, Figure (5.2) (**B**). This was due to the higher number of charges carried by the aluminium species compared to the charges borne by lactic acid. Furthermore, the conductivity σ of the aluminium-containing samples varied as follow: σ (aluminium hydroxide particles) < σ (aluminium polycations) < σ (aluminium monomers). The systems containing the aluminium polycations did not undergo any conductivity variation upon increase of lactic acid concentration whereas in the presence of the other aluminium species, conductivity increased.

Apart from the systems containing aluminium hydroxide particles, addition of lactic acid did not appear to affect the viscosity of the systems, Figure (5.2) (**C**). The absence of modification of viscosity for the majority of the samples signified that there was no formation of long chain polymeric complexes within the samples. In the case of Al hydroxide the residual charge on colloidal particles must be relatively small comparing to aluminium polycations (~ 0.15 charge per aluminium atom as calculated using the formal hydrolysis ratio of aluminium hydroxide close to 2.85). Therefore, assuming electrostatic character of initial interaction between lactic acid largely deprotonated at pH ~ 4.5 and positively charged surface of aluminium hydroxide, only 0.15 mole-equivalents (0.0225 $mg.mL^{-1}$) of lactic acid would be theoretically required to completely neutralise the charge of aluminium hydroxide particles. It is well known that in the vicinity of the point of electroneutrality colloidal particles become increasingly unstable towards aggregation and subsequent gelation or coagulation. This process was probably a reason behind the increase of viscosity of 'aluminium hydroxide - lactic acid' samples.

As a result of mixing together aluminium reference systems with lactic acid, aluminium underwent an acidic hydrolysis which modified its speciation within the samples. ^{27}Al NMR spectroscopy was intended to clarify the extent of that reaction.

5.3. ^{27}Al NMR spectroscopy

^{27}Al solution NMR measurements of the samples of aluminium species with various amounts of lactic acids were performed along with bulk measurements described above in order to establish molecular nature of this interaction. The signal at 80 ppm appearing in all the ^{27}Al NMR spectra acquired arises from aluminate-ions in the D_2O of the internal reference solution [3].

^{27}Al NMR measurements of the aluminium monomer - containing samples

The NMR spectra of the aluminium monomer-lactate samples and calculated speciation diagram are presented in Figure (5.3). As described by Karlik et al. [4], the ability of lactate to bind to aluminium ions is pH-dependent. At relatively low pH < 4 (as in the case of aluminium monomers) complexation

of Al^{3+} ions and lactic acid is hindered by predominantly protonated state of the latter. Nonetheless, the complex formation still occurs as evidenced by ^{27}Al NMR. The peak of the hexaaquo-aluminium monomer at 0 ppm in Figure (5.3) (**A**) decreases in intensity while, simultaneously, two new downfield signals appeared; a weak one centered at 14 ppm and another one centered at 6 ppm which had a high symmetry. After peak fitting of those new signals, Figure (5.3) (**C**), the 14 ppm signal represented 16 % of the 6 ppm signal. The peak fitting also allow one to quantify the aluminium-lactate complexes. The peak at 14 ppm has been assigned previously to $[(HLact^{-})_2Al^{3+}(H_2O)_2]$ [4] or (less likely) to $[(Lact^{2-})_2Al^{3+}(H_2O)_2]$ [5]. The 6 ppm signal has been attributed to $[H(Lact^{-})Al^{3+}(H_2O)_5]$ complex [5]. In all of these complexes, complexation occurs in the first coordination sphere of aluminium by direct substitution of water molecules around aluminium atom by lactate molecules. The increase of lactic acid concentration in aluminium-lactate solutions drives the complexation process as indicated by the increase of the NMR signals attributed to these complexes (Fig. 5.3A). However, the process somewhat steadies above [lactate] ~ 5 $mg.mL^{-1}$ and the aluminium-lactate fraction reaches only 17.55 % of the total aluminium concentration at [lactate] = 25 $mg.mL^{-1}$ due to the conditions of low pH adverse for complexation as discussed above.

The NMR signals of aluminium-lactate complexes have a relatively large bandwidth comparing to the signal of aluminium hexaaquocation at 0 ppm due to a gradual decrease in symmetry when changing from highly symmetrical structure of $[Al(H_2O)_6]^{3+}$ complex to less symmetrical bis-lactate complex and even less symmetrical mono-lactate complex. The signal of tris-lactate aluminium complex would be expected therefore to have a narrower bandwidth comparing with the first two aluminium-lactate compounds.

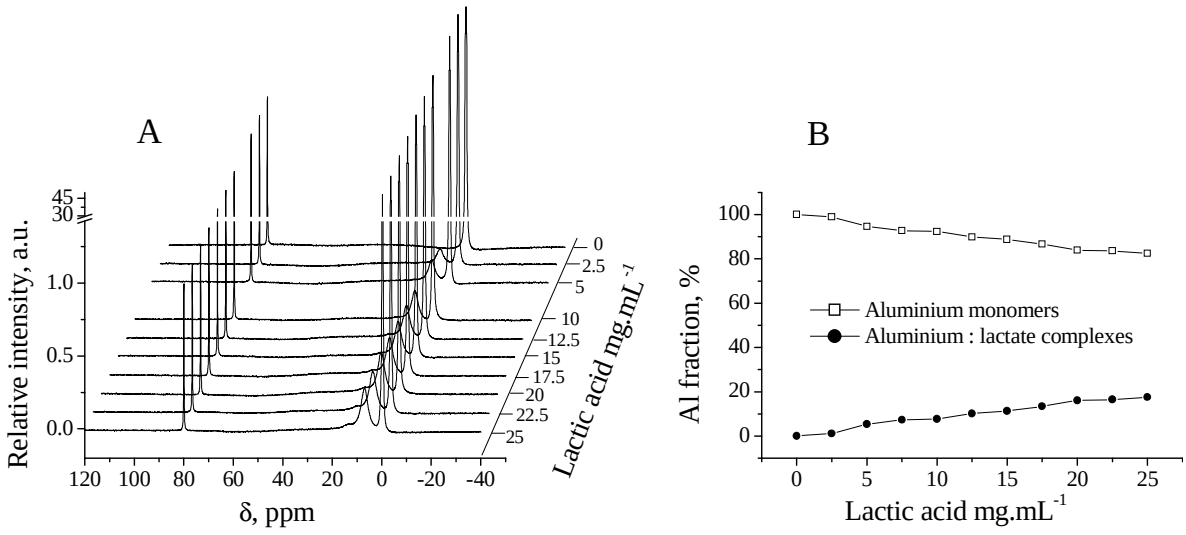

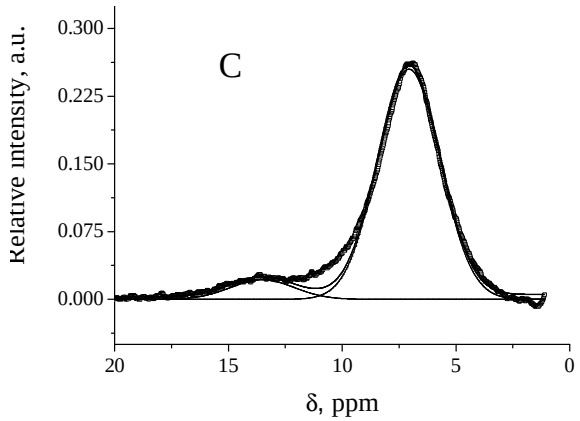

Figure 5.3. (**A**) ^{27}Al NMR spectra of the aluminium monomer - lactic acid samples as a function of total lactic acid concentration. T = 25 °C. (**B**) Speciation diagram in Al^{3+}-lactate system. (**C**) Peak-fitting of the truncated ^{27}Al NMR spectrum (lactic acid 25 mg.mL^{-1}). Line with square symbols represents original spectrum. Solid line represents theoretical spectrum which is the sum of all fitted peaks. Fitted peaks are shown by dotted and dashed lines.

^{27}Al NMR measurements for the Al_{13}-mer - lactate containing samples

Additions of lactic acid in the Al_{13}-containing samples (Figure (5.2) (**A**)) have significantly modified the aluminium species distribution in the samples as evidenced by the evolution of the NMR spectra of the samples shown in Figure (5.4) (**A**). The characteristic peak of the Al_{13} tetrahedral core at 63 ppm rapidly decreases upon addition of lactic acid completely disappearing at [lactate] ≥ 17.5 mg.mL^{-1} ([lactate] / [Al] ≥ 1.3).

As follows from Fig. 5.4 (A) a narrow peak at 0 ppm assigned to the monomeric aluminium species increases after adding 2.5 mg.mL^{-1} of lactic acid ([lactate] / [Al] = 0.18) and then starts to decrease. This is probably due to the fact that acid-induced breakdown of Al_{13} is stronger and faster than complexation with low levels of lactic acid. However, at higher lactic acid concentrations the complexation with Al-ions process probably becomes the most important contributor to the breakdown of Al_{13} species as indicated by the reciprocal trends in the Al_{13} concentration (peak at 63 ppm) and total Al-lactate concentration (peaks at 6-9 and 14-16 ppm). Unlike in the case of Al monomer - lactate interactions described above, in the case of Al_{13}-lactate system the major peak is at 14-16 ppm which can be attributed to the Al:lactate = 1:2 complex. This fact is possibly due to more preferential pH range of the interaction (pH ~ 4) which is maintained by the buffering action of the Al_{13}-mer breakdown.

The presence of the minor signal at 4 ppm indicates also partial acidic breakdown of the Al_{13}-mer polycations into aluminium monomers with the consequent transformation into aluminium dimers (20% of total aluminium content, Fig. 5.5, B) [6, 7]. The extent of the aluminium-lactate complex concentrations was emphasized by Figure (5.4) (**B**). 89.508 % of the aluminium fraction at the highest lactate concentration belongs to the sum of mono- and bis-lactate complexes; the < 10 % remaining corresponds essentially to aluminium monomers and dimers. It is reasonable to assume that at Al: lactate ratios higher than those studied in this work (maximum ratio at [lactate] = 25 mg.mL^{-1} was Al:

lactate = 1:1.86) the conversion of Al_{13} species into Al-bis-lactate complex will reach ~ 100% of total aluminium concentration.

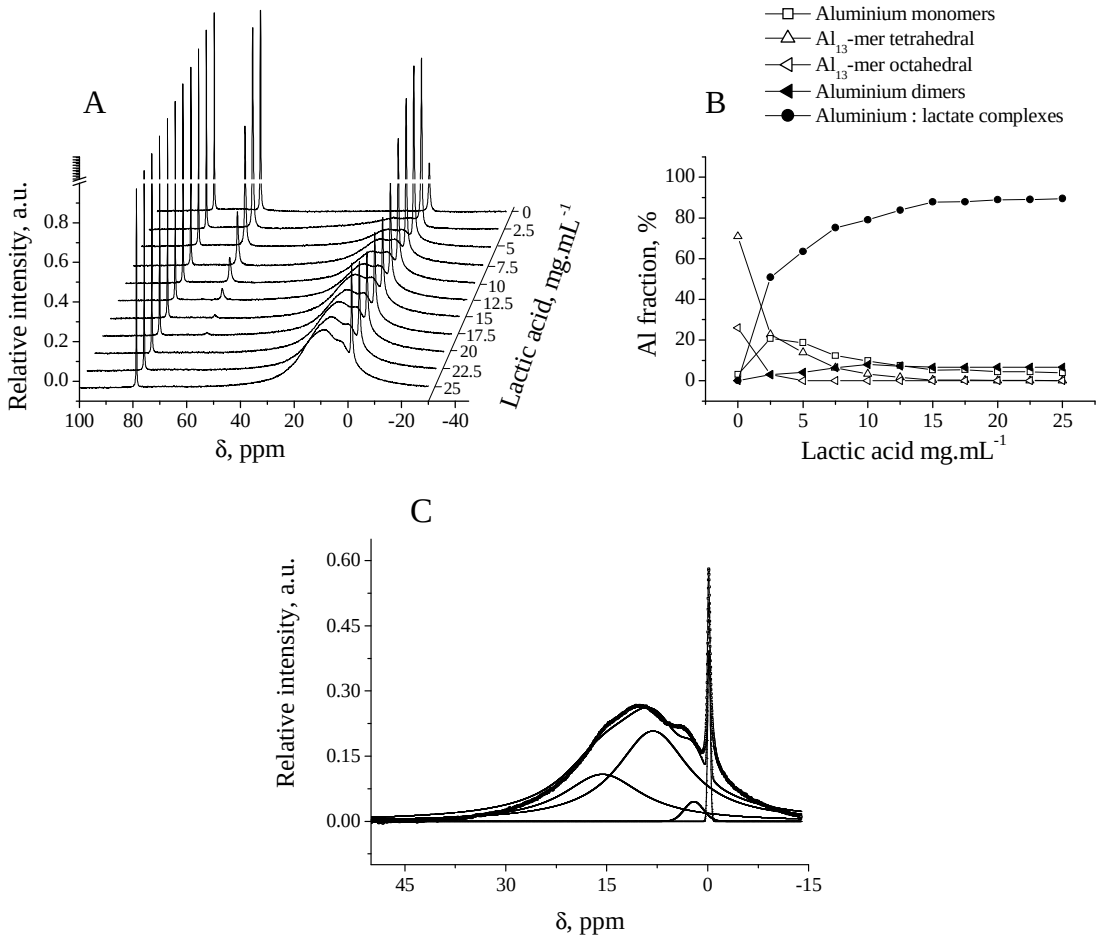

Figure 5.4. (**A**) ^{27}Al NMR spectra of the Al_{13} mer - lactic acid samples as a function of total lactic acid concentration. T = 25 °C. (**B**) Respective speciation diagram. (**C**) Peak fitting of the truncated ^{27}Al NMR spectrum (lactic acid 25 mg.mL^{-1}). Line with square symbols represents original spectrum. Solid line represents theoretical spectrum which is the sum of all fitted peaks. Fitted peaks are shown by dotted, dashed-dotted and dashed lines.

^{27}Al NMR outcome for the Al_{30}-mer - containing samples

Along with the signal of the Al_{30} tetrahedral core at 70 ppm present in Figure (5.5) **A**, a narrow peak at 63 ppm in the spectrum of the sample with no lactic acid reflected that the initial Al_{30}-mer reference system contained some Al_{13}-mers polycations. That quantity, after local integration and peak-fitting of the 63 ppm spectral signal, was less than 1 % of the total aluminium fraction of the sample.

From the spectra represented in Figure (5.5) (**A**), one can see that the Al_{30} tetrahedral core signal (70 ppm) disappeared when lactic acid was added to the solutions. The disappearance of the tetrahedral core of the polycations was concomitant with the decrease of the peak of the aluminium monomers at 0 ppm and the growth of the aluminium octahedral shell signal. The latter, after peak fitting (Figure (5.5) (**C**)), revealed the presence of three maxima at 3-4, ~ 7-9 and 14-16 ppm respectively. The minor signal

at 3-4 ppm corresponds to the aluminium dimers which appeared after the acidic breakdown of the aluminium polycations. Its fraction never exceeded 8 % of the total aluminium fraction. The other overlapped signals at ~ 7-9 and 14-16 ppm reflect the existence of aluminium-lactate complexes with different degree of coordination: mono- and bis-lactate chelates respectively. Those signals were already present in the systems containing initially the Al_{13}-mer. Both aluminium polycations have reacted in a similar way with lactic acid. The signal at 14-16 ppm is the predominant one. At the highest acid concentration, 92.016 % of the aluminium fraction was engaged in complexes, whereas the majority of the remainder corresponded to dimers.

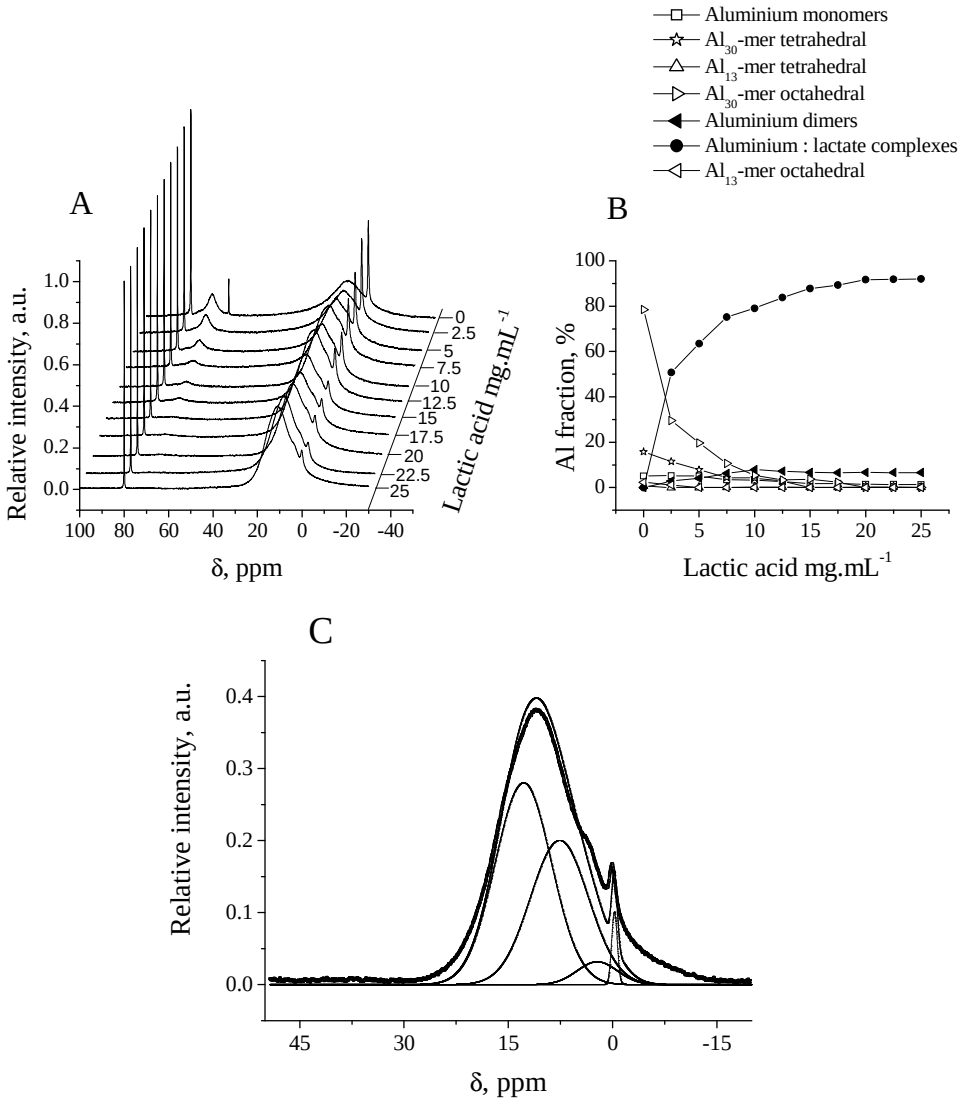

Figure (5.5) (**A**) ^{27}Al NMR spectra of the Al_{30} mer - lactic acid samples as a function of total lactic acid concentration. T = 25 °C. (**B**) Respective speciation diagram. (**C**) Peak fitting of the truncated ^{27}Al NMR spectrum (lactic acid 25 mg.mL^{-1}). Line with square symbols represents original spectrum. Solid line represents theoretical spectrum which is the sum of all fitted peaks. Fitted peaks are shown by dotted, dashed-dotted, short dotted and dashed lines.

^{27}Al NMR outcome for the aluminium hydroxide - containing samples

The amount of aluminium hydroxide was estimated from ^{27}Al NMR indirectly as a difference of the total aluminium content and the sum of the fractions of all soluble aluminium species (aluminium monomers, aluminium dimers and aluminium polycations) that could be detected by ^{27}Al NMR. Based on the integration of the spectra of the aluminium hydroxide-lactate systems, one can calculate on the speciation distribution diagram Figure (5.6) (**B**) the nearly exponential decrease of the aluminium hydroxide fraction upon addition of lactic acid to the samples. One needs to treat these data with certain degree of precaution as in the aluminium hydroxide - lactate system there was an increase in viscosity that could strongly affect the intensity of NMR signals.

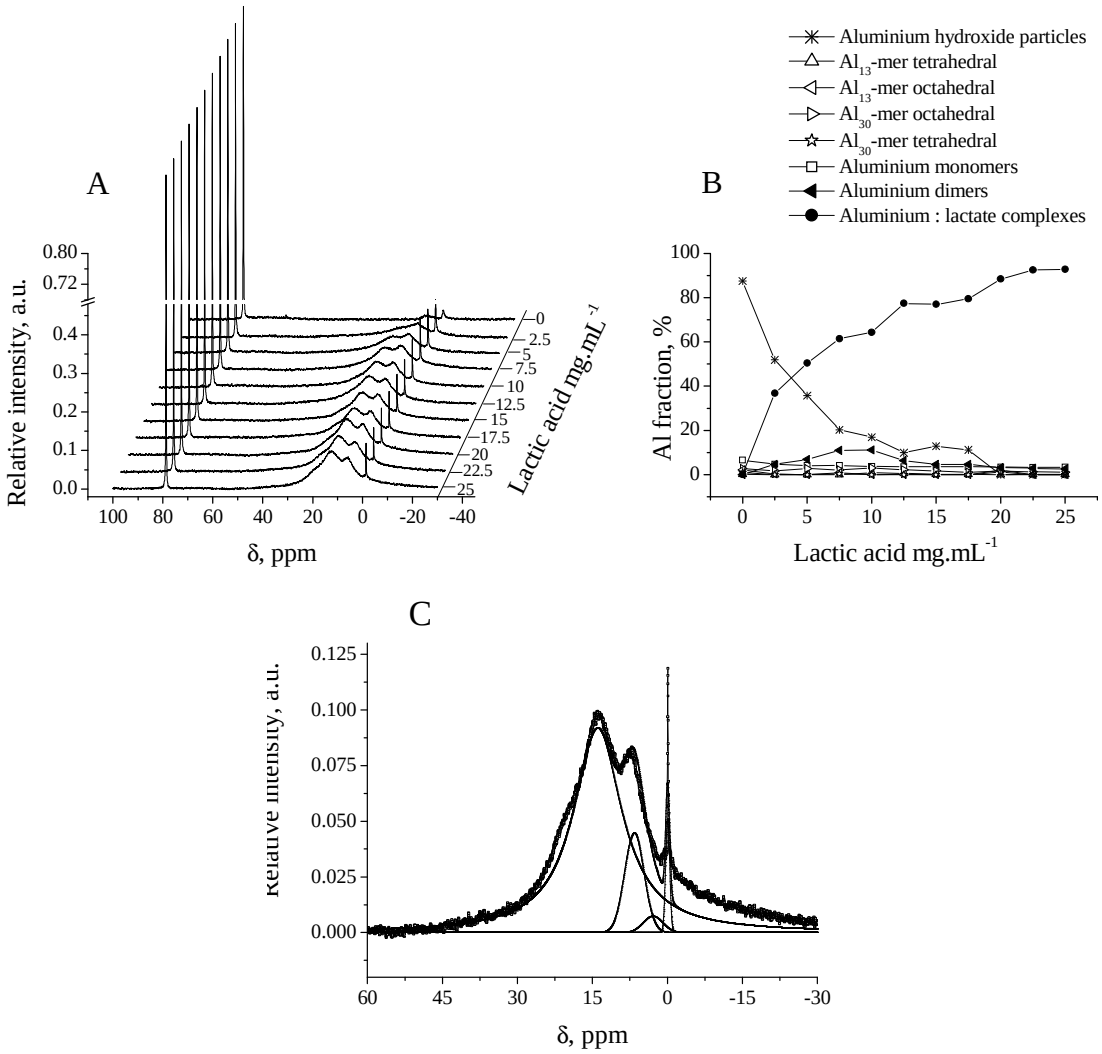

Figure 5.6. (**A**) ^{27}Al NMR spectra of the aluminium hydroxide - lactic acid samples as a function of total lactic acid concentration. T = 25 °C. (**B**) Respective speciation diagram. (**C**) Peak fitting of the truncated ^{27}Al NMR spectrum (lactic acid 25 mg.mL^{-1}). Line with square symbols represents original spectrum. Solid line represents theoretical spectrum which is the sum of all fitted peaks. Fitted peaks are shown by dotted, dashed-dotted and dashed lines.

Apart from the minor aluminium dimer signal at 4 ppm there are two other broad and overlapped signals detected in the ^{27}Al NMR spectra of aluminium hydroxide-lactic acid samples. After peak fitting (Figure (5.6) (**C**)), their maxima were found, similarly to the data obtained with the other aluminium reference systems, at ~ 7-9 and 14-16 ppm. The second signal mentioned was the largest one. These two signals in the region of octahedral aluminium (approx. 0-25 ppm), confirmed the breakdown of the aluminium hydroxide particles which leads to the formation of monomeric aluminium-lactate chelates. The aluminium fraction of the dimers never exceeded 11.93 % similarly to what was observed with the other aluminium reference systems. The gradual formation of the aluminium-lactate complexes reached 92.786 % at the highest acid concentration added.

As follows from the ^{27}Al NMR studies of solution chemistry of aluminium species in the presence of lactic acid, there are two major processes taking place when comparable amounts of aluminium species and lactic acid are present. The first rapid process is acidic breakdown of the products of aluminium-ion hydrolysis such as aluminium polycations and hydroxide. The presence of such reaction is supported by the initial increase of aluminium monomer signal at 0 ppm in the ^{27}Al NMR spectra when the concentration of lactic acid is relatively low. The second process is complexation of aluminium monomers formed as a result of acidic breakdown with lactic acid. The NMR data suggests the formation of mono- $[(Lact)Al(H_2O)_4]^{2+}$ and bis-lactate $[((Lact)_2Al(H_2O)_2]^{+}$ complexes of aluminium (where 'Lact' is lactic acid as a ligand). The aluminium-lactate complexes formed by chelation of one or two lactate molecules are quite strong ($K_{1,1}$= 2.36 ; $K_{1,2}$= 4.42) [16, 17] which assists the equilibrium shift in aluminium-ion-lactic acid system towards the formation of monomeric aluminium complexes with lactate. The complexation process is strongly pH-dependent and is hindered at pH < 4 due to the hindrance in the formation of deprotonated form of lactic acid - lactate (pK_a = 3.86). This explains the lower degree of complexation in the case of acidic $AlCl_3$ solutions (pH ~ 3) comparing to less acidic aluminium polycation and hydroxide lactate-containing samples. The formation of tris-lactate complex of aluminium is probably hindered by the insufficient amount of lactic acid (maximum lactate/Al ratio studied was 1.86). In the case of Al_{13}, Al_{30} and aluminium hydroxide relative fraction of bis-lactate complex comparing to mono-lactate is increasing with the increasing concentration of lactic acid. More than 80 % of total aluminium content present in these three systems is in the form of monomeric aluminium-lactate complexes. On the timescale of the experiment (24 hours) it was practically impossible to trace significant differences between hydrolysed aluminium species - Al_{13}, Al_{30} and hydroxide in terms of complexation with lactic acid. Relative stabilities of these species towards lactic-acid-assisted breakdown would play significant role on much shorter time scales.

5.4. ^{1}H nuclear magnetic resonance spectroscopy

Interactions of lactic acid with aluminium species was also studied using ^{1}H solution NMR spectroscopy. The conditions used to run the samples were detailed in the second part of the thesis, the Material and Methods section.

^{1}H NMR measurements of pure lactic acid samples

At room temperature, a ^{1}H NMR spectrum of a pure lactic acid solution in D_2O exhibited three signals, Figure (5.7) (including that from TMS). The resonances of the methine and the methyl protons were clearly resolved. The methine proton coupled with the methyl group resonated at + 4.40 ppm with the coupling pattern of a quadruplet and the methyl group coupled with the methine resonated at + 1.40 ppm as a doublet [9].

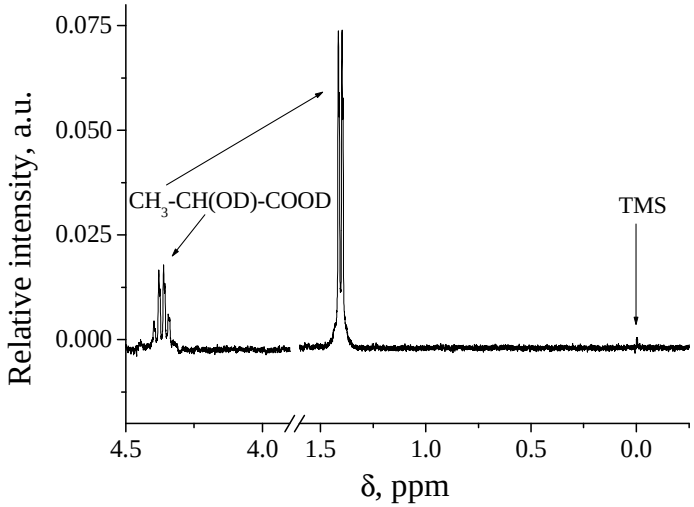

Figure 5.7. ^{1}H NMR spectrum of pure lactic acid 25 mg.mL^{-1} in D_2O.

^{1}H NMR measurements of aluminium species - lactic acid samples

The ^{1}H NMR spectra of lactic acid in the presence of aluminium chloride show significant changes as illustrated in Figure (5.8).

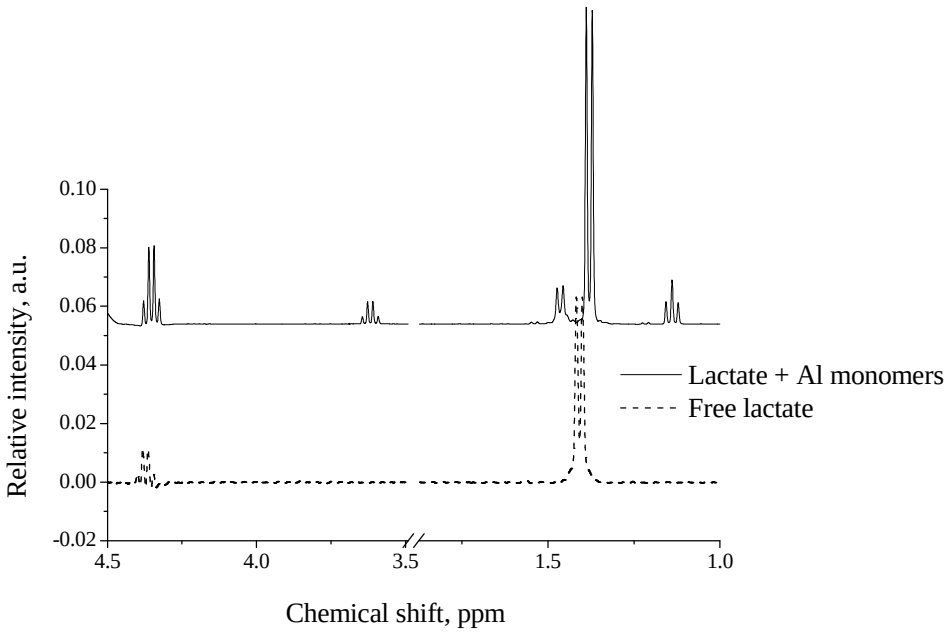

Figure 5.8. ^{1}H NMR spectra, run after 24 h aging, illustrating the shift effect induced by aluminium monomers on the lactic acid resonances.

When the free ligand solution was added to the aluminium species, new peaks appeared in the ^{1}H NMR spectra. The change of conformation of lactic acid when it's bound to aluminium as a chelating ligand has shifted upfield the signals of the free ligand. New sets of signals centred at 3.65 (linked to the methine proton), 1.46, 1.38 and 1.16 ppm (related to the methyl protons) were clearly visible together with the signals of the free ligand in some cases. The new sets of signals were assigned to different aluminium-lactate complexes where hydrogen was exchanged by aluminium. The lower the electronegativity of a directly bonded atom to another one, the larger the upfield shift created by the weakest element on the other element will be. That rule pointed out the shielding effect of aluminium on lactate proton resonances.

There is a clear dependence of the lactate signal intensity on the concentration of lactate in the $AlCl_3$-lactic acid samples. Together with the intensity, the multiplicity of the signals was modified upon lactate concentration variation. This phenomenon exhibited in the case of the methyl signals of aluminium hydroxide-based samples in Figure (5.9), was observed with all the aluminium species employed. At high lactate concentration, Figure (5.9) **c**, the resolution of the signal centred at 1.40 ppm was much better than at low lactate concentration, Figure (5.9) **a**. The 'multiplicity' is a result of increasing resolution with the increasing signal intensity.

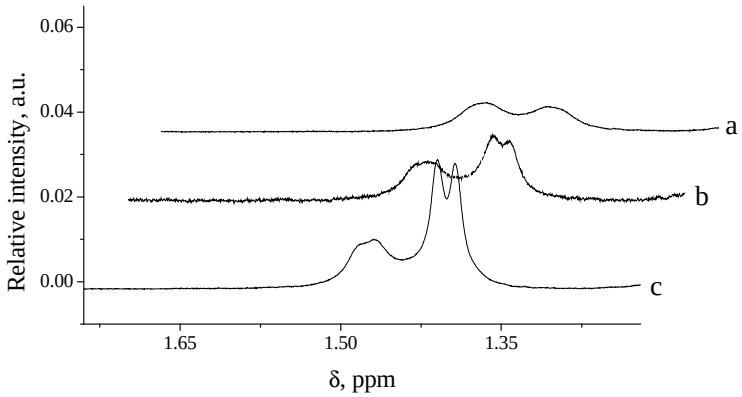

Figure 5.9. ^{1}H NMR lactate concentration - dependence on the resolution of the signals of the complexes formed in the case of aluminium hydroxide (0.15 $mol.L^{-1}$)-containing samples. (**a**) to (**c**) refer to lactic acid concentrations of 7.5, 15 and 25 $mg.mL^{-1}$.

Once the aluminium species initially present in the samples were broken down, the newly formed aluminium monomers interact with lactate and form complexes, giving rise to new ^{1}H NMR signals. The extent of the complexation of the aluminium species increases with the increasing concentration of lactic acid.

For aluminium monomers, five signals centered at 4.38, 3.65, 1.46, 1.38 and 1.16 ppm were detected in the presence of the highest lactic acid concentration (Figure (5.10)). The 4.38 and 1.38 ppm signals were attributed to the free ligand and the others to the aluminium-lactate assemblies. After integration

of the ^{1}H NMR spectra, the content in free ligand was found to increase (from 67 to 79 %) upon increase of lactic acid in the samples from 2.5 to 25 $mg.mL^{-1}$.

This was due to the excess ratio of the molecular concentration of the ligand compared to the molecular concentration of the aluminium monomers. Altogether, the aluminium-lactate complexes represented 21 % of the total proton fraction at the highest lactate concentration added, 13 % for the 1.46 ppm signal and 8 % for the 1.16 ppm signal. The 1.46 ppm signal was attributed to the less electronegative complex, the mono-coordinated one (the 6 ppm signal on the ^{27}Al NMR spectrum) and the 1.16 ppm signal to the five-membered ring chelate (the 14 ppm signal on the ^{27}Al NMR spectrum). In the bio-inorganic five-membered ring chelate, Al is coordinated with two coordinating oxygens, the negative donor groups of lactate. Five atoms are contained in the chelate ring. The oxygens of the donor hydroxyl and the carboxylate groups were both involved in the metal chelation in the case of the five-membered complexes. The two bindings explained the pronounced upfield shift of the 1.16 ppm signal. Since the 1.16 ppm signal is specific of the methyl, it appeared as a triplet. This occurs because there is a small interaction (coupling) with the methine protons.

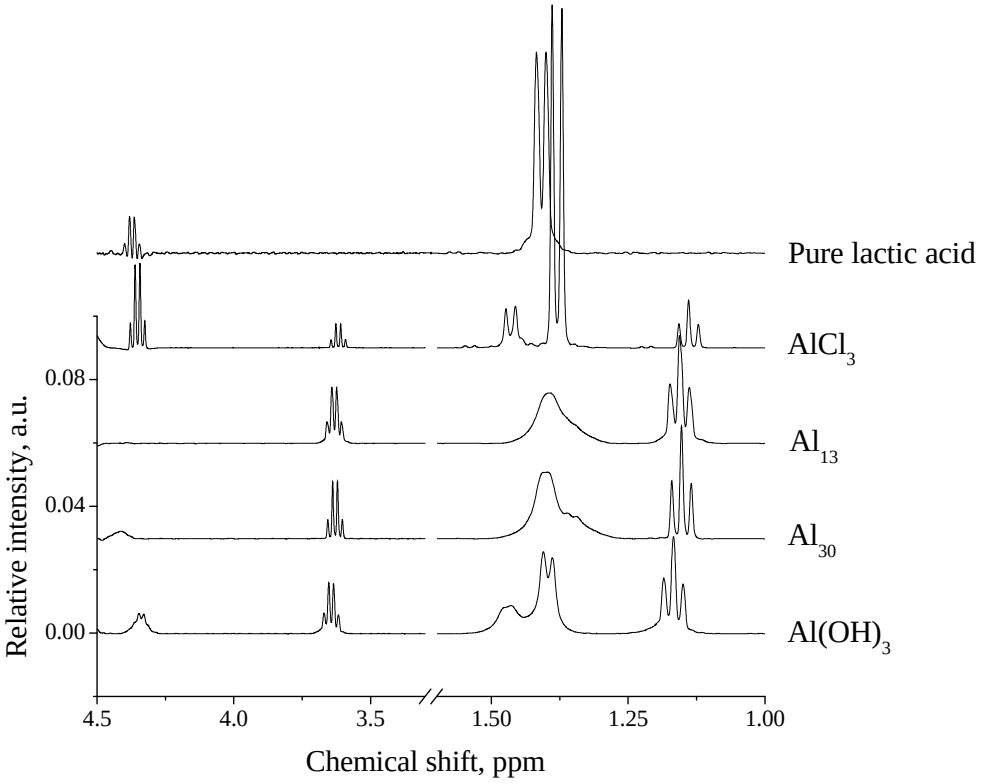

Figure 5.10. ^{1}H NMR spectra of pure lactic acid 25 $mg.mL^{-1}$ and with aluminium species 0.15 $mol.L^{-1}$.

In the presence of the Al_{13}-mers and the Al_{30}-mers polycations, the signal of the methine proton of the free ligand vanished (or almost vanished in the case of the Al_{30}-mers systems in Figure (5.10), and the signals associated with the complexes were dominant. The methyl protons in the complexes must be very similar to the ones of the free ligand, as the 1.46 and the 1.38 signals were almost completely overlapped as indicated by Figure (5.11). This observation was due to the occurrence of ligand

exchange. The change of magnetic environment was expected to produce the observed broadening effect. This result confirmed the variety of the structures of the complexes suggested in ^{27}Al NMR discussion. Due to the overlapping of the signals in the methyl region, the integrals of the signals could not be calculated.

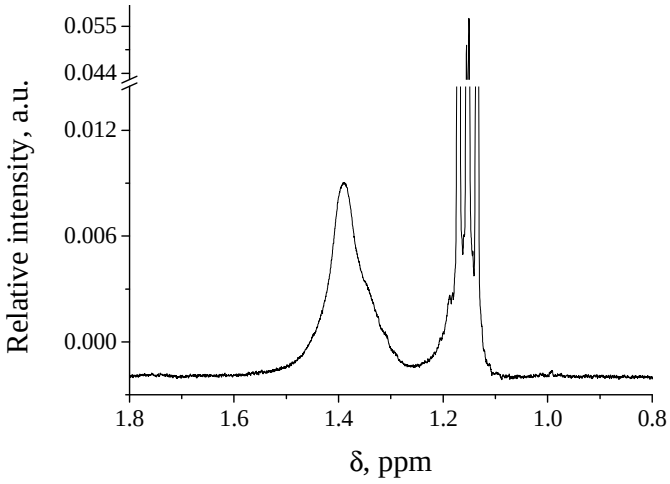

Figure 5.11. Illustration of the overlapping of the peaks situated around 1.40 ppm in the case of Al_{13}-mers-lactate 10 $mg.mL^{-1}$.

In the case of the aluminium hydroxides systems, similarly to what was observed in the presence of the other aluminium species, the methine and the methyl protons felt a different chemical surrounding from those experienced by pure lactic acid samples. In the aluminium hydroxide-containing solutions, the free ligand signals at 1.40 ppm and particularly the one at 4.40 ppm were more pronounced than in the aluminium polycations-lactate mixtures. The difference can be explained by the concentration of lactate in the polycation-based solutions being much lower than in the aluminium hydroxide-based solutions. The presence of the complexes in the aluminium hydroxide-containing mixtures accounted for 62 % of the total aluminium content of the samples.

The calculated three-bond coupling constant associated with a pure lactic acid sample was 7.00 Hertz (Hz). The same value was found for the aluminium monomers and the aluminium hydroxide-containing systems for the methine signal. That observation was explained by the free form of lactate remaining within the samples. The formation of chelates between aluminium and lactate gave rise to two new coupling constants, 7.08 and 7.12 Hz. The upfield shift of the new coupling constants was caused by the structural variation of lactic acid. Depending on the coordination environment of lactate in the aluminium-lactate compounds, the coupling constants are more or less upfield shifted.

Chelation of free aluminium monomers by lactic acid is manifested in ^{1}H NMR spectra by the appearance of new signals as discussed above and also by the shift of the existing signals not directly involved in the formation of chelate. Both processes are result of the profound change in the structure of lactate molecule that is strongly constrained by binding and affected by high electrostatic charge of Al^{3+}.

The distortion of structure of lactate bound to aluminium octahedrons observed in ^{1}H NMR spectra confirmed the nature of coordination of the pentacyclic chelate assemblies [6, 10-12].

5.5. Colloidal characterization of the complexes

Further colloidal characterisation of the samples of aluminium species containing lactic acid was undertaken using, particle size and zeta-potential measurements. The results are presented in Figure (5.12) as a function of lactic acid concentration.

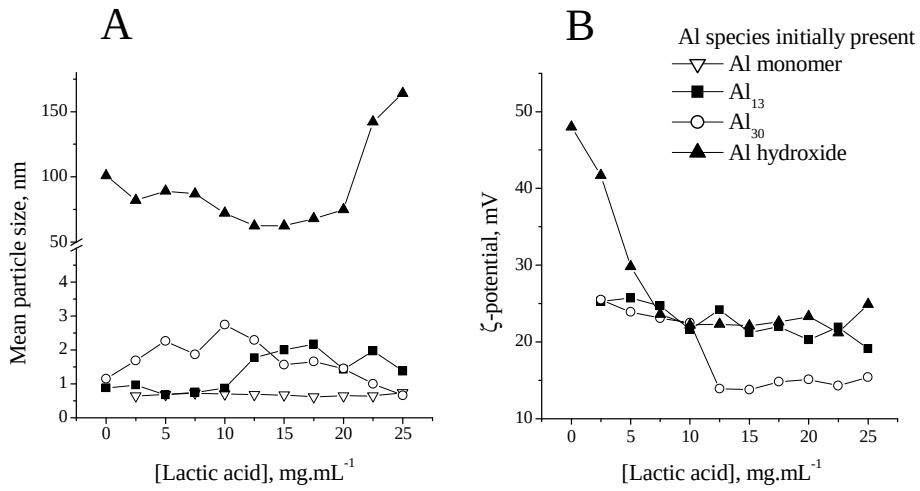

Figure 5.12. Evolution of (**A**) average particle sizes measured by DLS and of (**B**) zeta-potential of aluminium species-lactate samples as a function of lactic acid concentration.

In the case of the mixtures made of aluminium monomers, Al_{13}-mers and Al_{30}-mers polycations, the evolution of particle size upon lactic acid addition varied over a narrow range, from 0.6 to 3 nm. At the pH used in the study, these systems showed no aggregation. In the case of the samples prepared from the aluminium hydroxide sol, the main particle size of the mixtures fluctuated between 100 and 164 nm. Those results were expected since the aluminium hydroxide-containing samples were the only ones to show an increase of their viscosity upon lactic acid addition. Aggregation of aluminium hydroxide particles in the presence of lactic acid can be corroborated.

The zeta-potential measurements, Figure (5.12) (**B**) revealed that the samples were strongly positively charged at the pH range investigated. No charge reversal was observed upon lactic acid additions with any of the aluminium species used. As the concentration of lactic acid was raised in the samples, the formation of the aluminium-lactate assemblies produced a decreasing signal in the zeta-potential. This one was shifted from the zeta-potential of pure aluminium species (respectively 32 mV for Al_{13}-mers, 27 mV for Al_{30}-mers and 48 mV for aluminium hydroxide), to the zeta-potential of the composite particles. The zeta-potential of the aluminium monomers systems and their mean particle size and also the zeta-potential measurements of pure lactic acid solutions failed; the size of the compound lay below the measurement range of the equipment used.

The zeta-potential of the samples containing initially aluminium particle sols, reached a plateau after addition of 12.5 $mg.mL^{-1}$ of lactic acid.

Zeta-potential measurements indicate that there is no charge reversal in the aluminium species - lactic acid systems studied. The indicates that (1) there is no significant adsorption of lactic acid on highly charged aluminium species due to complete binding of most of lactic acid by aluminium monomers which are not 'seen' in the zeta-potential measurements due to exceedingly small size (< 0.6 nm) well below the threshold of DLS for such measurements (~ 4-5 nm); (2) DLS measurement detect only the positively charged species (mainly aluminium hydroxide) the amount of which is constantly decreasing with the increase of lactic acid, again, due to the species breakdown and chelation by lactate.

To evaluate the extent of the interactions between aluminium species and lactic acid, quantification of aluminium species and lactic acid after a contact time of 24 h was realised after a 30 min centrifugation at 3000 rpm by using respectively the Ferron assay and ^{1}H NMR spectroscopy.

5.6. UV-Vis spectroscopic quantification of speciation in Al-lactic acid systems

Quantification of aluminium species

To verify that the aluminium concentration in the samples was the same before and after addition of lactic acid, the total aluminum concentration was determined using the Ferron assay. The results are depicted in Figure (5.13); no precipitate was observed in the samples. Whatever the aluminium species initially present in the samples, the metal concentration remained stable to its initial value, 0.15 $mol.L^{-1}$, upon addition of lactic acid.

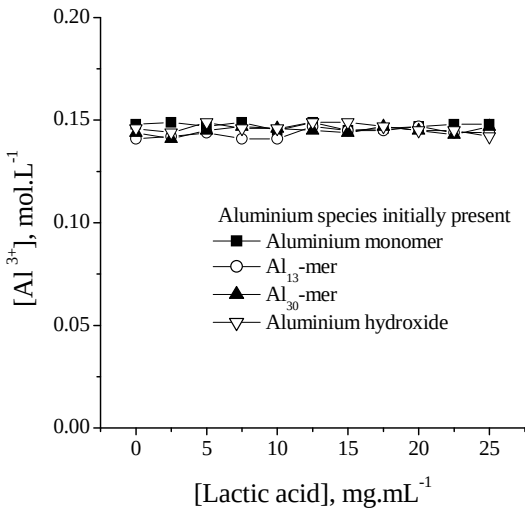

Figure 5.13. Free aluminium ion concentration in the samples determined by the Ferron assay.

Quantification of lactic acid

The methyl 1.40 ppm peak and the TMS signal in the pure lactic acid ^{1}H NMR spectra were integrated. A calibration line (Equation (5.1)) was calculated based on the plot (1.40 ppm / 0 ppm ratios) *vs.* lactic acid concentration (represented in Figure (5.14)).

$y = 5.3221\ x - 1.2605$ **Equation 5.1**

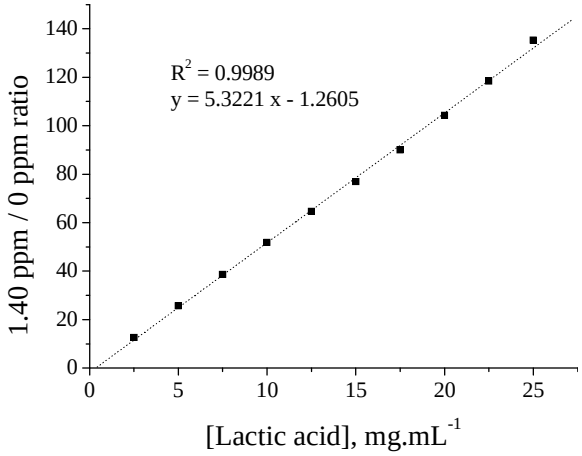

Figure 5.14. Calibration of lactic acid concentration realised by ^{1}H NMR manual integration of the methyl protons and the TMS signals.

Equation (5.1) was used as a standard to quantify the content in free lactic acid in the samples. The results were listed Table (5.2) for each aluminium species studied.

Table 5.2. Free lactic acid percentage in the supernatant solutions of the aluminium-lactate samples after centrifugation.

[Lactic acid] initial, $mg.mL^{-1}$	Free lactic acid, %			
	Aluminium monomers	Al_{13}-mers	Al_{30}-mers	Aluminium hydroxide colloids
2.5	45.29	9.47	9.47	88.10
5	42.29	4.74	97.02	99.72
7.5	71.55	98.08	99.76	99.92
10	73.21	94.40	84.97	98.66
12.5	77.44	77.63	90.38	98.82
15	79.88	77.89	93.50	97.91
17.5	80.02	90.80	84.36	99.76
20	86.04	79.07	89.10	99.23
22.5	84.57	84.02	91.08	98.81
25	83.66	87.21	88.75	99.31

With all the systems, the free lactic acid percentage in the supernatants increased with the increase of total acid concentration. This result was expected given the molecular ratios of the species in the samples. Apart from the aluminium monomer systems when lactic acid concentrations were between 2.5 and 15 $mg.mL^{-1}$, the acid concentration was in large excess compared to the aluminium species ones (cf. Table (5.1)). However, those observations did not prevent complexation of lactate with the aluminium species given that the free lactic acid percentages did not correspond to the total concentration of the acid initially introduced.

5.7. An infrared spectroscopic analysis of the aluminium-lactate structures

Fourier transform transmission infrared spectroscopy was used to provide additional insight into molecular structure of aluminium-lactate complexes.

A representative infrared spectrum of pure lactic acid sample at pH > 3 is shown in Figure (5.15).

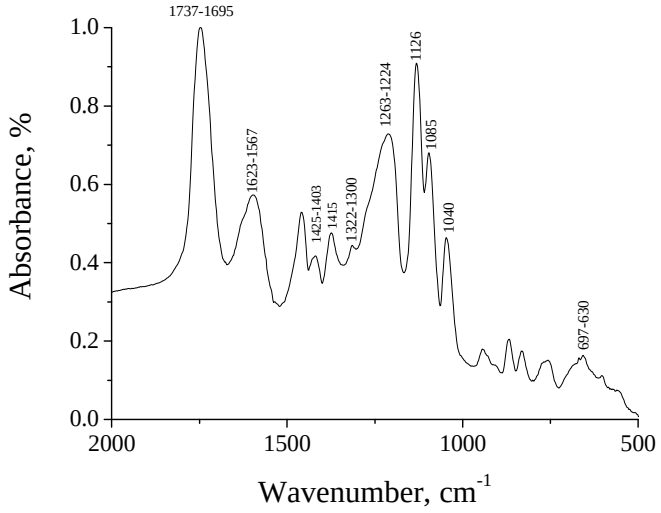

Figure 5.15. Infrared spectrum in the absorbance mode of pure lactic acid in its deprotonated (pH > 3) form, prepared as a KBr pellet. pH was adjusted by dropwise additions of HCl 1 mol.L^{-1}.

The lactic acid features in the spectrum revealed in Figure (5.15), were the alcohol absorption band between 697-630 cm^{-1} which arose from the bending vibration of the O-H (bending out-of-plane) and the alcohol absorption peaks at 1040, 1085 and 1126 cm^{-1} which were produced by the stretching vibration of the C-O free. The spectrum of the biomolecule was characterized also by the carboxylic acid absorption bands at 1263-1224 and 1322-1300 cm^{-1} of the stretching vibration of the O-C, the bands of the stretching vibration of the asymmetric and symmetric CO_2^- between respectively 1623-1567 and 1425-1403 cm^{-1}. The carboxylic acid band between 1737-1695 cm^{-1} was characteristic of the C=O stretch with the hydrogen of the carboxylic group free (H-non-bonded), and finally the peak at 1415 cm^{-1} was specific of the stretching vibration of the symmetric CO_2^-.

To observe specifically the effect of the aluminium species on the absorbance of lactate and not the absorbances due to the pure aluminium species, blank spectra of the aluminium reference systems were substracted from the spectra of the aluminium-lactate samples.

Table (5.3) gives the group wavenumbers for the functional groups encountered in pure lactic acid samples and in chelated lactate samples.

Table 5.3. Selected resonances in pure lactic acid sample and in chelated lactate samples.

	Infrared absorption frequencies					
	Stretching vibrations			Bending vibrations		
Functional class	Assignment	Wavenumber range, cm^{-1}	Reference	Assignment	Wavenumber range, cm^{-1}	Reference
Carboxylic acid	Asymmetric CO_2^-	1650-1540	[15]	C-O-H	1440-1395	[13]
	Symmetric CO_2^-	1450-1360	[15]	CO_2^- bound	775	[13]
	O-C	1320-1210	[13]	Wagging CO_2^- bound	540	[13]
	C=O (H-bonded)	1735-1705 (acids)	[13]	Rocking CO_2^- bound	430	[13]
	C=O (H-non-bonded)	1900-1700	[13]			
Alcohol	C-O free	1250-970	[13]	O-H (bending in-plane)	1440-1395	[13]
	C-O bounded	1125	[13]	O-H (bending out-of-plane)	770-650	[13]
Alkane				CH_3 deformation	1390-1370	[13]
Water				Scissoring vibration	1750-1580	[14]

The presence of aluminium species altered the spectrum of the pure lactic acid compound. Spectra of the different aluminium species-lactate mixtures are represented in Figure (5.16).

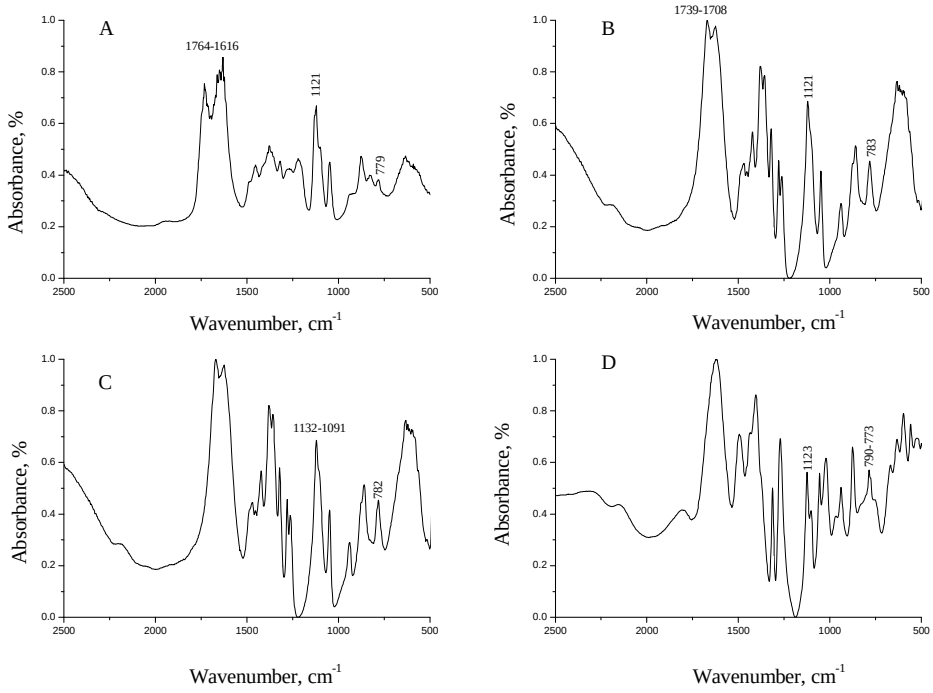

Figure 5.16. Infrared spectrum in the absorbance mode of the aluminium monomer – lactate samples (**A**), of the Al_{13} mer – lactate samples (**B**), of the Al_{30} mer – lactate samples (**C**) and of the aluminium hydroxide – lactate samples (**D**) with lactate concentration of 25 mg.mL^{-1}.

The NMR spectroscopic results revealed the formation of complexes between lactate and all the aluminium species tested. The infrared transmission data corroborated those previous conclusions. In the presence of all the aluminium species employed, characteristic bands of both the carboxylic acid and the alcoholic functions appeared in the aluminium-lactate spectra. Although carboxylates are derived from carboxylic acids, the lack of an O-H group makes their spectra radically different. The presence of any complexes between aluminium and lactate was detected by the stretching C-O vibration of the alcohol group and the bending of the bound -C=O vibration in the complexes. In the case of the aluminium monomers-lactate samples (Figure (5.16) **A**), the bending vibration of the carboxylic acid CO_2^- bound emerged at 779 cm^{-1} and the stretching vibration of alcohol C-O at 1121 cm^{-1}. The latter attribution can not be made more specific since the bound and the free form of the alcohol resonate at a similar range of wavenumbers. In the presence of the aluminium Al_{13}-mers and the Al_{30}-mers polycations, (Figure (5.16) **B** and **C**), the bound form of the carboxylic acid appeared at 783 and 782 cm^{-1} respectively and the alcoholic function at 1121 and between 1132-1091 cm^{-1} respectively. The two specific bands of the complexed lactate were also visible in the alumimium hydroxide-containing samples at 790-773 cm^{-1} for the bound carboxylic acid resonance and at 1123 cm^{-1} for the alcohol resonance. One more resonance was observed in the aluminium monomers, the Al_{13}-mers- and the aluminium hydroxide-containing samples respectively at 1764-1616, 1739-1708 and 1843-1774 cm^{-1} in addition to the absorbances already mentioned. The latter band was linked to the stretching vibration of the C=O (H-non-

bonded). The carbonyl vibration appeared also in the Al_{30}-lactate samples at 1719 cm^{-1}, as a peak not well-resolved though.

The absence of the C=O (H-bonded) carbonyl vibration in all the systems reinforced the idea developped in the ^{27}Al NMR discussion part regarding the structures of the aluminium-lactate complexes. The binding of aluminium by lactate did not implicate the carbonyl group of the carboxylic acid of lactate.

By using transmission infrared spectroscopy, the bonding arrangement in the aluminium-lactate assemblies was exposed. In all the systems, the hydroxyl oxygen in the carboxylate was coordinated to the aluminium atom while the involvement of the oxygen of the alcohol function was more dubious. There was no infrared spectroscopic evidence that the carbonyl oxygen was involved in the binding of lactate by aluminium.

5.8. Conclusions

Aluminium-lactate nanohybrid materials have been obtained by mixing aluminium monomers, Al_{13}-mers, Al_{30}-mers or aluminium hydroxide nano-sol solutions with varying amounts of lactic acid. The composition and formation mechanisms of these materials have been investigated using various solution and solid-state characterization techniques. The chosen time scale of ageing of aluminium-lactate mixtures (24 hours) allowed us to concentrate on the long-term interactions of aluminium species with lactate. All four aluminium-containing precursors used in this study possess significant positive surface charge which correlated well with the initial pH of the corresponding solutions.

The relevance of the study was shown by the speciation distribution of a pure lactic acid solution. The biomolecule was partly deprotonated from pH 3. The pH of the aluminium-lactic acid mixtures - above 3 with all the aluminium reference systems tested - was favourable to the formation of chelates between lactate and aluminium. After ageing, aluminium-lactate compounds were developed between the biomolecule and the inorganic species. The event was at the origin of the stabilization of the conductivity measurements and the initial decrease of the zeta-potential upon increase of lactic acid concentration up to 12.5 $mg.mL^{-1}$. Unlike in aluminium hydroxide-lactate systems, the hybrid particles of aluminium monomers and aluminium polycations with the biomolecule remained soluble.

The increasing concentration of lactic acid appeared to force all the aluminium species initially introduced to convert into monomers and dimers as a result of an acidic hydrolysis. Subsequently, the resulting hydrolysed products formed new aluminium-lactate assemblies. Depending upon whether the ^{27}Al or the ^{1}H NMR spectroscopic results were processed, the new assemblies represented 17-25 % of the fraction of aluminium when the aluminium monomers were the species initially present. Respectively 89.508 and 92.016 % of the fraction of aluminium was associated with the formation of complexes in the case of the Al_{13}-mers and the Al_{30}-mers systems. The aluminium hydroxide-based complexes contained 65-92.786 % of the fraction of aluminium.

With each aluminium reference system employed, several aluminium-lactate complexes were formed. Some of the complexes were specific to one aluminium reference system, while some were initial aluminium species-independent.

^{1}H NMR demonstrated that the number of coordination site within the aluminium-lactate entities varied. Although the carboxylate CO_2^- was always involved in the formation of the complexes, infrared transmission spectroscopy did not support the systematic participation of the carbonyl of the carboxylate and the oxygen of the alcoholic group in the complexes. Infrared spectroscopy suggested a greater contribution from the carboxylate group than from the alcoholic one in the formation of the aluminium-lactate complexes. The affinity of the carboxylic OH^- group for Al^{3+} is much higher than the one of the alcoholic OH^- group.

5.9. References

[1] O. Deschaume, K. L. Shafran, C. C. Perry, Langmuir, 2006, 22, 10078.

[2] (a) P. O. Astrand, E. Hultman, A. Juhlin-Dannfelt, G. Reynolds, Journal of applied physiology, 1986, 61, 338; (b) A. J. Downs, in Chemistry of Aluminium, Gallium, Indium and Tallium, Ed. by A. J. Downs, 1993, London, Chapman and Hall, 526 p.

[3] D. E. Saunders, Br. Med. Bull., 2000, 56, 334.

[4] S. J. Karlik, E. Tarien, G. A. Elgavish, G. L. Eichhorn, Inorg. Chem. 1983, 22, 525-529.

[5] F. Thomas, A. Masion, J. Y. Bottero, J. Rouiller, F. Montigny, F. Genévrier, Environ. Sci. Technol., 1993, 27, 2511.

[6] J. W. Akitt, B. E. Mann, J. Magn. Reson. 1981, 44, 584-589.

[7] J. W. Akitt, N. B. Milic, J. Chem. SOC.D, alton Trans. 1984, 981-984.

[8] J. D. Kubicki, d. Sykes, S. E. Apitz, J. Phys. Chem. A 1999, 103, 903-915.

[9] R. S. Dickins, C. S. Love, H. Pushmann, Chem. Commun., 2001, 2308-2309.

[10] J. W. Akitt, A. Farthing, J. Magn. Reson. 1978, 32, 345.

[11] J. W. Akitt, A. Farthing, J. Chem. Soc., Dalton Trans. 1981, 1606.

[12] J. W. Akitt, A. Farthing, O. W. Howarth, J. Chem. Soc., 1981, 1609.

[13] Brian C. Smith, in Infrared Spectral Interpretation: A Systematic Approach, 1999, CRC Press.

[14] S. Y. Venyaminov, F. G. Prendergast, Anal. Biochem., 1997, 248, 234.

[15] G. G. Bombi, B. Corain, A. A. Sheikh-Osman, Inorg. Chim. Acta, 1990, 171, 79.

[16] A. E. Martell, R. D. Hancock, R. M. Smith, R. J. Motekaitis, Coord. Chem. Rev., 1996, 149, 311.

[17] T. Kiss, I. Sóvágó, R. B. Martin, J. Pursiainen, J. Inorg. Biochem., 1994, 55, 53.

Part 6

Interactions of Aluminium Hydrolytic Species with Biomolecules

In this study, the interactions of the basic globular protein lysozyme (LSZ, isoelectric point 11.4) with Al_{13}-mers, Al_{30}-mers and colloidal hydroxides have been explored for a range of protein: aluminium ratios. Al_{13}-mers and Al_{30}-mers have properties which make them useful as models for the aluminium hydroxide surface and yet can be monitored in solution using ^{27}Al solution nuclear magnetic resonance (^{27}Al NMR) and infrared (IR) spectroscopies. The advantage of using colloidal aluminium hydroxide particles lies in the possibility of quantifying parameters such as zeta potential and size, while at the same time taking advantage of the high surface area to maximise the area available for molecular level interaction [11]. Colloidal, molecular and macroscopic variables have been monitored to study the modification of both inorganic and biomolecular phases. The results obtained have then been compared to the findings of a previous study that focused on the interactions of bovine serum albumin (BSA, isoelectric point 4.75) with a similar range of aluminium species [15].

6.1. Preparation of stock solutions and model aluminium - protein systems

Single species systems containing either $AlCl_3$, Al_{13}-mer, Al_{30}-mer and an aluminium hydroxide sol with particles size of 23 ± 3 and 100 ± 10 nm were prepared from crystalline $AlCl_3 \cdot 6H_2O$ (99 %, Fisher Scientific), in distilled deionized water as detailed previously [15]. The final aluminium concentration in the model solutions was 0.3 $mol.L^{-1}$, the purity of the resulting systems being checked by quantitative ^{27}Al solution NMR spectroscopy and a Ferron kinetic assay (Al_{13}-mer : 97 %; Al_{30}-mer : 92 % of the total aluminium content) [18-20]. ^{27}Al solution spectroscopy also demonstrated the absence of soluble aluminium species in aluminium hydroxide suspensions. Aqueous chicken egg white lysozyme and bovine serum albumin (BSA) solutions containing 50 mg/ml protein were prepared by dissolving the protein powder (Sigma) in distilled deionized water shortly before use.

Aluminium-protein systems were prepared at room temperature according to the procedure described previously [15]. The final aluminium concentration was 0.15 $mol.L^{-1}$, the protein concentration being

varied from 0 to 25 mg.mL^{-1} in steps of 2.5 mg.mL^{-1}. The range of lysozyme: aluminium molecular concentration ratios used was 1:67.8 to 1:6.8 for lysozyme: Al_{13}-mers, 1:29.4 to 1:2.9 for lysozyme: Al_{30}-mers and 1:0.092 to 1:0.009 for lysozyme: aluminium hydroxide particles (evaluated from the approximation of 100 nm diameter and 10 nm height cylindrical hydroxide particles, having a density of 0.3 g.cm^{-3}) (Table (6.1)).

Table 6.1. Lysozyme to aluminium species ratios used throughout the study.

LSZ concentration, mg/ml	LSZ : Al_{13}	LSZ : Al_{30}	LSZ : Al hydroxide 100 nm
2.5	1 : 67.8	1 : 29.4	1 : 0.092
5	1 : 33.9	1 : 14.7	1 : 0.046
7.5	1 : 22.6	1 : 9.8	1 : 0.031
10	1 : 17	1 : 7.4	1 : 0.023
12.5	1 : 13.6	1 : 5.9	1 : 0.018
15	1 : 11.3	1 : 4.9	1 : 0.015
17.5	1 : 9.7	1 : 4.2	1 : 0.013
20	1 : 8.5	1 : 3.7	1 : 0.012
22.5	1 : 7.5	1 : 3.3	1 : 0.010
25	1 : 6.8	1 : 2.9	1 : 0.009

The series of aluminium-protein containing samples were analyzed after solutions had been aged for 24 hours using a range of solution and colloidal techniques listed Figure (6.1). After careful centrifugation of the insoluble part of the samples, the precipitated solid was freeze-dried and analyzed using solid state techniques.

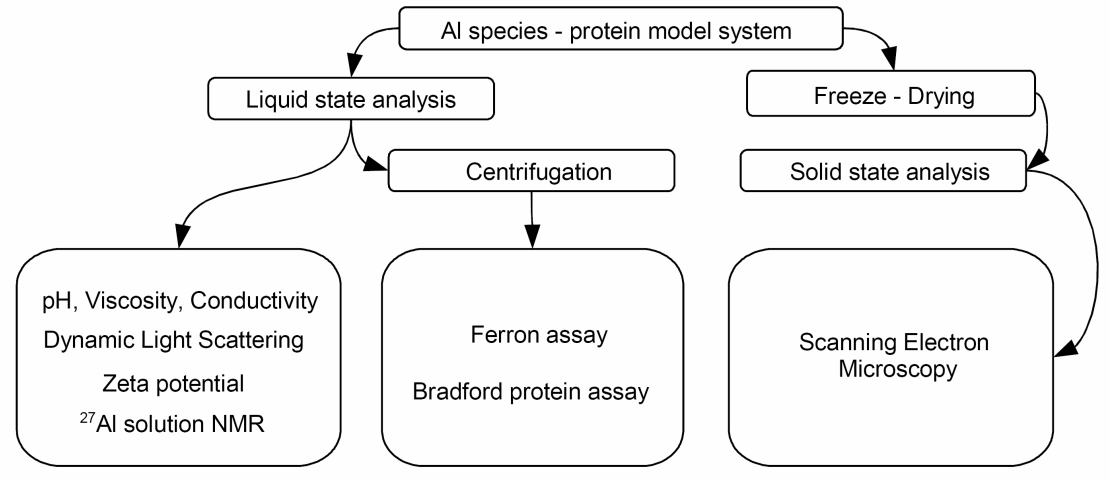

Figure 6.1. Range of analyses used to characterize solution, colloidal and solid state samples.

Solutions /colloids characterisation

All the solution characterisation procedures used throughout these studies have been used and described in detail in previous publications from our group. Briefly, ^{27}Al solution NMR spectra were acquired using a Jeol ECX400 spectrometer (Jeol, Tokyo, Japan) operating with a D_2O lock, single pulse method, X-pulse of 9.4 μs, 512 scans, relaxation delay 0.5 s. Quantification of the spectra was carried out using a peak-fitting algorithm [18, 19].

The free protein concentrations in the systems were determined after centrifugation at 3000 rpm for 10 min to remove any solids using a Thermo UV1 spectrophotometer for absorbance measurement. A Bradford total protein assay was used for protein quantification [21].

The pH and conductivity of the systems were measured with a PHM-250 pH-meter with Red Rod glass electrode and a temperature sensor, and a CDM-230 conductivity meter with two-plate conductivity probe and a temperature sensor (all from Radiometer Analytical, Villeurbanne, France). Viscosity was measured with an AND SV-10 vibro-viscometer (AND A&D Ltd., Tokyo, Japan) with gold-coated transducer and temperature sensor.

Dynamic light scattering (DLS) and zeta potential measurements of aluminium species - protein solutions were acquired using a Zetasizer Nano S from Malvern Instruments (Worcestershire, UK).

Preparation of solid materials, scanning electron microscopy

After centrifugation of the samples the resulting 'solid' materials were rinsed with water and centrifuged again. The pellet obtained was subsequently freeze-dried for 24 h using a Virtis freeze-drier before being mounted on Scanning Electron Microscope (SEM) stubs (TAAB) and coated with carbon using a standard procedure. A JSM-840A SEM (JEOL) operating at an acceleration voltage of 25 KeV and a working distance of 15 mm was used throughout the studies.

Comparative Fourier Transform Infrared (FTIR) study of protein conformation in the presence of aluminium species

In order to comparatively study the variation of protein conformation upon addition of the inorganic species to lysozyme and bovine serum albumin, a series of model aluminium-BSA and aluminium-lysozyme solutions were prepared similarly to the variable protein concentration samples, by maintaining the protein concentration at 25 mg/ml and varying the aluminium concentration from 0 to 0.15 $mol.L^{-1}$ by steps of 0.015 $mol.L^{-1}$, leaving the samples to age for 24 hours before freeze-drying for infrared spectroscopic analysis. For spectroscopic characterization of the resulting samples a standard KBr disc technique was used, 2 mg of freeze dried sample being mixed with 198 mg of KBr (Aldrich, IR grade, 99 %) and pressed into a disc at ~ 10 $tons.cm^{-2}$ pressure.

Spectra were recorded at 2 cm^{-1} resolution, the interferometer speed set to 0.4747 $cm^{-1}.s^{-1}$, 128 scans being averaged for each spectrum.

Two different techniques were applied in order to understand the molecular characteristics of the aluminium species: protein interactions, and to evidence any deep modification in their morphology, which can potentially lead to drastic changes in their properties. The amide I group of backbone C=O

vibrations was firstly used to obtain an assessment of protein conformation as a function of aluminium species concentration.

Spectra were truncated between 1800 and 1375 cm^{-1}, before applying a multiplicative scatter correction (MSC, GRAMS 32) to groups of spectra obtained for each aluminium species-protein system. Random noise and minor components were removed by use of a factor analysis algorithm (Minitab 14), conserving only the principal components (5 in all cases) for the reconstruction of the spectra, on the basis of their respective contribution to the original data.

For secondary structure assessment, the smoothed and baselined spectra were used between 1720 and 1490 cm^{-1} (amide I and II bands). Both bands were deconvoluted using automated curve fitting routine programmed using MatLab software. Peak positions corresponding to different structural elements of the two proteins were obtained from the literature [22, 23], their variation being limited to ± 2 cm^{-1} during the fit. 6 peaks were fitted to the amide I feature, corresponding to vibrations attributed to side chains vibrations (1613 cm^{-1}), β-sheets (1620 cm^{-1}), β-strands (1630 cm^{-1}), random coils (1646 cm^{-1}), α-helices (1654 cm^{-1}) and turns/H-bonded COOH (1680-1690 cm^{-1}). 2D correlation analysis was carried out by using a MatLab toolbox [24] written on the basis of the original work by Noda and Ozaki [25].

6.2. Macroscopic measurements: pH, conductivity and viscosity of the systems

Aspartic and glutamic acids have been demonstrated to bear the highest affinity for aluminium species in previous studies of aluminium-biomolecule interactions since these aminoacids have a carboxylate group in their side chain. Lysozyme only displays 6-7 of those acidic residues at its surface and exhibits a large positive charge at the pH considered, making the approach of the highly positively charged aluminium species difficult, and charge cancellation almost inexistent. Indeed pH, conductivity and viscosity measurements of the samples prepared from aluminium species and lysozyme did not show large changes, Figure (6.2), as those observed in the presence of BSA, due to the lower acidic residue content of the protein. In particular, pH remained within the domain of stability of the aluminium species (pH ~ 4.2-4.4) [18, 19].

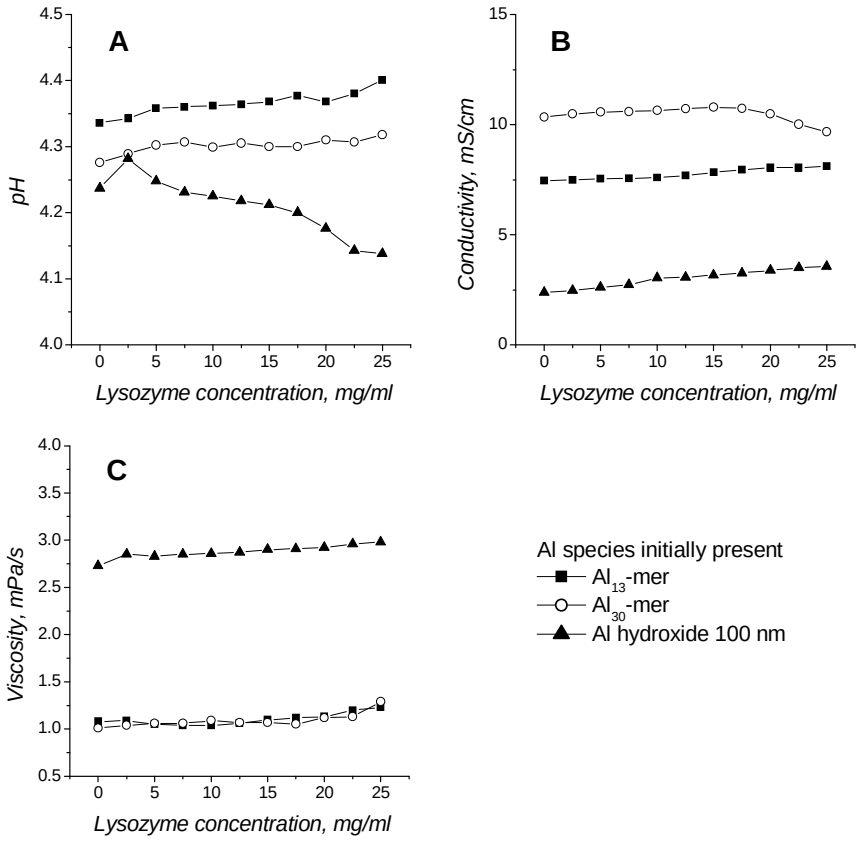

Figure 6.2. (**A**) pH, (**B**) conductivity and (**C**) viscosity of aluminium species - lysozyme samples prepared at various protein concentrations.

Both aluminium polyoxocation-containing systems (Al_{13}-lysozyme and Al_{30}-lysozyme) showed no significant increase of viscosity whatever the lysozyme concentration (viscosity values remained close to that of pure water and lysozyme solution at 1.00 ± 0.29 cP), indicating little or no gelation for the systems in question. In contrast, the viscosity of the aluminium hydroxide-lysozyme mixtures increased ~ 7 % upon lysozyme addition, demonstrating limited gelation.

6.3. Dynamic light scattering and zeta potential measurements

Evidence for the formation of bioinorganic assemblies was provided by the results of dynamic light scattering, where an evolution in the particle size of the model aluminium lysozyme systems (Figure (6.3)) was observed.

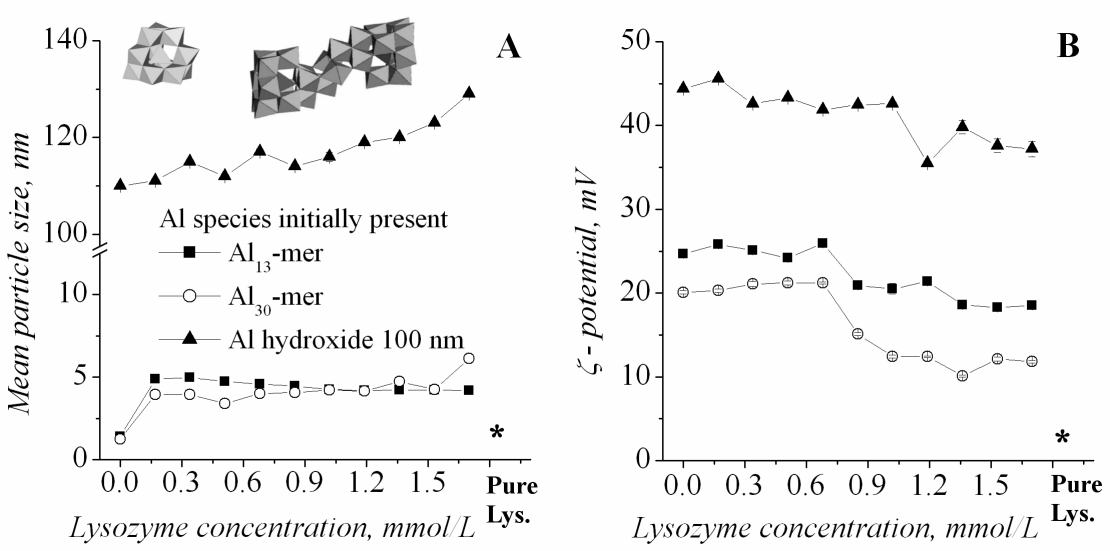

Figure 6.3. Polygonal representation of Al_{13} and Al_{30} (**A**) and evolution of (**A**) average particle sizes measured by dynamic light scattering; (**B**) zeta potential of aluminium species-lysozyme samples as a function of lysozyme concentration. Particle size R.S.D. < 0.3 % (measurements in triplicate). The particle size and zeta potential measured for pure lysozyme are presented as stars for comparison.

In the case of samples prepared from the aluminium hydroxide sol, the measured particle sizes increased steadily, from 110 nm to 129 nm with increasing lysozyme concentration (figure (6.3) **A**). Similarly to what has been found from analogous studies using bovine serum albumin [15], lysozyme probably covered the surface of aluminium hydroxide particles, but was however not inducing an electrostatically driven coagulation due to its positive charge in the pH domain considered. As followed from Figure (6.3), the particle size of the pure Al_{13}-mer and Al_{30}-mer solutions was found to be close to the actual sizes of these species (1 ± 0.1 and 2 ± 0.05 nm, respectively [6]). Once lysozyme was added, the average particle size in all cases increased to 5.18 ± 0.40 nm and 6.13 ± 0.38 nm respectively. For both aluminium polyoxocation-lysozyme samples the mean size of the suspension did not change with further increase of lysozyme concentration. The mean diameter of the lysozyme in solution as measured by DLS was ~ 1 nm (although from the literature the size of the lysozyme molecule is 3 nm x 3 nm x 4.50 nm [26, 27]). The mean particle size of aluminium polycation-lysozyme samples probably arose from some limited adsorption of polycation clusters onto an area of the "surface" of lysozyme that carried some negative charges under mildly acidic conditions [28] (pH < 5), thus allowing the protein to be "seen". Given that the ratio of aluminium to protein decreased as the protein concentration in solution increased and yet the mean particle size remained the same it would suggest that the DLS technique was measuring a specific molecular complex which, given the fact that the lowest Al_n : protein ratio used was 3:1, was likely to be formed from 1 lysozyme for 3 Al_{30} or 1 lysozyme for 6 – 7 Al_{13}, the ratio matching was this case the number of carboxylic acid moieties available at the surface of the lysozyme molecule.

The hypothesis above was supported by zeta potential measurements of the model systems in question (Figure (6.3) **B**). The zeta potential value for the aluminium polyoxocation-lysozyme system was

positive at all lysozyme concentrations measured, Al_{13}-containing samples having higher zeta potential values than Al_{30}-containing samples. In pure solutions of similar concentration, free lysozyme molecules bore a potential of 2 ± 0.80 mV at pH 4. The observed charge evolution can be explained by the adsorption of aluminium polyoxocations on the surface of the protein. For small additions of lysozyme, the potential observed was that for the free aluminium polycations alone, however as more and more lysozyme was added, the amount of free aluminium polycations was progressively reduced in comparison to the aluminium associated with the lysozyme-polycation conjugates, and the potential slowly decreased to reach a value corresponding to that of a lysozyme-polycation species.

For aluminium hydroxide, the value of the zeta potential was approximately twice as high as that of the aluminium polyoxocation-lysozyme solutions at similar concentrations and decreased with increasing amounts of lysozyme. The protein was probably adsorbed on the colloid surface, leading to a decrease in zeta potential produced by a compensation of some of the positive charge of the surface by the negatively charged groups of the protein, together with a masking of the hydroxide particles potential by the less charged biomolecules [11].

6.4. Residual concentrations of free lysozyme

To clarify the extent of aluminium species-lysozyme association after aging of the samples, free lysozyme concentrations were measured as a function of lysozyme concentration after removal of the insoluble matter by centrifugation (Figure (6.4)).

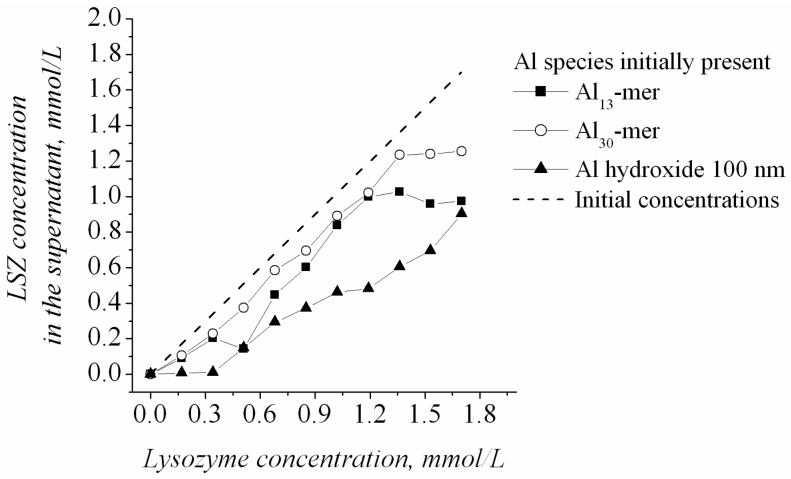

Figure 6.4. Free lysozyme concentration in the supernatant solutions of the aluminium species-lysozyme samples after centrifugation.

The amount of protein remaining in solution reflected phenomena such as adsorption to colloidal particles or electrostatic stabilisation of the protein by binding to strongly positive ions such as Al_{13}-mer and Al_{30}-mer. Therefore, residual protein concentration gave additional insights into the formation of colloidal, self-assembled composites.

The residual solution lysozyme concentration observed was lower than that added to the solutions (dotted line) for all the samples analysed.

Very little difference was observed between the samples with 'aluminium' alone and with the highest concentration of protein again producing evidence for a much weaker interaction of lysozyme with aluminium species than with BSA, which did lead to important modifications in the NMR signal [15].

The reduction of free lysozyme in solution was more pronounced for aluminium hydroxide / lysozyme systems due to the larger size of the particles to which the protein was bound, therefore enhancing the removal of the protein from solution on centrifugation.

In the case of aluminium polycation-lysozyme systems, lysozyme concentration reached a plateau above 17.5 $mg.mL^{-1}$ protein added. Although the protein concentration observed for this plateau was higher in the presence of Al_{30} (~ 18 ± 1 $mg.mL^{-1}$) than in the presence of Al_{13} (~ 15 ± 2 $mg.mL^{-1}$), the difference was not significant This difference was probably attributable to the differing stability of aluminium polycations-lysozyme assemblies, Al_{30}- lysozyme being the most stable species due to the higher charge and stability of Al_{30}-mer compared with Al_{13}-mer.

6.5. Quantitative ^{27}Al solution nuclear magnetic resonance

^{27}Al solution NMR spectroscopy was used to investigate the stability of the polycations in the presence of the protein [6, 19]. ^{27}Al NMR spectra acquired from the Al_{13}-lysozyme solutions showed peaks at ~ 63 ppm (tetrahedral core of the Al_{13}-mer) and ~ 0 ppm (octahedral signal of aluminium monomers) along with a signal at 80 ppm arising from aluminate ions of the internal reference solution (Figure (6.5) **A**) [29]. In the spectra of the Al_{30}-mer-lysozyme systems (Figure (6.5) **B**), along with the above mentioned signals at ~ 63 and ~ 0 ppm, a broader signal at 70 ppm was observed, which corresponded to the tetrahedral "core" aluminium nuclei of the Al_{30}-mer [30].

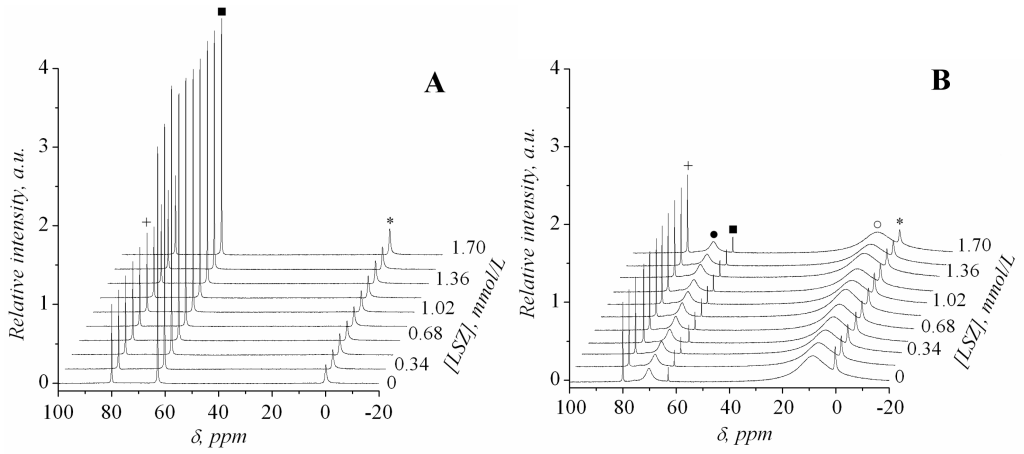

Figure 6.5. ^{27}Al solution NMR spectra of the Al_{13}-mer–lysozyme (T=25°C) (**A**) and Al_{30}-mer–lysozyme (T = 60°C) (**B**) samples, showing peaks attributed to * monomeric aluminium in octahedral environment, + monomeric aluminium in tetrahedral environment (reference solution), ■ aluminium in

the tetrahedral environment of Al_{13} tetrahedral cores, ●,○ aluminium, respectively in the tetrahedral environment of Al_{30} cores and the octahedral environment of Al_{30} shells.

On the basis of the ^{27}Al NMR spectra of the aluminium polyoxocation-lysozyme samples, aluminium speciation diagrams were calculated using an algorithm described previously [3, 7]. The diagrams included aluminium monomers, Al_{13}-mers, Al_{30}-mers, Figure (6.6).

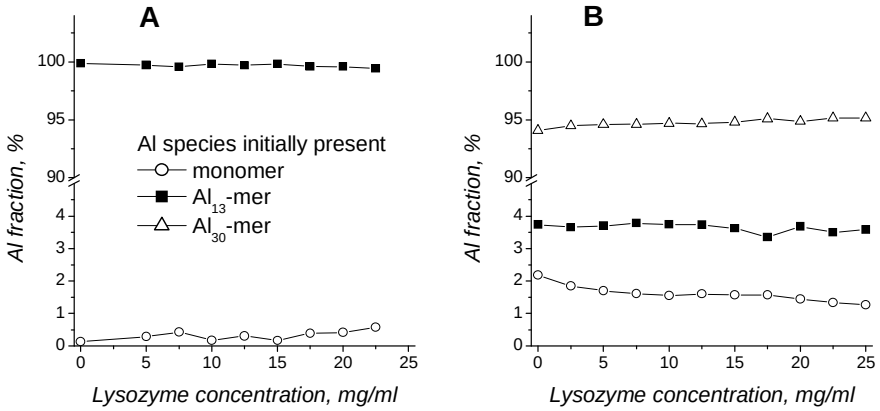

Figure 6.6. Speciation diagrams calculated from Figure (6.5) of the Al_{13}-mer-lysozyme (**A**) and Al_{30}-mer- lysozyme (**B**) samples as a function of total lysozyme concentration.

The concentration of small aluminium oligomers (e.g. aluminium dimers and trimers) was not taken into account in this study due to the very low concentration of these species, as indicated by the absence of the expected broad peak at ~ 2-4 ppm or its strong overlap with larger peaks at ~ 0 and ~ 10 ppm. In the case of the Al_{13}-mer-containing systems, the proportion of aluminium monomers increased very slightly as described above.

In opposition with the previous situation, monomer concentration appeared to decrease upon lysozyme addition in Al_{30}-lysozyme systems. Despite the signal broadening observed for Al_{30}-mer based systems, the corresponding species concentration, together with Al_{13}-mer concentration were not affected by the protein addition. The very weak effect of lysozyme on the NMR signal of the two polycations can not demonstrate a much weaker interaction with lysozyme than the interactions observed with BSA, which led to important modifications in the NMR signal.

6.6. Morphology of lysozyme samples monitored by scanning electron microscope

The solid products obtained by freeze-drying of various aluminium species-lysozyme samples were subjected to SEM analysis to observe the morphology of the prepared materials (Figure (6.7)). In the case of pure Al_{13}-mer and Al_{30}-mer systems, the freeze-dried material was disorganized, although recurrently, flake-shaped materials were observed. Upon lysozyme addition, the samples containing Al_{13}-mers changed progressively until finally they acquired a Velcro-like structural appearance for samples prepared in the presence of 25 $mg.mL^{-1}$ of lysozyme. For the Al_{30}-mer-based materials, the solid products obtained tended to organize themselves into structures characterized by sheets covered

with equally spaced parallel ribbons (Figure (6.7)). The 100 nm aluminium hydroxide based samples exhibited, in the absence and in presence of lysozyme, a morphology similar to the one observed for the Al_{30}-mer-lysozyme samples.

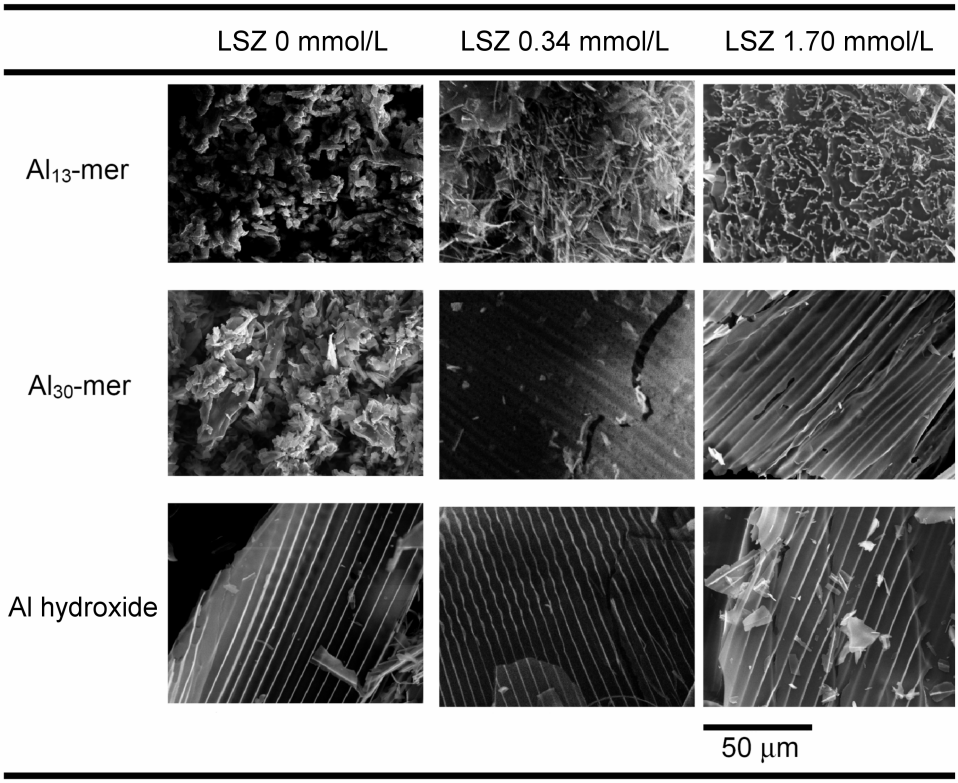

Figure 6.7. SEM pictures of aluminium species-lysozyme hybrid materials prepared by freeze-drying.

The reason for the "nanoribbon-sheet" morphology observed in the Al_{30}-mers and aluminium hydroxide-containing samples is unclear. This morphology could arise from the freeze-drying procedure. Further morphological and spatial chemical analysis is required to explain this phenomenon.

6.7. Comparative FTIR study of BSA and lysozyme / aluminium species systems

Among aminoacids, oxygen donors are usually the best aluminium ligands. The aminoacids most likely to bind aluminium are thus Asp–COO^-, Glu–COO^- or Ser–OH, Thr–OH or Tyr–O^-. Aluminium interaction with proteins can cause conformational changes, or link peptide chains together through their carboxylates moieties [31]. Both secondary structures and potential aluminium binding residues of BSA and lysozyme are shown in Figure (6.8).

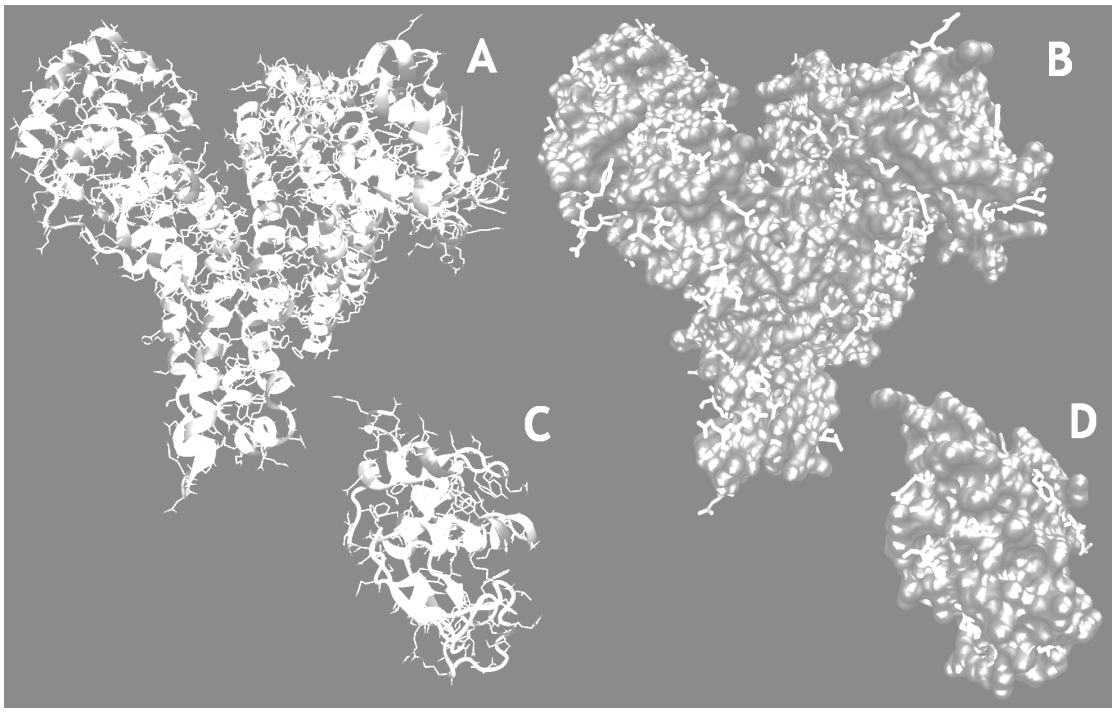

Figure 6.8. Structures of BSA obtained through modelling using the SAM-T06 server [32] (**A**,**B**) and lysozyme obtained from RCSB protein data bank file 2HU1 (**C**,**D**) showing the secondary structural motifs (**A**,**C**) and the surface residues prone to the binding of aluminium ions (**B**,**D**). Representation from Visual Molecular Dynamics software (VMD) [33].

Both proteins are composed of a large amount of α-helical and turn structures, a small amount of β-sheets being present in lysozyme (Figure (6.8) **A**-**C**). The BSA surface has a large number of strong possible binding sites, e.g. aspartic and glutamic acid residues, together with weaker binders, leading to a high negative surface charge under the pH range used in this study.

In contrast, the surface of lysozyme is mostly positive, and on average has much weaker binding sites for aluminium than BSA. The close proximity of binding sites and the average negative surface charge of BSA will lead to a large electrostatic potential in different points of the molecule that will favour the approach and binding of aluminium species, whereas the proximity of positively charged moieties will weaken the electrostatic field surrounding lysozyme, and thus disfavour binding.

In order to evidence these two different interaction tendencies, a comparative study of BSA and lysozyme in the presence of aluminium species was carried out using FTIR spectroscopy for the characterisation of samples prepared at fixed protein concentration and varying aluminium species concentration.

No strong conformational changes were observed upon aluminium species addition for BSA or lysozyme (Figure (6.9)), apart from a slight decrease (~ 5 %) in signal attributed to α-helices upon aluminium polycations addition to BSA, and a decrease, also minimal, of the signal attributed to turns upon addition of aluminium polycations to lysozyme. These variations can be explained by the defolding of both proteins induced by the Al polycations.

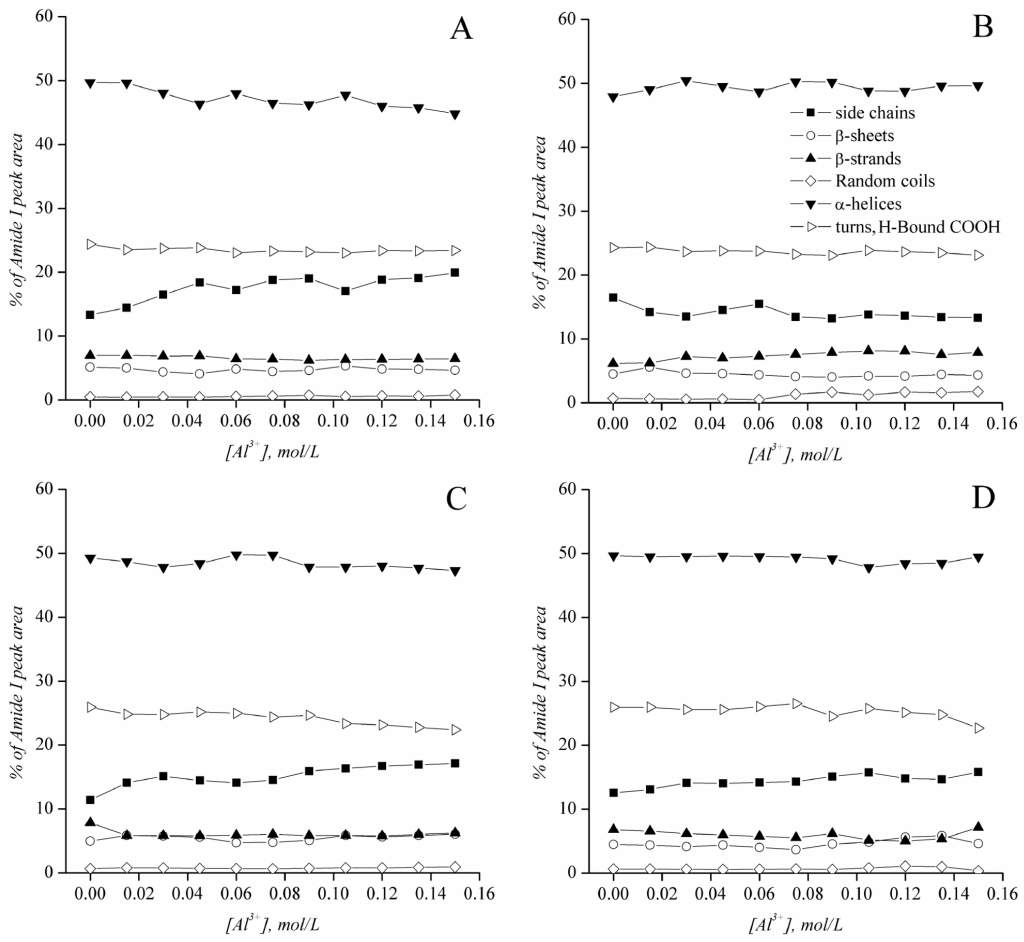

Figure 6.9. Contribution of different amide vibration bands to the area of the amide I band, determined by means of peak fitting for samples prepared from BSA-Al_{13} (**A**), BSA-aluminium hydroxide (**B**), lysozyme-Al_{13} (**C**) and lysozyme-aluminium hydroxide (**D**) systems.

The main modification observed affected the side chain vibrations, with a marked increase in the signal observed at 1613 cm^{-1} for the two proteins upon addition of Al_{13} and Al_{30}. Upon increase in aluminium hydroxide concentration, the same signal increased for lysozyme and decreased for BSA.

These observations demonstrated that interactions between aluminium species and the two proteins influenced mostly their side chains without profoundly affecting their conformation. In order to obtain more information on the nature of these interactions, 2D correlation analysis was used.

In BSA/aluminium polycation synchronous correlation maps, most of the spectral modifications can be attributed to the perturbation of carboxylic acid moieties of the protein (aspartic and glutamic acid residues) by the introduction of aluminium species, with strong positive autopeaks and cross peaks at 1405 and 1600 cm^{-1}. Small negative cross peaks were also present at 1740/1595 cm^{-1} and 1740/1405 cm^{-1} (Figure (6.9) **A**-**B**).

The peaks at 1740 and 1710 cm^{-1} can be attributed to the ν(C=O) vibration of COOH groups that were very sensitive to hydrogen bonding. The vibration of unbound groups can be found at up to 1762 cm^{-1} and can shift below 1700 cm^{-1} for bound groups [34]. Peaks in the 1400 and 1600 cm^{-1} regions were

respectively attributable to $\nu_s(COO^-)$ and $\nu_{as}(COO^-)$ of the deprotonated Glu and Asp residues. These two vibrations were susceptible to shifts by +60/-40 cm^{-1} from 1402/1579 cm^{-1} for Asp and from 1404/1556 cm^{-1} for Glu upon deformations induced by cation chelation. Therefore the shift observed here demonstrated the binding of aluminium species to deprotonated Glu and Asp residues. Furthermore, the correlation of COO^- groups with non H-bonded COOH indicated that the interaction of Al_{13} and Al_{30} with Glu and Asp residues occurred mostly at the surface of the protein, without affecting the secondary structure of the molecule.

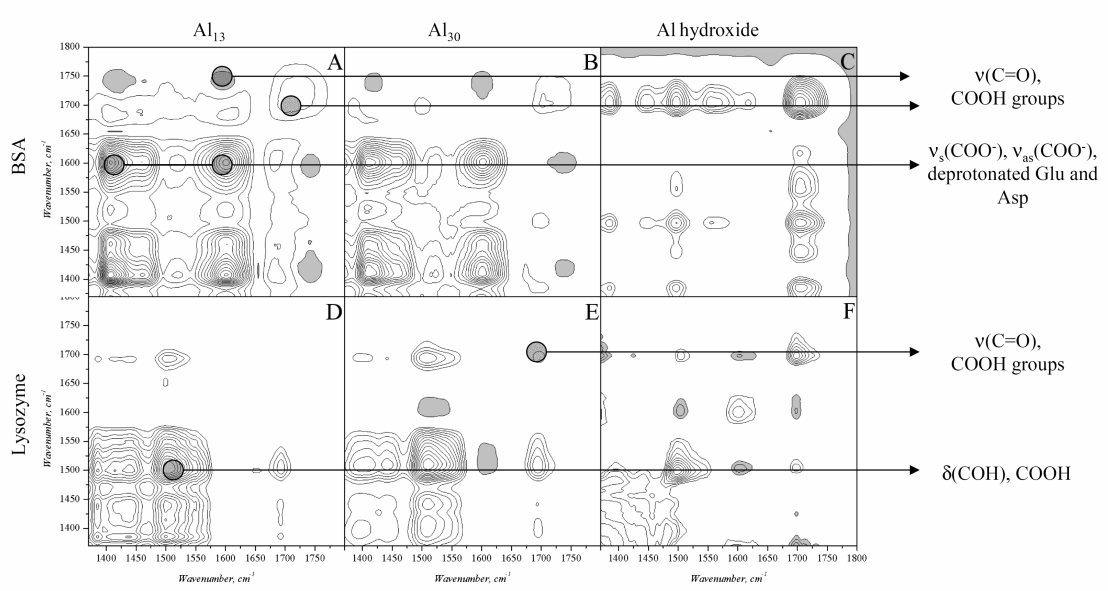

Figure 6.10. Summary of synchronous 2D-COS maps generated from transmission FTIR spectra of samples prepared at different aluminium species concentrations in the presence of a constant concentration of protein, 25 $mg.mL^{-1}$. **A**-**C**: BSA-Al_{13}, BSA-Al_{30} and BSA-aluminium hydroxide; **D**-**E**: lysozyme Al_{13}, lysozyme-Al_{30} and lysozyme-aluminium hydroxide.

For BSA/aluminium hydroxide systems, positive autopeaks and cross peaks were observed at 1380, 1500 and 1710 cm^{-1} (Figure (6.10) **C**). The correlations attributable to the COO^- groups were almost absent from the synchronous correlation diagram, and the signal from H-bonded COOH was mostly positively correlated to a signal at 1500 cm^{-1}, which was attributed to the δ(COH) vibrations of COOH, a vibration known to strongly shift upon hydrogen bonding (1264-1450 cm^{-1})[34]. Deprotonated tyrosine ring vibrations can also be observed in this spectral region, but the correlation of their evolution with the signal from COOH groups cannot be readily explained.

The asynchronous correlation diagram was similar to the map obtained in the presence of the two polycations (Figure (6.11)), however the vibrations related to COO^- groups correlated with more hydrogen bonded COOH groups. In addition, a correlation can be noticed between COOH groups being exposed to different hydrogen bonding modes. These two observations indicated that the presence of the hydroxide sol first perturbed the hydrogen bonding of COOH groups, or that COOH groups H-bond

to the surface of the hydroxide before being deprotonated, this last step being however less likely than in the presence of polycations due to the large size and low flexibility of the hydroxide particles.

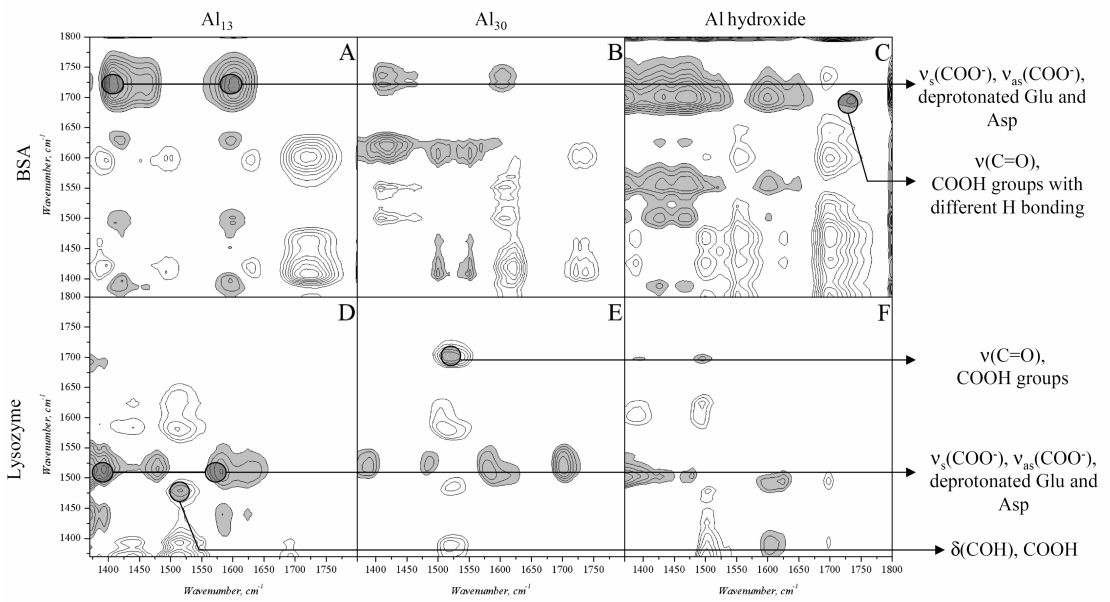

Figure 6.11. Summary of asynchronous 2D-COS maps generated from transmission FTIR spectra of samples prepared at different aluminium species concentrations in the presence of constant concentrations of proteins. **A**-**C**: BSA-Al_{13}, BSA-Al_{30} and BSA-aluminium hydroxide; **D**-**E**: lysozyme-Al_{13}, lysozyme-Al_{30} and lysozyme-aluminium hydroxide.

A different correlation scheme was observed for lysozyme-based samples, with a major autopeak at 1515 cm^{-1} in the presence of all aluminium species. Similarly to the case of aluminium hydroxide / BSA samples, this signal can be attributed to δ(COH) of COOH groups, this signal being positively correlated with a feature at 1695 cm^{-1}, attributed to strongly H-bonded COOH, and negatively correlated with a feature at 1606 cm^{-1}, attributable to $\nu_{as}(COO^-)$ vibrations.

However no negative correlation can be noticed with the weaker $\nu_s(COO^-)$ vibration. This signal can also be attributed to ν(CC) ring and δ(CH) of deprotonated Tyr residues [34], especially as asynchronous correlation was observed between features at 1475 and 1515 cm^{-1}. These two latter signals could be respectively attributed to complexing Tyr and protonated tyrosine, Tyr deprotonation leading to a characteristic shift of the ν(CC) ring and δ(CH) signal from 1500 to 1515 cm^{-1}. The signal at 1606 cm^{-1} was therefore attributed to ν(CC) ring and δ(CH) vibrations of the protonated residue. The correlation of the 1500-1515 cm^{-1} signals with the feature at 1695 cm^{-1} would be then attributable to a cooperative binding of aluminium species to Asp, Glu and Tyr residues (Figure (6.12)) leading to a deprotonation of the latter residue, the pK_a of Tyr being far higher (10.2) than the pH used during our experiments.

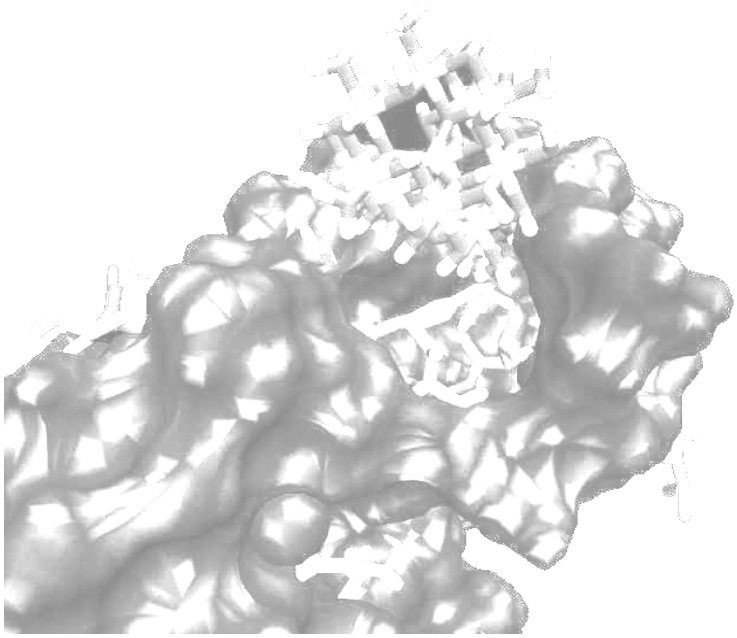

Figure 6.12. Possible binding mode of Al_{13} to lysozyme, involving one tyrosine residue and other residues favourable to binding in the β-sheet region. Representation using VMD [33] after energy minimisation and 5 ps MD equilibration of the assembly using Accelrys MS Discover and the Compass generalised force field.

6.8. Conclusions

The interactions of lysozyme, a biomolecule present in human and animal body fluids, with different aluminium species have been studied. The results from FTIR analysis of aluminium species/protein systems demonstrated the likely interaction mechanisms leading to the formation of hybrid materials. For both BSA and lysozyme, the assembly of Al_{13} and Al_{30} with the proteins led to the formation of hybrid species observable by means of dynamic light scattering (particle size superior to both pure aluminium species and pure protein particle sizes) and zeta potential measurements (potential stabilising to the value of the hybrid species upon increase in protein concentration). However, the assembly of aluminium species with both proteins only led to a minor change in their secondary structure, the main changes being observed for the protein surface groups as demonstrated from secondary structure quantification carried out for different protein: aluminium ratios. Polycations were demonstrated to bind Asp and Glu residues of BSA, leading to a deprotonation of their carboxylic acid groups, as demonstrated from 2D correlation spectroscopy. This deprotonation would have led to the increasing acidity of the solutions observed from pH measurements reported previously [15].

In the case of lysozyme interacting with aluminium species, as well as for BSA interacting with aluminium hydroxide particles, only a perturbation of the hydrogen bonding of Asp and Glu COOH moieties can be noticed. This result demonstrated the weaker interaction of the soluble aluminium species with lysozyme, arising from the high positive electrostatic potential on the protein. The similarity of the interactions between aluminium hydroxide and both proteins was due to the rigidity

and large dimensions of the colloid, which decreased the probability of contact between potential binding sites on protein and mineral surfaces. The correlations observed in the case of lysozyme could also demonstrate a cooperative binding of the aluminium species to acidic aminoacids and tyrosine leading to a deprotonation of the later residue. This hypothesis however requires further experimentation to be confirmed. The variety of interactions observed between proteins bearing different physicochemical properties and aluminium species constitutes a useful base for the choice of polymers and biopolymers for the fabrication of novel aluminium-based materials, either from stable bioinorganic core-shell particles (comprising aluminium at the surface or in the bulk of the materials) or by self-assembly of composite networks having the ability to phase-separate from the initial liquid medium.

6.9. References

[1] S. M. Bradley and R. A. Kydd, Catal. Lett., 1991, 8, 185.

[2] E. Montarges, A. Moreau and L. J. Michot, Appl. Clay Sci., 1998, 13, 165.

[3] J. Gregory and J. Duan, Pure Appl. Chem., 2001, 73, 2017.

[4] J. J. Fitzgerald and A. H. Rosenberg, in *Antiperspirants and Deodorants*, ed. K. Laden, Marcel Dekker, 1999, pp. 83-137.

[5] C. C. Perry and K. L. Shafran, J. Inorg. Biochem., 2001, 87, 115.

[6] K. L. Shafran and C. C. Perry, J. Chem. Soc., Dalton Trans., 2005, 2098.

[7] J. P. Jolivet, in *Metal Oxide Chemistry and Synthesis: From Solution to Solid State*, J. Wiley and Sons Ltd., Chichester, 2000.

[8] W. H. Casey, Chem. Rev. C, 2006, 106, 1.

[9] G. Berthon, Coord. Chem. Rev., 1996, 149, 241.

[10] W. R. Harris, G. Berthon, J. P. Day, C. Exley, T. Peder Flaten, W. F. Forbes, T. Kiss, C. Orvig and P. F. Zatta, J. Toxicol. Environ. Health, 1996, 48, 543.

[11] K. Rezwan, L. P. Meier, M. Rezwan, J. Voros, M. Textor and L. J. Gauckler, Langmuir, 2004, 20, 10055.

[12] G. Furrer, B. L. Phillips, K.-U. Ulrich, R. Pöthig and W. H. Casey, Science, 2002, 297, 2245.

[13] D. R. Parker, T. B. Kinraide and L. W. Zelazny, Soil Sci. Soc. Am. J., 1989, 53, 789.

[14] J. J. Comin, J. Barloy, G. Bourrie and F. Trolard, Eur. J. Agron., 1999, 11, 115.

[15] O. Deschaume, K. L. Shafran and C. C. Perry, Langmuir, 2006, 22, 10078.

[16] E. Bergfors, B. Trollfors and A. Inerot, Journal of Allergy and Clinical Immunology, 2004, 113, S294.

[17] J. Berkowitz, M. A. Anderson and R. C. Graham, Water Res., 2005, 39, 3918.

[18] K. L. Shafran, O. Deschaume and C. C. Perry, J. Mater. Chem., 2005, 15, 3415.

[19] K. Shafran, O. Deschaume and C. C. Perry, Adv. Eng. Mater., 2004, 6, 836.

[20] P. M. Jardine and L. W. Zelazni, Soil Sci. Soc. Am. J., 1986, 895.

[21] C. M. Stoscheck, Methods Enzymol., 1990, 182, 50.

[22] T. J. Lenk, T. A. Horbett, B. D. Ratner and K. K. Chittur, Langmuir, 1991, 7, 1755.

[23] A. Muga, H. H. Mantsch and W. K. Surewicz, Biochemistry, 1991, 30, 7219.

[24] J. E. Berry and Y. Ozaki, 2D-CoS Toolbox, *Matlab Code*, 2001, Uegahra (Japan), Kwansei-Gakuin University.

[25] I. Noda, A. E. Dowrey, C. Marcott, G. M. Story and Y. Ozaki, Appl. Spectrosc., 2000, 54, 236A.

[26] W. G. Burton, K. D. Nugent, T. K. Slattery, B. R. Summers and L. R. Snyder, J. Chromatogr., 1988, 443, 363.

[27] A. A. Vertegel, R. W. Siegel and J. S. Dordick, Langmuir, 2004, 20, 6800.

[28] K. Rezwan, L. P. Meier and L. J. Gauckler, Biomaterials, 2005, 26, 4351.

[29] J. W. Akitt, J. Chem. Soc., Faraday Trans. 2, 1986, 82, 377.

[30] L. Allouche, C. Gerardin, T. Loiseau, G. Ferey and F. Taulelle, Angew. Chem. Int. Ed., 2000, 39, 511.

[31] P. Rubini, A. Lakatos, D. Champmartin and T. Kiss, Coord. Chem. Rev., 2002, 137.

[32] G. Shackelford and K. Karplus, Proteins: Structure, Function, and Bioinformatics, 2007, 69, 159.

[33] W. Humphrey, A. Dalke and K. Schulten, J. Mol. Graphics, 1996, 14, 33.

[34] A. Barth, Prog. Biophys. Mol. Biol., 2000, 74, 141.

Part 7

Insight into Structural Transition and Complexation of Mucin in the Presence of Aluminium Species

During this work, aluminium-mucin samples were prepared from model solutions of aluminium species (aluminium monomers, Al_{13}-mers, Al_{30}-mers, and aluminium hydroxide sol with 100 ± 11 nm particle size) and different amounts of mucin. The samples were analyzed using a range of solution and colloidal techniques including pH, conductivity, viscosity measurements together with ^{27}Al NMR and quantification of the free protein and aluminium fraction after centrifugation of the phase-separated materials. The samples were finally freeze-dried and analyzed using Fourier transform infrared spectroscopy and SEM as solid-state techniques.

7.1. Potentiometric titrations, pH and conductivity of aluminium-mucin solutions

Potentiometric titrations

The affinity of mucin to aluminium species has been tested by potentiometric titrations. Fully automated potentiometric titrations were carried out on mucin alone and on mucin in the presence of the Al_{13}-mer polycation. Figure (7.1) shows the titration results of mucin in the absence and in the presence of the Al_{13}-mer polycation as a function of pH.

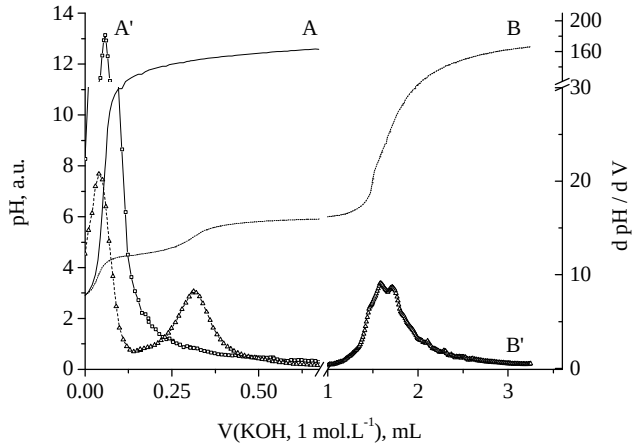

Figure 7.1. Potentiometric first and derivative titration curves of 2.5 mg of mucin alone ((**A**) and (**A'**) respectively) and 2.5 mg of mucin with 0.15 mol.L^{-1} Al_{13}-mer polycation ((**B**) and (**B'**) respectively) against 0.1 mol.L^{-1} KOH.

Alone, the pure mucin titration curve (Figure (7.1) **A**) underwent one main inflexion point which happened between pH 4 and 12. The trend of a pure mucin titration curve is related to the composition of its sequence. Although the detailed compositions and structures of mucins are diverse depending on their origin, they display some common features like regions enriched with acid aspartic, acid glutamic [1], cysteine [2], serine [3] and threonine [4]. The side chain groups of those amino acids have pK_as ranging from 4 to 13. The broad pH interval of the deprotonation of mucin is related to sequential deprotonation of its amino acid functional groups. Once mixed together with the Al_{13}-mer polycation, the potentiometric titration curve (Figure (7.1) **B**) of mucin revealed two more inflexion points providing a first indication of the existence of binding sites. They were caused by the delayed deprotonation of the protein, due to its electrostatic interactions with the metal. The mucin pK_as' were perturbed from its pure pK_as' values.

pH and conductivity of aluminium species-mucin samples prepared at various mucin concentrations.
pH and conductivity measurements of the samples prepared from aluminium species and mucin were carried out simultaneously, after ageing the samples for 24 h. The data are presented in Figure (7.2).

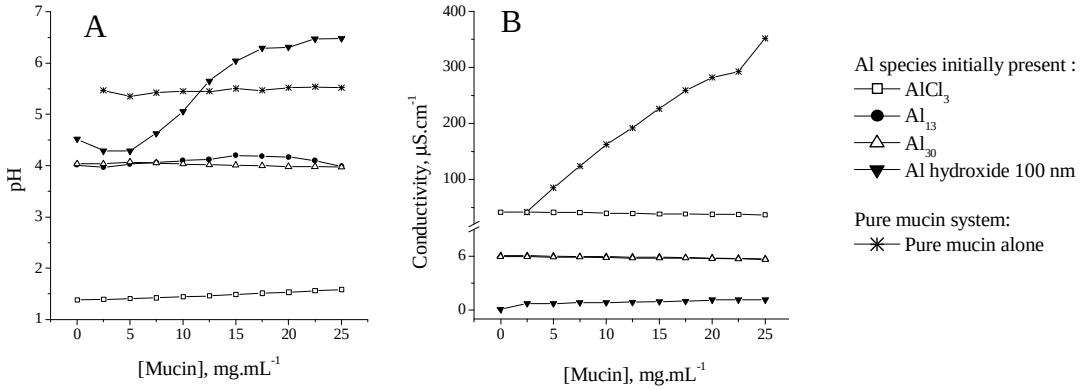

Figure 7.2. pH (**A**) and conductivity (**B**) of aluminium species-mucin samples prepared with various mucin concentrations.

On the pH diagram (Figure (7.2) **A**), pH increased for the aluminium hydroxide-based systems starting from mucin concentration of 5 $mg.mL^{-1}$ was observed. It probably reflected the partial conversion of the colloids into smaller aluminium hydroxide particles with release of hydroxide ions. With the Al_{13}-mer, Al_{30}-mer and $AlCl_3$ based systems, no pH variation was noticed. The deprotonation and further binding of the protein by the aluminium species was yet proven by potentiometric titration. It is likely that the pH stability was the result of a reorganisation of the mixed species. Ionised sites on mucin could have been instantly bound by the aluminium species, the phenomenon occurring before the pH was measured, i.e. within the 24 h of aging of the samples.

Pure mucin conductivity increased upon an increase of its concentration. This corresponded to an increase in the charge density of the protein. Increases of mucin concentration had a relatively low effect on the conductivity of the systems (Figure (7.2) **B**). The stability of the conductivity of the aluminium-mucin samples reflected the neutralisation of the negative charges of mucin by the positively charged aluminium species. The event occurred with all the different aluminium species employed.

7.2. Visual aspect and viscosity properties of the aluminium-mucin samples

Visual aspect

The gel-like aspect of the aluminium-mucin samples and the absence of precipitate in the samples were first appreciated by simple visual examination. When they were not mixed together, the mucin and the aluminium hydroxide particles did not gel as represented in Figure (7.3) **A** and **B**. Once combined, the two molecules demonstrated a synergistic effect on their ability to establish a gelled material (Figure (7.3) **C**).

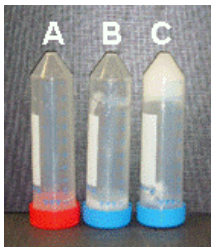

Figure.7.3. Solution samples of mucin 25 $mg.mL^{-1}$ (**A**), aluminium hydroxide particles 0.15 $mol.L^{-1}$ (**B**) and a mixture of aluminium hydroxide particles 0.15 $mol.L^{-1}$ and mucin 25 $mg.mL^{-1}$ (**C**).

The Al_{13}-mers and the Al_{30}-mers polycations had the same property to form a gel when they were blended with mucin. The gelation of mucin in the presence of aluminium species rather than aggregation [5] was visible by eye as a viscous opalescent gel developed in the samples upon mucin concentration increase, Figure (7.4).

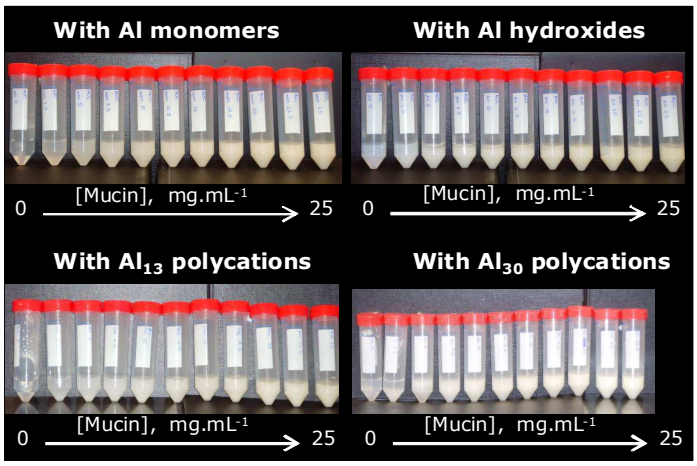

Figure 7.4. Gelation behaviour of increasing concentration of mucin 24 h after mixing with different aluminium species 0.15 mol.L^{-1}.

The elastic material depicted in Figure (7.3) **C** did not pour freely, rather had the consistency of syrup or honey. It can resist and recover from stretching, compression or distortion applied by a force (to an unknown extent as no measure was performed).

Viscosity

Among the properties that underwent the most dramatic changes at the gel point was the viscosity, Figure (7.5).

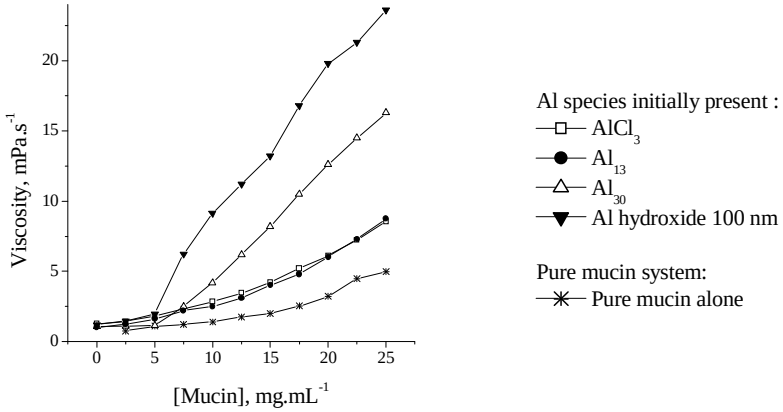

Figure 7.5. Viscosity of aluminium species - mucin samples prepared at various protein concentrations. The measurements were performed at 24 h aging.

Measurements demonstrated that the gelation of mucin by aluminium species modified the viscosity of native mucin. Furthermore, the viscosity of the different aluminium species solutions increased upon increase of mucin concentration. The gel point was noticed after addition of 22.5 mg.mL^{-1} of mucin in the samples which contained initially the $AlCl_3$, and the aluminium polycation species. Mucin addition of 20 mg.mL^{-1} led to the gel point of the aluminium hydroxide-based samples. The viscosity

measurements were sensitive to the aluminium speciation of the samples. In the case of the aluminium hydroxide-mucin systems where that observation was the most pronounced, viscosity increased 4.7 times in presence of 25 mg.mL^{-1} of protein compared to the viscosity of the pure mucin stock solution, confirming an increase in the density of the gel formed.

7.3. Residual concentrations of mucin and aluminium cations

To clarify the extent of aluminium species - mucin association after aging of the samples, free supernatant mucin and aluminium concentrations were measured after the removal of the insoluble matter by centrifugation as described in the experimental section. The results are presented in Figure (7.6) for the samples prepared from Al_{13}-mer, Al_{30}-mer and aluminium hydroxide sols.

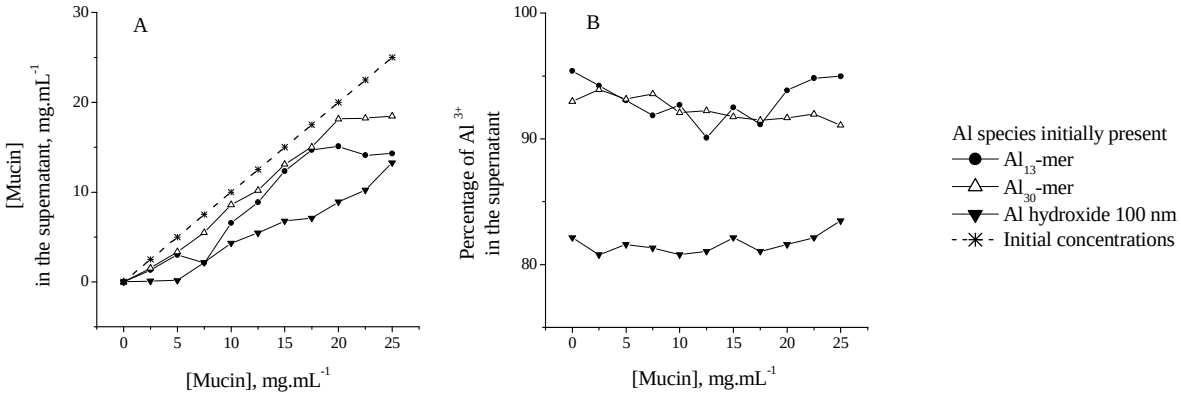

Figure 7.6. (**A**) Free mucin concentration and (**B**) aluminium cation concentration in the supernatant solutions of the aluminium-mucin samples after centrifugation.

The average measurement error of the experiments performed in triplicate, did not exceed 0.03 mg.mL^{-1} for mucin and 5.20 % for aluminium ions. Mucin concentration was determined with the Bradford protein assay, Figure (7.6) **A** and aluminium concentration by Ferron spectrophotometric assay, Figure (7.6) **B**.

As follows from Figure (7.6) **A**, the free mucin concentration in the supernatant of the aluminium species-mucin samples increased with increase of total protein concentration for all three aluminium systems. The mucin concentration in the supernatants was lower than the one introduced initially in the samples. Part of the mucin contained in the Al_{13}-mer, Al_{30}-mer and aluminium hydroxide systems was involved in the formation of new aluminium-mucin assemblies. For samples containing one of the aluminium polycations, “free” mucin concentration reached the maximum at a total mucin level of 20 mg.mL^{-1}. On the other hand, the equilibrium of the formation of the aluminium hydroxide-mucin composites seemed to require the highest quantities of protein as no plateau phase was attained.

The results obtained with the Ferron spectrophotometric assay (Figure (7.6) **B**) confirmed the existence of bio-inorganic complexes. The aluminium cation content of the supernatants was lower than was initially present in the samples. Similarly to what was observed with the Bradford protein assay, it was with the aluminium hydroxide-containing systems that the quantitative loss of aluminium species was

the most pronounced. Increase in mucin concentration caused very little variation of the percentage of the aluminium cation in the supernatants.

The residual mucin and aluminium ion concentrations in the supernatant solutions revealed the existence of aluminium-mucin assemblies; the extent of the complexation being the most significant for the aluminium hydroxide systems.

7.4. Characterisation of the aluminium species in the bio-inorganic assemblies by ^{27}Al NMR

^{27}Al solution NMR

The identification and the measure of the amounts of individual aluminium species have been carried out using quantitative ^{27}Al solution NMR spectroscopy according to a procedure developed earlier in our group [6, 7]. The NMR spectra of all of the aluminium species-mucin systems were acquired and are displayed in Figure (7.7).

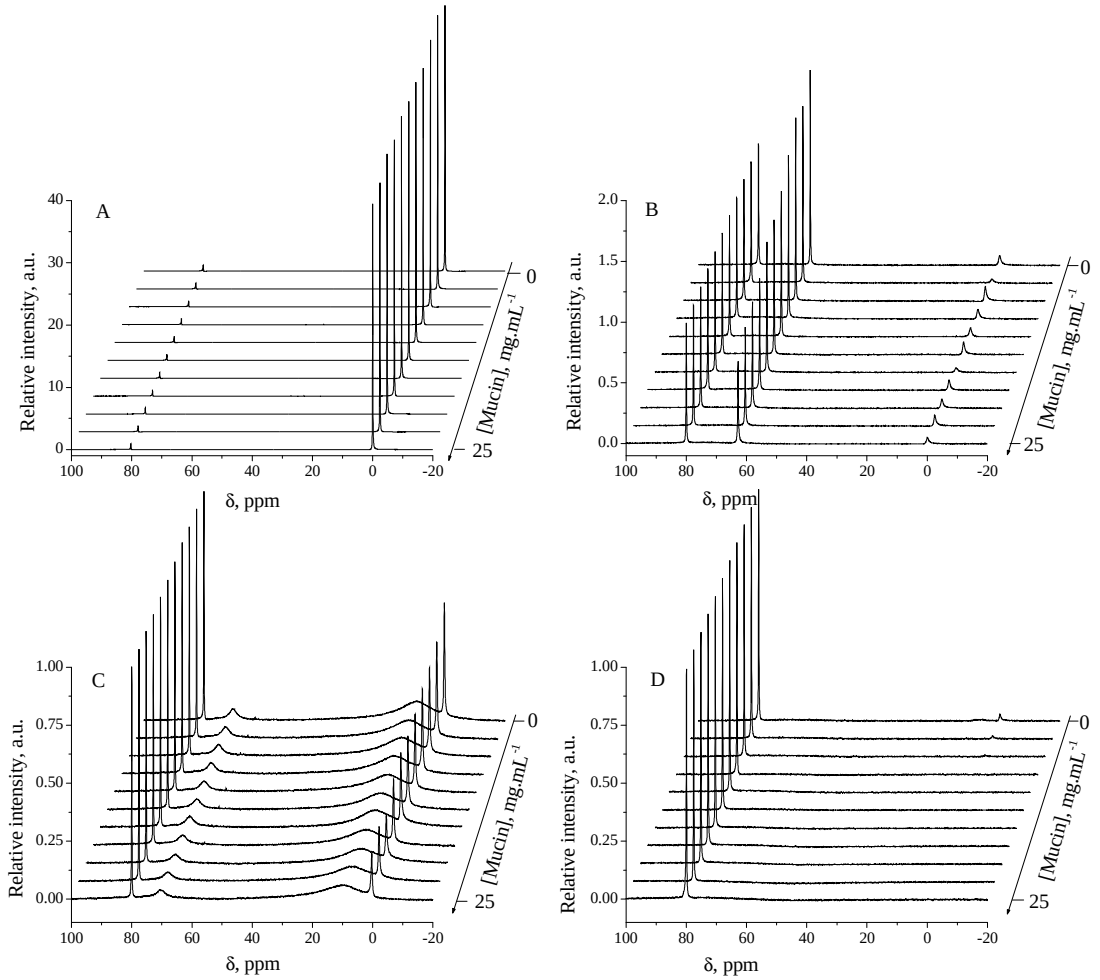

Figure 7.7. ^{27}Al solution NMR spectra of the $AlCl_3$-mucin (**A**), Al_{13}-mer-mucin (**B**), Al_{30}-mer-mucin (**C**), and aluminium hydroxide-mucin (**D**) samples as a function of total mucin concentration. The peak at 80 ppm arises from the internal reference solution of aluminate ions in D_2O.

^{27}Al NMR spectra acquired from the $AlCl_3$-mucin samples (Figure (7.7) **A**), revealed one prominent peak at 0 ppm (octahedral signal of aluminium monomers) whose intensity did not vary upon increase

of mucin concentration along with a signal at 80 ppm arising from aluminate-ions of the internal reference solution [8]. Spectra of solutions made of Al_{13}-mer and mucin (Figure (7.7) **B**), showed peaks at ~ 63 ppm (tetrahedral core of the Al_{13}-mer) and ~ 0 ppm. The intensity of the characteristical peak of the aluminium polycation decreased when the concentration of mucin was increased. In the spectra of the Al_{30}-mer-mucin systems (Figure (7.7) **C**), along with the mentioned signal at ~ 0 ppm, two broader signals at 70 and at ~ 9 ppm were observed. They corresponded respectively to the tetrahedral 'core' aluminium and the octahedral aluminium shell atoms of the Al_{30}-mer [9]. Spectra of the initial aluminium hydroxide systems (Figure (7.7) **D**) presented two peaks; one related to the aluminate-ions, and the second one was the monomers' peak [8]. The second mentioned peak disappeared after addition of mucin in the samples.

Local peak integration (Figure (7.8)) demonstrated a small decrease in concentrations of the aluminium species initially present. This main spectral change observed under protein additions, without the appearance of monomer concentration increase, confirmed that the addition of protein catalyzed the formation of a gel in solution. Apart from the aluminium monomer-containing samples where some aluminium dimers were detected, the speciation of aluminium appeared to be unaffected by the protein.

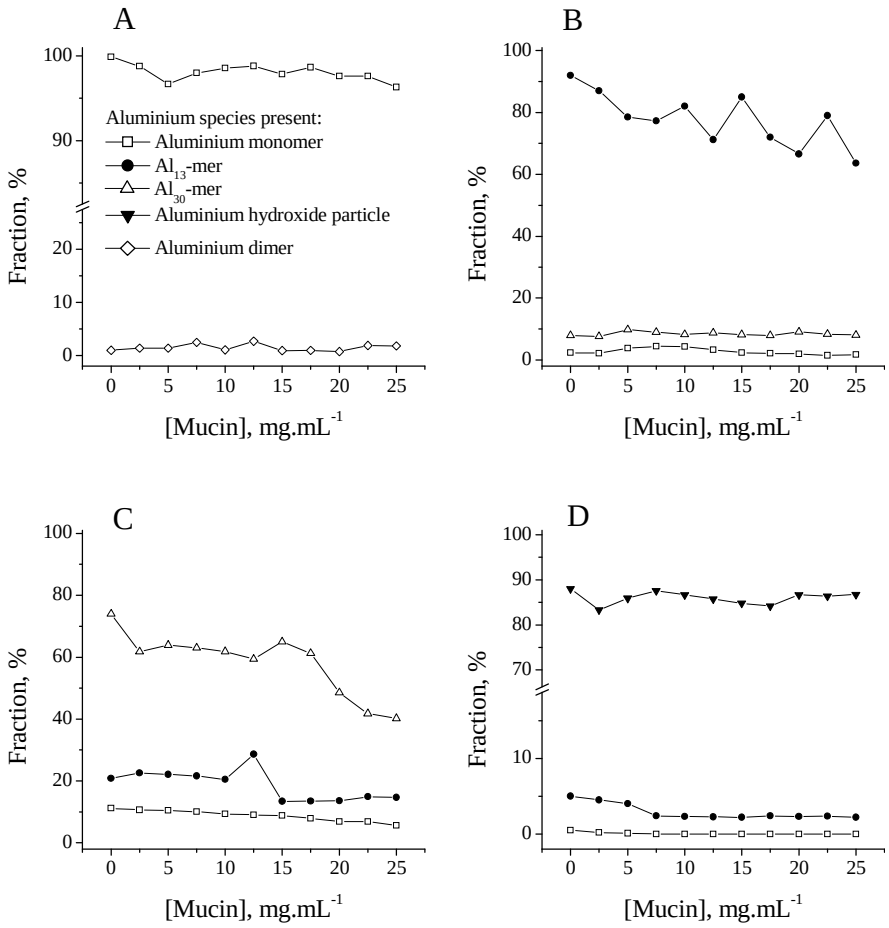

Figure 7.8. Speciation diagrams determined by local integration of the peaks of the ^{27}Al NMR spectra of the samples prepared from $AlCl_3$ (**A**), Al_{13}-mer (**B**), Al_{30}-mer (**C**) and aluminium hydroxide particles (**D**) 0.15 $mol.L^{-1}$ with mucin.

The addition of the mucin to the systems caused a limited decrease of the initial signals. No formation of new signals was observed. Mucin acted as a stabilising agent on the aluminium species. Those results were verified by aluminium solid-state nuclear magnetic resonance.

^{27}Al solid-state NMR

^{27}Al solid-state NMR (SSNMR) was performed on the aluminium polycation-containing samples. The characteristic signal of an aluminium polycation reference system, the Al_{13}-mers, exhibited two resonances as represented in Figure (7.9). They corresponded to the signals of the tetracoordinated (noted Al_{IV}) [10, 11, 12] and the hexacoordinated (noted Al_{VI}) aluminium [13, 14].

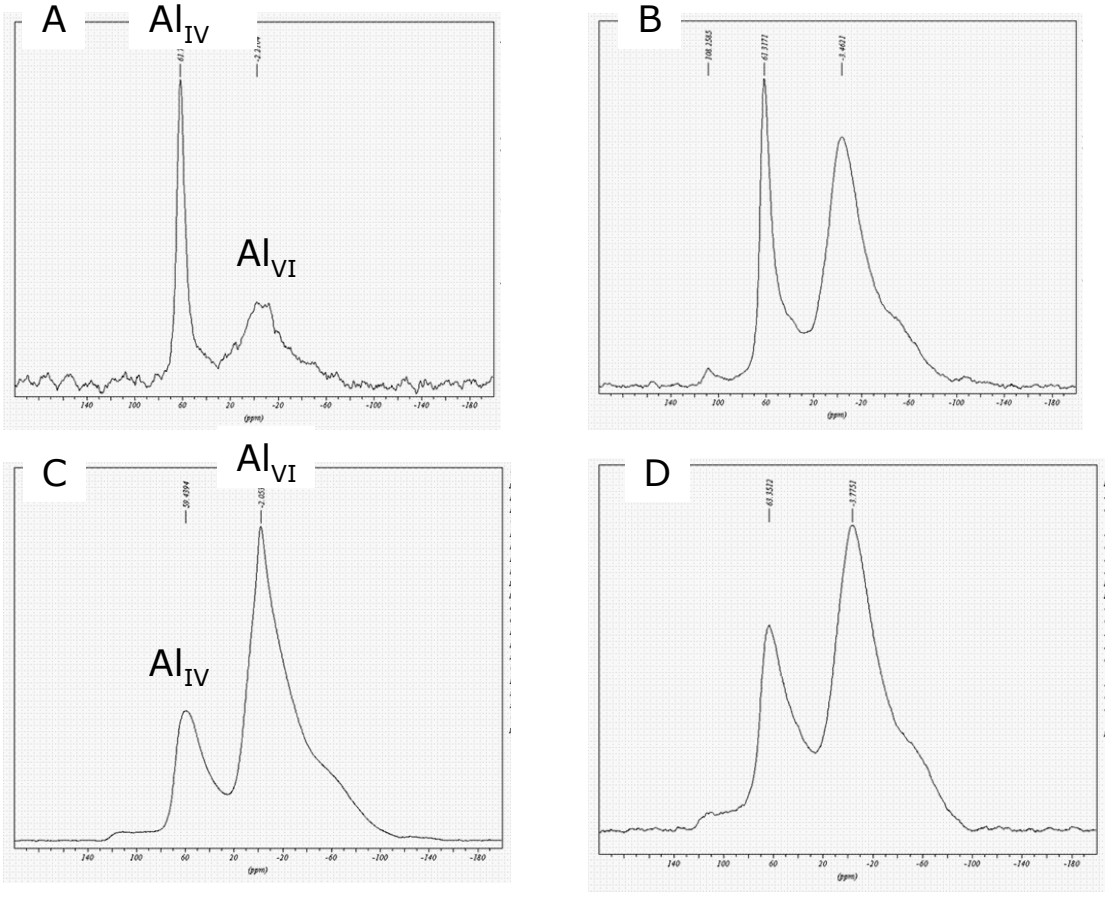

Figure 7.9. ^{27}Al solid-state NMR spectra of Al_{13}-mer 0.15 mol.L^{-1} (**A**), Al_{13}-mer in presence of 25 mg.mL^{-1} of mucin (**B**), Al_{30}-mer 0.15 mol.L^{-1} (**C**), Al_{30}-mer in presence of 25 mg.mL^{-1} of mucin (**D**). Vertical scales (not showed) represent the intensity in arbitrary units, normalized to the maximum peak height in each spectrum. Asterisks denote spinning side bands.

In the spectrum of the Al_{13}-mer reference system, one can noticed a narrow signal at 61.787 ppm and one smaller and broad peak at -2.210 ppm as shown on Figure (7.9) **A**. The first signal noted peak 1, was stable in the presence of mucin, whereas the second one, peak 2, was shifted to higher chemical shifts. Together with the shielding of peak 2, one can observe the decrease of the peak 1: peak 2 intensity ratio (the data are compiled in Table (7.1)).

The characteristic signal of an Al_{30}-mer reference system exhibited two broad peaks: one at 59.439 ppm and one stronger at - 2.054 ppm (Figure (7.9) **B**). Although both peaks were still there in presence of mucin, peak 1 was shifted to higher chemical shifts whereas peak 2 was shifted to lower chemical shifts (the chemical shift values are presented in Table (7.1)).

Table 7.1. Relative intensities of peak 1 and peak 2 observed in samples containing an aluminium polycation without and with mucin.

[mucin], $mg.mL^{-1}$	Chemical shift, ppm			
	Peak 1		Peak 2	
	Samples with Al_{13}-mer	Samples with Al_{30}-mer	Samples with Al_{13}-mer	Samples with Al_{30}-mer
0	61.787	59.439	-2.210	-2.054
25	61.317	63.351	-3.462	-3.775

The presence of the characteristic signals of the aluminium polycations in the samples containing some mucin suggested that mucin did not break down the aluminium species. The shift of the octahedral signals suggested the complexation of the polycations with the protein.

The decrease of the peak 1: peak 2 ratios in the case of samples containing the Al_{13} polycation implied that the octahedral aluminium detected had been formed during the addition of mucin, with a concentration effect on the protein. The chemical shift of peak 2 for all the aluminium polycation-containing samples can be attributed to the formation of aluminium-mucin assemblies. The shielding of peak 1 for the Al_{30}-containing systems could be due to the conversion of some Al_{30} polycations into Al_{13} polycations.

Now that the proof of the existence of new assemblies between aluminium and mucin were demonstrated by means of several techniques, DLS measurements were undertaken to get more information about the aluminium-mucin assemblies.

7.5. Dynamic light scattering measurements

The binding of the aluminium species by BSA was proved to be electrostatically driven [15]. Based on that knowledge, we hypothesized that the new assemblies formed between the different positively charged aluminium species used in our work and mucin were interacting electrostatically.

Although this hypothesis could have been reinforced with zeta-potential data, the results obtained with that latter technique were not useful owing to their lack of reproducibility. Instead, DLS measurements were conducted to evidence the existence of electrostatic interactions in the samples. The particle size of pure mucin samples was determined by dynamic light scattering and the results are presented in Figure (7.10).

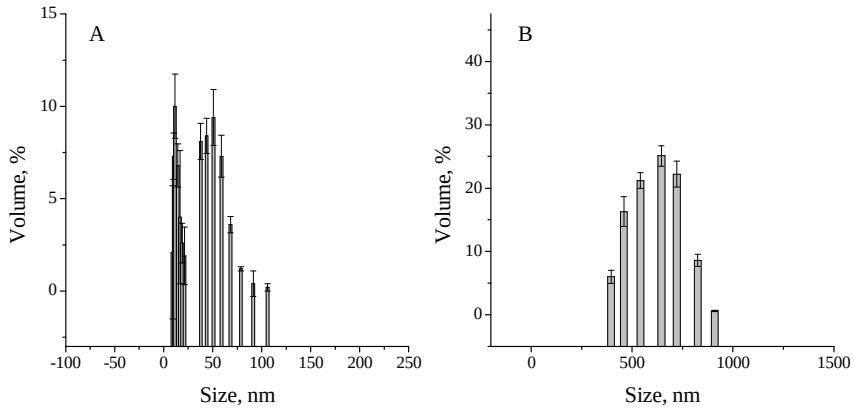

Figure 7.10. Size distributions of 2.5 (**A**) and 25 (**B**) mg.mL^{-1} mucin aqueous solutions.

The mucin alone can be considered as a mixture of particles having different gelation states. It can be clearly seen that at 2.5 mg.mL^{-1} (Figure (7.10) **A**), the mucin solution showed a bimodal size distribution; the smaller particles have a mean diameter 10.20 ± 1.74 nm and the larger particles 50.70 ± 1.51 nm. The same trend was observed for mucin concentrations of 5 and 7.5 mg.mL^{-1}. The bimodal trend can be explained by the structural dumbbell-like structure of the mucin molecule. That characteristical aspect represented in Figure (7.11) was evidenced by [16] by means of atomic force microscopy and transmission electron microscopy.

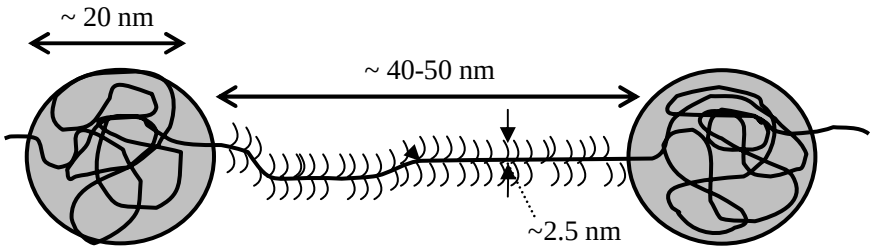

Figure 7.11. Schematic diagram of a dumbbell-like mucin molecule showing two globular structures per chain separated by a glycosylated spacer.

The lower particle size value distinguished the globular structure of the protein whereas the higher value the long glycosylated spacer of the peptide backbone.

Upon increase of the concentration of the mucin in the solutions, the mean size of the samples increased linearly from 50.7 ± 10.26 to 655.42 ± 55 nm. Furthermore, once the concentration of the protein reached the threshold of 10 mg.mL^{-1}, the size distribution of mucin samples became unimodal (example of a homogeneous size distribution is illustrated by Figure (7.10) **B**). According to the manufacturer, mucin contains about 1 % of bound sialic acids whose ionization is pH-dependent. Under the studied pH conditions, sialic acids were in their ionised form, which decreased the colloidal stability of mucin [17]. The variation of the general trend of the size distribution of the protein arose

from the increase of intermolecular binding in solution which promoted further gelation-aggregation into larger particles.

The increase of mucin concentration promoted an increase of the mean particle size of the pure mucin solutions (Figure (7.12)). The rise of the mean particle size was due to the formation of intermolecular interactions within the mucin network.

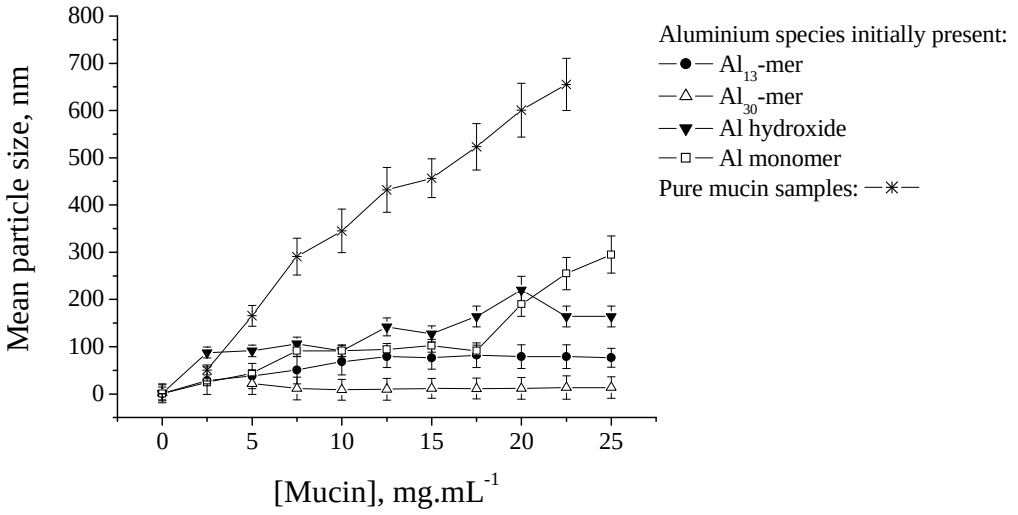

Figure 7.12. Evolution of average particle sizes of aluminium species-mucin samples as a function of mucin concentration measured by DLS at a scattering angle of 90°.

Figure (7.12) also shows the effect of addition of aluminium species (0.15 mol.L^{-1}) on the particle size distribution of mucin. There was a significant change in the new assemblies' particle size distribution. The mean particle size of all the suspensions containing some aluminium species was below the values obtained for pure mucin solutions.

Furthermore, the variation of the mean particle size was dependent on the nature of the aluminium species present in the samples. An increase in the distribution size was noticed upon mucin concentration increase in the aluminium hydroxide and the aluminium monomer-containing samples whereas additions of the protein to the aluminium polycations affected the particle size in the blends to a lesser extent. The conjecture is that the positively charged aluminium species interfered with the intermolecular interactions present in the mucin network. The aluminium species added to mucin adsorbed on, the surface of mucin and caused further gelation due to the formation of intramolecular polymeric bridges between smaller particles. At the same time, the mucin particles, which had more complete coverage by the aluminium species, tended to de-aggregate due to electrostatic repulsion. More mucin particles were fully covered by aluminium species, which led to de-aggregation of larger particles. Aluminium apparently inhibited the oligomerisation of the protein and conferred greater stability on the new assemblies.

7.6. Conformational assessment of the mucin in aluminium - protein hybrid materials.

Infrared spectroscopy measurements were intended to confirm the above-mentioned model and to study the conformation of mucin alone and in the presence of aluminium species.

The conformation of mucin in the absence and in the presence of aluminium species was studied spectroscopically by Fourier transform attenuated total reflectance (ATR–FTIR) and KBr pellet transmission.

ATR–FTIR analysis

First the infrared absorptions of the freeze-dried pure mucin samples were measured by ATR–FTIR. The spectra obtained for different mucin concentrations and an example of the component amide I band curve fitted are represented in Figure (7.13) **A** and **B** respectively.

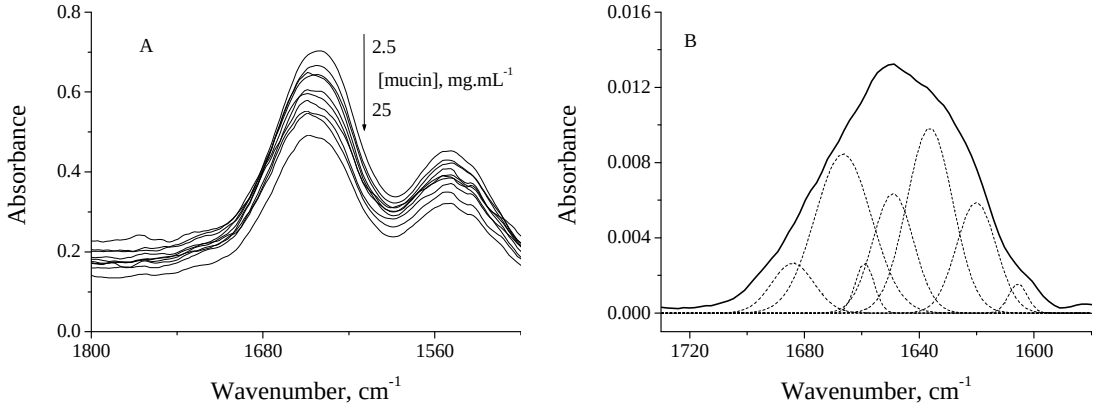

Figure 7.13. (**A**) Mucin adsorption at different concentrations followed by ATR-FTIR. (**B**) Amide I band with fitted component peaks for the 25 mg.mL^{-1} pure mucin sample.

The amide I band is a summation of several component bands, each arising from specific secondary structures located within the protein. Figure (7.14) highlights the fraction of each secondary structure found in the pure mucin sample.

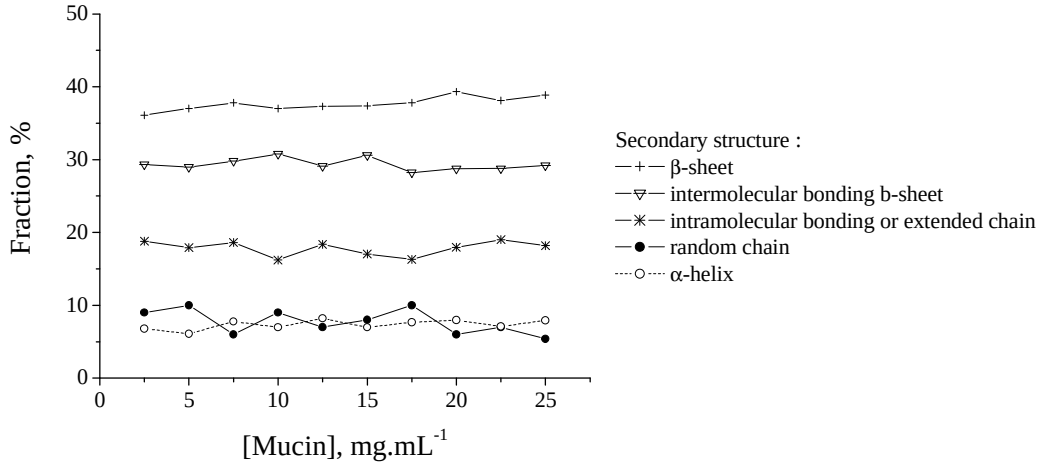

Figure 7.14. Secondary structure distribution of the pure mucin solutions against the concentration of the protein determined by ATR-FTIR. Standard deviations errors obtained from data collection in triplicate were within ± 3.2 %.

Curve fitting analysis of component bands demonstrated that the proportion of each secondary structure present in the pure mucin did not vary upon increase of the concentration of the protein. Among the conformations encountered, between 25 and 40 % of the total fraction of secondary structure consisted of β-sheet structures. 30 % of the protein was organised into intermolecular interactions and in between 15 and 20 % in intramolecular interactions. Random chains and α-helices were less abundant structures, present in equal proportions.

Upon increase of the concentration of the protein, DLS measurements emphasized an increase of the mean size of pure mucin samples. It was presumably attributed to the formation of electrostatic intermolecular interactions. The infrared spectroscopic data was able to support this assumption.

The conformation of mucin in the presence of different aluminium species was then studied. The enlargement of the amide I band of the mixtures of aluminium species with mucin (presented in Figure (7.15) stressed a variation of the λ_{max} in the region 1800-1600 cm^{-1} in the presence of aluminium species. The λ_{max} 1670 cm^{-1} of a pure mucin sample shifted to lower wavenumbers in the presence of all the aluminium species employed.

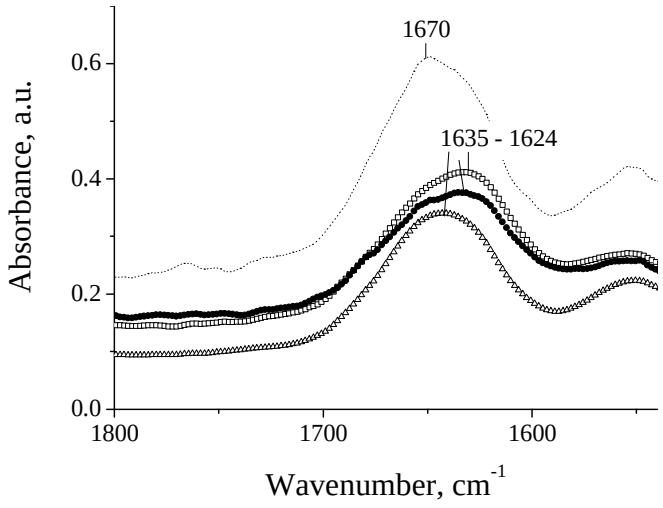

Figure 7.15. Enlargement of the ATR-FTIR spectra of pure mucin spectrum (25 mg.mL^{-1}) and aluminium (0.15 mol.L^{-1})-mucin (25 mg.mL^{-1}) combinations showing the shift of the λ_{max} of the amide I band.

Significant changes in peak position and their relative intensities were observed in the presence of aluminium species, suggesting that aluminium caused conformational changes for the mucin. The speciation diagrams of the secondary structures of the aluminium-mucin samples endorsed the idea. The results are presented in Figure (7.16).

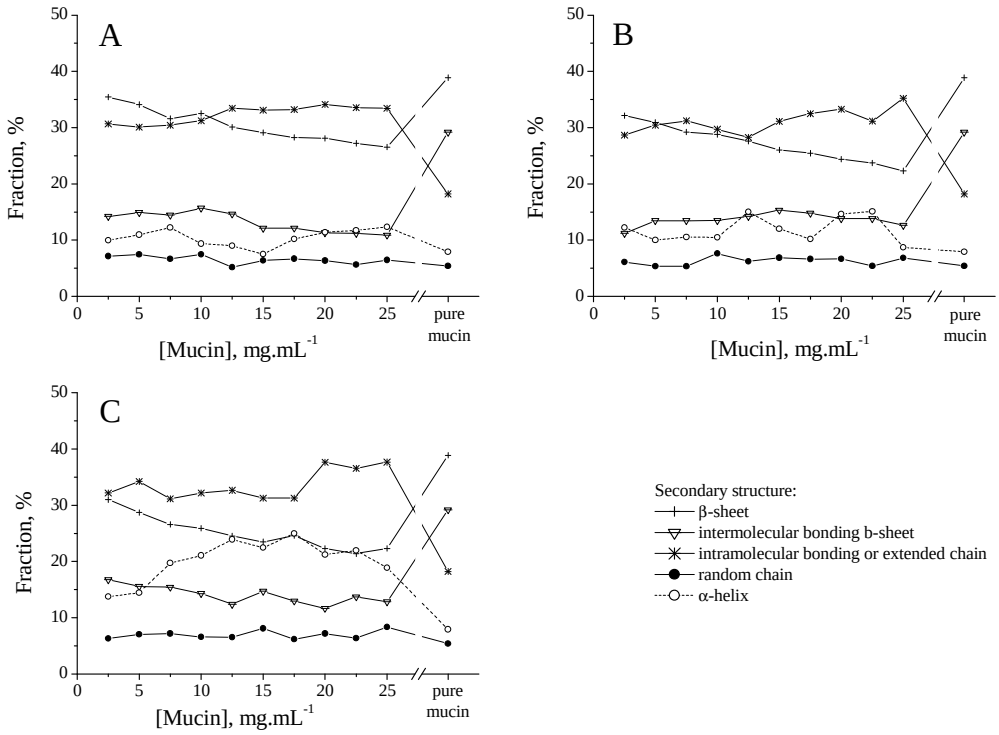

Figure 7.16. Secondary structure distribution of the Al_{13}-mers-mucin (**A**), the Al_{30}-mers-mucin (**B**) and the aluminium hydroxide-mucin (**C**) mixtures against the concentration of the protein determined by ATR-FTIR. Standard deviations errors obtained from data collection in triplicate were within ± 2.8 %.

In the presence of aluminium species, the intramolecular bonding or extended chain structures were either the most numerous from the beginning of mucin addition in the mixtures as in the case of the aluminium hydroxide-containing samples, or became the most significant after additions of 12.5 or 5 $mg.mL^{-1}$ of protein to the Al_{13}-mers and Al_{30}-mers solutions respectively. Upon increase of the concentration of mucin, the fractions of the β-sheet and the intermolecular bonded conformations decreased while an increase of the fraction of the α-helices was observed. The presence of the α-helices was limited for the aluminium polycations systems and more pronounced for the aluminium hydroxide samples. The random chain organisation was insensitive to the presence of aluminium and its fraction was stable in the protein. These observations supported the interpretations of the DLS results. Due to the decrease of the intermolecular bonding, oligomerisation of the protein was inhibited. The important quantity of intramolecular bonding suggested that the presence and the complexation of the aluminium species with mucin favoured the formation of compact structures such as α-helices at the expense of β-sheets.

The conformation of mucin was subsequently analyzed by the KBr transmission method. Similarly to the procedure performed for ATR-FTIR analysis, the spectra collected by KBr transmission spectroscopy were peak fitted and their integration have provided secondary structure distribution within the samples. The distribution diagrams are represented in Figure (7.17).

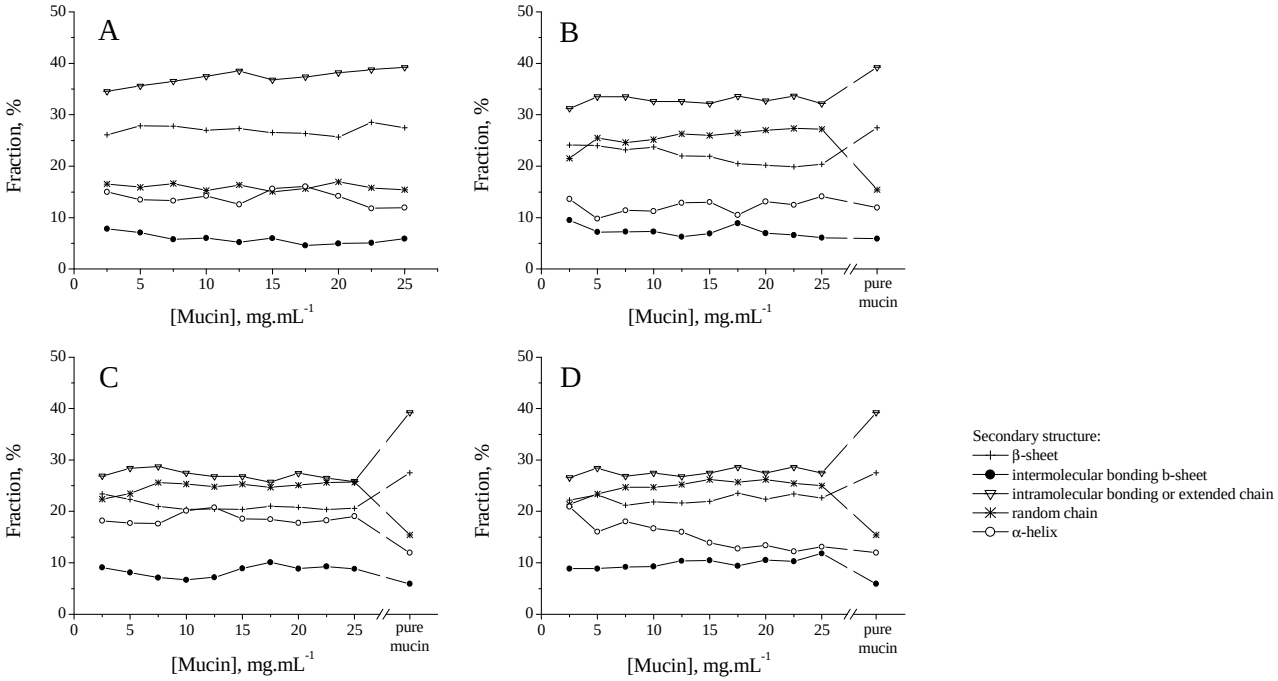

Figure 7.17. Secondary structure distribution of the pure mucin samples (**A**), the Al_{13}-mers-mucin (**A**), the Al_{30}-mers-mucin (**B**) and the aluminium hydroxide-mucin (**C**) mixtures against the concentration of the protein determined by KBr transmission. Standard deviations errors obtained from data collection in triplicate were within ± 3.1 %.

In its native conformation, mucin is mainly made of intramolecular bonding and organised in β-sheet structures. Addition of aluminium species did not modify that general trend notwithstanding the occurrence of a combination of electrostatic interactions, covalent linkages and hydrogen bonding between aluminium and the protein. Increase of the concentration of mucin in the samples did not change the proportion of each secondary structure. Binding of aluminium to mucin led to structural stabilisation of the host protein. Furthermore, the conformation of mucin was aluminium species-independent because no real difference was evidenced between the different aluminium species employed on the secondary structure distribution.

The importance of intramolecular interactions in the aluminium-containing samples was likely to facilitate polymer chain entanglement and was responsible for the higher value of random chain organisation. Although the intramolecular bonding was yet present in pure mucin samples, the absence of complexation with aluminium species within the pure mucin solutions may explain the lower fraction of random chain structures in those samples.

The results obtained with both infrared spectroscopic techniques were next compared. Figure (7.18) expresses it.

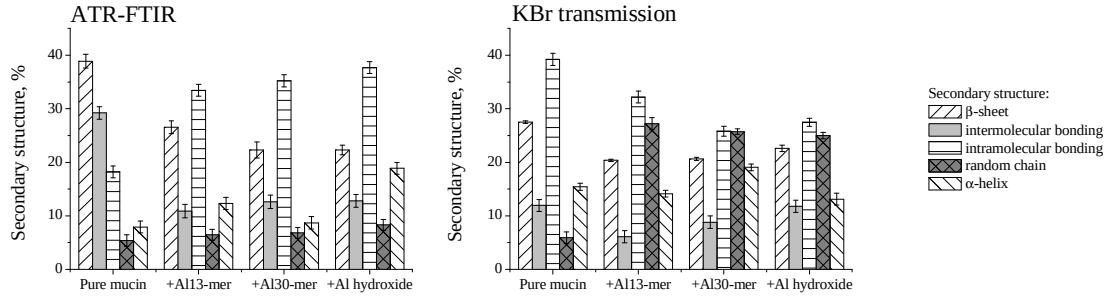

Figure 7.18. Comparison of the secondary structure distribution of the aluminium (0.15 mol.L^{-1})-mucin 25 mg.mL^{-1} mixtures determined by ATR-FTIR and KBr transmission.

The infrared spectroscopic data of the aluminium-mucin materials summarised in the above figure, demonstrated that the ATR spectra were not identical to transmission spectra.

The mucin native conformation was organised into a much more compact structure when analyzed by KBr transmission than by ATR-FTIR. Although both sampling techniques featured high intermolecular bonding content, the fraction of random chains was more prominent with the KBr transmission analysis than with the ATR-FTIR one.

The difference stated can be related to the sample preparation. The quality of transmittance measurements could have been adversely affected by the sample preparation, step which is not required for ATR-FTIR analysis.

7.7. SEM observations

The solid products obtained by freeze-drying of various Al species-mucin samples were subjected to SEM analysis. By increasing the mucin concentration from 2.5 to 25 mg.mL^{-1} in the samples, the SEM morphology of the solutions evolved from dispersed small spheres to stacked sheet structures covered with scattered spheres (Figure (7.19)). The conformation of the mucin obtained from the infrared spectroscopic data showed an increase of the proportion of the intramolecular interactions within the protein itself upon increase of the concentration of the protein. The increase of the intramolecular interactions can have affected the structure of the pure protein and caused the formation of stacked sheets.

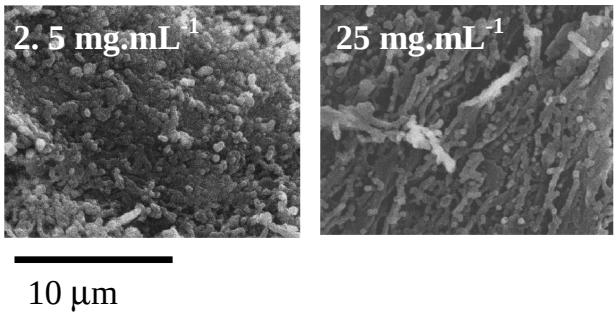

Figure 7.19. SEM images of the pure mucin solutions at 2.5 and 25 mg.mL^{-1} mucin concentration centrifuged at 3000 rpm for 30 min and freeze-dried prior to observation.

In the case of pure Al_{13}-mer (Figure (7.20)), the freeze-dried material is disorganized on the micrometer level. Once in the presence of mucin, the polycation formed smaller sized structures. The samples containing Al_{13}-mers changed progressively until finally they exhibited small and spherical configurations. Carbon, oxygen and aluminium were uniformly observed in the sample at the highest mucin concentration as revealed by their elemental mapping.

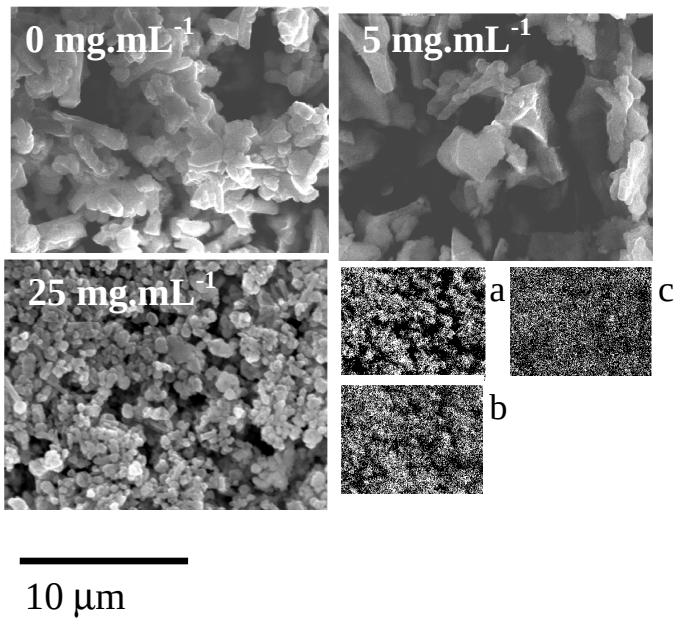

Figure 7.20. SEM pictures of aluminium-mucin hybrid materials prepared by freeze-drying from Al_{13}-mers with various mucin amounts. In (**a**), (**b**), (**c**) are represented the elemental mapping of the same region than in the 25 mg.mL^{-1} hybrid material using respectively CKα_{1-2}, OKα_1 and AlK α_1 energies.

A similar picture to the one drawn for the Al_{13}-containing samples was observed for the Al_{30}-mer-based materials (Figure (7.21)). Freeze-drying of pure Al_{30}-mer solutions led to structures heterogeneous in shape. As mucin concentration increased, spheres with uniform sizes about micron size in diameter were prevalent. The dense assemblies observed in the aluminium polycation-mucin solutions can be explained based on the conclusions obtained from infrared spectroscopy. We saw that electrostatic interactions occurring between the aluminium species and the protein favoured the folding of the mucin into a more compact α-helical pattern. The condensed helical conformation may justify the formation of the spherical structures. Again, the elemental mapping of carbon, oxygen and aluminium exposed their uniform incorporation in the aluminium-mucin assemblies.

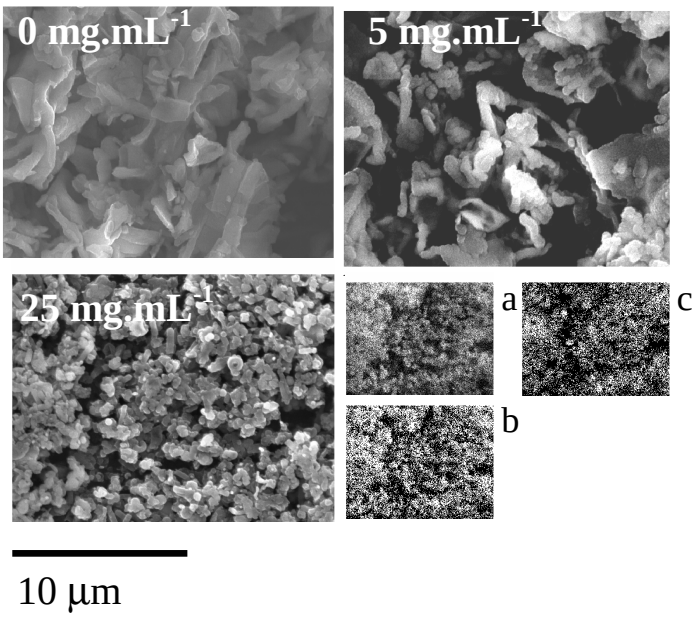

Figure 7.21. SEM pictures of aluminium-mucin hybrid materials prepared by freeze-drying from Al_{30}-mers with various mucin amounts. In (**a**), (**b**), (**c**) are represented the elemental mapping of the same region than in the 25 mg.mL^{-1} hybrid material using respectively CKα_{1-2}, OKα_1 and AlK α_1 energies.

The presence of mucin also modified the morphology of the aluminium hydroxide-containing samples, Figure (7.22). From small spheres, the aluminium hydroxide particles organised themselves into aluminium-mucin heterostructures.

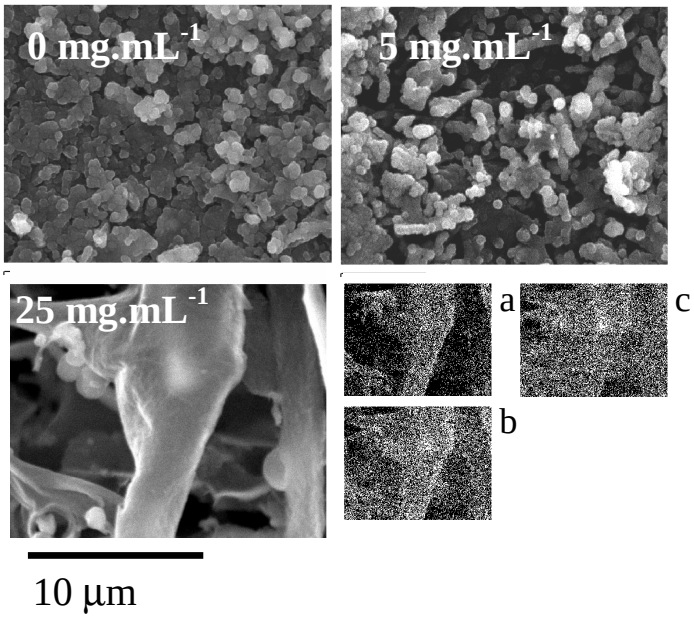

Figure 7.22. SEM pictures of aluminium-mucin hybrid materials prepared by freeze-drying from Al hydroxide with various mucin amounts. In (**a**), (**b**), (**c**) are represented the elemental mapping of the same region than in the 25 mg.mL^{-1} hybrid material using respectively CK$\alpha_{1\text{-}2}$, OKα_1 and AlK α_1 energies.

The initial small and spherical morphology of the aluminium hydroxides was identical to the morphology of the samples resulting from the blend of aluminium polycations and mucin. SEM observations made on samples prepared from aluminium polycations supported the idea that increases in mucin concentration led to partial transformation of polycations into aluminium hydroxide colloids. The fact that the Al_{13} and Al_{30}-based materials obtained by freeze-drying apparently were soluble in water over the whole mucin concentration range could be explained by either the relatively small fraction, or the extremely fine size of the aluminium hydroxide particles formed in both cases.

Summarizing the SEM observations of the morphology of aluminium-mucin systems, the effect of aluminium speciation was important. With increasing size of aluminium species, the spherical shape of the protein got organized into sheet-like structures.

7.8. Conclusion

This study aimed to improve the understanding of the gelation behaviour of mucin induced by the presence of different aluminium species. Here we describe the use of infrared and nuclear magnetic resonance spectroscopies and other physico-chemical techniques to investigate on the molecular-level, the interactions between mucin and aluminium species. The contribution of the electrostatic interactions among the aluminium-mucin complexes formed was confirmed as evidenced by potentiometric titrations and DLS measurements.

The binding of aluminium species to mucin was found to bring about transition of native β-sheet structures to more compact organisation involving intermolecular bonding with the resultant

stabilisation of the protein as evidenced by DLS measurements and Fourier transform infrared spectroscopy. The formation of small spheres in the aluminium polycation-containing mixtures was verified by SEM observations. In the case of the aluminium hydroxide systems, the conformational change of the protein due to its complexation was accompanied as demonstrated by SEM, with the formation of sheet-like structures. The tendency of mucin to gel in the presence of aluminium species was the most pronounced with the aluminium hydroxide particles.

7.9. References

[1] G. Zayas, J. Dimitry, A. Zayas, D. O'Brien, M. King, BMC Pulmonary Medicine, 2005, 5, 11.

[2] D. J. Thornton, J. R. Davies, I. Carlstedt, J. K. Sheehan, Airway Mucus: Basic Mechanisms and Clinical Perspectives, 1997, D. F. Rogers, M. I. Lethem, eds., pp. 19-39, Birkhäuser Verlag, Basel.

[3] C. Wickstrom, J. R. Davies, G. V. Eriksen, E. C. I. Veerman, I. Carlstedt, Biochem. J., 1998, 334, 685.

[4] R. Bansil, E. Stanley, J. T. Lamont, Annu. Rev. Physiol., 1995, 57, 63.

[5] T. A. Gerken, R. Gupta, N. Jentoft, Biochemistry, 1992, 31, 639.

[6] K. L. Shafran, O. Deschaume, C. C. Perry, Adv. Eng. Mater., 2004, 6, 836.

[7] K. L. Shafran, C. C. Perry, Dalton Trans., 2005, 2098.

[8] J. W. Akitt, Prog. Nucl. Mag. Res. Sp., 1989, 21, 1.

[9] L. Allouche, C. Gerardin, T. Loiseau, G. Férey, F. Taulelle, Angew. Chem.Int. Ed., 2000, 39, 511-514.

[10] D. Coster, J. J. Fripiat, Chem. Mater., 1993, 5, 1204.

[11] K. J. D. MacKenzie, J. Temuujin, K. Okada, Thermochim. Acta, 1999, 327, 103.

[12] J. Y. Bottero, J. M. Cases, F. Fiessinger, J. E. Poirier, J. P hys. Chem., 1980, 84, 2933.

[13] S. M. Bradley, R. A. Kydd, R. F. Howe, J. Colloid Interface Sciences, 1993, 159, 405.

[14] W. E. E. Stone, G. E. Shafei, J. Sanz, S. A. Selim, J. Phys. Chem., 1993, 97, 10127.

[15] O. Deschaume, K. L. Shafran, C. C. Perry, Langmuir, 2006, 22, 10078.

[16] G. E. Yakubov, A. Papagiannopoulos, E. Rat, R. L. Easton, T. A. Waigh, Biomacromolecules, 2007, 8, 3467.

[17] T. A. Waigh, A. Papagiannopoulos, A. Voice, R. Bansil, A. P. Unwin, C. D. Dewhurst, B. Turner, N. Afdhal, Langmuir, 2002, 18, 7188.

Part 8

Summary and Perspectives

8.1. Hydrolysis ratio and experimental parameters

The first part of the thesis was methodology-based. It was partly devoted to the preparation of the ground floor materials for the latter part of the project, the aluminium-biomolecule studies. After the determination of the speciation of four aluminium reference systems by ^{27}Al solution NMR, a comparative study of three aluminium quantification techniques was performed. Though quantification of aluminium concentration resulted in good consistency between gravimetry, spectrophotometric and ^{27}Al solution NMR techniques, NMR was preferred over the other techniques. The benefits of NMR lie in its quick implementation and its ability to achieve speciation information unlike the two other methods.

The specified aluminium reference systems synthesized ($AlCl_3$, Al_{13}- and Al_{30}-mers and $Al(OH)_3$) were used for fundamental studies of the phenomena of aggregation and gelation. Based on qualitative visual observations of aluminium-gelling agent mixtures, an absence of deprotonated sites on the gelling agents appeared unfavourable to the establishment of aluminium-ligand complexes. Beside, pH-dependent gelling agents were found to be the best destabilization agents of the aluminium systems. These agents were able to produce gels, with this ability being exploited later in the project. Gelation was also observed in highly basic solutions such as with the K_3PO_4-containing samples and some of the Na_2SiO_3-containing samples. However, the use of those agents has to be avoided in order to maintain the aluminium speciation in the samples.

Among the aluminium reference systems employed, the aluminium hydroxide suspension was the most prone to form a composite gel-like structure in the presence of gelling agents. Extrapolation of the results to mixtures made of aluminium species and biomolecules suggested that negatively charged functionalities such as carboxylate functions and the side chains of certain amino acids (aspartic acid, glutamic acid, etc.) present in biomolecules will have the most important impact on their gelation with aluminium species. We consequently assumed that assemblies formed between aluminium and biomolecules would be predominantly driven by electrostatic interactions since the aluminium polycations are highly positively charged and the aluminium hydroxide colloids are also positively

charged. Hydrogen bonding could also control the adsorption of new assemblies between aluminium species and the biomolecules. To further observe the intricate relations existing between aluminium species and ligands, the number of organic polymers tested as gelling agents could be extended. Further functionalities for potential co-gellant applications would be exposed.

Knowing that all of the aluminium species tested are able to gel, the next section of work was undertaken to explore the mechanisms leading to the sol-gel transformation of aluminium ions into Al (oxy) hydroxides and oxides in aqueous solution. To pursue that aim, the effects caused by the addition of a soft base, Trizma-base, to aluminium reference systems was investigated using a combination of four complimentary techniques for monitoring pH, conductivity, viscosity and parameters of ultrasound (ultrasonic velocity and attenuation). The present work led to the generation of new kinetic data about the gel formation process. pH measurements revealed that the aluminium species present initially were neutralised and converted first into monomeric aluminium ions. Upon increase of the hydrolysis ratio *h* of the media, conductivity results demonstrated that the species started to condense into polynuclear species. From $h \sim 3$, the Keggin and the aluminium molecular clusters were converted into Al (oxy) hydroxides from the viscosity data. The event was initiated by the aggregation of primary nuclei of Al (oxy) hydroxides into larger clusters. Its further development corresponds to the sol-gel transition phenomenon that was characterised by the formation of weak gels as attested by ultrasonic titrations. The variation of the differential ultrasonic attenuation measurements corroborated the succession of the events occurring during conversion of aluminium ions into Al (oxy) hydroxides. Furthermore, the sequence of the sol-gel transition was dependant on the initially aluminium species present. Upon further addition of base, the resulting gels started to dissolve and form smaller negatively charged particles as well as aluminates as a final product of dissolution under basic conditions. The findings can be extrapolated to the characterisation of colloidal processes in different metal-containing solutions. Additionally, the impact of variables such as temperature or the presence of anions or ligands on the gel formation process could complement the conclusions established here. The procedure followed here could interestingly be applied to composite gels in order for example to investigate the viscosity of composite materials.

8.2. Gelation studies

A potentiometric method was developed and optimised for the determination of the formal hydrolysis ratio *h* for the exhaustive and quantitative speciation-fractionation of aluminium in aqueous solutions. The method uses the point of complete precipitation of aluminium hydroxide as a reference ($h = 3.0$) in order to calculate the initial formal hydrolysis ratio of aluminium hydrolytic species. Additional data processing of the first-derivative titration curves was performed by peak-fitting. Peak-fitting was used to refine the position of the inflexion points and resolve overlapping inflexions better. Several solutions of pure hydrolytic species including aluminium monomers ($AlCl_3$), Al_{13}-mers, Al_{30}-mers and aluminium hydroxide particles were used as ‘reference standards’ to validate the proposed potentiometric method. Other important variables in the potentiometric determination of the hydrolysis ratio have also been optimised including the concentration of aluminium.

In the presence of aluminium reference systems above 0.04 mol.L^{-1}, there is a problem of assigning the major inflexion point (h = 3.0) which arises from higher local pH gradients. Moreover, the use of concentrations higher than 0.012 mol.L^{-1} provided underestimated values of the formal hydrolysis ratio of the systems. The use of high aluminium concentrations during the course of titrations can also lead to the formation of a gel as already discussed in the previous section. The optimum range of aluminium concentrations for the titrimetric determination of the formal hydrolysis ratio was found to be between 0.004 and 0.012 mol.L^{-1}.

The type and strength of alkali (Trizma-base, NH_4OH, $NaHCO_3$, Na_2CO_3 and KOH) employed for the titrations had an effect on the pH-metric determination of the 'formal' hydrolysis ratio. On the basis of the comparison of five different alkalis, the optimum window of alkali strength for the determination of the 'formal' hydrolysis ratio of Al species in solution is in the range of $8.0 \leq pK_a \leq 10.4$ (*e.g.* Trizma, NH_4OH or Na_2CO_3). The conclusions were corroborated by reference values obtained from ^{27}Al solution NMR measurements. Once the parameters of the potentiometric method were optimised, the determination of the 'formal' hydrolysis ratio was cross-verified using quantitative ^{27}Al solution NMR. The absence of major difference between the potentiometric and the spectroscopic techniques in the determination of h, proved the robustness of our method. Finally, the method appeared to be an accurate and easy technique in its implementation as illustrated by its use in the determination of the 'formal' hydrolysis ratio of a commercial sample of basic aluminium chloride.

From the results discussed above, the developed potentiometric method is an excellent route to the qualitative analysis of aluminium-containing solutions due to its low cost, relative ease and good control over reaction factors. Unlike with ^{27}Al solution NMR, by using potentiometry, it is possible to calculate the aluminium speciation of an aluminium ions solution which contains an insoluble phase (e.g. aluminium hydroxide).

8.3. Interactions of aluminium species with biomolecules

In the final part, a thorough study of aluminium-biomolecule systems was undertaken. Experiments consisted of mixing together a pure aluminium reference system with varying amounts of a biomolecule. Four aluminium-containing systems were employed: aluminium monomers ($AlCl_3$), Al_{13}-mers, Al_{30}-mers and aluminium hydroxide particles while three bioligands were tested: lactic acid, lysozyme and mucin. The choice of the biomolecules was based on their different physico-chemical properties and their occurrence in the human body. The composition and formation mechanisms of these materials have been investigated using various solution and solid-state characterization techniques. The study of aluminium-biomolecule assemblies made it possible to highlight and characterise new bio-materials.

In the first study, lactic acid, a strongly binding ligand, was used. Lactic acid, due to its acidity, broke down all the aluminium reference systems tested into aluminium monomers by acidic hydrolysis. After ageing, aluminium-lactate compounds were formed between the biomolecule and the resulting

aluminium hydrolysed products. The existence of chelate complexes was evidenced by ^{27}Al and ^{1}H solution NMR spectroscopies and KBr transmission infrared spectroscopy of the solid products.
Al_{13}-mers, Al_{30}-mers and aluminium hydroxide particles were the most responsive species to the presence of lactic acid. However, aluminium-lactate nanohybrid materials were detected with all the aluminium systems employed. Some of these chelate complexes were mono-coordinated while the majority contained lactic acid acting as a bidentate ligand.
Lactic acid is a chelator of Al^{3+} ions. It can be used in biological systems to remove abnormal by high concentrations of aluminium from the body. The chelating agent forms a water soluble chemically inert form, the chelate, which will enter the bloodstream and be excreted harmlessly.

The second biomolecule employed as a ligand, was a basic globular protein, lysozyme. The evolution of both the inorganic and biomolecular phases was compared with results of previous studies focusing on interactions of aluminium species with bovine serum albumin (BSA). For both BSA and lysozyme, the assembly of Al_{13} and Al_{30} with the proteins led to the formation of hybrid species observable by means of dynamic light scattering (particle size superior to both pure aluminium species and pure protein particle sizes) and zeta potential measurements (potential stabilising to the value of the hybrid species upon increase in protein concentration). Specific charge-stabilised bioinorganic assemblies involving aluminium species and lysozyme were observed to form in contrast to the gel like structure formed on interaction of BSA with aluminium species. The chemical and structural alterations of the two proteins on interaction with the inorganic species were investigated using infrared spectroscopy (secondary structure determination and 2D correlation spectroscopy) and showed that the interactions involve mostly acidic surface groups (Asp, Glu), through strong complexation and deprotonation in the case of BSA interactions with Al_{13} and Al_{30}, through hydrogen bonding in the case of lysozyme interactions with the same species, and also through hydrogen bonding in the presence of aluminium hydroxide particles.

The last compound tested was mucin, a protein which is found in the dynamic, interactive mucosal defensive system of the human body. The mucin molecule with isoelectric point at pH ~ 4.79-6.24 represents a very weak polyacid showing a range of acidities and, therefore, an inhomogeneous distribution of negative charges. Thus, for most cases studied, the interaction between mucin and positively charged aluminium polycations or aluminium hydroxide nanoparticles will be predominantly electrostatic. Such interactions presumably lead to coverage of mucin molecules by smaller aluminium polycations.
The resulting aluminium-mucin complexes were characterised by a gel-like structure. The binding of aluminium species to mucin was found to bring about a transition of native β-sheet structures to more compact organisation involving intermolecular bonding with the resultant stabilisation of the protein as evidenced by DLS measurements and Fourier transform infrared spectroscopy.
The re-organisation of the new assemblies was observed in the form of small spheres by SEM in the case of the systems made initially of aluminium polycations. Interesting curved sheeted morphology

materials were obtained from aluminium hydroxide-mucin systems, which will require further characterisation including mechanical testing.

The objective of scrutinising the effects of aluminium species on the structures of biomolecules of different properties was achieved. The present work led to the generation of new morphological data about the interactions occurring between aluminium polynuclear and hydroxide species and different biomolecules. For the first time, conformational analyses were performed on a wide range of aluminium species and biomolecules. The isoelectric point of the ligand seemed to have the most important influence on the formation of new conformational assemblies. The advancements brought about by the conformational studies will enable one to imagine new bio-related materials.